RUTHENIUM-BASED ANTICANCER DRUGS THAT TARGET DNA THROUGH MULTIPLE BINDING MODES

By:

Rachel Louise Mowll

A thesis submitted in partial fulfilment of the requirements for the degree of Doctor of Philosophy

The University of Sheffield
Faculty of Science
Department of Chemistry

May 2019

1. Abstract

The primary aim of this work was to assess the potential of ruthenium complexes as effective treatment for non-small cell lung cancer before going forward into animal studies. The main candidates were the previously studied DRuT ($[Ru(tpm)(dppz)Cl]^+$) and PRuT ($[Ru(tpm)(phen)Cl]^+$), which were known to be cytotoxic towards A2780 and A2780 CIS human ovarian carcinoma cells.

DRuT and PRuT were synthesised and characterised and their DNA binding properties were investigated. A restriction enzyme inhibition experiment showed that PRuT binds covalently to DNA but DRuT does not. It was known that DRuT binds reversibly to DNA by intercalation, however it was not known whether PRuT binds reversibly to DNA and if so, by what mechanism. A competition DNA titration experiment found that PRuT does bind reversibly to DNA but with a lower affinity than DRuT. From this it was inferred that PRuT may be a groove binder.

The mechanisms of action of DRuT and PRuT in A2780 CIS cells were investigated. An ICP-MS experiment showed that at timepoints up to 3 hours PRuT enters cells more quickly than DRuT. PFGE showed that neither DRuT nor PRuT causes DNA double strand breaks in treated cells. FACS analysis showed that DRuT causes cells to accumulate in S phase of the cell cycle and that it inhibits DNA replication. It was also shown that PRuT causes cell cycle arrest in early S phase; DNA replication appears to initiate but not continue. A PCR inhibition experiment confirmed that DRuT inhibits DNA replication at a lower concentration than PRuT. DNA fibre analysis showed that both DRuT and PRuT decrease DNA replication fork speed, but DRuT slows the replication rate more than PRuT. Rad51 immunofluorescence was used to determine whether PRuT causes more replication fork collapse than DRuT, however the results were inconclusive. A TMRE assay showed that DRuT and PRuT cause mitochondrial damage, with DRuT causing a larger effect than PRuT.

The cytotoxicities of DRuT and PRuT were measured in A549 non-small cell lung cancer cells. It was found that DRuT is cytotoxic but PRuT is not. DRuT's mechanism of action in this cell line was therefore investigated. It was found that DRuT causes Chk1 phosphorylation, but not Chk2 or γ-H2AX phosphorylation. FACS analysis showed that DRuT only causes replication inhibition at concentrations much higher than the IC_{50}, unlike in A2780 CIS cells where the effect is observed at IC_{50} concentration. A TMRE assay showed that DRuT causes a small amount of mitochondrial damage, although the effect is smaller than in A2780 CIS cells.

Overall it was concluded that DRuT could be a potential drug candidate for treating non-small cell lung cancer, and should be considered for taking forward into animal studies. However more information about its mechanism of action in A549 cells is needed.

Contents

1 Abstract **I**

Acknowledgements **VI**

Abbreviations **VII**

2 Introduction **1**

2.1 The role of DNA in cell biology 1

2.1.1 Structure of DNA 1

2.1.1.1 Targeting DNA 2

2.1.1.1.1 Irreversible binding 2

2.1.1.1.2 Reversible binding 2

2.1.2 The central dogma of molecular biology 4

2.1.3 The cell cycle 5

2.1.4 DNA replication 5

2.1.5 Transcription 7

2.1.6 Translation 7

2.1.7 DNA repair 8

2.1.8 Cell death 9

2.2 Cancer 11

2.2.1 Cancers with unmet needs 12

2.2.1.1 Non-small cell lung cancer 12

2.2.2 Causes of cancer 13

2.2.3 Hallmarks of cancer 15

2.2.3.1 Self-sufficiency in growth signals or sustaining proliferative signalling 16

2.2.3.2 Insensitivity to antigrowth signals or evading growth suppressors 16

2.2.3.3 Evading apoptosis or resisting cell death 17

2.2.3.4 Limitless replicative potential or enabling replicative immortality 18

2.2.3.5 Sustained angiogenesis or inducing angiogenesis 18

2.2.3.6 Tissue invasion and metastasis or activating invasion and metastasis 19

2.2.3.7 Enabling characteristics and emerging hallmarks 20
2.3 Treatment of cancer 22
2.3.1 Surgery 22
2.3.2 Radiotherapy 22
2.3.3. Chemotherapy 23
2.3.4 Immunotherapy 23
2.3.5 Targeted therapy 24
2.4 Metal-based chemotherapy 25
2.4.1 Platinum-based chemotherapy 25
2.4.1.1 Cisplatin: discovery and mechanism of action 25
2.4.1.2 Cisplatin: problems and alternative analogues 28
2.4.2 Ruthenium-based chemotherapy 32
2.4.2.1 Ruthenium drugs with covalent binding properties 32
2.4.2.2 Ruthenium complexes with non-covalent binding properties 34
2.4.2.3 The DNA light switch effect 36
2.5 Ruthenium (II) tris-(1-pyrazolyl)methane complexes 39
2.6 Aims 48

3 Synthesis and Binding Studies 49
3.1 Aims 49
3.2 Synthesis 50
3.3 Characterisation 54
3.4 Binding studies 59
3.4.1 Covalent binding 59
3.4.1.1 DNA ICP-MS 59
3.4.1.2 NMR 62
3.4.1.3 Restriction enzyme experiment 68
3.4.2 Non-covalent binding 72
3.4.2.1 DNA titrations 72
3.5 Conclusion 77

4 Mechanistic studies in a human ovarian carcinoma model 78

4.1 Introduction 78
4.2 Cellular uptake 79
4.3 Effects on DNA 81
4.3.1 Pulsed field gel electrophoresis 81
4.3.2 Fluorescence-activated cell sorting 83
4.3.3 Polymerase chain reaction inhibition 88
4.3.4 DNA fibre analysis 91
4.3.5 Rad51 immunofluorescence 94
4.3.5.1 Protocol optimisation 95
4.3.5.2 Comparison of DRuT and PRuT 103
4.4 Mitochondrial effects 105
4.4.1 Mitochondrial membrane potential 105
4.4.2 Autophagy and mitophagy 107
4.5 Conclusion 115

5 Mechanistic studies in a human non-small cell lung cancer model 117
5.1 Introduction 117
5.2 MTT toxicity assay 118
5.3 Effects on DNA 120
5.3.1 Western blots 120
5.3.2 FACS analysis 123
5.4 Mitochondrial effects 127
5.4.1 TMRE assay 127
5.4.2 Autophagy and mitophagy 129
5.5 Conclusion 135

6 Conclusion and future work 136
6.1 Conclusion 136
6.2 Future work 140

7 Experimental 141
7.1 Synthesis 141

7.1.1 Synthesis of 1,10-phenanthroline-5,6-dione (DPQ) 141
7.1.2 Synthesis of DPPZ 141
7.1.3 Synthesis of $[Ru(tpm)Cl_3]$ 142
7.1.4 Synthesis of $[Ru(tpm)(phen)Cl]^+$ 142
7.1.5 Synthesis of $[Ru(tpm)(dppz)Cl]^+$ 143
7.1.6 Synthesis of $[Ru(tpm)(dppn)Cl]^+$ 144
7.1.7 Synthesis of $[Ru(bpy)_2Cl_2]$ 144
7.1.8 Synthesis of $[Ru(bpy)_2(dppz)]^{2+}$ 145
7.1.9 Synthesis of $[Ru(bpy)_3]^{2+}$ 145
7.1.10 Formation of chloride salts 146
7.1.11 Preparation of stock solutions 146
7.2 Biological studies 147
7.2.1 Cell culture 147
7.2.2 DNA ICP-MS 147
7.2.3 NMR 148
7.2.4 Restriction enzyme inhibition 148
7.2.5 DNA titrations 149
7.2.6 Cellular uptake ICP-MS 149
7.2.7 Pulsed-field gel electrophoresis 149
7.2.8 Fluorescence-activated cell sorting 150
7.2.9 Polymerase chain reaction inhibition 151
7.2.10 DNA fibre analysis 151
7.2.11 Rad51 immunofluorescence 152
7.2.12 TMRE assay 153
7.2.13 ptfLC3 transfection and imaging 153
7.2.14 MTT assay 154
7.2.15 Western blotting 155
7.2.15.1 Lysate preparation 155
7.2.15.2 Western blotting 155

8 References **156**

Acknowledgements

I have had assistance from many technical and research staff with experiments. I would particularly like to thank the following people for their contributions. Neil Bramall for performing ICP-MS analysis, Sue Bradshaw for performing NMR analysis, Dr Emad Ahmed Abdel Gaber for advising and assisting me with PFGE, Dr Darren Robinson for advising and assisting me with microscopy, Julie Swales for performing FACS analysis, Dr Helen Bryant for assistance with Rad51 immunofluorescence, Maria Davies for assistance with ptfLC3 transfection and Dr David King for assisting me with DNA fibre analysis.

Multiple past and present members of the Thomas and Smythe research groups gave me invaluable assistance and advice throughout my research. I would particularly like to thank Dr Mike Walker for inducting me into the Thomas group and Dr Dave Turton and Jackie Price for their extensive help in the Smythe lab. I would also like to thank all members of the Smythe group for helping me find my feet in a cell biology lab when I was clueless. Thank you also to Dr Joe Clarke for his continued support throughout the PhD process.

Finally I would very much like to thank my supervisors Professor Carl Smythe and Professor Jim Thomas for all their help in supporting me with this project. I could not have achieved what I have without their advice, support and encouragement.

Abbreviations

$[complex]_{50\%}$ = concentration of complex of interest at a 50% reduction in fluorescence

$[DNA]_T$ = total DNA concentration

[free complex] = concentration of unbound complex

$[H33258]_{50\%}$ = concentration of H33258 at a 50% reduction in fluorescence

3D = 3-dimensional

A = adenine

A_{260} = absorbance at 260 nm

A_{280} = absorbance at 280 nm

AF488 = Alexa Fluor 488

AF555 = Alexa Fluor 555

AF568 = Alexa Fluor 568

ATP = adenosine triphosphate

bp = base pairs

bpy = 2,2'-bipyridine

BRCA1 = breast cancer 1, early onset

BRCA2 = breast cancer 2, early onset

BrdU = bromodeoxyuridine

BSA = bovine serum albumin

C = cytosine

CCCP = carbonyl cyanide m-chlorophenyl hydrazine

Cdk2 = cyclin-dependent kinase 2

CldU = chlorodeoxyuridine

CT-DNA = calf thymus DNA

CTR1 = copper transporter-1

DMEM = Dulbecco's Modified Eagle Medium

DMF = dimethylformamide

DMF-d7 = deuterated dimethylformamide

DMSO = dimethyl sulfoxide

DNA = deoxyribonucleic acid

DPPN = benzo[i]dipyrido[3,2-a:2',3'-c]phenazine

dppz = dipyrido[3,2-a:2’,3’-c]phenazine

DPQ = 1,10-phenanthroline-5,6-dione

dpq-df = dipyrido (3,2-a:2′,3′-c) quinoxaline-difuran

DRuT = $[Ru(tpm)(dppz)Cl]^{+}$

DRuT-H_2O = $[Ru(tpm)(dppz)H_2O]^{+}$

DSB = double strand break

EBSS = Earle’s Balanced Salt Solution

EDTA = Ethylenediaminetetraacetic acid

EMT = epithelial-mesenchymal transition

EPR = enhanced permeability and retention

ER = endoplasmic reticulum

ERCC1 = excision repair cross-complementing-1

FACS = fluorescence-activated cell sorting

FCCP = carbonyl cyanide-4-(trifluoromethoxy) phenyl hydrazone

FDA = Food and Drug Administration

FSG = fish skin gelatin

G = guanine

G0 phase = gap phase 0

G1 = gap phase 1

G2 phase = gap phase 2

GFP = green fluorescent protein

H33258 = Hoechst 33258

hnRNA = heteronuclear RNA

HPV = human papilloma virus

HR = homologous recombination

HRP = horseradish peroxidase

HSA = human serum albumin

HU = hydroxyurea

ICP-MS = inductively-coupled plasma mass spectrometry

IdU = iododeoxyuridine

IF = immunofluorescence

K = binding constant

K_{app} = apparent DNA-binding constant of complex of interest

M phase = mitosis phase

m/z = mass over charge

MAPK = mitogen-activated protein kinase

MLCT = metal-to-ligand charge transfer

MMR = mismatch repair

mRNA = messenger RNA

MTT = 3-(4,5-dimethylthiazol-2-yl)-2,5-diphenyltetrazolium bromide

NER = nucleotide excision repair

NMR = nuclear magnetic resonance

NSCLC = non-small cell lung cancer

PBS = phosphate-buffered saline

PBS-tx = 0.15% BSA and 0.1% Triton X-100 in PBS

PCR = polymerase chain reaction

PFA = paraformaldehyde

PFGE = pulsed-field gel electrophoresis

phen = 1,10 phenanthroline

PI = propidium iodide

ppm = parts per million

PruT = $[Ru(tpm)(phen)Cl]^+$

PtT = platinum (II) terpyridine

Py = pyridine

RFP = red fluorescent protein

RNA = ribonucleic acid

ROS = reactive oxygen species

RPM = revolutions per minute

RPMI-1640 = Roswell Park Memorial Institute 1640

rRNA = ribosomal RNA

S phase = synthesis phase

T = thymine

TBS = Tris-buffered saline

TBS-T = 0.1% Tween-20 in TBS

TKPTS = mouse kidney proximal tubule

TMRE = tetramethylrhodamine, ethyl ester

tpm = tris-(1-pyrazolyl)methane

tpphz = tetrapyridophenazine

tRNA = transfer RNA

U = uracil

UV = ultraviolet

VDAC1 = voltage-dependent anion-channel 1

WHO = world health organisation

X = molar equivalent of complex compared to DNA

ΔF_{sat} = change in fluorescence at the point of saturation

ΔF_x = change in fluorescence

2. Introduction

2.1 The role of DNA in cell biology

One major feature that distinguishes living organisms is their ability to pass on genetic information to their offspring. All living cells store this information in the same way – as a sequence of four monomers in a long linear polymer called deoxyribonucleic acid (DNA).

2.1.1 Structure of DNA

The monomers of DNA, known as nucleotides, consist of a sugar (deoxyribose), a phosphate group and one of four bases (the purines adenine (A) and guanine (G), and the pyrimidines thymine (T) and cytosine (C)). The monomers are linked by the phosphates and sugars, which form the polymer backbone, and it is the sequence of the bases that forms the genetic code (Figure 1).

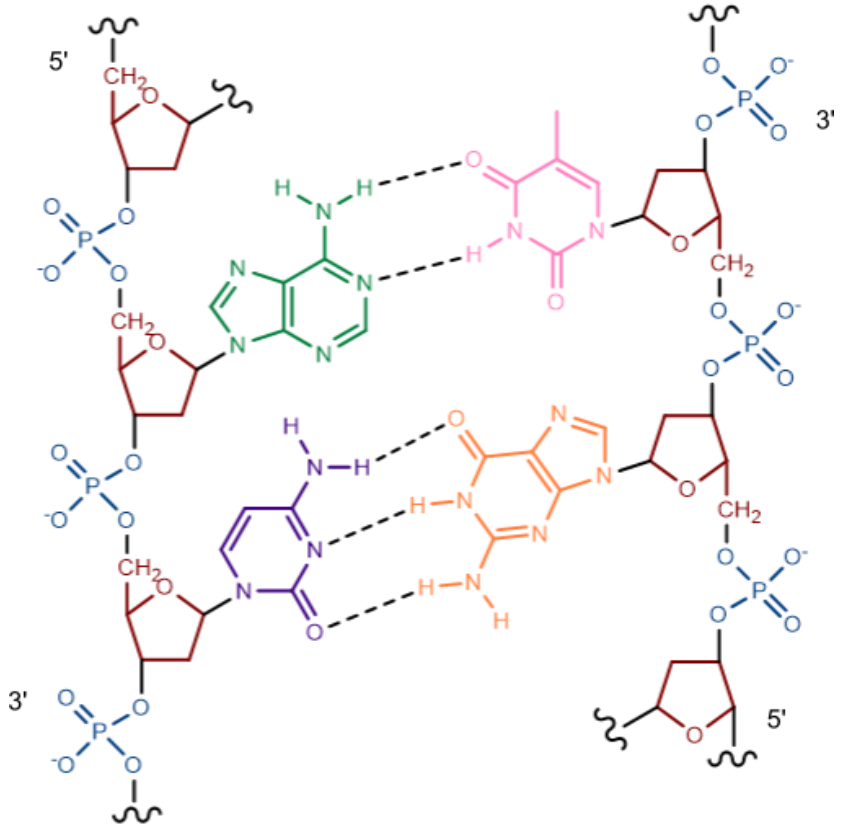

Figure 1: The structure of DNA. Sugar shown in red, phosphate in blue, adenine in green, thymine in pink, cytosine in purple and guanine in orange. The strands run in opposite directions with one end denoted 5' and one 3'.

Even before Watson and Crick's discovery of the molecular structure of DNA, it was known that the amount of A+G is equal to the amount of C+T in DNA, and this information was critical for solving its structure.[2] The most common conformation of DNA, named B-DNA, was found to be a right-handed double helix with a diameter of 20 Å,[3] consisting of two antiparallel strands. The strands contain complementary base pairs which are held together by hydrogen bonds – A with T and G with C (Figure 1).[2] The helical structure of DNA is stabilised both by the hydrogen bonds between complementary bases and by vertical π-stacking between bases.[3] The helix contains two grooves running down its length – a wide major groove and a narrow minor groove.[3] One consequence of the relatively weak hydrogen bonds between base pairs is that during the process of DNA replication, the two strands can be separated easily, and each single strand can be used as a template for the synthesis of a new strand with complementary base pairs. The complementarity between strands provides the basis by which accurate copying of the information contained within DNA can occur (see section 2.1.4), and ensures that, during the process of cell proliferation, daughter cells acquire accurate copies of the genome contained in parental cells.

2.1.1.1 Targeting DNA

Many chemotherapeutic drugs act to kill cancer cells by binding to their DNA, causing damage and leading to cell death. There are several ways small molecules can bind to DNA, and these are outlined below.

2.1.1.1.1 Irreversible binding

Irreversible binding is achieved by covalently binding to the bases of DNA. Several components of tobacco smoke bind to DNA in this way including polycyclic aromatic hydrocarbons and N-nitrosamines, specifically forming bulky adducts that ultimately lead to tumour formation.[4] The chemotherapy drug cisplatin also binds irreversibly to DNA (see section 2.4.1.1), as well as mustard agents[5] which have historically been used as chemotherapeutics.

2.1.1.1.2 Reversible binding

Electrostatic binding

As shown in Figure 1, DNA has anionic groups along its backbone; therefore cationic species readily bind to DNA. Spermine and spermidine (Figure 2) are naturally occurring polyamines that protonate

at biological pH.[6] Due to their ability to bind to DNA they have many functions within the cell. Although the electrostatic interaction with the DNA backbone is a large factor in their binding, polyamines can interact with DNA in other ways, such as interacting with the bases and groove binding. Polyamines help to stabilise DNA structure and have a role in condensing it,[6] as multivalent cations like polyamines decrease the repulsion between the negative charges on the backbone as well as bending the polymer.[7]

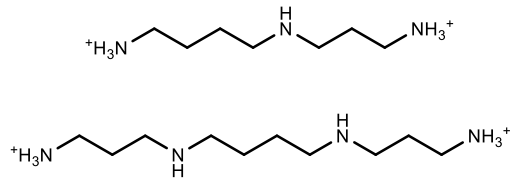

Figure 2: The structures of the polyamines spermine (top) and spermidine (bottom), which bind electrostatically to polyanionic DNA.

Intercalation

Intercalation was first proposed by Lerman in the early 1960s.[8] Planar aromatic molecules can fit in between the base pairs of DNA, and this unwinds the helix and separates the base pairs.[9] Lerman noted that intercalation had an effect on the viscosity of the DNA solution, a feature which can be used to test whether new compounds intercalate.[8]

A characteristic example of an intercalator is ethidium bromide (Figure 3). Like many organic intercalators it is a planar, polyaromatic, electron deficient system which can slot between base pairs. The interaction is stabilised by a variety of intermolecular interactions including the hydrophobic effect, π-stacking, van der Waals interactions and hydrogen bonding. The lengthening of the helix also decreases repulsion between anionic phosphate groups on the DNA backbone. The lengthening of the helix is what gives rise to the change in DNA viscosity.[10]

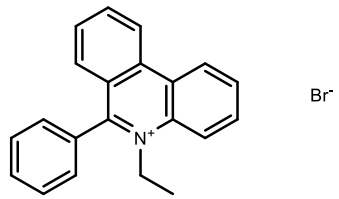

Figure 3: The structure of the organic intercalator ethidium bromide.

Groove binding

Groove binders fit into one of the grooves of DNA, due to intermolecular interactions such as the hydrophobic effect. They often bind in the minor groove and usually have a crescent shape which optimises the fit.[9] Netropsin (Figure 4) is an example of a groove binding molecule which binds in the minor groove of DNA.[11] It binds preferentially to sites with several A-T pairs and interferes with replication and transcription.[12]

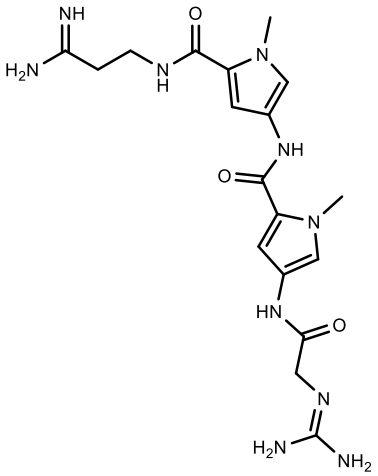

Figure 4: The structure of the minor groove binder netropsin.

2.1.2 The central dogma of molecular biology

Proteins make up most of the mass of a cell, excluding water.[13] The information stored in DNA is used to instruct the synthesis of proteins, with a section of DNA that codes for a protein being known as a gene, although this is not 'read' directly by the cell. Another important class of biopolymer, closely related to DNA, is used for this purpose – ribonucleic acid (RNA). The sugars in the backbone of RNA are ribose, and the base T in DNA is replaced by uracil (U). During the process of transcription, relevant sections of DNA are copied into a functionally identical base sequence in the form of RNA. This RNA is known as messenger RNA (mRNA). The process of synthesising proteins, known as translation, can then occur. The sequence of bases in the RNA is grouped into codons, each of which consists of three bases that correspond to a specific amino acid. Amino acids are polymerised in sequences specified by RNA to form proteins; the direction of information transfer, carried out by the processes of transcription and translation, is described as the central dogma of molecular biology (Figure 5).[14]

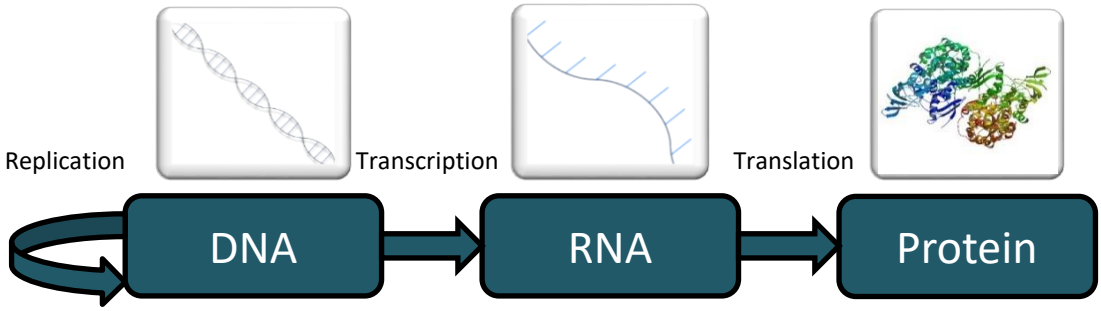

Figure 5: A representation of the central dogma of molecular biology showing the flow of information from DNA to DNA, DNA to RNA and RNA to protein. PDB ID: 3J09

2.1.3 The cell cycle

DNA replication occurs within the cell cycle, the process by which cells ensure viability during periods of proliferation. The cell cycle consists of 4 distinct phases (Figure 6). Significant morphological change is observed during S (synthesis) phase, when DNA replication takes place allowing each chromosome to give rise to a pair of sister chromatids, and M (mitosis) phase, in which all organelles are distributed to facilitate the creation of two viable daughter cells. During mitosis, the sister chromatids are separated and the cell divides into two. There are also two G (gap) phases, G1 and G2 (see Figure 6) in which cells grow and monitor both their extra-cellular and intra-cellular environment. During these G phases, checks on the fidelity of proliferation, known as checkpoints, operate to ensure that entry into a subsequent phase is unlikely to result in loss of genomic information in daughter cells. Checkpoints ensure that cell cycle progression may be delayed, to ensure that all previous essential processes such as resolution of environmental or replication-induced DNA damage, have been properly completed.[15]

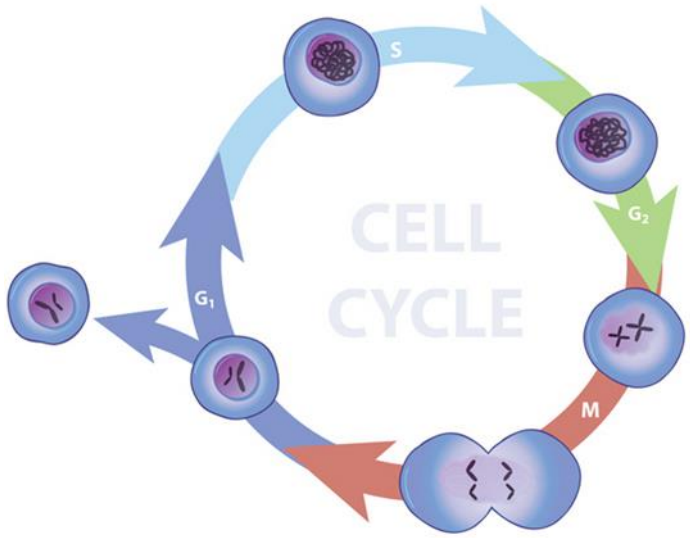

Figure 6: The stages of the cell cycle. Including S (synthesis) phase, M (mitosis) phase, and G1 and G2, the gap phases. Reproduced from Essentials of Biochemistry.[16]

2.1.4 DNA replication

The first necessary stage in DNA replication involves the unwinding of the DNA double helix, carried out by DNA helicases and single-stranded DNA-binding proteins, at specific DNA sequences termed replication origins.[17] Replicative DNA helicases move along the DNA helix separating the two strands, whilst single-stranded DNA-binding proteins bind to and stabilise each single DNA strand, to prevent reannealing and to protect the exposed single-stranded DNA. These assemblies prevent DNA from

forming hairpin structures which hinder DNA synthesis.[18] The separated strand structure formed is called a replication fork. Each strand then acts as a template for the synthesis of a new strand, and this is performed by DNA polymerases. As template-directed DNA replication only occurs in the 5' to 3' direction and the two strands in a DNA duplex run in opposite orientations, it follows that only one strand will be correctly orientated for continuous DNA synthesis. This newly synthesised strand is referred to as the leading strand. Because replicative DNA polymerases are unable to synthesise new DNA strands de novo and can only extend existing strands, a short RNA primer, synthesised by DNA Pol α primase, is first paired with the template strand, followed by a short section of DNA. DNA polymerase δ then uses this as a starting point for polymerisation of the leading strand.[19] In the other DNA strand – the lagging strand – DNA is synthesised in the 5' – 3' orientation in short segments called Okazaki fragments. Each fragment requires a new RNA primer and then, after the primers are removed, the fragments are "stitched together" by a DNA ligase.[19] Since both the leading and lagging strands are synthesised by the same replication machinery the lagging strand loops around in order to be replicated (Figure 7).

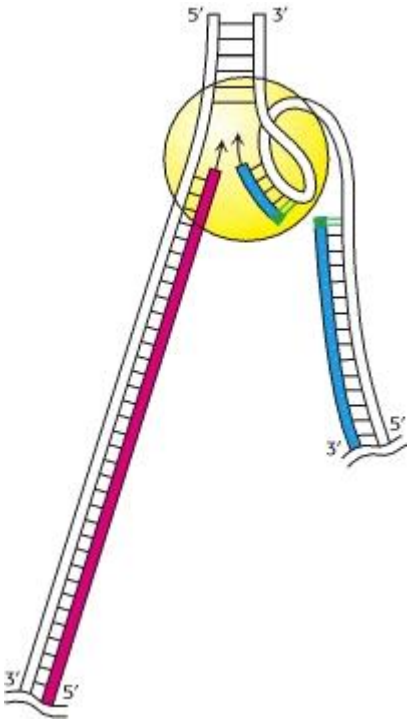

Figure 7: The simultaneous replication of the leading (pink) and lagging (blue) strands, showing how the lagging strand loops back on itself so it can be replicated in the 5' – 3' direction. Reproduced from Biochemistry.[20]

Replication stress occurs when the progress of replication forks is hindered so that replication is unable to occur. This is known as replication fork arrest, and occurs where replication forks encounter DNA or chromatin secondary structure, or DNA damage lesions. Under experimental conditions, replication stress can be induced in cell lines by treating with hydroxyurea (HU), which depletes pools of nucleotides,[21] resulting in almost complete blockage of total cellular replication. If the replication block is removed relatively quickly, the arrested replication forks are capable of restarting.[22] However,

prolonged exposure to replication stress results in replication fork stalling, and successful restart under these circumstances requires homologous recombination (HR), a form of DNA repair. Alternatively, DNA ahead of a stalled replication fork may be replicated by a fork traveling in the opposite direction. Chromosomal DNA contains many thousands of replication origins, and initiation of replication (termed "firing") does not occur at each simultaneously. Rather, large cohorts of origins fire at discrete and reproducible points within S phase, and this has the effect of minimising the risk that a chromosomal region will go unreplicated.[23] If a replication fork is not restarted, it may collapse, resulting in fork abandonment and generating 'chicken foot' structures. These structures can be processed by cellular DNA repair machinery, leading to double strand breaks (DSBs) in the DNA.[21]

2.1.5 Transcription

Transcription is the process by which messenger RNA (mRNA) is generated using DNA as a template. mRNA acts as an intermediate carrier of genetic information between genomic DNA and the protein synthetic machinery.[24] During transcription, the relevant region of chromosomal DNA is cleared of chromatin–associated protein, the DNA is unwound and RNA is synthesised using one of the separated DNA strands as a template.[25] As the RNA strand is synthesised, RNA polymerases catalyse the formation of phosphodiester bonds which link the ribonucleotides. The chain moves away from the DNA strand and the double strand of DNA reforms, and is reassembled into chromatin.[26] A large amount of RNA can be made quickly from one strand of DNA if required by the cell. Transcription generates long non-coding RNA, which may be involved in the regulation of gene expression, ribosomal RNA (rRNA), a component of the ribosome which together with ribosomal proteins is involved in the catalysis of protein synthesis,[27] and heteronuclear RNA (hnRNA) which in eukaryotes, undergoes splicing to remove introns to enable the generation of mature mRNA.

2.1.6 Translation

Translation is the process by which proteins are synthesised from mRNA. It is governed by the genetic code, which was delineated in the 1960s and determines how nucleotide sequences are interpreted to facilitate protein synthesis. As discussed above, a set of three nucleotides forms a codon and since there are four nucleotides, there are 64 different possible codons. Each codon represents either an amino acid in a polypeptide sequence, or a signal to stop translation. Since there are only 20 amino acids, individual amino acids are specified by one or more codons. For example, there are six codons which code for arginine, and the codons UAA, UAG and UGA all signal a stop in translation.[28] Therefore, sequences

of RNA are 'read' by the ribosome and codons are translated into amino acid sequences in the process of protein synthesis. Transfer RNA molecules (tRNAs) also play a major role in the translation process; linked via their 3' hydroxyl group to specific amino acids,[29] they act as adaptor molecules via anticodons, a set of three nucleotides complementary to those found in mRNA. As mRNA threads through the ribosome, each incoming tRNA-amino acid complex binds to the cognate codon in the mRNA, which is followed by the catalytic transfer of the pre-existing peptide chain to the incoming amino acid-tRNA complex. As proteins are synthesised from the N-terminus to the C-terminus, each amino acid in turn attacks the carbonyl group of the previous amino acid in the emerging peptide, displacing the tRNA that was linked to it, leading to an extended chain with a tRNA molecule bonded only to the last amino acid added.[30]

Once a protein has been synthesised it must fold into its final shape, known as its tertiary structure. This consists of sections of secondary structure, such as α helices and β sheets.[31] The folded form of a protein is its lowest energetic form, favoured due to the intramolecular interactions formed between atoms within the protein and the exclusion of water from hydrophobic sections.[32] Many proteins do not fold into their final conformations on their own and require additional proteins known as molecular chaperones which recognise any sections of incorrectly folded protein.[29]

Proteins (and sometimes RNA) are the final products of the information stored in DNA, and the information held in the sequence of proteins is not usually used to make other proteins, or RNA or DNA in living organisms.[14]

2.1.7 DNA repair

Several events, such as exposure to heat or radiation, and even spontaneous reactions, can lead to DNA damage. There are various types of DNA damage, some are due to modification of the bases. These include base oxidation and methylation. Bases can also be mismatched, i.e. not paired with the correct base. Bases can be cross-linked in various ways, and finally DNA can suffer DSBs, where both strands are broken.

Clearly DNA damage is undesirable as it can lead to proteins being incorrectly synthesised, and if this damage is passed to daughter cells it becomes permanent. Although DNA mutations lead to evolution in the long term, the vast majority do not have a positive effect and it is more desirable for the DNA to be repaired. Problems with DNA repair are associated with many diseases, including several types of cancer.[33] The two most common DNA repair pathways are called base excision repair and nucleotide excision repair, and both repair modified bases. In base excision repair, proteins called DNA glycosylases recognise damaged bases. The damaged base is then removed and an enzyme called AP

endonuclease cuts the backbone after which DNA polymerase adds a new nucleotide and the backbone is joined again.[34] Nucleotide excision repair removes bulky DNA adducts, after the damage is detected as a distortion in the double helix. One strand of the DNA is cut on either side of the damage and removed by a DNA helicase. The chain can then be re-synthesised and repaired.[35]

Both of these repair mechanisms rely on the fact that one strand of the double helix is undamaged and can be used as a template for the repair of the other strand. However, sometimes both strands are broken at the same time; this is known as a DSB. This event can be repaired by non-homologous end joining, where the two ends are joined back together, however this usually results in a mutation at the damage site, and ends which were not originally joined together can accidentally get 'repaired'.[36] Alternatively, the sister chromatid can be used as a template to guide the repair in a process known as HR, which usually occurs during and just after DNA synthesis.[37] When DNA damage is present and has not yet been repaired it can interfere with the cell cycle, delaying entry into S or M (mitosis) phase. DNA damage which cannot be repaired often leads to the initiation of apoptosis, a process which is induced by many anticancer drugs.[38]

2.1.8 Cell death

When cells are injured beyond repair, either physically or chemically, they die. In the case of unplanned cell death, known as necrosis, water enters cells and they swell and burst, causing inflammation.[39] However, cells can also die in a more controlled way. When it is beneficial to an organism for a cell to die, it will enter a process of programmed cell death, a common mechanism for this being apoptosis. During apoptosis the cell breaks up into smaller, membrane-enclosed apoptotic bodies which are phagocytosed (engulfed) by neighbouring cells.[39]

Proteases known as caspases play a vital role in apoptosis, and there are two subcategories – initiator and executioner caspases. Initiator caspases are present in an inactive form before apoptosis, and when a cell needs to undergo apoptosis they form dimers, activating and cleaving each other.[40] Executioner caspases directly induce events leading to cell death and are activated by initiator caspases. They then cleave other proteins within the cell including structural and signalling proteins as well as other caspases and other targets resulting in cell death.[40]

There are two key pathways to apoptosis, extrinsic and intrinsic. Extrinsic apoptosis is initiated from outside the cell. Cells have receptors on their surfaces and protein ligands from other cells can bind to them, sending a signal that the cell should initiate apoptosis.[41] For example, one death receptor found on the surface of cells is called Fas and is activated by a Fas ligand binding to it. Fas contains a death domain inside the cell which, when bound by a Fas ligand, binds adaptor proteins which in turn bind

initiator caspases, allowing the caspases to become activated, leading to apoptosis.[42] The intrinsic pathway to apoptosis is initiated by the cell itself in response to various stresses. This latter mechanism is also known as the mitochondrial pathway as it involves mitochondria releasing certain proteins, a process regulated by the Bcl-2 family of proteins, some of which encourage, and some of which depress, this release.[42] One such protein which is released from the mitochondria is cytochrome c, which once released binds to an adaptor protein. A group of adaptor proteins form a heptamer which activates initiator caspases, inducing apoptosis.[43]

2.2 Cancer

Cancer is a group of diseases characterised by abnormal and uncontrolled cell growth arising from genomic instability. As well as growing and dividing to form a tumour, malignant cancer cells (unlike those of a benign tumour) invade other tissues in a process known as metastasis. Cancer arises from a single cell which undergoes a series of mutations causing it to become cancerous.[44] These changes give the cell an evolutionary advantage over its neighbours within its micro-environment, and so its offspring will begin to take over, dominating the surrounding normal cells. Even within a tumour different cancer cells may then undergo distinct mutations.[45] As well as dividing more frequently than normal, terminally differentiated, cells, cancer cells do not die in conditions unsuited to normal cells. They often do not stop dividing when the Hayflick limit is reached, as discussed in section 2.2.3.4.[45] It is metastasis, the process whereby cancer cells migrate to new areas of the body and form tumours there, which is the most dangerous aspect of cancer, as it means that even if a single tumour is removed by radiation and/or surgery, undetectable residual cells may go on to cause other tumours in different areas of the body.

The variation in the genetic composition of tumours between patients with similar forms of cancer makes it difficult to pin down exact causes in specific cases. However it is known that so-called "founder" mutations must occur in proto-oncogenes (genes that promote proliferation) and/or tumour suppressor genes (genes that are anti-proliferative). Proto-oncogenes acquire gain-of-function mutations while tumour suppressor genes undergo loss-of-function mutations. In addition, mutations that affect a cell's DNA damage response, or that interfere with the apoptotic process, are common in many cancers.[45] For example, the tumour suppressor gene p53, which induces apoptosis, is mutated in over 50% of cancers.[44] Mutations leading to cancer can arise from exposure to certain chemicals, known as carcinogens, such as those found in tobacco smoke, or ionising and ultraviolet (UV) radiation. In some circumstances, mutations that confer predisposition to cancer may be inherited, such as in familial retinoblastoma or Li-Fraumeni Syndrome.[46] Most cancers show mutations in a combination of these areas.[47]

Cancer can be classed by the type of cell it originates in, with the most common form being carcinoma, a cancer originating in the epithelial cells that form the skin and line internal organs and body cavities. The majority of lung and ovarian cancers, the types that are the focus of this thesis, are carcinomas. The other forms of cancer are sarcoma, leukaemia, lymphoma, myeloma and central nervous system cancers.

2.2.1 Cancers with unmet needs

Although much progress has been made in recent years in the treatment of cancer, highlighted by the recent announcement that as many people now survive cancer as die from it,[48] the progress for some types of cancer has been a lot faster than for others, and some cancers, in particular those of the lungs, pancreas, oesophagus and brain, have particularly low survival rates and are known as cancers with unmet needs.[49] These cancers represent a particular challenge for the scientific community to develop new and effective treatments. There is also a need to improve the prevention and detection of these cancers in conjunction with improved treatment options.

2.2.1.1 Non-small cell lung cancer

The majority of lung cancers (80-85%)[50] are non-small cell lung cancer (NSCLC). This category is further split into three types based on the type of cells the cancer originated in: adenocarcinoma, squamous cell cancer and large cell carcinoma.

In England and Wales around 10% of people diagnosed with lung cancer will survive for 5 years; this varies with the type and stage of the cancer. Just 5% of sufferers will survive for 10 years. This compares to 50% 10 year survival across all cancers in 2010-2011, 78% for breast cancer, 84% for prostate cancer, and 57% for bowel cancer.[48] These facts illustrate the need to find more effective treatments for NSCLC and improve survival rates.

As with all cancers the severity of NSCLC can be defined by its stage.[51] Stage I is the least severe and means that the cancer is confined to the lungs. Stage II cancer is in the lung and has spread to nearby lymph nodes. Stage III cancer has spread to lymph nodes in the middle of the chest. Stage IV is the most severe form and is characterised by cancer that has spread to either both lungs, the fluid around the lungs or another part of the body.

The treatment for NSCLC depends on the stage of the cancer.[52] For stage I and II cancers the tumour will often be removed by surgery. Chemotherapy is also often given after surgery to kill any remaining cancer cells. This is known as adjuvant chemotherapy. For stage III disease a combination of chemotherapy and radiotherapy is often used if surgery is not possible. For stage IV NSCLC chemotherapy is usually the main treatment, and radiotherapy is also sometimes used for palliative treatment.

2.2.2 Causes of cancer

Cancer research UK lists the major causes of cancer as: smoking, obesity, sun and UV exposure, poor diet, lack of physical activity, alcohol, infection, air pollution and radon, changes in hormone levels, workplace exposures, genetic factors and age. It states that 4 out of 10 cancers could be prevented by changes in environmental and lifestyle factors.[53] However, the percentage of cancers that are thought to be avoidable has decreased over time. In 1964 the World Health Organisation (WHO) stated that '*the majority of human cancer is potentially preventable*'. In 1981 a review paper on the causes of cancer in the United States, published by Doll and Peto in the Journal of the National Cancer Institute, reported that some individuals had even estimated the percentage of preventable cancers as 80 or 90%.[54] However the WHO website now states that between 30-50% of cancer cases are preventable,[55] in line with Cancer Research UK's estimate.

As cancer is a result of DNA mutations, the causes of cancer are factors that can cause these mutations. Age is the largest single risk factor for cancer. The longer a person lives, the greater the chance of DNA mutations occurring by chance. It is also thought that changes in the microenvironment in tissues due to ageing may promote cancer.[56] Inherited faulty genes are also a risk factor which cannot be prevented by environmental or lifestyle changes.

The largest preventable risk factor for cancer is still smoking. In 2010 tobacco exposure caused 19.4% of all new cancer cases.[57] Smoking increases the risk of a number of cancers, in particular lung cancer. Compounds found in cigarette smoke, such as benzene, cause DNA damage, leading to cancerous mutations over time.[4]

The second largest cause of cancer in the UK is obesity. The risk of a large number of types of cancer is increased by obesity, including breast, kidney and bowel cancers.[58] The link between obesity and cancer is not as well understood as that between smoking and cancer, although it is thought to be due to the effects of excess fat on the body. Excess body fat causes an increase in growth factors such as insulin, which encourages cells to grow and proliferate. Inflammation is also caused which can promote cancer, and fat can also influence sex hormones which can cause cell proliferation in the breasts and womb of post-menopausal women. The distribution of body fat affects how great the cancer risk it causes is, and abdominal fat in particular is a risk factor. However, the reason for this is not yet understood.[58]

Exposure to UV light from the sun or sunbeds is another risk factor for cancer and is primarily associated with skin cancer.[59] This is because UV radiation can cause DNA damage which, like carcinogens in cigarette smoke, can lead to cancerous mutations.

Poor diet can cause cancer in a number of ways. If it leads to weight gain and obesity then cancer risk is increased due to the aforementioned reasons. In addition some specific foods, namely red and

processed meats, have been linked with increased risk of bowel cancer. One reason for processed meats increasing cancer risk may be because they contain nitrates which are converted in the body to N-nitroso compounds which are carcinogenic.[60] In addition, balanced diets, high in fruit, vegetables and fibre, decrease the risk of a number of cancers, and therefore diets lacking in these elements can be considered to be a risk factor for cancer.[61]

Similarly to a good diet, exercise is known to help prevent cancer. In women high levels of oestrogen can promote breast cancer, and exercise lowers oestrogen levels. Additionally, exercise reduces insulin levels. Exercise also helps to prevent bowel cancer which is thought to be due to quicker progress of food through the bowel reducing exposure to carcinogens, as well as decreasing inflammation in the bowel.[62]

Drinking alcohol is a risk factor for cancers of the head and neck as well as breast, bowel and liver cancers. Acetaldehyde is a breakdown product of alcohol in the body and is carcinogenic by damaging DNA and inhibiting repair. It has been found to cause increased growth of liver cells. Alcohol also increases oestrogen levels and can increase the production of reactive oxygen species (ROS), high levels of which can damage DNA.[63]

Some infections can increase cancer risk; the most well-known of these is the human papilloma virus (HPV) which causes cervical cancer among others. HPV infects epithelial cells and uses the cell's DNA replication machinery to replicate itself. In terminally differentiated cells this is achieved by the degradation of p53 and disruption of normal retinoblastoma protein (pRB) function. This causes aberrant growth and proliferation in infected cells, leading to cancer.[64]

Two further environmental cancer-causing factors are air pollution and radon gas. Carcinogenic compounds in air pollution can cause lung cancer[65], as can Radon gas.[66]

Finally, elevated hormone levels are linked to certain types of cancer, some of which are mentioned above. Hormone replacement therapy and the contraceptive pill can increase the risk of certain cancers in women, however the contraceptive pill has also been found to protect against other cancers.[67]

As stated above, smoking is by far the largest preventable risk factor for cancer. Smoking primarily causes lung cancer which currently has relatively low survival rates, meaning that smokers are at a high risk of dying from cancer. The number of people who smoke is decreasing following the wide publication of its health risks, which should lead to a decrease in the number of lung cancer cases, however currently, more effective treatments are urgently needed.

2.2.3 Hallmarks of cancer

In 2000 Hanahan and Weinberg published a landmark paper entitled "The Hallmarks of Cancer".[44] This set out to explain the current understanding of *"rules that govern the transformation of normal cells into malignant cancers"*. They outlined 6 *"acquired capabilities"* or hallmarks of cancer, and these are shown in Figure 8. These represent the ways in which cancer cells override their inbuilt anticancer defence mechanisms, and the authors suggest that these characteristics are common to most, if not all, human cancers.

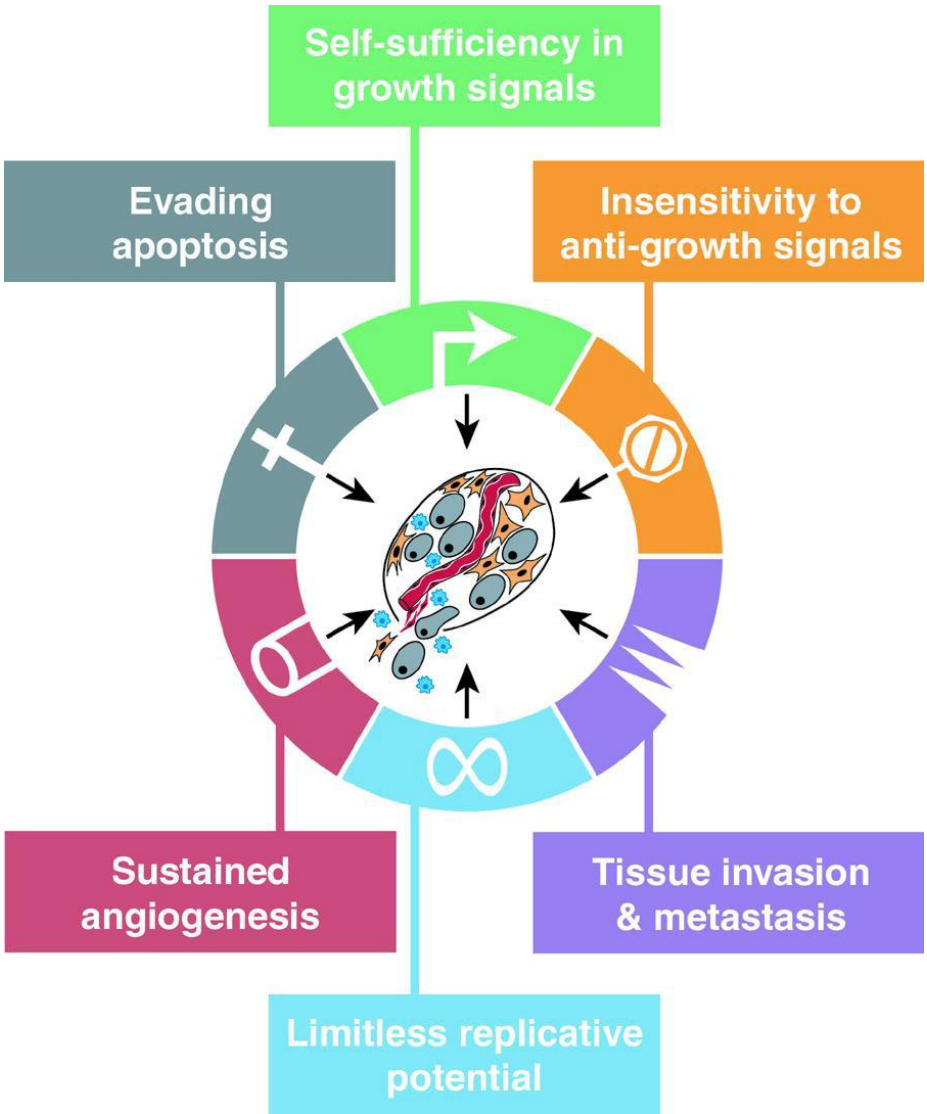

Figure 8: A diagram demonstrating the hallmarks of cancer, as of 2000. Reproduced from The Hallmarks of Cancer.[44]

In 2011 a second review was published entitled Hallmarks of Cancer: The Next Generation.[45] Here the original hallmarks were updated in line with research from the previous decade.

2.2.3.1 Hallmark 1: Self-Sufficiency in Growth Signals or Sustaining Proliferative Signalling

Healthy cells do not grow or divide unless they receive extracellular signals prompting them to do so. These signals operate through low molecular weight ligands, or growth factors, that bind to transmembrane receptors. However, cancer cells generate their own growth signals; these are usually oncogenes imitating normal growth signals.[44]

Some cancer cells are able to synthesise growth factors, which normally only come from extracellular sources. Growth factor receptors themselves may also be overexpressed, which can make cells more sensitive to normal levels of extracellular growth factors.[44] Highly overexpressed or modified growth factors can also cause ligand-independent signalling, leading to cell growth in the absence of growth factors. The type of extracellular receptors expressed by cells can also be altered in cancer cells, favouring those involved in growth signalling. Proteins involved downstream in growth signalling can also be altered. Ras proteins are an important example of this as they are often altered to allow them to release signals that promote mitosis when they normally would not.[68] Normal negative feedback mechanisms are also disrupted, allowing higher than usual levels of growth signalling,

In addition, signalling between different cell types in tumours is likely to contribute to growth signalling.[44]

Intuition would suggest that increased growth signalling would always lead to increased tumour growth, however this is not always the case. Research has shown that excessive overexpression of growth-related proteins such as Ras can lead to cell senescence or apoptosis. In cell cultures it has been shown that very high levels of Ras can lead to cells entering senescence, whereas cells with lower levels of Ras continue to proliferate. A similar effect has been observed in mouse models of cancer and even in human melanoma. It seems likely, therefore, that cancer cells balance their levels of growth signals to avoid triggering senescence or apoptosis, or else that they disable the mechanisms that promote senescence and apoptosis.[45]

2.2.3.2 Hallmark 2: Insensitivity to Antigrowth Signals or Evading Growth Suppressors

Like growth factors, signals that inhibit cell growth are sensed by extracellular receptors. These can cause cells to enter quiescence (cell cycle phase G0) or enter a permanent postmitotic state which is associated with differentiation. Cell cycle checkpoints play a large role in determining whether a cell continues through the cell cycle or enters one of the aforementioned states.[44]

pRB is an important part of the process for cells becoming quiescent, as, when hypophosphorylated, it normally inhibits proliferation by preventing transcription factors from inducing the transition from G1

to S phase. TGFβ is a factor that usually prevents proliferation by a number of mechanisms, including inhibiting the phosphorylation of pRB.[45]

These protective mechanisms are disrupted in cancer cells. This may be through the downregulation or alteration of TGFβ receptors or pRB may also gain a loss-of-function mutation.[45]. Further downstream signalling mechanisms may also be disrupted.

P53 is another important protein which inhibits cell growth by stopping cell cycle progression if cell stress sensors are activated; it can even trigger apoptosis under conditions of extreme stress. As previously stated, p53 is mutated in a large number of cancers.[45]

Contact inhibition is an effect whereby cells in culture stop proliferating when they contact other cells, and therefore form a monolayer. However cancer cells lose this capability, and indeed, in tumours, proteins related to this mechanism are often mutated.[45]

A second antigrowth mechanism, cells entering a terminally differentiated state, must also be avoided by cancer cells. This often occurs through overexpression of the c-Myc transcription factor which inhibits differentiation and instead promotes cell growth.[44]

2.2.3.3 Hallmark 3: Evading Apoptosis or Resisting Cell Death

All normal cells have the capability to die by apoptosis, either through receiving extracellular signals, or through the mitochondrial apoptosis mechanism. Cancer cells exist in stressed circumstances and should undergo apoptosis, however they are able to circumvent these mechanisms so they can continue to survive.

Mutation of the p53 tumour suppressor gene is observed in over 50% of human cancers.[44] This protein usually induces apoptosis in response to a range of cellular stresses, in particular DNA damage, and therefore cancer cells with p53 mutations can be unusually resistant to DNA damage.

Cancer cells can also activate antiapoptotic signalling pathways such as the PI3 kinase-AKT/PKB pathway. In addition they can become resistant to extracellular signals for apoptosis such as FAS by upregulating a decoy receptor.[44]

Apoptosis is not the only way a cell can die, and research into other mechanisms such as autophagy and necrosis is also ongoing. Autophagy can promote either cell survival or cell death. Autophagy signalling is inhibited in some cancers, leading to decreased cell death, however some cancer treatments induce autophagy which cells use to avoid death.[45] In necrotic cell death, debris enters the surrounding area and recruits immune inflammatory cells. These immune inflammatory cells can promote cancer through a variety of mechanisms. So while apoptosis protects against cancer, necrosis may overall promote it.[45]

2.2.3.4 Hallmark 4: Limitless Replicative Potential or Enabling Replicative Immortality

In addition to cancer cells overcoming their reliance on environmental growth signals to proliferate, they must also disable internal systems that limit their replicative potential. This system is governed by the length of telomeres, protective repeating sections of DNA at the end of chromosomes. As DNA replication can only occur in the 5' to 3' direction, the replication machinery is unable to fully replicate the 3' ends of the chromosomes during each cell cycle. For this reason telomeres are shortened by 50-100 base pairs (bp) during every cell division. Once telomeres reach a critical length they are no longer able to protect the chromosomes, and can potentially fuse together by non-homologous end joining. This inevitably leads to cell death.[44]

Telomerase is a specialised polymerase which adds new sections of DNA onto existing telomeres, lengthening them. This is upregulated in around 90% of cancer cells,[45] enabling them to prevent excessive shortening of the telomeres. Cells may enter senescence in response to increased growth signals as a protection mechanism, so cancer cells must also overcome this. Upregulated telomerase is correlated with the ability to circumvent senescence.[45]

More recent evidence has suggested that shortened telomeres may actually promote tumourigenesis by causing increased DNA mutations. However as more developed cancers display upregulated telomerase, this may appear at a later stage and stabilise the growing number of cancer cells. Telomerase has also recently been shown to have some cancer-promoting functions independent of telomeres.[45]

2.2.3.5 Hallmark 5: Sustained Angiogenesis or Inducing Angiogenesis

Angiogenesis is the growth of new blood vessels, and it is essential for any new tissue to survive by allowing cells to be provided with oxygen and nutrients from the bloodstream, and allowing them to remove waste products and carbon dioxide. Clearly this includes new tumours. Initially cancerous tumours lack the necessary blood vessels, however they are able to gain the ability to induce angiogenesis in order to grow larger. It appears that the ability to induce angiogenesis is 'switched on' in tumours at a certain stage of development.[45]

The induction of angiogenesis is based on the balance of signalling factors that either promote or inhibit angiogenesis. Tumours 'switch on' angiogenesis by changing the balance of these signals. For example, VEGF, which promotes angiogenesis, is often upregulated and thrombospondin-1, which inhibits it, is often downregulated. These transitions have a variety of causes, for example p53 causes the upregulation of thrombospondin-1, so loss of p53 function can cause a decrease in thrombospondin-1 levels.[45]

The blood vessels produced within tumours are less healthy than those in normal tissues. According to Hanahan and Weinberg they display *'precocious capillary sprouting, convoluted and excessive vessel branching, distorted and enlarged vessels, erratic blood flow, microhemorrhaging, leakiness, and abnormal levels of endothelial cell proliferation and apoptosis'*.[45] Different types of tumour also display different types of vasculature, with some containing sections that lack blood vessels and others containing large numbers.

As well as the endothelial cells that make up blood vessels, other types of cells are essential to support the vasculature in tumours. Pericytes are cells that, in normal tissue, are associated with the outer surface of endothelial tubes of blood vessels. These are also found in tumours and are essential for maintaining the tumour vasculature. Cells originating from bone marrow have also been found to play a role in tripping the angiogenic switch as well as protecting the vasculature.[45]

2.2.3.6 Hallmark 6: Tissue Invasion and Metastasis or Activating Invasion and Metastasis

Metastasis is the property of cancer that is most detrimental to human health; it is the cause of 90% of human cancer deaths.[69] This is the ability of tumours to invade surrounding tissue, and for cancer cells to then travel to other sites in the body and form tumours in these new locations. In the new locations nutrients are likely to be in plentiful supply, allowing metastases to grow rapidly.[44]

In order to invade new tissues and metastasise, cancer cells must disable systems that keep them tethered to neighbouring cells. Proteins from the immunoglobulin and calcium-dependent families regulate cell-cell adhesion, and these are affected in cancerous cells. In addition, proteins which adhere cells to the extracellular matrix, such as integrins, are also affected. For example, cancers often lose the function of E-cadherin, a protein which couples adjacent cells and consequently releases antigrowth signals. The specific forms of integrins expressed by cancer cells are also altered to enable the cells to adapt to the extracellular matrix in their new environments.[44]

Extracellular proteases are another class of proteins that are vital to cancer cells' ability to invade and metastasise. One of their functions is matrix degradation and they are upregulated whereas protease inhibitors are downregulated.[44]

In the years between the publication of the first and second Hallmarks of Cancer papers, research into invasion and metastasis revealed much more about the process, and the process known as the invasion-metastasis cascade was described. The first stage is invasion into local tissues, followed by cancer cells entering blood and lymphatic vessels, the transport of the cells through these vessels, their escape into other tissues, the growth of micrometastases (small collections of cancer cells), and finally growth into new tumours.[45]

The epithelial-mesenchymal transition (EMT) programme, which is usually used in embryonic development and wound healing, is hijacked by tumour cells to allow them to invade and metastasise. Additionally, multiple cell types are involved in allowing cancer cells to gain this capability. There is still debate as to the exact mechanism of metastasis in different cancers, and research into this area continues.[45]

2.2.3.7 Enabling Characteristics and Emerging Hallmarks

In addition to the original 6 hallmarks, the 2000 paper described the property of genome instability as an enabling characteristic of cancer.[44] It was remarked that in order for cancer cells to undergo all the mutations necessary to give them the hallmarks, they must have particularly unstable genomes. Loss of p53 function is involved in this, as it normally responds to DNA damage. Other proteins involved in the sensing and repair of DNA damage, and in the control of mitosis, are often lost in cancer cells, contributing to the genomic instability that allows normal cells to become cancerous. As mentioned above, it is also thought that shortened telomeres in cancerous cells increase the rate of mutations.[45]

A second enabling characteristic is tumour-promoting inflammation. Inflammation of varying degrees is common in tumours and they have been found to contain immune system cells. This inflammation has been found to promote tumour growth by a number of means, for example by introducing growth factors into the tumour microenvironment. Inflammation can often be detected very early on in tumour development, and it allows cancer cells to acquire hallmark capabilities, and therefore it is considered an enabling characteristic.[45]

The first emerging hallmark described in 2011 is reprogramming energy metabolism. Normal cells process glucose by glycolysis mainly under anaerobic conditions, however cancer cells have been observed to use glycolysis even in conditions where oxygen is present. Glycolysis is less efficient than the usual method of adenosine triphosphate (ATP) production, mitochondrial oxidative phosphorylation, and therefore cancer cells must upregulate glucose receptors and take up a large amount of glucose. Many tumours also have a hypoxic environment, and can continue to produce ATP in these conditions using glycolysis. However the reason for the use of glycolysis by cancer cells is under debate.[45]

The second emerging hallmark is evading immune destruction. The immune system would be expected to attack growing tumours, and yet tumours are able to grow despite this. Evidence suggests that the immune system does indeed suppress the formation of tumours in some circumstances, however there are clearly many instances in which it is not effective. Tumours have been found to evade the immune system by disabling immune cells, as well as through other mechanisms, and research is ongoing in this area.[45]

The two papers on the hallmarks of cancer set out the general characteristics of cancer cells. The 2011 paper also goes on to describe the characteristics of the tumour microenvironment and the different types of cells found in it.[45] 7 years on research continues, but these hallmarks serve as a useful overview of the properties of cancer.

2.3 Treatment of cancer

Current cancer treatments may involve surgery to physically remove tumours, radiation which kills cancer cells (which are less resilient to DNA damage than normal cells)[70] or drugs, which either inhibit signalling pathways controlling proliferation, or damage DNA. Although cancer cells can withstand DNA damage, chemotherapeutic drugs, like radiation, cause sufficient damage to selectively induce cancer cell death. Often cancer treatment involves using more than one of these approaches, for example removing a tumour surgically followed by chemotherapy to kill any remaining cancer cells. Current chemotherapeutic regimes remain problematic because of the limited selectivity of the drugs for cancer cells. Thus chemotherapeutics used tend to damage normal proliferating cells as well as cancer cells, leading to severe side effects.

2.3.1 Surgery

Surgery to remove cancerous tissue is the preferable treatment option for many types of cancer. In particular early-stage cancers which have not metastasised may be cured entirely by surgery. Usually the tumour will be removed, as well as a small amount of healthy tissue from the surrounding area to ensure that as far as possible all cancerous tissue has been removed. Nearby lymph nodes may also be removed in case they contain any cancer cells.

2.3.2 Radiotherapy

Radiotherapy involves the use of radiation to treat a tumour. The radiation is usually X-rays and causes DNA damage in cancer cells leading to cell death. It may be used prior to surgery to de-bulk a tumour, or following surgery to kill any remaining cancer cells.

There are immediate and long-term side effects associated with radiotherapy. Rather than affecting the whole body, like the side effects of chemotherapy, these side effects tend to affect the area that has been irradiated. Typical early side effects include skin redness and peeling, inflammation of the mouth and digestive tract, nausea and diarrhoea. Late side effects occur months or years after radiotherapy and include a range of effects dependent upon on the area treated.[71]

2.3.3 Chemotherapy

Chemotherapy is treatment for cancer using drugs. It aims to induce the death of cancer cells while preserving healthy cells. There is a large range of chemotherapy drugs and treatment can involve one or a combination of drugs. Like radiotherapy it may be used to de-bulk a tumour prior to surgery, or it may be used following surgery to kill remaining cancer cells. It may also be used to treat metastases. Some types of cancer are particularly sensitive to chemotherapy, and in these cases it may be used alone.

Chemotherapy drugs are often used in combinations. They are usually given intravenously, although in some cases they can also be taken orally. Treatment is given in cycles, typically of a few weeks. This allows healthy cells to repair themselves in the breaks between treatments, and maximises the chances of all cancer cells going through a division at the time of treatment.

Different chemotherapy drugs have different mechanisms of action, however they all target the process of cell division. This is one reason why chemotherapy tends to cause severe side effects. It causes damage to healthy cells that divide rapidly including hair, bone marrow, skin and the lining of the digestive tract.[72] As with radiotherapy there are also long-term side effects of chemotherapy. These include infertility,[73] fatigue,[74], second cancers[73] and mild cognitive impairment.[75]

2.3.4 Immunotherapy

Surgery, radiotherapy and chemotherapy are the mainstays of traditional cancer treatment. However, new research has produced new emerging types of treatment, one of which is immunotherapy. This involves harnessing the body's immune system to attack the cancer.

One category of immunotherapy is monoclonal antibodies.[76] These antibodies target proteins on the surface of cancer cells. Successful antigens must be expressed homogenously on the surface of cancer cells but must have low expression levels in healthy cells. Some monoclonal antibodies work by a process called antibody-dependent cell-mediated cytotoxicity. This makes cancer cells more obvious to immune system cells. Monoclonal antibodies can also block growth factor receptors on the surface of cancer cells, inhibiting their ability to grow and proliferate. Some monoclonal antibodies are conjugated to drugs or radioactive substances, allowing these to act in a more targeted way. Finally, monoclonal antibodies known as checkpoint inhibitors can block proteins which cancer cells overexpress, that prevent T cells from attacking the cancer cells.[76]

Another type of immunotherapy is treatment with synthetic cytokines. These are signalling proteins which are produced by immune cells and are important in the immune system.[77]

Some cancer vaccines are currently under development and in clinical trials. These do not prevent cancer like traditional vaccines, but recognise proteins expressed by cancer cells, allowing the immune system to attack them. There are various types of cancer vaccine under development.[78]

Adoptive cell transfer is a type of immunotherapy that is in its infancy but is currently undergoing clinical trials. One type involves a sample of the patient's T cells being taken and genetically engineered to recognise proteins on the surface of cancer cells.[79]

Overall, immunotherapy is a diverse field of cancer research, and is expected to become more advanced in the future, hopefully improving treatment for a wide range of cancer types.

2.3.5 Targeted therapy

Targeted therapy is a general term which refers to treatments which specifically target cancer cells, as opposed to chemotherapy which is indiscriminate and affects all cells. Monoclonal antibodies (see above) are classed as a type of targeted therapy.

There are several types of targeted therapy known as cancer growth inhibitors. These can block growth factors in a number of ways, decreasing the cancer cells' abilities to grow and divide. For example, antiangiogenics prevent blood vessels from growing within tumours. These are often VEGF inhibitors which prevent VEGF from binding to receptors and therefore preventing blood vessel growth.[80]

PARP inhibitors are another type of targeted therapy and are currently used to treat some ovarian cancers. PARP is a DNA repair protein. Cancers that have mutations in BRCA genes have defective DNA repair systems, and in these cases inhibition of PARP means they can no longer repair DNA damage, leading to cancer cell death. Olaparib is a PARP inhibitor which is currently used to treat ovarian cancer,[81] and it is also undergoing clinical trials to determine its effectiveness in treating other cancer types, including lung cancer.[82]

In the future, as the understanding of the underlying mechanisms of cancer improves, more targeted therapies should be developed. These should treat cancers more effectively and have fewer side effects. However, it will be necessary to determine whether each patient's individual cancer is likely to respond to a certain type of targeted therapy, and those who will not respond to any available targeted therapies will continue to rely on more traditional treatment options.

2.4 Metal-based chemotherapy

Since the discovery of the anti-cancer properties of the platinum complex cisplatin there has been an explosion in the study of metal complexes as potential drugs.

Drugs are traditionally organic molecules, however inorganic molecules have different properties which enable them to be utilised in ways which would be difficult to accomplish with purely organic molecules. When targeting a biological site, the shape of the molecule binding to it is very important, and the range of geometries of metal complexes allows their 3D shapes to be controlled relatively easily.[83] Metal complexes can also undergo redox reactions and ligands can easily be modified and be substituted to change biological targets.[83] Specifically with regards to anticancer drugs, cationic metal complexes complement the polyanionic nature of DNA, making them suitable candidates to target this biomolecule.

2.4.1 Platinum-based chemotherapy

Cisplatin (Figure 9) is one of the most widely-used anticancer drugs. As a molecule it has been known since 1845 when it was first synthesised and named Peyrone's chloride.[84] A square planar platinum complex with two chloride ligands and two ammonia ligands can form two geometric isomers. In the cis form the chloride ligands are adjacent to each other, whilst in the trans isomer they are opposite each other. As insinuated by its name, cisplatin is the cis isomer and the trans isomer is known as transplatin.

It wasn't until over a century after cisplatin's initial discovery that its biological effects were discovered. This discovery was completely accidental as metal complexes were not generally considered to be suitable drug candidates at the time.

2.4.1.1 Cisplatin: discovery and mechanism of action

In the 1960s Barnett Rosenberg was undertaking experiments investigating the effect of an electric or magnetic field on cell division, as he thought these fields might play a role in the process. He used an electric field in a chamber of the bacteria Escherichia coli in a setup that included platinum electrodes. When the field was turned on the bacteria elongated, becoming around 300 times longer than normal. This unusual effect was caused by platinum complexes in the growth chamber derived from the electrodes, which weren't as inert as previously thought. One of these complexes was found to be cisplatin.

Experiments in animal models of cancer followed, and cisplatin was found to cause tumour regression in mice. After this clinical trials began in 1971 and cisplatin was approved for use by the US Food and Drug Administration (FDA) in 1978. It made a huge impact in cancer treatment, particularly in the treatment of testicular and ovarian cancers. Its most dramatic impact was on the treatment of testicular cancer, leading to a cure rate of over 80%.[85] It is still used widely today to treat a range of cancers, typically in combination with other therapies.

Since cisplatin's biological effects were discovered researchers have been working to understand its mechanism of action. This mechanism is subject to debate,[86] however the currently best understood mechanism involves cisplatin's ability to covalently bind to cellular DNA, and is presented below.

Cisplatin is a neutral molecule and it remains in this form once intravenously injected, as the chloride concentration outside of cells is around 100 mM.[85] Inside cells the chloride concentration is much lower at around 2-10 mM.[85] This encourages the chloride ligands of cisplatin to exchange with water ligands. This leads to a positively charged, activated form of cisplatin. The negatively charged DNA backbone means that the cisplatin molecules are now attracted to DNA. The two most Lewis acidic sites on DNA are the N7 sites on the guanine and adenine bases. The water ligands on the activated cisplatin molecule are weakly bound and so they readily substitute for the guanine and adenine N7 nitrogens. This is considered a form of irreversible, covalent binding.

This process forms DNA adducts. Since cisplatin, as a cis isomer, has its two chloride ligands at a fixed 90 degree angle, it is able to form specific types of crosslinks, when one molecule binds to two sites. Although it can potentially form DNA-protein crosslinks and protein-protein crosslinks, the crosslinks that are believed to be primarily responsible for cisplatin's cytotoxicity are DNA-DNA crosslinks. These can be either interstand (binding once to each DNA strand) or intrastrand (binding twice to one strand). The most common crosslink observed is intrastrand, and it thought these are responsible for the therapeutic action of cisplatin as they cause a kink in the DNA double helix that is believed to disrupt various DNA processing mechanisms. Indeed a positive linear correlation has been reported between the amount of DNA binding and cytotoxicity.[87]

These crosslinks ultimately lead to the disruption of several cellular processes. DNA replication and RNA transcription are both inhibited, the cell cycle is affected, and apoptosis is induced.[88] The DNA distortion is found by DNA damage recognition proteins, such as those involved in the mismatch repair (MMR) complex.[88] This may inhibit DNA transcription. These DNA damage recognition proteins may lead to further DNA damage signalling which can be pro- or anti-apoptotic depending on the circumstance.

Cisplatin treatment leads to a transient S-phase cell cycle arrest, followed by a permanent G2/M phase arrest.[88] Cell cycle checkpoints are activated. Cell cycle arrest is one of several possible consequences

of DNA damage and it may be anti-apoptotic. It can induce nucleotide excision repair (NER) which can repair the damage caused by cisplatin and allow cells to survive.

P53 senses the DNA damage and can activate cell cycle arrest and DNA repair mechanisms, or induce apoptosis. ATM and ATR are activated and ATR in particular phosphorylates p53 at serine-15.[88] Chk1 and Chk2 are activated by ATR and ATM respectively. The mitogen-activated protein kinase (MAPK) cascade is activated, which involves phosphorylation of p53.

The amount of DNA damage must exceed a threshold where repair capabilities are overwhelmed to activate apoptosis.[88] When apoptosis is induced Bax translocates to the mitochondria and cytochrome c is released. Caspases are then activated.

It is clear that the mechanisms leading to apoptosis following cisplatin treatment are multifaceted and complex. Increased understanding of these can help alternative treatments to be developed and resistance to be overcome.

Recent studies - on cisplatin's effects away from DNA - have questioned the traditional view of cisplatin's mechanism of action. The majority (around 99%[89]) of cisplatin in a cell does not bind to DNA and its activity needs to be clarified. Cisplatin has been shown to have cytotoxicity towards enucleated cells,[90] so there are clearly proapoptotic mechanisms it induces that aren't linked to DNA damage. Some possible mechanisms by which cytoplasmic cisplatin can cause cell death have been identified, and these are outlined below.

Cisplatin can cause the accumulation of ROS and nitric oxide in the cytoplasm[85] which can directly lead to cell death by permeabilising the mitochondria. This occurs through the opening of the permeability transition pore, a multi-protein complex connecting the inner and outer membranes of the mitochondria, which opens to activate cell death.[91]

Further research into the signalling pathways leading to mitochondrial membrane permeabilisation induced by cisplatin has shown that the activation of the pro-apoptotic Bcl2 family protein Bax and possibly Bak, as well as voltage-dependent anion-channel 1 (VDAC1), which is a component of the permeability transistion pore complex, play a role. This may be downstream from the production of ROS.[92]

The activation of p53 is an important aspect of cisplatin's mechanism of action. P53 is stabilised in response to DNA damage allowing it to act as a transcription factor, inducing either cell cycle arrest or apoptosis. Cytosolic p53 can also induce apoptosis by localising to the mitochondria,[93] and both of these pathways are thought to play a role in cisplatin-induced apoptosis.[94] Interestingly, p53 transcriptional activity was found to be required for cisplatin to generate ROS in HCT116 human colorectal carcinoma cells. The ROS appear to lead to the activation of p38α, a kinase which has p53 as a target, leading to

apoptosis. It is believed that once activated, p38α regulates p53 levels, maintaining p53 activation. However this mechanism of action differs in different cell lines.[94]

Cisplatin has also been shown to cause an endoplasmic reticulum (ER) stress response.[85] In particular, this occurs in mouse kidney proximal tubule (TKPTS) cells, which is particularly relevant to off-target toxicity effects of cisplatin in the kidneys. However this mechanism could also be relevant to tumour cells. This pathway was shown to be dependent on cyclin-dependent kinase 2 (Cdk2) activity, a kinase which is usually associated with controlling cell cycle progression.[90, 95]

The fact that within each type of cancer there can be great variation in the responses of individual patients to cisplatin treatment is difficult to explain in terms of the DNA damage hypothesis. In addition, as previously stated testicular cancer is particularly responsive to cisplatin treatment, but studies thus far have been unable to relate the sensitivities of different testicular tumours to differences in cellular processing of Pt-DNA adducts, etc.[86] Testicular cancer's particular sensitivity has been linked to reduced DNA repair ability in testicular tumours, but it is likely that there are additional factors involved.[85]

A recent review of current research into mechanisms of cisplatin resistance[86] points out that in recent years the scientific community's understanding of cancer has become more nuanced. Issues such as cancer stem cells, the heterogeneity of cancers and the importance of considering the microenvironment of each cancer are highlighted and these should be taken into account in increasing our understanding of cisplatin's mechanism of action.

The review also points out the possibilities in combining indiscriminate cytotoxic agents such as cisplatin with newer targeted treatments to work in a synergistic manner.

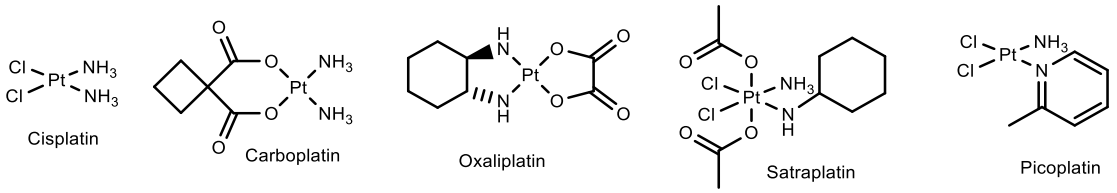

Figure 9: Platinum-based drugs. Cisplatin is the archetypal drug and the others have been developed to overcome issues with it such as toxicity and resistance.

2.4.1.2 Cisplatin: problems and alternative analogues

Overall cisplatin has revolutionised cancer treatment and has increased survival rates in many types of cancer, however soon after it was introduced issues became apparent. It has low solubility and can only be administered intravenously. However the biggest issue which was noticed quickly was its side effects. As it is not a targeted drug and acts in all cells in the body it has a number of off-target effects.

These are particularly noticeable in parts of the body with cells that are rapidly replicating. Cisplatin is toxic, especially to the kidneys (nephrotoxicity) and digestive tract.[84] It is also toxic to the ears (ototoxicity).[96]

A potential solution to this problem came from collaborative work between Johnson Matthey Plc and the Institute of Cancer Research. The cisplatin analogue carboplatin (Figure 9) was synthesised and was found to be less toxic. In particular it causes greatly reduced nephrotoxicity compared to cisplatin, as well as reduced toxicity towards the gastrointestinal tract and neurotoxicity.[84]

The rationale behind the structure of carboplatin is that platinum complexes with more labile ligands are more toxic.[97] In carboplatin, cisplatin's chloride ligands are replaced with the less labile bidentate 1,1-cyclobutanedicarboxylate ligand, leading to an aquation rate around three orders of magnitude slower than cisplatin.[98-99] DNA adduct formation is therefore slower for carboplatin and so it is administered at a higher concentration. The aquated form of carboplatin is the same as the aquated form of cisplatin and so, apart from their differing rates of aquation and reactivities, their mechanisms of action are the same.[97] Carboplatin was found to be as effective as cisplatin in the treatment of ovarian cancer, while being less toxic, and is therefore generally used preferentially in the treatment of ovarian cancer today.[84]

Another issue with cisplatin which was discovered later than its toxicity was the fact that some cancers are resistant to it. This can be intrinsic resistance, as in the cases of some colorectal, prostate, lung and breast cancers, or resistance acquired through cisplatin treatment, such as in the case of some ovarian cancers.

Numerous studies over the years have investigated the mechanisms behind cisplatin resistance. A number of different possible mechanisms have been discovered and more than one is usually found to take place in any given cisplatin-resistant cancer.[84]

Cisplatin-resistant cells are often found to have a lower intracellular platinum concentration following cisplatin treatment than non-resistant cells. This can be the result of both decreased influx and increased efflux.

Cisplatin influx probably takes place both by passive diffusion and active transport mechanisms. In particular the transporter copper transporter-1 (CTR1) has been implicated in the transport of cisplatin across cell membranes.[84] $Ctr1^{-/-}$ cells have been found to accumulate less cisplatin and to become more cisplatin-resistant upon treatment.[100] Various efflux-related proteins may also play a role in cisplatin resistance, although it is believed that decreased influx plays a larger role.[84]

Another mechanism implicated in cisplatin resistance is cisplatin binding to sulfur residues within cells. Platinum is a soft metal and sulfur is a soft ligand so the two bind with a higher affinity than platinum and the nitrogen atoms in DNA base pairs. Sulfur is found in the amino acids cysteine and methionine

and molecules rich in these such as glutathione are thought to bind to cisplatin molecules inside cells, effectively deactivating them. Evidence for this has come from cell studies and studies of samples from cancer patients. For example, a comparison between different ovarian cancer cell lines revealed the amount of glutathione they contained correlated to resistance to cisplatin.[101] This effect has also been shown for other sulfur-rich molecules, providing evidence that it is due to the binding of cisplatin to sulfur.[84] Interestingly, although this binding can cause resistance, it may also play a role in the cytotoxic effect of cisplatin by causing oxidative stress within cells.[85]

As well as the above mechanisms relating to preventing cisplatin reaching DNA, there are also resistance mechanisms that act after binding has occurred. One of these is through DNA repair mechanisms repairing the damage done by cisplatin. Cisplatin-resistant cell lines have been found to remove DNA crosslinks caused by cisplatin more effectively than cisplatin-sensitive lines.[102]

NER is a mechanism for removing cisplatin from DNA. The endonuclease ERCC1 (excision repair cross-complementing-1) cuts the DNA in this mechanism and is associated with cisplatin resistance. It is more abundant in some cisplatin-resistant cell lines[103] and cell lines without functional ERCC1 can have decreased resistance.[104]

The MMR DNA repair mechanism is also implicated in cisplatin resistance, but in contrast to NER, decreased MMR capability can increase cisplatin resistance.[105] It is thought that the reason for this is that normally MMR proteins recognise cisplatin adducts and attempt to repair them. When this fails apoptosis is triggered.[84]

DNA DSBs caused by cisplatin are generally repaired by HR. Two genes involved in this, breast cancer 1, early onset (BRCA1) and breast cancer 2, early onset (BRCA 2) are mutated in some cancers which makes them more sensitive to cisplatin. However, in cancers with mutations that restore BRCA1 and BRCA2 function, cisplatin resistance is increased.[85]

As well as repairing DNA damaged by cisplatin, cells can also adapt to tolerate cisplatin lesions on DNA. DNA polymerases β and η can perform translesion synthesis, bypassing cisplatin adducts.[106]

The disruption of apoptotic signalling pathways is a final mechanism of cisplatin resistance, and one that has come to be better understood in recent years. It can manifest in a range of ways, affecting the detection of DNA damage, the signals to induce apoptosis, and the execution of apoptosis.[85] For example, many p53 deficient cell lines are resistant to cisplatin.[94]

As a response to cisplatin- and carboplatin- resistant tumours, new platinum-based drugs were developed in an attempt to combat this resistance.[107] Oxaliplatin (Figure 9) is one such drug which is currently used to treat colorectal cancer.[84] The accumulation of oxaliplatin in cancer cells is less dependent on CTR1 than cisplatin and carboplatin at certain concentrations, showing that it must have another mechanism for entering cells.[100] In addition, oxaliplatin-DNA adducts are not recognised by

MMR proteins,[84] giving two possible reasons for the fact that oxaliplatin does not display cross-resistance with cisplatin for some cell lines.[84] It is also less toxic than cisplatin due to its oxalate ligands which, like in carboplatin, are less labile than chloride ligands.[97] Due to this decreased toxicity oxaliplatin is used to treat patients who cannot tolerate cisplatin.[107]

Some platinum-based drugs are currently in clinical trials. One of these is satraplatin, which is orally active, and another is picoplatin (both shown in Figure 9), which was specifically designed to overcome resistance. The methyl group on the pyridine ligand sterically protects the platinum centre from nucleophilic attack, meaning that sulfur-containing molecules cannot deactivate the drug.[97]

An aim for new metal-based cancer drugs is higher selectivity for cancer cells[108] and recently there has been work aimed towards delivering platinum-based drugs specifically to tumours based on a variety of methods.[109] This would hopefully decrease side effects caused by the drugs acting on other areas of the body. Nanoparticles are effective in this role due to the enhanced permeability and retention (EPR) effect,[109] whereby macromolecules and nanoparticles show an enhanced accumulation in solid tumours.[110] A major reason for this effect is that tumours have leaky vasculature compared to other tissues, due to improper formation of blood vessels, as well as decreased lymphatic drainage. Nanoparticles also spend longer in the bloodstream as they are too large to be excreted by the kidneys but too small to be detected by the reticuloendothelial system.[111] Carbon nanotubes are usually toxic and insoluble, but they can be functionalised to make them useful in biological applications. Cisplatin has been encapsulated inside such nanotubes, and can be more cytotoxic in this form than when free.[112] Attaching platinum-based drugs to functionalised gold nanoparticles[113] or nanorods[114] can also be effective in increasing the drug's cytotoxicity and its cellular uptake. Other inorganic nanoparticles can also be effective delivery systems.[109]

Drugs can be targeted to tumours by exploiting receptors that are overexpressed in cancer cells as nanoparticles can be functionalised with receptor-binding molecules.[109] Polymers are another delivery method, which has led to the development of ProLindac, a nanopolymer consisting of the active fragment of oxaliplatin bound to hydroxypropylmethacryl-amide,[109] which works through a combination of the EPR effect and the fact that, at low pH within tumours, the polymer will release the active complex.[97] ProLindac has shown promising anticancer activity in phase I and II trials, and is currently undergoing phase III trials treating head and neck cancer.[107]

As mentioned previously, DNA is a very common target for potential drugs in cancer research,[83] but as demonstrated in section 2.1.1.1.2, covalently binding to it is not the only way it can be targeted. Early studies of intercalating metal complexes involved square planar platinum (II) terpyridine (PtT) complexes. PtTS (Figure 10) was found to increase the viscosity of DNA and unwind the double helix, consistent with an intercalative mode of binding.[115] PtTC (Figure 10) was thought to also bind to DNA covalently due to its labile chloride ligand.[115] Crystal structures confirmed that PtT complexes are

capable of inserting between base pairs.[116-117] As was noted at the time, complexes with the terpyridine ligand bind well to DNA due to the large, planar aromatic nature of the ligand, similarly to the known intercalator ethidium (Figure 3).[115]

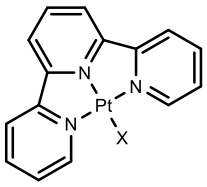

PtTC: X = Cl
PtTS: X = S-CH_2-CH_2-OH

Figure 10: The structure of platinum terpyridine intercalators investigated in the 1970s.

2.4.2 Ruthenium-based chemotherapy

After the initial discovery of cisplatin, the largely unexplored d-block was searched for other potential anticancer drugs. The anticancer properties of some ruthenium compounds were first discovered in the 1960s. In 1964 it was reported that a Ru (II) substituted phenanthroline (phen) complex inhibited tumour growth in mice.[118] Ruthenium's diverse coordination chemistry is well understood due to its uses in other applications[119] and its oxidation states (II) (III) and (IV) can all be stable under physiological conditions,[120] making it an attractive metal to use for potential anticancer drugs.

2.4.2.1 Ruthenium drugs with covalent binding properties

Covalent interaction with DNA can be an important part of cytotoxic activity. For example, a study of three ruthenium polypyridyl complexes with one, two or three labile chloride ligands showed that the complex with three chlorides was the most cytotoxic and formed the highest number of interstrand crosslinks with DNA.[121]

Since the toxicity of platinum drugs is an issue, ruthenium drugs represent an interesting alternative as they have been shown in some cases to be better tolerated.[122] To date, three ruthenium-based drugs, NAMI-A, KP1019 and IT-139, have entered clinical trials (Figure 11).

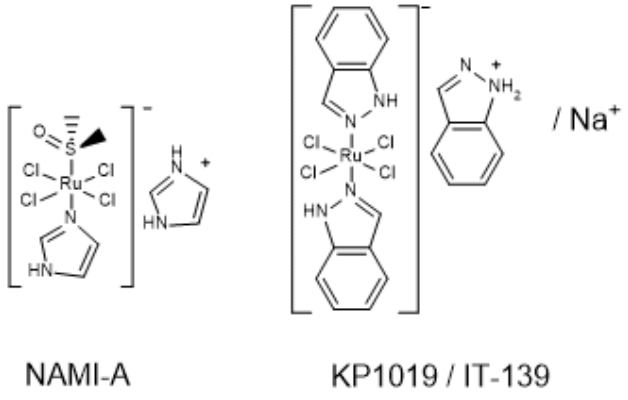

Figure 11: The ruthenium based drugs that have undergone clinical trials.

NAMI-A is an antimetastatic agent[123] which treats metastases without effectively treating the primary tumour. Its antimetastatic properties were discovered in mice in 1992.[124] A phase I trial published in 2004 showed that blister formation on the hands and feet is the dose-limiting toxicity.[125] It was observed that in this trial, as well as in another ruthenium complex trial, a patient with NSCLC achieved stable disease, leading to a hypothesis that ruthenium complexes may be effective treatments for this type of cancer in particular. In 2014 NAMI-A was studied in a phase I/II trial of patients with NSCLC in combination with gemcitabine, an antimetabolite which is currently used to treat bladder, pancreas, ovary, breast cancers and NSCLC. However, the trial concluded that this drug combination was only moderately tolerated with significant side effects, and was less effective than gemcitabine alone.[126]

KP1019 (Figure 11) is another ruthenium-based drug to have undergone clinical trials. It was studied in a phase I clinical trial in 2008.[127] In contrast to NAMI-A, KP1019 was well tolerated and caused few side effects. The dose-limiting factor was in fact not a side effect, but the volume required for infusion due to low solubility.[128] Due to this solubility issue the sodium salt analogue, IT-139, also known as NKP-1339, was taken forward into further clinical trials. IT-139 is more soluble than KP1019. IT-139 underwent a clinical trial in 2016 and was also found to be well tolerated. In this trial a maximum tolerated dose was determined. The anti-tumour activity was described as modest, and it was suggested that IT-139 could be studied in combination with other chemotherapeutics.[129]

Work in cellular models has shown that KP1019 is taken up rapidly into cells[130] and causes them to die by the intrinsic mitochondrial pathway to apoptosis.[127] There have been various hypotheses about its mechanism of action. It has been found to bind to transferrin and albumin, two transporter proteins found in the blood stream.[128] Transferrin is a protein that transports iron (III). Tumour cells overexpress transferrin receptors[127] as they require more iron than most cells due to their rapid division.[120] This means that theoretically the drug can specifically target tumour cells.[127] This phenomenon has been observed for other transferrin-binding drugs. Transferrin bound to iron enters cells by receptor-mediated endocytosis,[127] meaning that molecules bind to transmembrane receptor proteins which enter the cell inside acidic endosomes. It is thought that the acidic environment could then cause the drug to be

released into the cell.[128] Due to the EPR effect, KP1019 binding to albumin may also help it to accumulate in tumours.[127] Much of the research into KP1019/IT-139 has focussed on their transferrin binding properties, however they also have a high binding affinity with albumin, and this is found in much higher concentrations in the blood. In the KP1019 clinical trial patient blood samples showed ruthenium bound to albumin, but no detectable ruthenium bound to transferrin.[127] One hypothesis for how these two transport proteins may both play a role in the delivery of KP1019/IT-139 to tumour cells is that the drug bound to human serum albumin (HSA) may act as a reservoir that supplies the drug for transport into cells by transferrin.[128]

The ability of ruthenium drugs to act in this way is thought to contribute to their reduced toxicity in comparison to platinum drugs, as well as the possibility that they are converted to their active form only within the reducing tumour environment, known as 'activation by reduction'.[120] This is because Ru (III) complexes are relatively inert compared to Ru (II) complexes which consequently substitute their labile ligands faster. There is some evidence for the validity of this hypothesis in vitro, however it is not yet known whether it actually occurs in vivo.[128]

2.4.2.2 Ruthenium complexes with non-covalent binding properties

Ruthenium complexes that bind reversibly to DNA have also been extensively studied. This began with the investigation of the ligands 2,2'-bipyridine (bpy) and phen in octahedral complexes. $[Ru(phen)_3]^{2+}$ was investigated due to its kinetic inertness and well-known photophysical properties.[116] This complex was found to bind to DNA and it was initially thought that it bound via intercalation due to results consistent with other known intercalators, such as unwinding of the double helix.[116] These types of complexes had the added complication of having optical isomers that were found to bind differently to DNA. One of the three ligands will lie in the correct orientation to intercalate into the double helix. It was found that the right handed Δ isomer bound with greater affinity than the left handed Λ isomer, which was explained in terms of the positions of the two non-intercalating ligands with regards to the right-handed double helix, and was used as evidence for an intercalative binding mode (Figure 12).[116] As can be seen, in theory the two non-intercalating phen ligands in the Λ isomer clash with the DNA backbone, whereas those of the Δ isomer fit well into the helix.

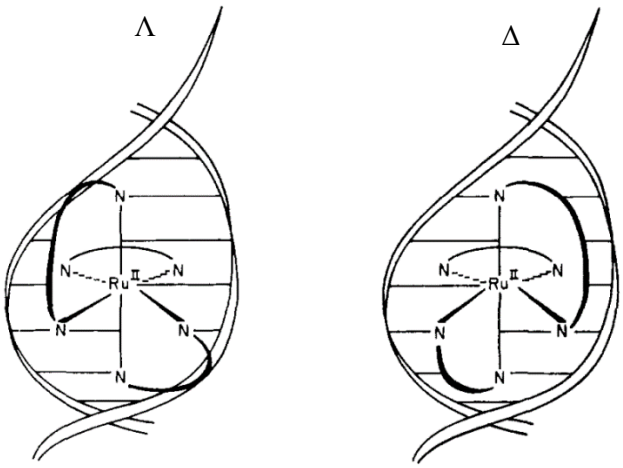

Figure 12: The proposed reason for the difference in binding affinities of Δ- and Λ-$[Ru(phen)_3]^{2+}$, showing the greater affinity of the Δ isomer with the DNA helix.[116]

However, Barton and co-workers went on to suggest that this molecule not only binds by intercalation from the major groove, but also surface binds.[131] Nuclear magnetic resonance (NMR) studies on tris-phen complexes with different metals found evidence of this binding mode, and that it occurs in the minor groove. However, they also found evidence of the intercalative mode of binding in the major groove, especially for the Δ isomer, and concluded that both isomers bind by more than one mode.[132-133]

The true binding mode was subject to further discussion in the literature until in 1992 a study by Chaires and co-workers found no evidence of multiple binding modes.[134] Binding studies comparing the complex to the known intercalators ethidium and daunomycin found that it had a smaller binding constant and the binding was essentially electrostatic in nature, rather than being due mainly to van der Waals interactions as required by classical intercalation. A viscosity study was also performed which found that the complex did not increase the relative specific viscosity of a DNA solution, behaving more similarly to the groove binding control Hoechst 33258 (H33258). It was suggested that the Λ isomer, which behaved most similarly to H33258, binds by groove-binding, whereas the Δ isomer decreased the relative specific viscosity of the DNA which, it was suggested, could be explained by a partial intercalation mode of binding where the phen ligand could not fully insert itself between base pairs. This could cause a kink in the double helix, explaining the decrease in relative specific viscosity.[134]

Further work showed that both isomers bind by different single binding modes.[135] It was concluded that neither isomer could bind via any classical mechanism such as groove binding or intercalation due to the 3D structures and steric interactions.

2.4.2.3 The DNA light switch effect

Polypyridyl ligands were extended with more aromatic rings to form the dipyrido[3,2-a:2',3'-c]phenazine (dppz) ligand (Figure 13). With a larger planar aromatic area, complexes with this ligand are usually unambiguous intercalators. Two well-known intercalators are $[Ru(bpy)_2(dppz)]^{2+}$ and $[Ru(phen)_2(dppz)]^{2+}$ (Figure 13). These complexes are particularly interesting because they demonstrate what is known as the DNA light-switch effect. A complex displaying this effect has luminescent properties, but these are quenched when it is dissolved in water. However when it intercalates into DNA it is again luminescent. $[Ru(bpy)_2(dppz)]^{2+}$ is luminescent in other solvents including ethanol and acetonitrile and demonstrates a MLCT (metal to ligand charge transfer). In this case, the charge transfer goes from the ruthenium atom to a singlet π* state on the dppz ligand, which undergoes intersystem crossing to a triplet excited state located on the phenazine nitrogen atoms. In the presence of water the luminescence is quenched because the solvent hydrogen bonds to the phenazine nitrogen atoms.[136] Intercalation into DNA prevents hydrogen bonding with water, which quenches the excited state.[137]

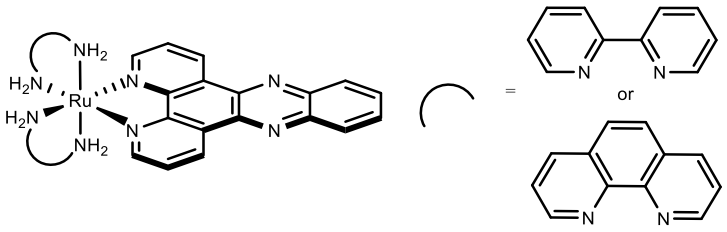

Figure 13: Complexes that display the DNA light switch effect, including the intercalating dppz ligand.

The wavelength maxima for these complexes were found to shift depending on the base composition of the DNA they are bound to and the emission intensity depends on the helical form of the DNA. Triple helical DNA gave the most intense luminescence, whereas A-form double stranded DNA (an alternative conformation which has a deep, narrow major groove and a shallow, wide minor groove compared to B-DNA[3]) gave the lowest intensity. These observations were attributed to how well these types of DNA allow the complex to intercalate and shield the phenazine nitrogen atoms from water. The deep, narrow major groove in A-DNA makes intercalation from this position more difficult.[138]

DNA light-switch complexes have been developed which selectively bind to specific types of DNA. For example the luminescence of $[Ru(bpy)_2(dpq\text{-}df)]^{2+}$ (where dpq-df =dipyrido (3,2-a:2′,3′-c) quinoxaline-difuran) is enhanced in the presence of G-quadruplex DNA compared to other forms of DNA[139]. $[Ru(phen)_2(dppz)]^{2+}$ can also be used to detect aptamer-protein binding. An aptamer is a nucleic acid sequence specifically designed to bind to a target molecule.[140] When the complex is in a solution containing an aptamer, its luminescence decreases when the protein that binds to the aptamer is added, due to the binding of fewer complexes to the DNA.[141]

Compounds that display the DNA light-switch effect can potentially act as imaging agents. Metal-based imaging agents for cells show potential as an alternative to traditional stains. In particular, d^6 octahedral polypyridyl complexes have some attractive properties for this application.[142] Their MLCT excitations are often in the visible region of the electromagnetic spectrum, whereas excitation in the UV region, which can damage DNA, is more common for traditional organic dyes. They also tend to have higher Stokes shifts (the difference in energy between absorption and emission maxima), reducing the problem of autofluorescence which increases background signal.[142] However, often a lack of uptake into cells has limited their applicability.[142]

A dinuclear ruthenium polypyridyl complex $[(Ru(phen)_2)_2(tpphz)]^{4+}$ (where tpphz is tetrapyridophenazine) has been found to image live cells by displaying the light switch effect when binding to DNA.[137] (Figure 14 a, b). Using higher resolution imaging this complex also specifically images DNA in live cells. Co-staining with the DNA-specific stain DAPI compared to co-staining with general nucleic acid stain SYTO-9 confirmed this. Changes in DNA between cells in different stages of the cell cycle could be observed as high magnification images showed individual chromosomes (Figure 14 c). This complex can also be delivered into cells through a polymersome (a polymeric vesicle) to specifically image mitochondria inside live cells (Figure 14 d).[143]

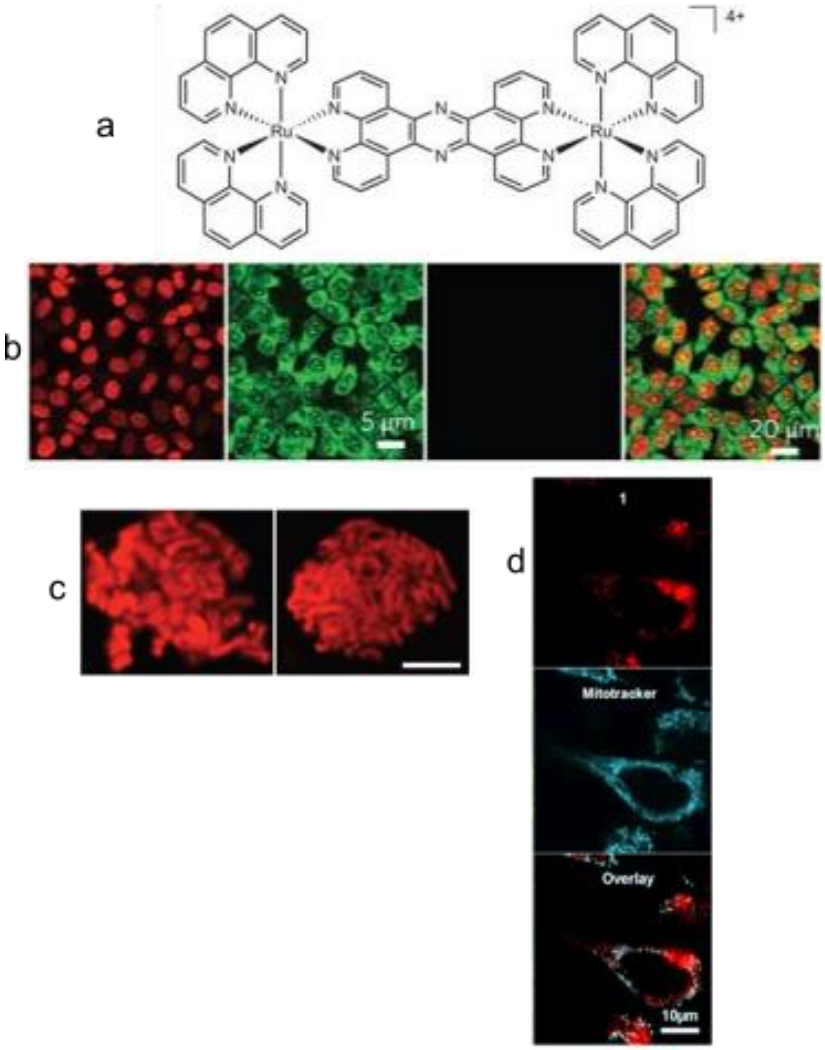

Figure 14: a) Dinuclear ruthenium complex $[(Ru(phen)_2)_2(tpphz)]^{4+}$, b) staining of live cells by the complex (shown above) (red) compared to the commonly used stain SYTO 9 (green) and a dead cell stain (purple),[142] c) chromosomes imaged by the compound d) cellular localisation of the compound encapsulated in a polymersome (red), compared with mitotracker red (cyan).[143]

2.5 Ruthenium (II) tris-(1-pyrazolyl)methane complexes

Many metal complexes have been investigated within the Thomas and Smythe groups with regards to their ability to bind to DNA and therefore act as, for example, imaging agents or potential drugs.[144-147] The structure of a class of ruthenium polypyridyl complexes that have been investigated as potential cytotoxic drugs, $[Ru(tpm)(N\text{^}N)X]^{n+}$, where tpm is tris-(1-pyrazolyl)methane, N^N is a polypyridyl ligand and X is a monodentate ligand, can be seen in Figure 15.

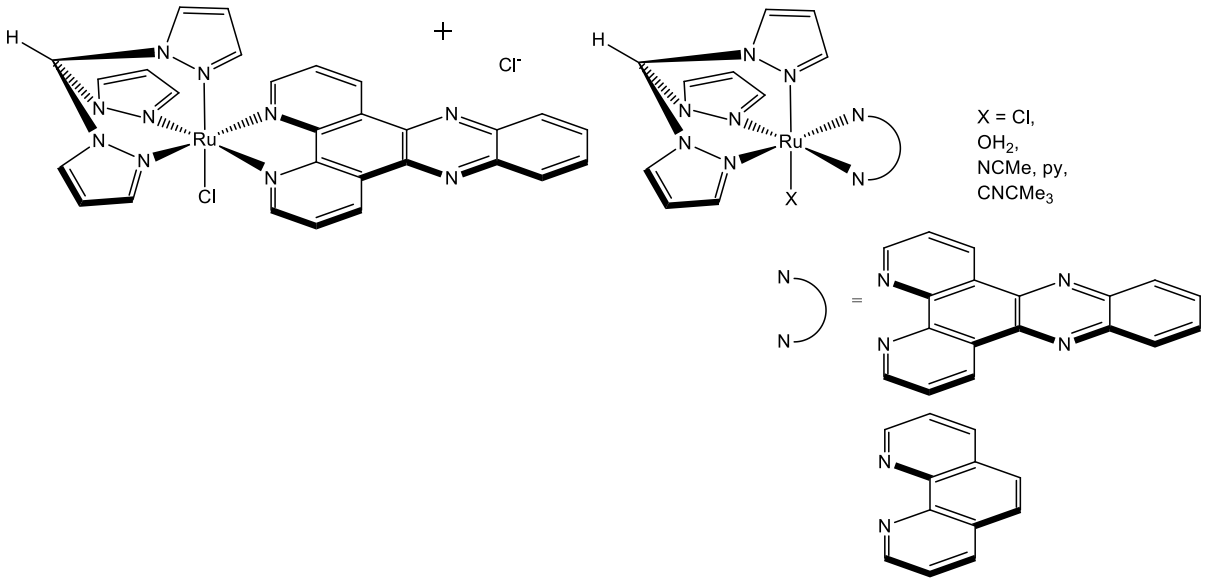

Figure 15: The general structure of the complexes $[Ru(tpm)(dppz)Cl]^+$ (DRuT), $[Ru(tpm)(phen)Cl]^+$ (PRuT), $[Ru(tpm)(dppz)(OH_2)]^+$ (DRuT-H_2O), $[Ru(tpm)(dppz)(NCMe)]^{2+}$, $[Ru(tpm)(dppz)(py)]^{2+}$ and $[Ru(tpm)(dppz)(CNCMe_3)]^{2+}$.

The tpm ligand is tri-dentate, capping one face of the octahedron. This is helpful as it circumvents the issue of enantiomers which are formed in octahedral complexes with three bidentate ligands, as discussed in the example of $[Ru(phen)_3]^{2+}$ in section 2.4.2. The tpm ligand is analogous to the ligand tris(1-pyrazolyl)borate, a well-studied molecule described as a scorpionate ligand due to its tridentate coordination mode being compared to a scorpion. Two binding sites hold the metal as if between a scorpion's pincers, with a pseudo-axial ligand binding from above, comparable to the scorpion's sting.[148]

A range of Ru (II) tpm complexes shown in Figure 16 were investigated with regards to their potential as anticancer drugs by measuring their cytotoxicities in two cancer cell lines, A2780 and A2780 CIS. These are both human ovarian carcinoma cell lines, with A2780 CIS cells being a cisplatin-resistant derivative of the parental A2780 line. Results are shown in Figure 16 and Table 1. IC_{50} values provide a way to compare the relative cytotoxicity of potential drugs, and in this context the IC_{50} is the concentration of a substance required to bring about a 50% reduction in viable cell numbers after a defined incubation period starting with a proliferating cell population. Numbers of viable cells were

determined indirectly using an MTT (3-(4,5-dimethylthiazol-2-yl)-2,5-diphenyltetrazolium bromide) assay which measures total metabolic activity in the cell population (for further details see chapter 5: mechanistic studies in a human non-small cell lung cancer model). IC_{50} values depend on the conditions of the particular experiment and so they are not generally comparable between experiments. For this reason a comparative control is required, and in this experiment cisplatin was used.

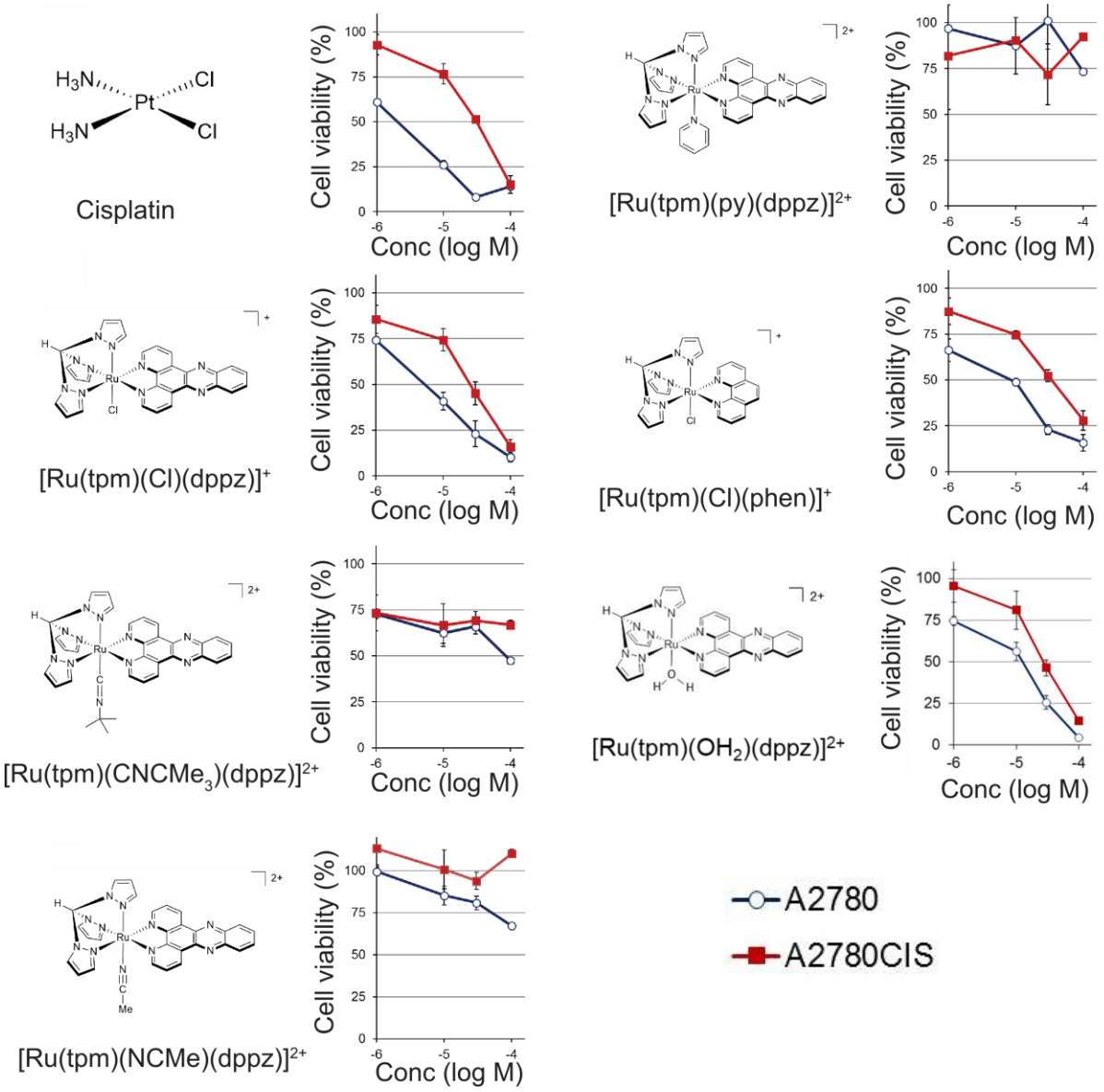

Figure 16: Comparisons of cytotoxicities of several Ru (II) tpm complexes in A2780 and A2780 CIS cell lines, as well as a comparison to cisplatin. The graphs show compound concentration (log M) (x axis) against cell metabolic activity (%) (y axis). It can be seen that DRuT, DRuT-H_2O and PRuT show significant cytotoxicities, in contrast to the other three Ru (II) tpm complexes.

Table 1: IC_{50} values over 48 hours for various Ru (II) tpm complexes and cisplatin in A2780 and A2780 CIS cell lines, as well as resistance factors.

Compound	**IC_{50} (μM)**		
	A2780	**A2780 CIS**	**Resistance Factor**
Cisplatin	2 ± 1	33 ± 5	16.5
DRuT	7 ± 5	19 ± 2	2.7
PRuT	13 ± 4	38 ± 1	2.9
DRuT-H_2O	14 ± 5	30 ± 7	2.1
$[Ru(tpm)(dppz)(NCMe)]^{2+}$	> 100	>100	N/A
$[Ru(tpm)(dppz)(py)]^{2+}$	>100	>100	N/A
$[Ru(tpm)(dppz)(CNCMe_3)]^{2+}$	>100	>100	N/A

Figure 16 and Table 1 confirm that the A2780 cell line is more sensitive to cisplatin than A2780 CIS. The IC_{50} values obtained for cisplatin in both cell lines are similar to those found in the literature,[149] confirming that the results of this experiment are reliable. Three of the ruthenium complexes tested showed promising results (DRuT ($[Ru(tpm)(dppz)Cl]^+$), PRuT ($[Ru(tpm)(phen)Cl]^+$) and DRuT-H_2O ($[Ru(tpm)(dppz)(OH_2)]^+$)). For these complexes the percentage of viable cells can be seen to steadily decrease with increasing complex concentration for both cell lines, and in each case there is a smaller difference in sensitivity between A2780 and A2780 CIS cells than for cisplatin. This indicates that A2780 CIS cells are less resistant to these complexes than to cisplatin. The lowest IC_{50} values over 48 hours were found for DRuT (7 μM for A2780 and 19 μM for A2780 CIS). This complex has a lower IC_{50} value for A2780 CIS cells than cisplatin and a relatively small difference between the two cell lines, suggesting a possible lack of cross resistance. DRuT-H_2O, analogous to DRuT but with a water ligand in place of the chloride, has higher IC_{50} values than DRuT for both cell lines, but again is more cytotoxic than cisplatin towards A2780 CIS cells. PRuT, which has the non-intercalating phen ligand rather than the intercalating dppz ligand, also shows significant cytotoxicity towards both cell lines, although its IC_{50}s are higher than for DRuT and DRuT-H_2O in both cell lines, and higher than cisplatin even for the A2780 CIS cell line. It has a larger difference between its IC_{50} values for the two cell lines than DRuT or DRuT-H_2O, suggesting more cross resistance with cisplatin.

In contrast to these three complexes, some complexes tested did not show significant cytotoxicity in either cell line. Three examples are included in Table 1 and Figure 16, $[Ru(tpm)(NCMe)(dppz)]^{2+}$, $[Ru(tpm)(py)(dppz)]^{2+}$ (where py = pyridine) and $[Ru(tpm)(CNCMe_3)(dppz)]^{2+}$. All of these complexes have IC_{50} values of > 100 μM for both cell lines. A common feature shared between these complexes not present in the three cytotoxic complexes is the presence of a non-labile monodentate ligand where the other complexes have labile chloride and water ligands. This strongly suggests that having a labile ligand in this position of the complex is important for cytotoxicity. This is mirrored by other studies

into ruthenium polypyridyl complexes that found a larger number of labile ligands led to increased cytotoxicity[121] (see section 2.4.2). Based on the known mechanism of action of cisplatin, it was hypothesised that these labile ligands are replaced by water ligands in aqueous solution, then allowing the complexes to bind covalently to DNA. This suggests an importance of covalent DNA binding to the cytotoxicity of DRuT, DRuT-H_2O and PRuT. This would also mean that once aquated, DRuT and DRuT-H_2O are identical. For this reason, DRuT and DRuT-H_2O were used interchangeably in some experiments.

Of the three cytotoxic complexes, DRuT and DRuT-H_2O have an intercalating ligand whereas PRuT does not. Since PRuT is the least cytotoxic this suggests that both a labile ligand and an intercalating ligand could contribute to cytotoxicity. This implies that a combination of covalent and non-covalent DNA binding modes could optimise cytotoxicity in this class of complexes.

To determine how the structures of the complexes relate to their biological activities they were compared to each other and cisplatin in a range of experiments. It was shown by increases in the relative specific viscosity of a DNA solution that DRuT-H_2O intercalates into DNA, whereas PRuT does not (Figure 17). Other complexes analogous to DRuT with various ligands in position X (Figure 15) have also been found to bind to DNA by intercalation, but certain ligands in this position, such as 4-aminopyridine, can inhibit intercalation.[150]

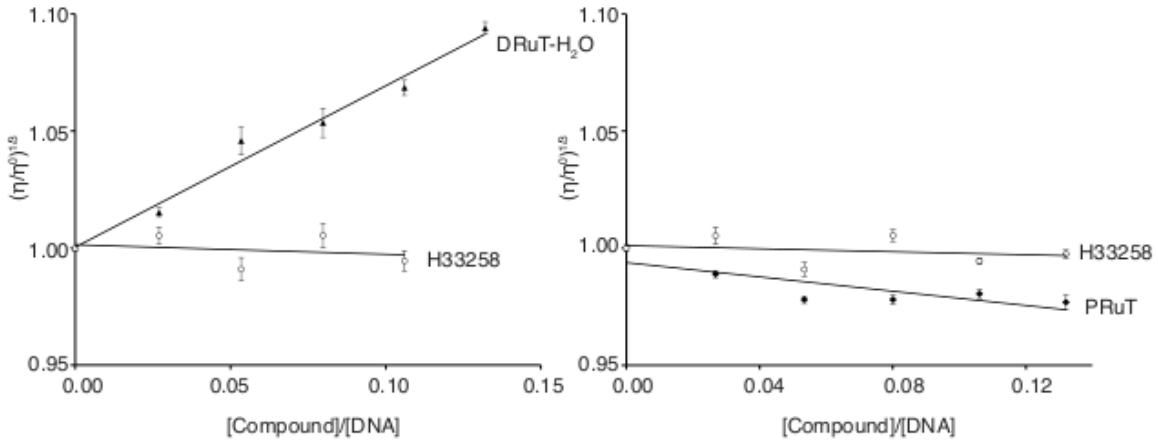

Figure 17: Graphs showing the change in relative specific viscosity when DRuT-H_2O and PRuT are titrated into a solution of DNA, compared with a groove binding control H33258. As expected, DRuT-H_2O increases the relative specific viscosity of the solution, indicating that it intercalates, whereas PRuT does not.

It was shown that DRuT causes cells to undergo apoptosis as it causes characteristic fragmentation of nuclei and the production of cleaved caspase-3, a caspase that is activated during apoptosis (Figure 18).[151]

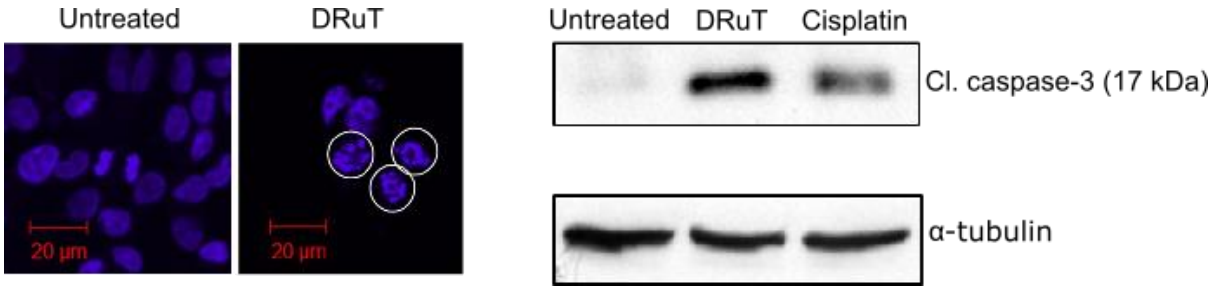

Figure 18: A microscopy image showing A2780 CIS cells treated with DRuT or untreated, and stained with DAPI. DRuT-treated cells have fragmented nuclei, a feature of apoptosis. A western blot showing that DRuT and cisplatin treatment cause the cleavage of caspase-3, another feature of apoptosis.

Clearly both DRuT and PRuT cause cell death, however their structural differences and different cytotoxicities mean they may be acting through different mechanisms. In order to investigate this, experiments were performed to determine which pathways to cell death each complex activates.

Flow cytometry was used to investigate the effect of DRuT on the cell cycle and DNA replication (Figure 19). Cell cycle analysis showed that treatment with DRuT increases the proportion of cells in S phase, suggesting that they are accumulating in this phase and are unable to progress further through the cell cycle. A bromodeoxyuridine (BrdU) incorporation assay (see chapter 4: mechanistic studies in a human ovarian carcinoma model for more details) showed that DRuT severely inhibits synthesis of DNA. This could be a reason for its cytotoxic effect – when cells are unable to replicate their DNA they may undergo apoptosis.

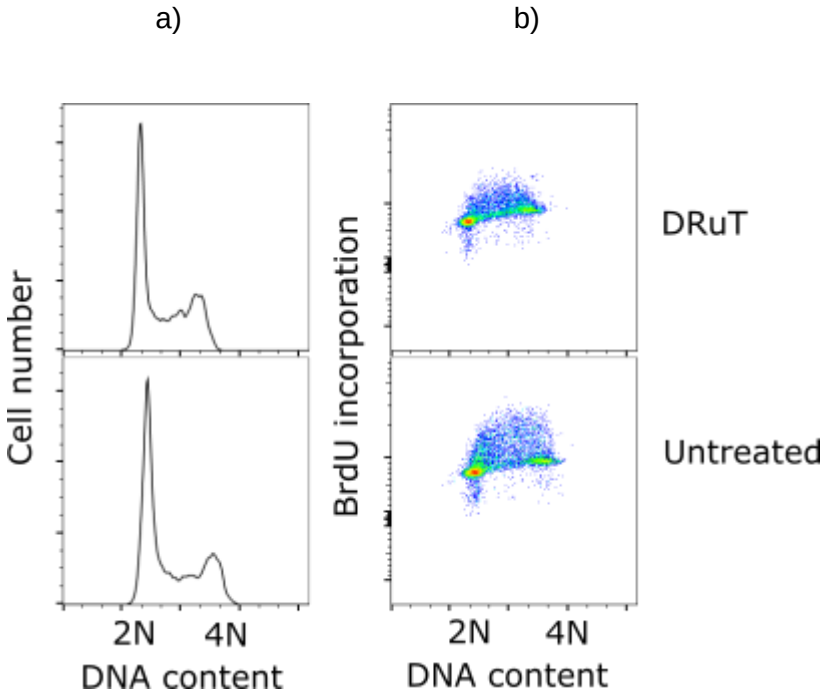

Figure 19: Graphs showing the results of flow cytometry experiments a) PI staining of A2780 CIS cells against cell number indicating that treatment with DRuT increases the proportion of cells in S phase, b) PI staining against BrDu incorporation

(measured as FITC intensity) with cell count represented as colour contours, revealing rates of DNA replication, indicating that treatment with DRuT inhibits replication. Cells were treated with 20 μM DRuT for 18 hours.

The levels of several proteins were probed after treatment with DRuT, DRuT-H_2O and PRuT by western blotting (Figure 20). Particularly interesting were the results for phosphorylated Chk1 and Chk2, two checkpoint kinases involved in the cell cycle. Chk1 has various functions relating to regulation of the cell cycle, and is activated in response to replication stress.[152] Activation requires that it be phosphorylated on serines 317 and 345 by ATR (ATM- and Rad3- related protein kinase).[153]

It was shown that treatment of A2780 CIS cells with DRuT, DRuT-H_2O and PRuT causes the phosphorylation of Chk1 on serine 345. Cisplatin was also found to activate Chk1. The activation of Chk1 by DRuT is consistent with the results from the flow cytometry assay which show the disruption of replication.

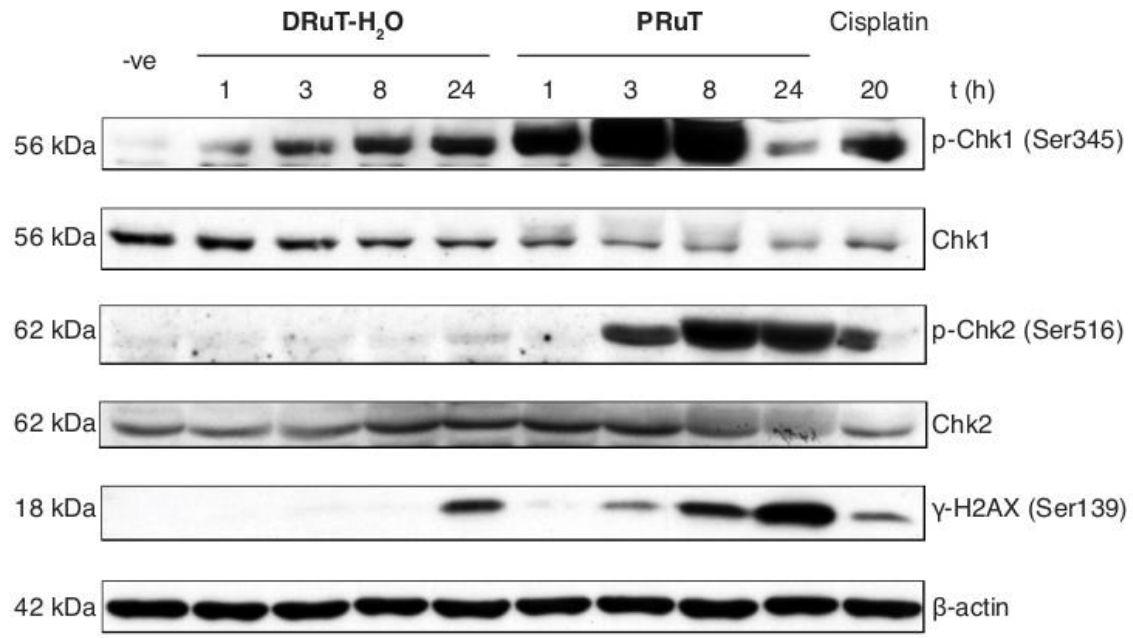
DRuT-H2O
PRuT
Cisplatin
-ve
1
3
8
24
1
3
8
24
20
t (h)
56 kDa
p-Chk1 (Ser345)
56 kDa
Chk1
62 kDa
p-Chk2 (Ser516)
62 kDa
Chk2
18 kDa
γ-H2AX (Ser139)
42 kDa
β-actin

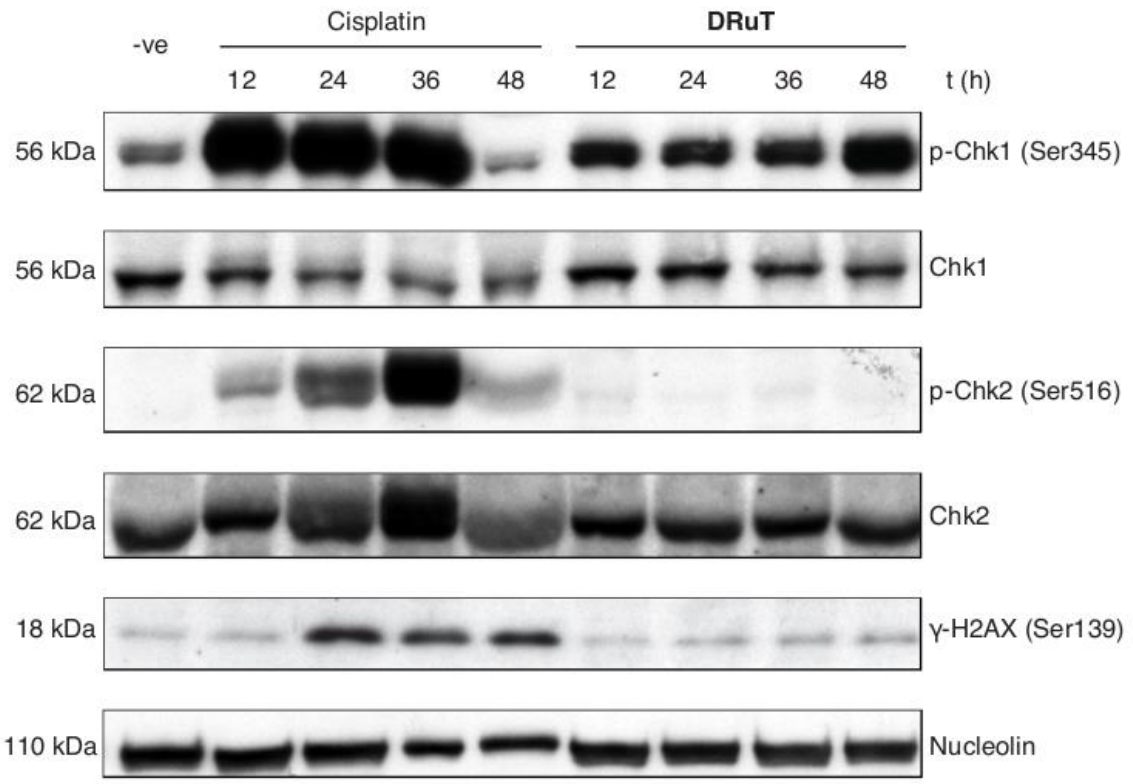
Cisplatin
DRuT
-ve
12
24
36
48
12
24
36
48
t (h)
56 kDa
p-Chk1 (Ser345)
56 kDa
Chk1
62 kDa
p-Chk2 (Ser516)
62 kDa
Chk2
18 kDa
γ-H2AX (Ser139)
110 kDa
Nucleolin

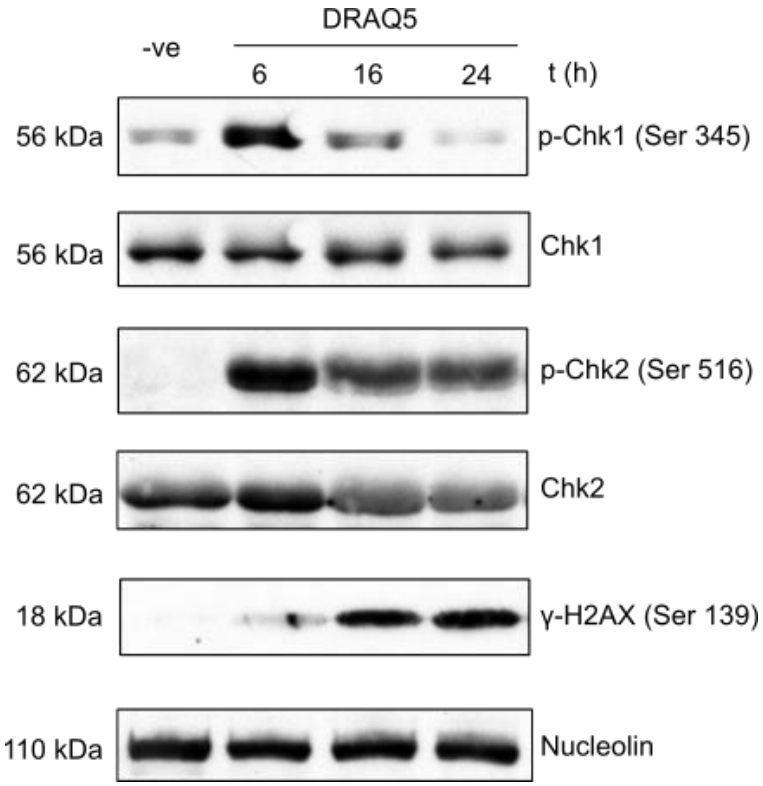

Figure 20: Western blots showing the effect on the levels of various proteins in cells treated with various concentrations of DRuT, DRuT-H_2O, PRuT, and cisplatin and DRAQ5 as comparisons. α-tubulin, nucleolin and β-actin are used as loading controls. Phosphorylated Chk 1 is an indication of DNA damage in each case, and phosphorylated Chk2 and γ-H2AX indicate DSB formation in cells treated with PRuT, cisplatin and DRAQ5.

To compare the cellular response produced by the ruthenium complexes to traditional chemotherapeutic agents such as cisplatin, the activation of Chk2 was investigated. Chk2 is activated in response to DNA DSBs such as those caused by cisplatin, and can lead to apoptosis.[154] The activation of γ-H2AX, a histone which is phosphorylated in response to DNA DSBs,[155] was also investigated. As expected, cisplatin treatment caused activation of both Chk2 and γ-H2AX, but neither was activated by DRuT or DRuT-H_2O, suggesting that these complexes do not cause DSBs in DNA and activate apoptosis by a different mechanism to cisplatin. Some phosphorylation of γ-H2AX was observed after 24 hours of treatment with DRuT-H_2O, however this is likely due to DSBs in DNA caused directly by apoptosis, rather than leading to it.

In contrast, PRuT treatment caused a very different response in A2780 CIS cells, causing phosphorylation of Chk2 and γ-H2AX in addition to Chk1. This is similar to the effect of cisplatin, suggesting that PRuT too causes DSBs in DNA leading to apoptosis. Another control used was the organic intercalating dye DRAQ5. Although this isn't directly comparable to the ruthenium complexes it is an interesting comparison to see if the same effect on cells as DRuT and DRuT-H_2O can be induced by a molecule that only intercalates. DRAQ5 was found to activate Chk1, Chk2 and γ-H2AX, indicating that it causes DNA DSBs, and that the combination in DRuT and DRuT-H_2O of an intercalating ligand and a labile ligand may be essential for the activation of the specific pathway to apoptosis they induce, by interfering with DNA replication.

The cytotoxicity that DRuT and DRuT-H_2O share, particularly DRuT in a cisplatin resistant cell line, while not inducing Chk2 phosphorylation, may prove to be important. This is due to the fact that Chk2 activation is associated with the side effects caused by cisplatin in healthy cells.[154] As the two major issues with cisplatin treatment are its side effects and resistance, the fact that DRuT shows potential to combat both of these clearly warrants further investigation.

A useful comparison comes from a complex reported, $[Ru(terphenyl)(en)Cl]^+$, (Figure 21) which shares some features with DRuT, i.e. it is a Ru (II) complex with an intercalating ligand and a labile Cl ligand. This complex has been shown to initiate a different pathway to apoptosis, shown by activation of p21 and p53 DNA damage pathways,[156] indicating that the cellular response to DRuT will not be shared by all other similar complexes.

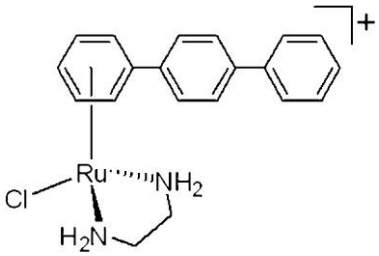

Figure 21: The structure of $[Ru(terphenyl)(en)Cl]^+$. [156]

2.6 Aims

The primary aim of this research project is to identify a ruthenium complex that could be an effective treatment for NSCLC, with the aim to eventually taking this compound forward into animal studies.

To achieve this goal, the primary compounds which will be studied are DRuT and PRuT. The studies already outlined on these two compounds regarding DNA binding and action in human ovarian carcinoma cell lines will be built upon. Once the mechanisms of action of DRuT and PRuT are adequately understood in A2780 and A2780 CIS cells, the NSCLC cell line A549 will be used to determine whether either DRuT or PRuT could be an effective treatment for this cancer. The compounds' toxicities will be established, and if either compound is toxic then its mechanism of action will be explored in A549 cells to determine whether it is the same or different to that in A2780 and A2780 CIS cells.

The first results chapter will discuss the DNA binding properties of DRuT and PRuT in A2780 CIS cells. It is already known that DRuT-H_2O is an intercalator, but whether PRuT binds reversibly to DNA is unknown. It is also unknown whether DRuT or PRuT bind covalently to DNA, and if so whether one does with a higher affinity than the other.

The second results chapter will aim to determine in more detail the mechanisms of action of DRuT and PRuT in A2780 CIS cells. Specifically, effects caused by DNA binding, such as replication inhibition, will be explored, as will potential damage to mitochondria.

The third results chapter will be used to determine whether DRuT or PRuT could be an effective treatment for NSCLC. The toxicities of DRuT and PRuT will be measured in A549 cells, and then their mechanisms of action will be determined. Again, this will focus on effects caused by DNA binding and effects on the mitochondria.

Together, the results will be used to make a judgement as to whether DRuT or PRuT should go forward as a drug candidate for NSCLC in animal studies.

3. Synthesis and Binding Studies

3.1 Aims

Before conducting DNA binding studies, the complexes DRuT and PRuT, which had been previously found to have interesting cytotoxic properties, had to be synthesised. As controls for subsequent experiments, two other ruthenium complexes, $[Ru(bpy)_3]^{2+}$ and $[Ru(bpy)_2(dppz)]^{2+}$, were selected for synthesis. These were chosen on the basis of their known DNA binding properties; $[Ru(bpy)_2(dppz)]^{2+}$ is an extensively studied intercalator and $[Ru(bpy)_3]^{2+}$ only binds weakly via electrostatic interactions. The next logical complex in the series of DRuT and PRuT is $[Ru(tpm)(dppn)Cl]^+$, as each complex extends the aromatic polypyridyl ligand. For this reason $[Ru(tpm)(dppn)Cl]^+$ was also synthesised. This complex has previously been synthesised in the Thomas group but has not been studied in biological systems.[1] An extended intercalating ligand, dppn (benzo[i]dipyrido[3,2-a:2',3'-c]phenazine) (Figure 22), is the polypyridyl ligand in this complex, and an additional aim was to compare the biological activity of $[Ru(tpm)(dppn)Cl]^+$ to that of DRuT. If the presence of an intercalating ligand in DRuT (compared to PRuT) has a positive effect on cytotoxicity, then $[Ru(tpm)(dppn)Cl]^+$ has the potential to be yet more cytotoxic. The dppn ligand is also associated with the photo-generation of singlet oxygen, the reactive species involved in photodynamic therapy.[157] Therefore the incorporation of dppn may lead to dual cytotoxicity through DNA targeting and singlet oxygen sensitisation.

The aforementioned complexes were synthesised utilising literature and Thomas group methodology.[1, 158]

Following the successful synthesis, the second aim was to further investigate the DNA binding modes of DRuT and PRuT. As outlined in Chapter 1, previous studies had indicated that DRuT intercalates into DNA and PRuT does not. However further studies were needed to determine whether either or both complexes covalently bind to DNA, in addition to determination of what, if any, reversible binding mode PRuT displays. By answering these questions, the biological mechanisms of action of these complexes can be further understood.

These binding studies were carried out using a range of techniques: inductively coupled plasma-mass spectrometry (ICP-MS), NMR spectroscopy and a restriction enzyme inhibition assay were used to assess covalent binding in both cellular and cell-free conditions, whilst non-covalent binding to DNA was investigated through fluorescent competition titration experiments.

3.2 Synthesis

$[Ru(tpm)(dppz)Cl]^+$ (DRuT), $[Ru(tpm)(phen)Cl]^+$ (PRuT), $[Ru(tpm)(dppn)Cl]^+$, $[Ru(bpy)_3]^{2+}$ and $[Ru(bpy)_2(dppz)]^{2+}$ were synthesised. DRuT, PRuT and $[Ru(tpm)(dppn)Cl]^+$ were produced using methods previously developed in the Thomas group (Figure 22).

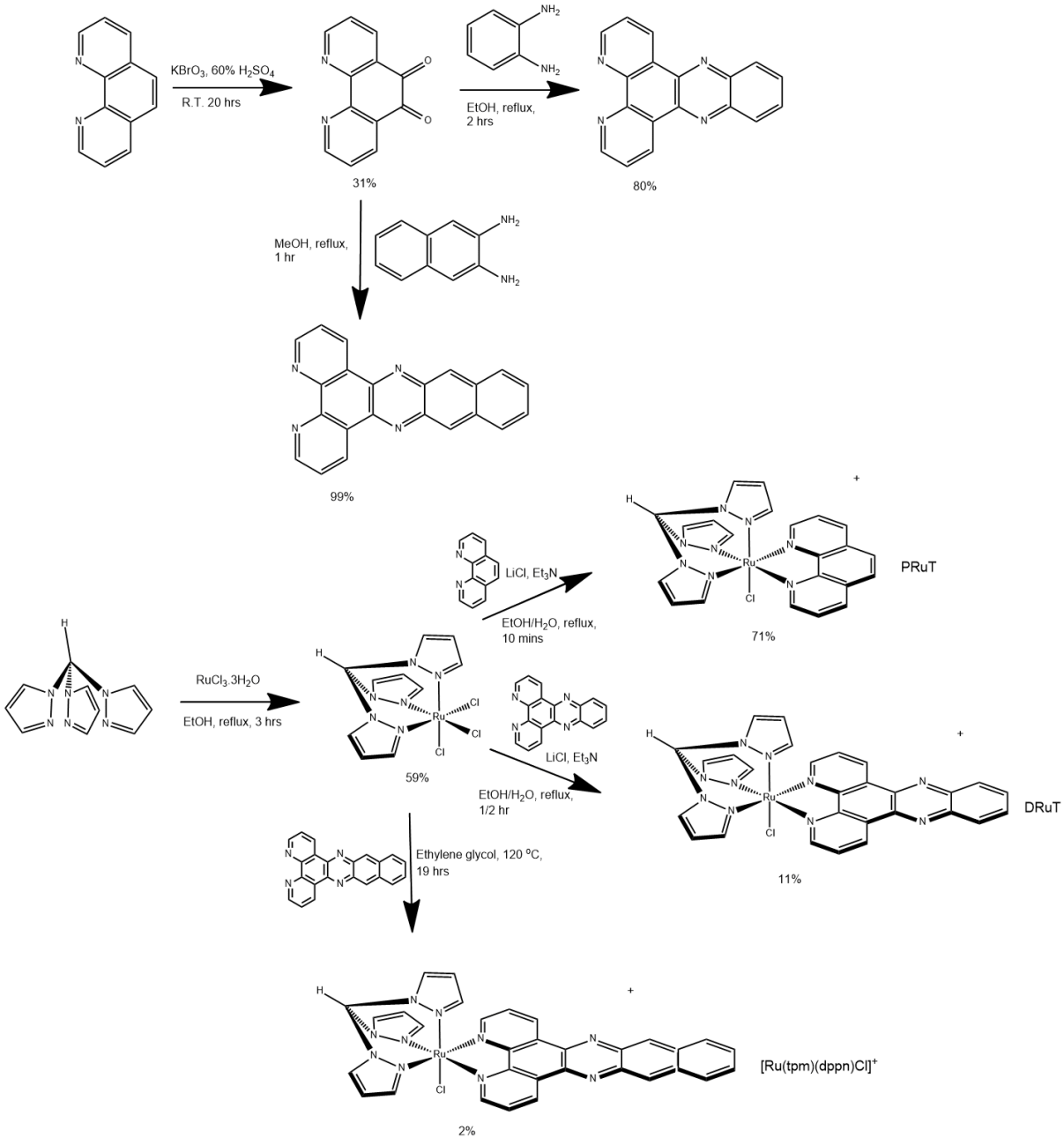

Figure 22: The synthetic route taken to obtain DRuT, PRuT and $[Ru(tpm)(dppn)Cl]^+$.

Prior to forming the complexes, the individual ligands had to be synthesised. First, the dppz ligand was synthesised from the starting material 1,10-phenanthroline. This was oxidised at the 5 and 6 positions to form 1,10-phenanthroline-5,6-dione (DPQ). Two common methods are recognised for this reaction,

one involving a mixture of concentrated nitric and sulfuric acids and heating for 3 hours. However a more recent synthesis,[159] used here, has the advantage of milder conditions. In this method phen is stirred at room temperature with potassium bromate in 60% sulfuric acid overnight. The product was purified by recrystallisation, but the yield was not very high at 31%. This could be due, in part, to the fact that the neutralisation step may lead to a reduced yield if not fully optimised as DPQ is soluble in both acidic and alkaline conditions. However, despite the diappointing yield, sufficient DPQ was produced to move onto the next step.

The DPQ was refluxed for two hours with phenylene diamine in ethanol to give dppz in a procedure used extensively in the Thomas group.[1, 158] The product was recrystallised from ethanol/water. This was a fairly high yielding reaction at 80%.

Dppn was synthesised in an analogous manner.[1] DPQ was refluxed with 2,3-diaminonaphthalene in methanol for an hour in the absence of light and the resulting orange precipitate was collected and washed giving a pure product with a yield of 99%.

The ruthenium complexes DRuT, PRuT and $[Ru(tpm)(dppn)Cl]^+$ were synthesised by first adding the TPM (Tris(1-pyrazolyl)methane) ligand* to $RuCl_3.3H_2O$, in a synthesis reported by Meyer et al.,[160] before reacting with the appropriate polypyridyl ligand in a process reported previously by the Thomas group.[1, 158] $[Ru(tpm)Cl_3]$ was synthesised by refluxing $RuCl_3.3H_2O$ with TPM in ethanol for 3 hours, with the product precipitating from solution. The yield was moderate, at 59%, and no further purification was required.

DRuT was synthesised by the reaction of $[Ru(tpm)Cl_3]$ with dppz in ethanol/water for 3 hours. Triethylamine was added 10 minutes into the reflux to reduce the Ru (III) to Ru (II). Lithium chloride was also present in the reaction mixture to prevent dissociation of the remaining chloride ligand. Addition of aqueous ammonium hexafluorophosphate caused the precipitation of the product as hexafluorophosphate salt.

DRuT was purified by column chromatography on alumina with 1:1 – 60:40 acetonitrile:toluene as the mobile phase. The product appeared as a deep red/purple band, and several other bands were observed. This purification proved difficult with the best results achieved by dissolving the crude product in the minimum volume of acetonitrile, followed by the addition of diethyl ether to precipitate the product, which was then collected and further purified by column chromatography. The yields for this reaction were low, with 11% being the highest achieved. It may be noted that different (possibly shorter) reaction times may lead to improved yields, possibly due to fewer side-products forming. A promising alternative synthetic route has been investigated by other members of the Thomas group in currently unpublished work where the dppz is first reacted with $[Ru(DMSO)_4(Cl)_2]$, with TPM then being reacted with the product.

*TPM kindly donated by Sam Ashworth, synthesised using a Thomas group method.[1]

PRuT was synthesised in an analogous way to DRuT, with phen being used in the place of dppz. Since the purification of DRuT by column chromatography had proved problematic, the approach of dissolving in acetonitrile and precipitating with diethyl ether was taken for PRuT. After this step the product was pure and so column chromatography was not required. The yield of PRuT (71%) was much higher than DRuT, likely due to the lack of column chromatography. In addition the reflux for this reaction was only 10 minutes long, reducing the opportunity for side products to form.

$[Ru(tpm)(dppn)Cl]^+$ was synthesised[1] by heating $Ru(tpm)Cl_3.3H_2O$ with dppn in ethylene glycol to 120 ^oC for 19 hours in the absence of light. Again it was precipitated by the addition of aqueous ammonium hexafluorophosphate and collected by filtration. Some of the crude product was purified by column chromatography on alumina with a gradient of 2:1 toluene:acetonitrile to pure acetonitrile as the mobile phase.

In addition to the cytotoxic complexes DRuT, PRuT and $[Ru(tpm)(dppn)Cl]^+$, the controls $[Ru(bpy)_3]^{2+}$ and $[Ru(bpy)_2(dppz)]^{2+}$ were synthesised by the synthetic route illustrated in Figure 23.

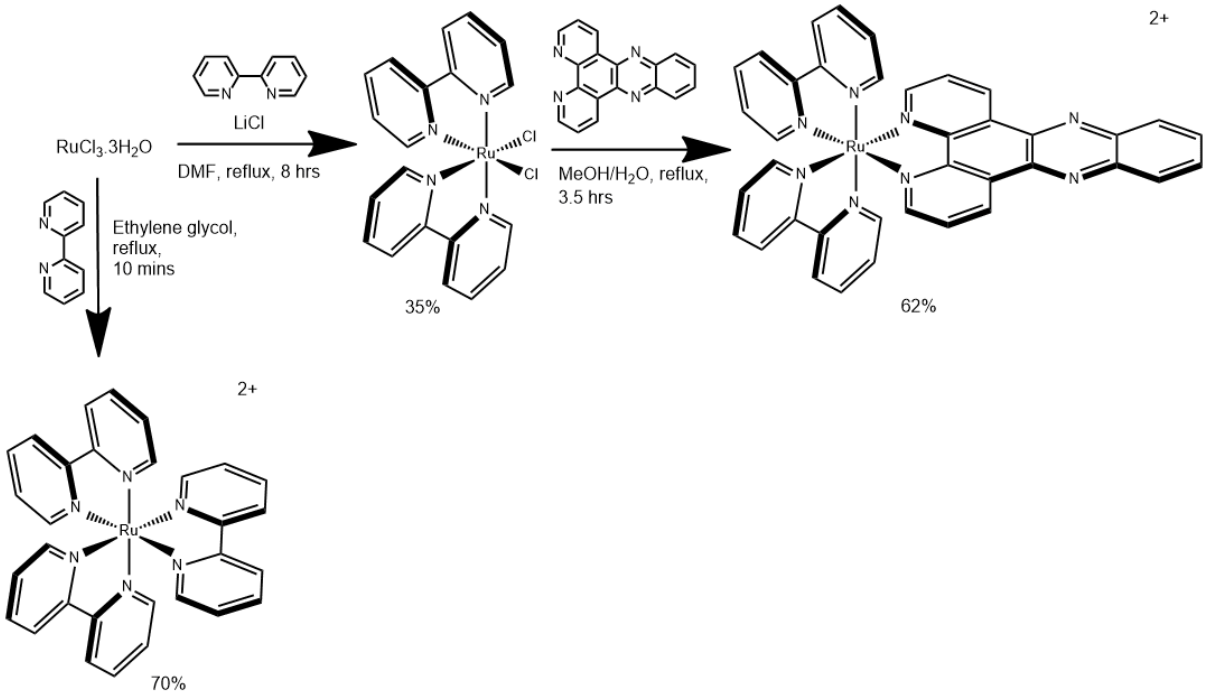

Figure 23: The synthetic route taken to obtain $[Ru(bpy)_3]^{2+}$ and $[Ru(bpy)_2(dppz)]^{2+}$.

$[Ru(bpy)_3]^{2+}$ was formed from $RuCl_3.3H_2O$ in a short 10-minute reflux with bpy in ethylene glycol, and precipitated by the addition of aqueous ammonium hexafluorophosphate. The yield was acceptable at 70% and no further purification was required.

The method reported by Meyer was used to synthesise $[Ru(bpy)_2Cl_2]$,[161] in which $RuCl_3.3H_2O$ is refluxed with bpy in dimethylformamide for 8 hours. Addition of lithium chloride to the reaction mixture helps prevent the substitution of the final two chloride ligands. After refluxing, addition of acetone and cooling to 4 ^oC overnight induced precipitation of the pure product. The yield of 35% was

lower than that reported in the literature[161] and could be due to inefficient cooling (Meyer's method specified cooling to 0 °C), or product being lost when washed with water.

The synthesis of $[Ru(bpy)_2(dppz)]^{2+}$ was based on a method by Amouyal et al.[162] $[Ru(bpy)_2Cl_2]$ was reacted on with dppz by refluxing in methanol/water for 3.5 hours and the product was precipitated by the addition of aqueous ammonium hexafluorophosphate. The product was purified by dissolution in the minimum volume of acetonitrile followed by addition of diethyl ether and collection of the resulting precipitate to give a moderate yield of 62%.

Each of the complexes was isolated as an acetonitrile-soluble hexafluorophosphate salt. However, these salts are insoluble in water and therefore inappropriate for biological studies. The complexes were therefore transformed into their water soluble (apart from DRuT) chloride salts. This was achieved by dissolving in the minimum volume of acetone and adding tetrabutylammonium chloride dissolved in acetone. The chloride salts formed are insoluble in acetone causing them to precipitate from solution, allowing them to be collected.

PRuT, $[Ru(bpy)_3]^{2+}$ and $[Ru(bpy)_2(dppz)]^{2+}$ could then be dissolved in phosphate-buffered saline (PBS) to give stock solutions for use in biological studies. However the chloride salt of DRuT has low water solubility and therefore was predissolved in dimethyl sulfoxide (DMSO) to a concentration of 10 mM before further dilution for each experiment. As a control for the addition of DMSO, an equivalent amount was added to other samples in biological experiments to ensure consistency.

3.3 Characterisation

All compounds were characterised by ^{1}H NMR and electrospray mass spectrometry. The ^{1}H NMR spectra of DRuT and PRuT are shown in Figure 24.

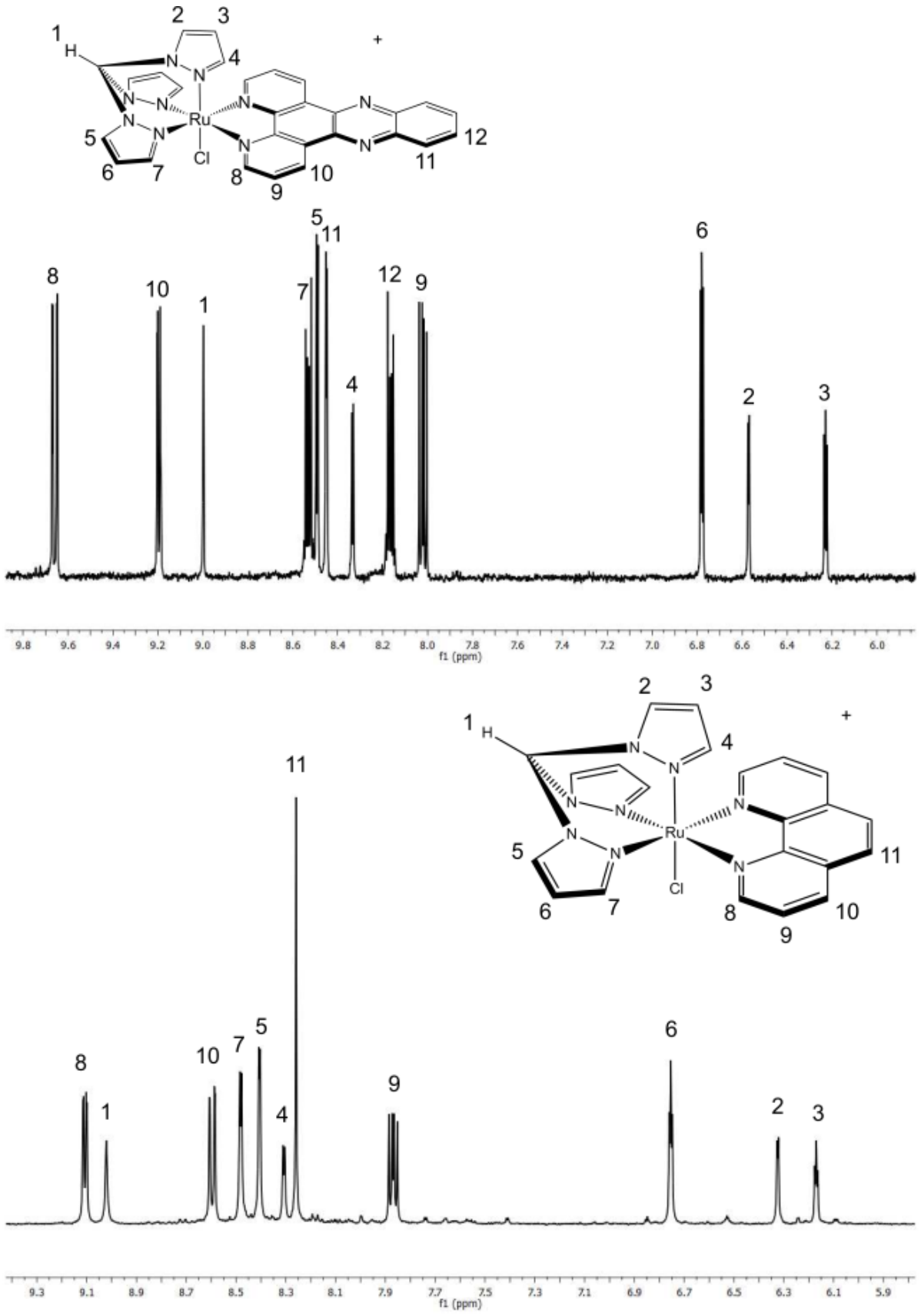

Figure 24: ^{1}H NMR spectra of DRuT (above) and PRuT (below) as PF_6 salts in acetonitrile.

These ^{1}H NMR spectra of DRuT and PRuT are in agreement with those previously assigned in detail by Walker.[1] The assignments are shown in Figure 24. In both spectra the three most downfield signals correspond to three of the tpm pyrazole protons. The spectrum for DRuT is the most complicated, so the spectrum for PRuT will be discussed first. For PRuT the group of peaks between 7.8 and 8.7 ppm (parts per million) correspond to the remaining tpm pyrazole protons and the three pairs of phen protons furthest from the nitrogens. The singlet peak at around 9 ppm corresponds to the remaining tpm proton and the furthest upfield peak corresponds to the pair of phen protons closest to the nitrogens.

For DRuT the tpm protons appear at similar chemical shifts to those in PRuT. Some dppz protons appear between 7.9 and 8.5 ppm, with one pair at 9.2 ppm. The peak corresponding to the pair of protons closest to the coordinated nitrogens is shifted upfield compared to the corresponding protons in PRuT to around 9.6 ppm.

The ^{1}H NMR spectra for $[Ru(bpy)_3]^{2+}$ as a PF_6 salt in acetonitrile is shown in Figure 25.

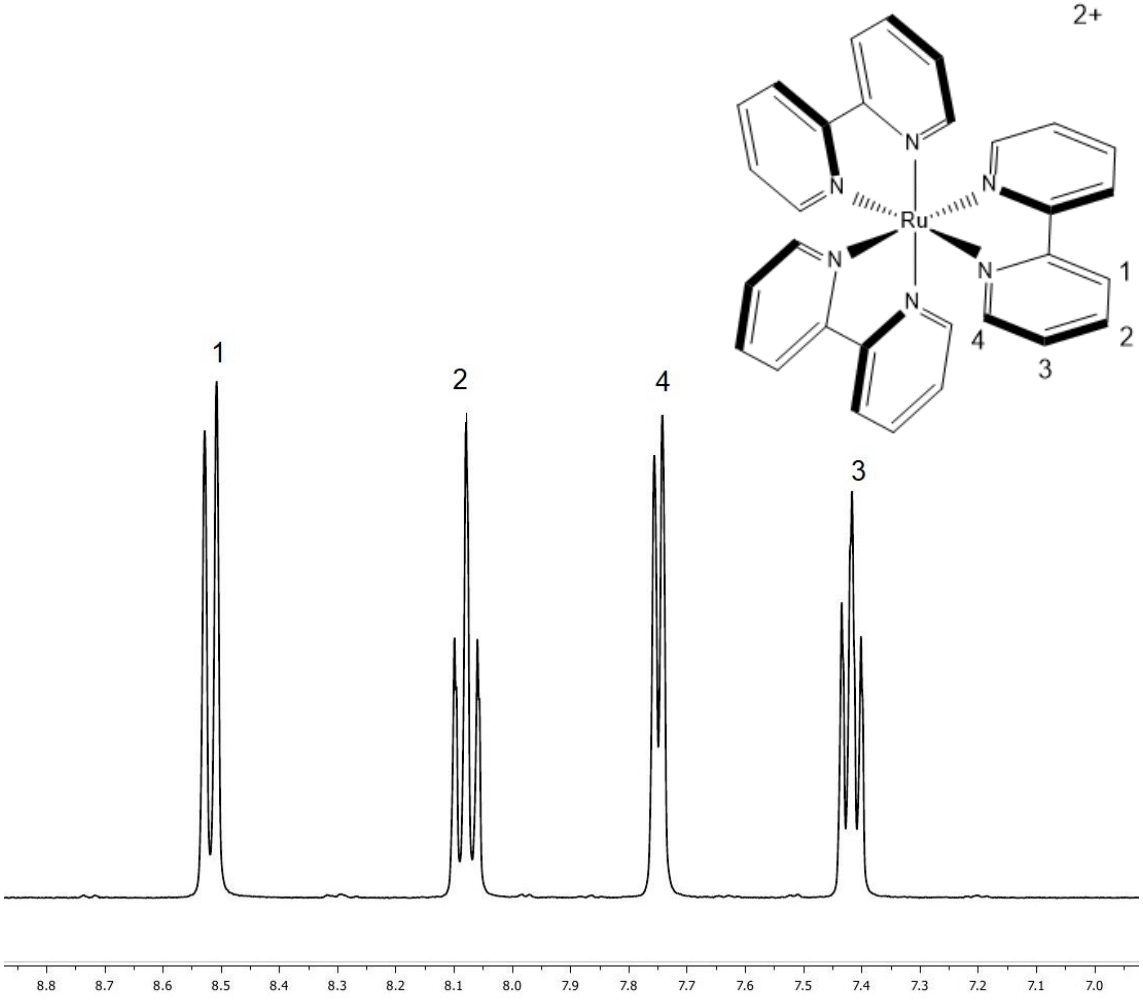

Figure 25: The ^{1}H NMR spectrum of $[Ru(bpy)_3]^{2+}$ as a PF_6 salt in acetonitrile.

In this spectrum the four peaks correspond to the four proton environments in the bpy ligands. As the three ligands are identical their corresponding protons are in equivalent environments. So each peak

represents six protons. The two doublets correspond to the protons on the 3 and 6 positions of the pyridine rings, as these are split by one proton each, and the triplets correspond to the protons on the 4 and 5 positions as these are split by two protons each.

The ^{1}H NMR spectrum of the other control complex, $[Ru(bpy)_2(dppz)]^{2+}$, as a PF_6 salt in acetonitrile, is shown in Figure 26.

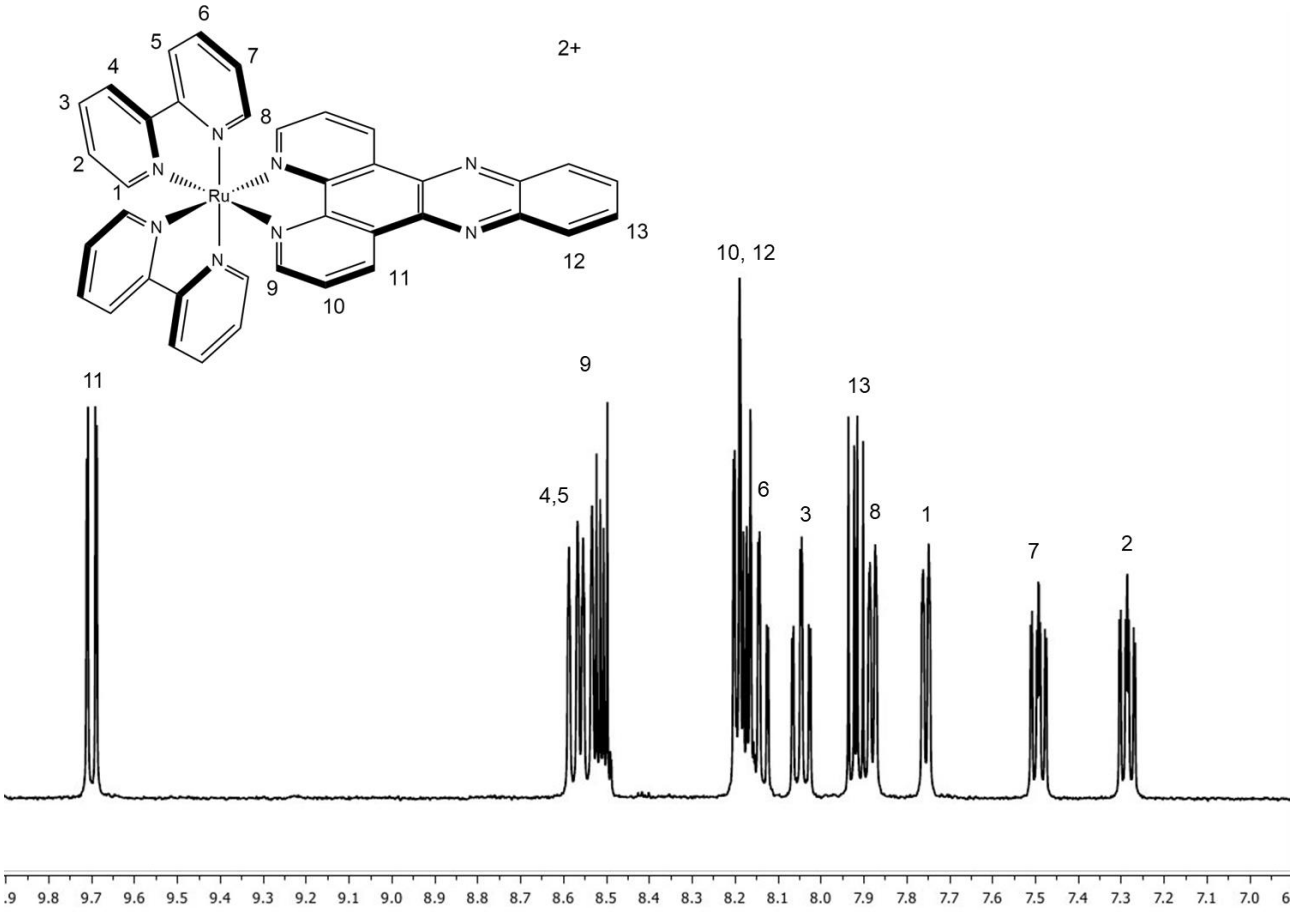

Figure 26: The ^{1}H NMR spectrum of $[Ru(bpy)_2(dppz)]^{2+}$ as a PF_6 salt in acetonitrile.

This spectrum is more complicated than that for $[Ru(bpy)_3]^{2+}$ due to the larger number of proton environments, however the peaks integrate to the correct number of proton environments and are in agreement with spectra reported in the literature.[162]

Figure 27 shows the ^{1}H NMR spectrum of $[Ru(tpm)(dppn)Cl]^{+}$ as a PF_6 salt in acetonitrile.

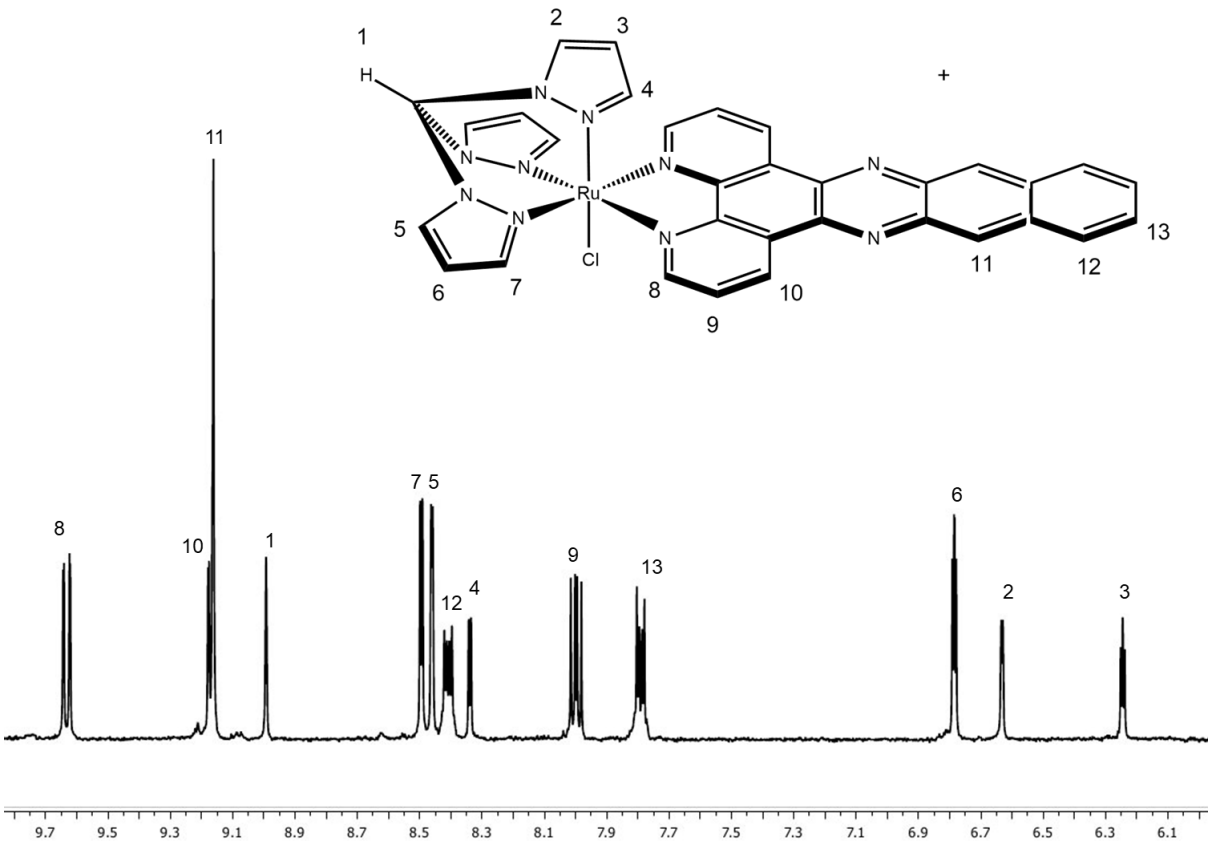

Figure 27: The ^{1}H NMR spectrum of $[Ru(tpm)(dppn)Cl]^{+}$ as a PF_6 salt in acetonitrile.

This spectrum has again been assigned by Walker,[1] and it is similar to the DRuT spectrum. The peak corresponding to the pair of protons on the dppn ring next to the phenazine ring is shifted to around 9.2 ppm, and the two peaks corresponding to the pairs of protons on the last ring of the dppn ligand are at 7.8 and 8.4 ppm.

3.4 Binding Studies

Complexes in the ruthenium TPM polypyridyl class have the potential to bind to DNA in various ways. The presence of a polypyridyl ligand means they are likely to bind reversibly. Furthermore, differences between these ligands lead to different reversible binding modes, as has been confirmed from viscometry experiments (see chapter 2: introduction). Since both DRuT and PRuT have a labile ligand in the monodentate binding site they also have the potential to bind covalently to DNA in a cisplatin-like manner.

Studies were undertaken to determine whether reversible or irreversible binding occurs for each complex, with the aim to better understand their similarities and differences, and gain further insight into each complex's biological mode of action.

3.4.1 Covalent Binding

DRuT and PRuT could bind covalently to DNA through their monodentate binding sites. The chloride ligand may be predicted to substitute for water in an aqueous environment. This water ligand may then substitute for nucleobases, particularly the N7 sites in guanine and adenine. It is possible that this could work in a similar way to cisplatin, i.e. the complexes only aquating after being taken up into cells due to the lower chloride concentration, followed by the more highly charged complexes being attracted electrostatically to DNA. Unlike cisplatin, the complexes only have one labile ligand, and as such they would be unable to cross link DNA. However DRuT and PRuT could form bulky adducts which are also damaging.

Studies were undertaken to determine whether this potential covalent binding of the complexes to DNA occurs.

3.4.1.1 DNA ICP-MS

ICP-MS is a technique which allows elements, and in particular metals, to be detected at very low concentrations. It allows for detection of smaller amounts of metals than other techniques which might be considered for similar applications such as atomic absorption spectroscopy.[163]

Use of ICP-MS in the detection of quantities of metal associated with DNA has been reported extensively in the literature, in particular to detect the covalent binding to DNA of platinum drugs.[163]

This technique has also been used to study the covalent binding of ruthenium drugs[164] and an analogous approach was taken here. This technique was chosen as it could be performed on DNA extracted from treated cells, rather than using DNA in a cell-free environment. This makes the results more applicable to the biological mechanisms of action of the complexes, as just because a molecule can bind to DNA in a cell-free environment, it won't necessarily bind to DNA in cells. Cellular DNA is supercoiled, and is present as chromatin being tightly bound to nucleosomal histone proteins, making its form very different to, for example, calf thymus DNA (CT-DNA) which consists of shorter DNA fragments and is commonly used in *in vitro* studies.

For this experiment, A2780 CIS cells were treated with DRuT or PRuT for 24 hours. This timepoint was chosen to ensure that the complex had reached its target and had time to react. The cells were then harvested, lysed and the DNA extracted using a mammalian genomic DNA purification kit. Proteins in the sample were degraded using Proteinase K and the sample was added to a silica column. Due to the salts and alcohol in the buffers used the nucleic acids bind to the column. The column was washed to remove impurities and salts, and this step should also remove any non-covalently bound ruthenium species from the DNA. The nucleic acids were then eluted from the column using a slightly basic buffer. Finally, RNAse A, an endoribonuclease which catalyses the cleavage of phosphodiester bonds in single stranded RNA, was used to remove RNA from the samples.

The purity of the extracted DNA was evaluated by measuring the A_{260}/A_{280} values, the ratio between the absorbances at 260 nm and 280 nm. 260 nm corresponds to the maximum absorbance for nucleic acids and 280 nm is the maximum absorbance for proteins, so this ratio can be used to assess the purity of nucleic acid samples to ensure that they are free from protein contamination. A ratio of around 1.8 is considered to be pure DNA. A lower ratio can indicate protein contamination in the sample. A higher ratio can be caused by RNA contamination since a ratio of around 2.0 is expected for pure RNA.[165] However the ratio can also be affected by factors such as the alkalinity of the buffer.[166] In this experiment, A_{260}/A_{280} ratios between 1.6 and 1.9 were deemed acceptable, and samples which had ratios that fell outside of this range were discarded.

After the A_{260}/A_{280} ratios were measured in elution buffer, ethanol precipitation was used to precipitate the DNA which was then redissolved in TMAH/EDTA buffer for ICP-MS analysis.

Three control compounds were used in this experiment. Cisplatin was used as a positive control for covalent binding and to validate the method used compared to literature results. Two ruthenium complexes, $[Ru(bpy)_3]^{2+}$ and $[Ru(bpy)_2(dppz)]^{2+}$ were also used. Neither of these complexes have any labile ligands and therefore are unable to covalently bind to DNA. However they can non-covalently bind to different extents. $[Ru(bpy)_2(dppz)]^{2+}$ is an intercalator whereas $[Ru(bpy)_3]^{2+}$ exhibits weak electrostatic binding.[167] In this experiment if significant quantities of either of these complexes were

found to be associated with DNA then the validity of the experiment would be called into question, as it should only detect covalently bound complexes.

ICP-MS analysis revealed that the DNA extracted from cisplatin-treated cells had an associated platinum content of 20.7 pg Pt per μg DNA. This is in approximate agreement with results obtained by Yamada et al[163] in an experiment treating human colorectal cancer cells with cisplatin and measuring platinum bound to the DNA by ICP-MS. Agreement between this and literature results supports the legitimacy of the experimental procedure used.

The mass of ruthenium per μg DNA for $[Ru(bpy)_3]^{2+}$ and $[Ru(bpy)_2(dppz)]^{2+}$ was 0.084 pg and 0.049 pg respectively. These results are several orders of magnitude smaller than those for cisplatin, supporting the assumption that the DNA purification process satisfactorily removed any non-covalently bound ruthenium. The results for DNA extracted from cells treated with DRuT and PRuT are shown in Figure 28.

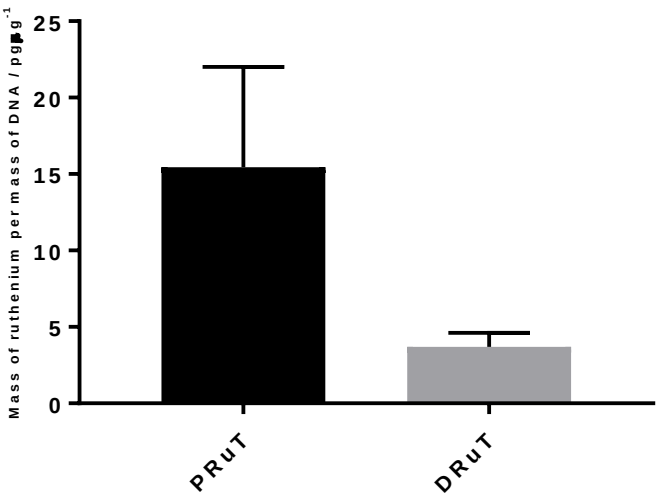

Figure 28: The mass of Ru/mass of DNA, determined by ICP-MS, of DNA extracted from A2780 CIS cells treated with DRuT and PRuT (50 μM) for 24 hours. Error bars represent standard deviation based on four repeats.

The masses of ruthenium per μg DNA for DRuT and PRuT were 3.70 pg and 15.44 pg respectively. This suggests that both DRuT and PRuT covalently bind to DNA in cells, as their results are significantly higher than those for the control ruthenium complexes. It also suggests that PRuT binds around four times more frequently than DRuT under the experimental conditions used.

These results contradict the idea that the difference in biological mechanisms of action between DRuT and PRuT can be explained solely by one species covalently binding to DNA and the other not. However it is still possible that the frequency of DNA modifications could affect the cellular response to the complexes. It could be that PRuT modifies DNA to an extent above a threshold that induces a different response than a lower degree of modification by DRuT, which the cell may deal with through a different pathway.

There was a much larger degree of variability between experiments for PRuT than any of the other complexes (see error bars in Figure 28). This could be explained by the fact that by the end of the 24 hour treatment period cell cultures treated with PRuT were observed to contain a comparatively much larger number of dead or dying cells. It is likely that complex uptake in dying cells may consequently have been more variable, perhaps allowing the complexes to flood in once the cell membranes have lost integrity.

Unfortunately there are issues with this experimental approach which limit the conclusions that can be drawn from the results. No attempt was made to control for the variation in uptake rates between the complexes into the cells. Different rates of uptake would be expected due to the different charges and lipophilicities of the complexes, particularly between DRuT and PRuT and the ruthenium control complexes. The control complexes have a 2+ charge which could prevent them from easily crossing the lipid membrane. If these complexes do not enter the cell then they would not have the opportunity to bind to the DNA and this means they may not be valid controls. In addition, if the rate of uptake between DRuT and PRuT is different, then the difference in the results could be due to differing amounts of ruthenium in the cell and not related to differences in covalent DNA binding.

An obvious alternative experiment is to use ICP-MS to investigate DNA binding in cell-free conditions, which would overcome the issue of cellular uptake. However this would have the issue of the result not necessarily being relevant to what would happen in cells. It would, however, be an interesting comparison alongside the results from this experiment performed in cells.

3.4.1.2 NMR

As a way to further investigate binding to DNA, cell-free NMR studies were undertaken. The reactivities of DRuT and PRuT with guanosine, an analogue for the guanine bases in DNA, were investigated. This approach has been used in the literature by researchers looking to determine how reactive compounds are likely to be with DNA, including platinum and ruthenium complexes.[168-169] The advantage is that this technique unambiguously detects covalent binding. However obviously this *in vitro* technique is far removed from the intracellular environment and the fact that a compound can react with guanosine doesn't necessarily mean that it will react with guanine residues in the DNA of living cells.

As previously stated, it is likely that the chloride ligand in DRuT and PRuT would substitute for a water ligand in an aqueous environment. This ligand may then substitute for the N7 atom in guanine (or guanosine), thereby covalently binding to DNA.

An initial experiment involved simply monitoring a mixture of DRuT or PRuT with guanosine by NMR. The mixture was dissolved in D_2O containing 1/50 DMF-d7 (deuterated dimethylformamide) in order to aid dissolution of the ruthenium complexes. DRuT or PRuT and guanosine were mixed in a 1:1 ratio at 200μM concentration and the reaction was monitored over 48 hours by ^1H NMR. Water suppression was used, which is a technique allowing other peaks to be seen more clearly when there is a large solvent peak from water.[170] It was used in this case due to the low concentrations of reagents.

The reaction between guanosine and a compound of interest is monitored by observing the change in the guanosine H8 peak at 8 ppm (Figure 29). H8 is the closest proton to N7 in the guanosine molecule and so it is strongly affected by changes to N7. However, both DRuT and PRuT also have peaks at around 8 ppm which changed during the course of the experiment, partially obscuring the guanosine peak. For this reason it was impossible to tell whether changes in the spectra were due to a reaction between the complexes and guanosine, or just the substitution of the chloride ligand for water.

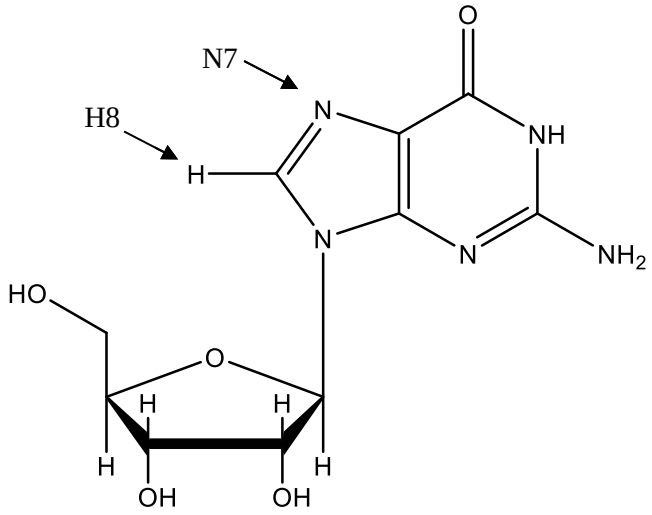

Figure 29: A diagram of guanosine. The position of N7, where DRuT and PRuT have potential to bind, is shown, as well as H8, the closest proton to N7.

To investigate this further the reaction between the complexes and water was separated from the reaction between the complexes and guanosine. Studying the overall reaction in this way makes the assumption that the aquation reaction would occur before the reaction of the resulting complex with guanosine.

Solutions of DRuT and PRuT were dissolved in 1/50 DMF-d7 in D_2O and the reactions were monitored by ^1H NMR until no more changes were observed (Figure 30).

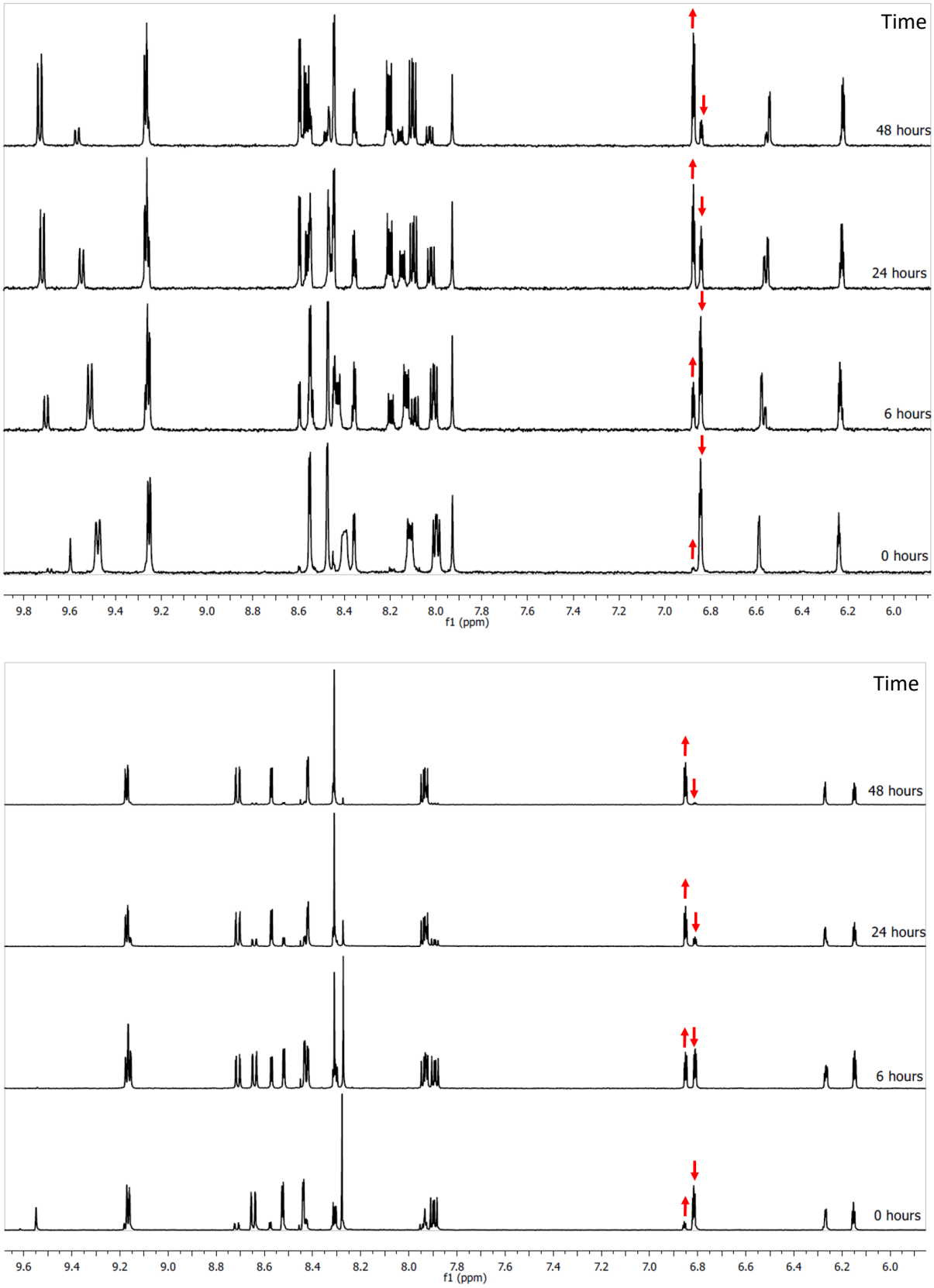

Figure 30: ^{1}H NMR spectra showing the reaction between DRuT (above) and PRuT (below) at a concentration of 200 μM with D_2O over 48 hours, showing that PRuT exchanges its chloride ligand with D_2O faster than DRuT.

These spectra show that PRuT aquates more quickly than DRuT. For DRuT the peak close to 6.8 ppm, corresponding to a TPM pyrazole proton, can be easily used to monitor the progress of the reaction.

The reaction is clearly underway after 6 hours, and yet after 48 hours the original peak can still be seen, indicating that the reaction has not yet gone to completion. The reaction was complete after 120 hours. For PRuT, the progress of the reaction can also be monitored by observing the peak at 6.8 ppm. In this case a spectrum taken immediately after mixing reveals the reaction is already underway. The reaction nears completion after 24 hours and no further changes are observed after 48 hours.

The electrospray mass spectra for the complexes before the reaction confirm the identities of the complexes. Peaks at m/z (mass over charge) 633 for DRuT, and at m/z 531 for PRuT, correspond to the M^+ for the complexes without a counterion. The mass spectra taken after changes in ^1H NMR spectra had stopped show that chloride ligands were exchanging for coordinating water, with new peaks at m/z 616 and m/z 514 corresponding to [(DRuT-H_2O) – $2H^+$] and [PRuT-H_2O) – $2H^+$] respectively.

To investigate the reaction between the complexes and guanosine separately from the reaction with water, the complexes were allowed to react to completion with water (120 hours for DRuT and 48 hours for PRuT) after which time guanosine was added to the aquated complexes (again in a 1:1 ratio with the complex at 200 μM) and the reaction was monitored (Figure 31).

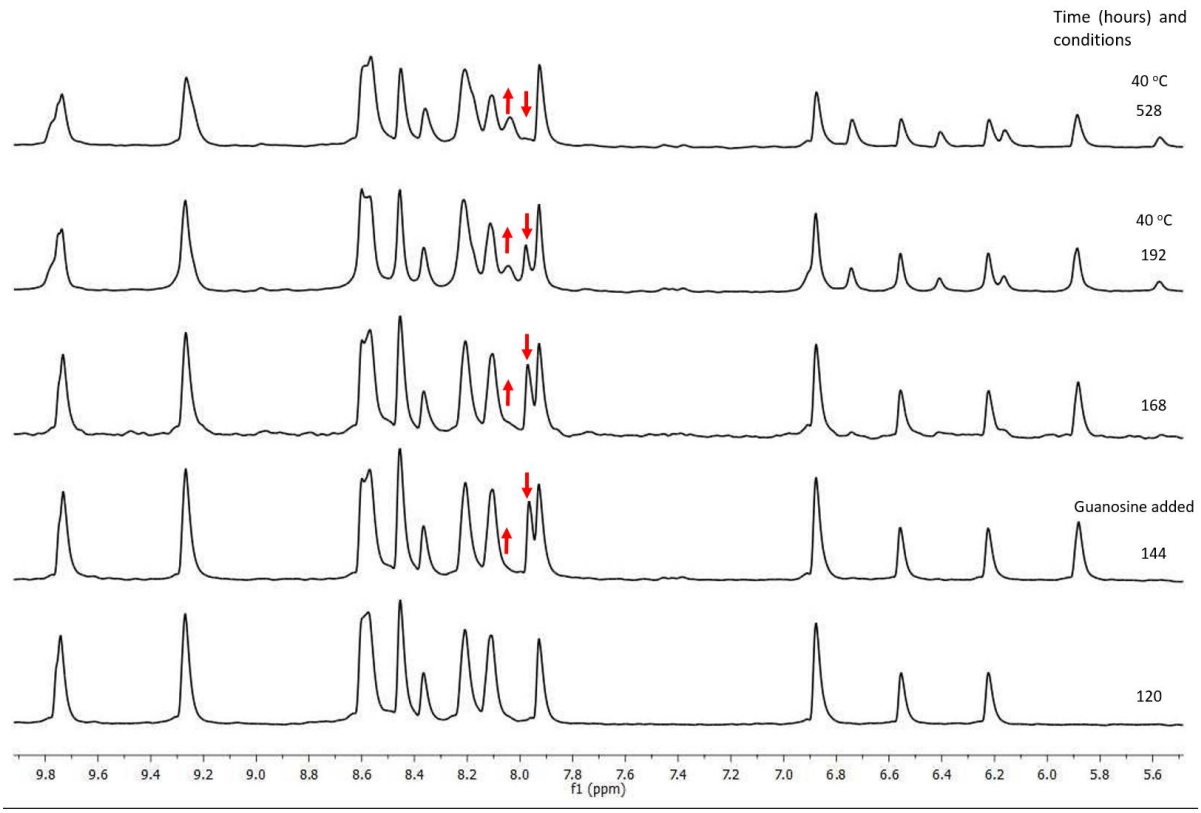

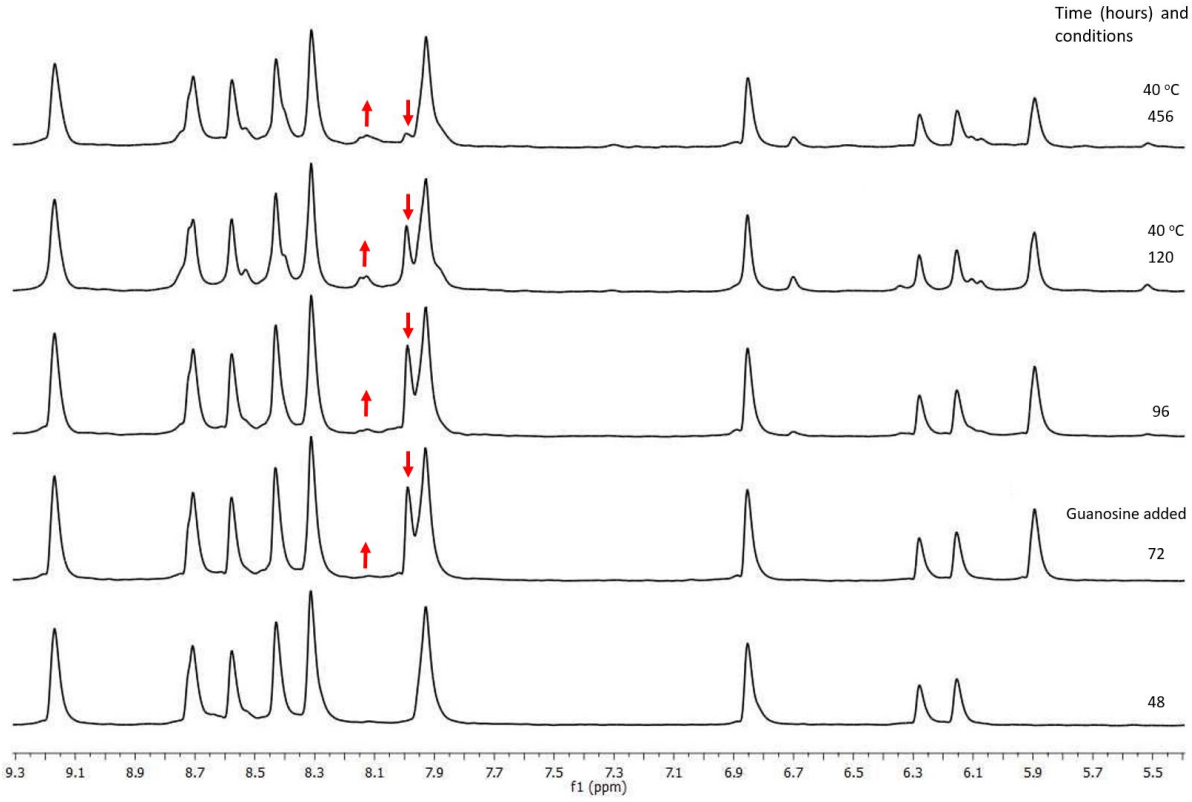

Figure 31: ^{1}H NMR spectra showing the reaction between DRuT (above) and PRuT (below) with guanosine after being allowed to react fully with water, over 2 weeks, showing that both react at a similar rate when heated to 40 °C.

The spectra in Figure 31 show that as the solutions were monitored at room temperature for 48 hours, in both cases little to no changes in any peaks were observed, indicating no reaction. Because of this the solutions were heated to 40 °C, chosen due to this being close to the temperature cell cultures are incubated at (37 °C). After 24 hours under these conditions changes in the spectra are observed for both DRuT and PRuT. In both cases the guanosine H8 peak at about 8 ppm reduces in size and the other peaks from the complexes shift. In particular, in both cases the two peaks between 6 and 6.5 ppm corresponding to two TPM protons can be seen to shift. These protons would be expected to be affected significantly by the complexes reacting at the D_2O position, as this is directly opposite these TPM protons in the octahedral geometry.

The reactions were observed to continue upon further incubation at 40 °C. Although it appears that DRuT may react slightly faster, the rates of reaction did not appear to be significantly different between the two complexes, indicating that they do not have significantly different reactivities towards guanosine. However, PRuT reacts faster than DRuT with water. The reaction with water changes the charge of the complexes from +1 to +2, and these more highly charged complexes would be attracted to polyanionic DNA more strongly. Due to this the aquated complexes may react more quickly with guanosine/DNA than the chloride complexes, essentially meaning that the aquation is the rate-limiting step and PRuT would react more quickly overall. However this would be difficult to verify by NMR

due to the difficulties already described when trying to monitor the reaction with guanosine before the reaction with water is complete.

One notable feature of these results is the relatively slow speed of reaction between the aquated complexes and guanosine, even at 40 ^{o}C. Both DRuT and PRuT have cellular effects within the timescale of hours, as evidenced by western blots (see chapter 2: introduction), whereas the reactions observed by NMR were on the timescale of days. If the covalent reaction of the complexes with DNA is the cause of their effects in cells then this should occur much more quickly than the NMR data implies. Therefore, these results appear to contradict the ICP-MS results by suggesting that a covalent reaction between the complexes and DNA is unlikely to occur within the timescale that the complexes begin to cause downstream markers of DNA damage.

This technique is obviously an imperfect way to measure the potential of a molecule to bind with cellular DNA. The concentration of guanosine used here is not the same as the concentration of guanine bases in a cell, and the form of cellular DNA is completely different from free guanosine. This will have an impact on the rate of reaction observed in an experiment compared to the actual rate of reaction in cells.

3.4.1.3 Restriction enzyme experiment

The results from the ICP-MS and NMR experiments are in apparent contradiction and as both methodologies have different strengths and weaknesses it is difficult to determine which result should be used to draw conclusions as to the covalent DNA binding behaviour of DRuT and PRuT. To clarify this situation, a third experiment was performed involving a restriction enzyme digest.

Restriction enzymes are a class of endonucleases which hydrolyse both strands of the DNA backbone at a specific site, based on the ability of each enzyme to recognise a unique palindromic DNA sequence. They cut DNA leaving a 3' hydroxyl and a 5' phosphate on either side of the strand break. Found naturally in bacteria and archaea, they are extensively used in molecular biology laboratories as an invaluable tool in gene cloning. There are various classes of restriction enzyme, but those most commonly used in laboratories are type II. These cut DNA at specific positions at their recognition site. Due to this their behaviour can be easily predicted, giving rise to their applications.

It has been shown that covalent modification of DNA can inhibit restriction enzymes.[171] In particular, platinum complexes such as cisplatin exhibit this effect. So a compound's ability to inhibit restriction enzymes can be used to test whether or not it covalently binds to DNA. Platinum complexes with only one binding site, which can therefore only form monoadducts with DNA, have also been shown to inhibit restriction enzyme activity. [171] This suggests that if DRuT and PRuT covalently bind to DNA they should cause a similar inhibition.

Cisplatin was used as a positive control for this experiment and the restriction enzyme that was chosen was EcoRI. This is because this enzyme has been used for similar experiments in the literature[172] and its recognition site is GAATTC. This includes guanine bases, so an effect should be observed even if the complexes only bind to these bases.

There is some evidence in the literature of highly sequence-specific intercalators inhibiting restriction enzymes, however sequence-neutral intercalators did not have this effect.[173] For this reason it was thought preferable to separate any non-covalently bound complex from the DNA sample (whether this is reversibly bound complex or free complex in solution) after incubation and prior to the restriction enzyme reaction. Two methods were trialled for this separation: a PCR (polymerase chain reaction) purification kit and ethanol precipitation.

PCR purification kits are generally used for purifying small quantities of DNA after PCR reactions. They use silica columns and buffers to bind, wash and elute the DNA. This technique separates the DNA from impurities such as salts, and so should separate the DNA from platinum and ruthenium complexes.

Ethanol precipitation involves precipitating DNA in ethanol and sodium acetate. The precipitate is collected, followed by repeated washes with 70% ethanol. Assuming a sufficient number of washes are performed, this should remove platinum and ruthenium complexes.

The ethanol precipitation method gave the greatest recovery of DNA for samples incubated with DRuT and PRuT and the PCR purification kit gave the greatest recovery for samples incubated with cisplatin, so these methods were employed in these respective cases.

Plasmid DNA was selected for this experiment, as a plasmid which has been cleaved at a single site is easily distinguished from uncleaved material. Plasmids can exist in three different topological forms: supercoiled, nicked (where one DNA strand has been cleaved) and linearised (where both DNA strands have been cleaved). These three forms may be distinguished by agarose gel electrophoresis.[174] The supercoiled form is also arguably relevant to cellular DNA which is also supercoiled. The plasmid used was FCHo1-pmCherryC1 which has a size of 7322 base pairs and was chosen as it contains one EcoRI restriction site. If the EcoRI enzyme is not inhibited the plasmid would be expected to be fully linearised. So after the restriction enzyme reaction, the more supercoiled and nicked plasmid remaining in the sample, the more the enzyme has been inhibited, and therefore the more the complex being tested has covalently bound to the plasmid.

The plasmid (0.5 μg) was incubated with cisplatin, DRuT and PRuT at various concentrations in water for 5 hours. The reason for the time chosen was that this is similar to the minimum time at which cellular effects are observed after treatment. After this incubation, in the case of cisplatin-treated samples, DNA was purified using a Qiaquick PCR purification kit according to the manufacturer's instructions and the DNA was eluted in water. For DRuT- and PRuT- treated samples after incubation, ethanol and sodium acetate (final concentration 100 mM) were added and the samples cooled to -20 ^{o}C to induce DNA precipitation. Following centrifugation (13000 RPM (revolutions per minute), benchtop centrifuge), DNA pellets were washed 5 times with 70% ethanol and then dissolved in water.

Half of the DNA recovered from all samples was then treated with EcoRI (0.5 μL, 12 unit/μL, where 1 unit of restriction enzyme will digest 1μg DNA in a 50 μL reaction in 60 minutes) for 2 hours in an appropriate buffer in the presence of bovine serum albumin (BSA), according to the manufacturer's instructions. The products of the reactions were analysed by gel electrophoresis using an agarose gel containing ethidium bromide and subsequently imaged and visualised by ethidium bromide-induced fluorescence using a Bio-Rad Gel Doc EZ Gel Documentation System and proprietary software.

Initially the same set of concentrations of all three complexes was used, however for higher cisplatin concentrations virtually no DNA was recovered after the PCR purification kit was used. It was hypothesised that this was because the cisplatin was crosslinking plasmids, i.e. reacting with two at once. This could lead to high molecular weight DNA species being formed, if several plasmids were linked together by several cisplatin molecules. These high molecular weight species would not elute

from the DNA purification column, perhaps offering an explanation for the low yield obtained. As cisplatin treatment was a positive control, and inhibition of the EcoRI was observed at the low cisplatin concentrations for which the DNA yield was acceptable, only these low concentrations were used subsequently.

As shown in Figure 32, cisplatin partially inhibits EcoRI as expected. In lane 4 the linearised plasmid can be seen at the expected molecular weight. In lanes 1-3 a second band is observed at a higher molecular weight, corresponding to a non-linearised form. The appearance of this form confirms that the EcoRI has failed to cut and linearise the plasmid as efficiently as in the control lane with no cisplatin. This is what would be expected based on the knowledge that cisplatin binds covalently to DNA. The samples shown have low cisplatin concentrations and so the EcoRI inhibition is only partial. However, EcoRI inhibition increases with increasing cisplatin concentration (see graph in Figure 32). It is expected that if the samples with higher cisplatin concentrations could be recovered, they would show higher levels of inhibition of EcoRI, and possibly complete inhibition.

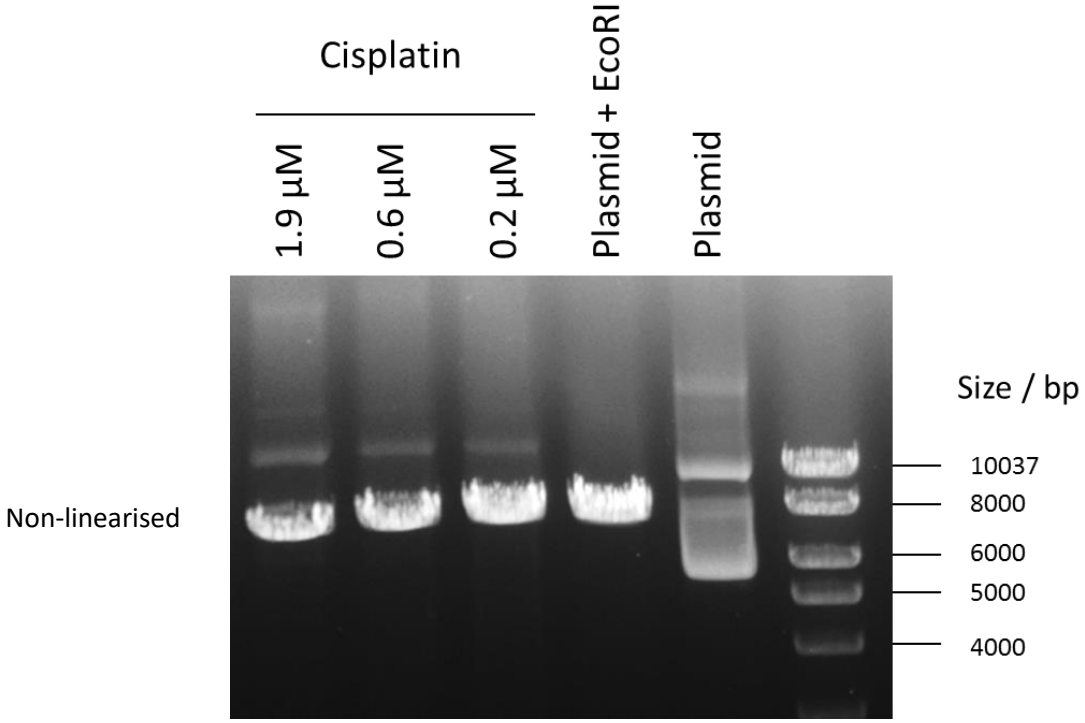

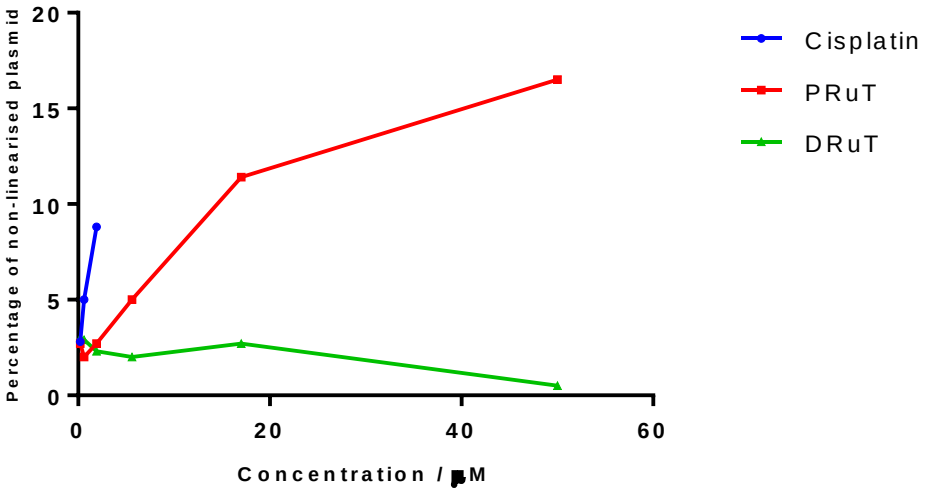

Figure 32: An example image of agarose gel electrophoresis stained with ethidium bromide. This shows the extent of inhibition of EcoRI acting on the plasmid FCHo1-pmCherryC1 in response to treating the plasmid with various concentrations of cisplatin. A graph showing the percentage of non-linearised plasmid detected in each lane against the concentration of cisplatin, PRuT and DRUT.

Figure 32 shows that observable EcoRI inhibition is caused by PruT treatment of the plasmid, but not DRuT treatment. This is confirmed by the presence of non-linearised plasmid following PRuT treatment but not DRuT treatment. This suggests that PRuT is capable of covalently binding to DNA at a level detectable by this technique and DRuT is not.

The graph in Figure 32 shows the intensity of the linearised plasmid band compared to the intensity of the whole lane for each condition. A higher percentage of non-linearised plasmid corresponds to a higher amount of inhibition of EcoRI and therefore may represent a greater degree of covalent DNA binding. This analysis reveals that the level of inhibition is higher for cisplatin than for PRuT at equivalent concentrations. So although PRuT demonstrates some covalent DNA binding it does not have as large an effect as cisplatin. This is not unexpected as cisplatin can bind in a bidentate manner to DNA, whereas PRuT could only bind in a monodentate manner due to only having one potential binding site. This could also suggest that PRuT does not have such a high affinity for DNA as cisplatin. However, there is a clear difference in the effectiveness of DRuT which does not show any covalent DNA binding in this experiment. The difficulty in obtaining DNA samples treated with higher concentrations of cisplatin means conclusions drawn about the differences between cisplatin and ruthenium complex treatment in this experiment should be considered with caution.

One potential pitfall of this experiment is that a non-covalently bound molecule could also inhibit a restriction enzyme in some circumstances. However, restriction enzymes have very high affinities for their restriction sites and would likely out-compete most reversibly bound small molecules unless these were highly sequence-specific. If a non-covalent interaction was to cause restriction enzyme inhibition in this experiment, DRuT would be predicted to cause such an effect due to its strong reversible binding affinity for DNA, meaning that DRuT is in effect a control for this experiment. As DRuT does not cause

any observable inhibition it appears that in this experiment only covalent modification of DNA inhibits the restriction enzyme.

These results support the conclusion reached from the ICP-MS results, confirming that PRuT covalently binds to DNA, and at a higher level than DRuT. However the ICP-MS results suggested that DRuT could covalently bind at about a quarter of the rate of PRuT, and this was not detected in this experiment. This experiment does contradict the NMR data which suggests that neither complex is likely to bind over the timescale of a few hours. However, since the NMR experiment was in cell-free conditions using guanosine, not DNA, it is easy to discount this data in favour of the ICP-MS and restriction enzyme experimental conclusions.

In summary, these results suggest that PRuT does exhibit covalent DNA binding and there is some conflicting evidence that DRuT can also form covalent bonds to DNA.

3.4.2 Non-Covalent Binding

DPPZ is well known to be an intercalating ligand, and so DRuT would be expected to strongly bind reversibly to DNA in the form of intercalation. The viscosity data showed this to be the case for DRuT-H_2O (see chapter 2: introduction) and due to their similar structures it is reasonable to assume this to also be true for DRuT.

On the other hand, as discussed in the introduction, phen and its metal complexes are not considered to be intercalators. Indeed viscosity experiments support this conclusion, showing that PRuT does not intercalate. Therefore, the potential reversible binding mode of PRuT is less easy to predict. The work done in the Covalent Binding section indicates that it does covalently bind to DNA and it is possible that this is its only mode of DNA binding (apart from electrostatic attraction to the backbone), as is the case for cisplatin. However, as a polypyridyl ligand phen does have a binding affinity for DNA in a non-intercalative manner, so it is worth exploring the possibility that PRuT could exhibit some form of non-covalent DNA binding. For example it is possible that it is a groove binder.

3.4.2.1 DNA Titrations

As many ruthenium polypyridyl complexes are luminescent and display the DNA light switch effect, it is common to probe their reversible DNA binding affinities by titrating them into a solution of DNA

and observing the increase in their luminescence. This can be used to determine binding constants. However, as DRuT and PRuT are not luminescent this simple but powerful technique cannot be used.

One alternative is to perform a competitive DNA titration. In these experiments a second compound is used which displays an increase in luminescence upon binding to DNA and has well studied reversible DNA binding characteristics (e.g. DAPI and H33258). A solution of either molecule is added to a solution of DNA and the luminescence spectrum is recorded. The compound of interest is then titrated in and any decrease in luminescence indicates that the luminescent compound has been displaced by the compound of interest reversibly binding to the DNA. In some cases this technique is also used to determine the binding constant of the compound of interest.[175]

A competitive DNA titration was performed using CT-DNA to determine whether PRuT could displace H33258. A solution of 20 μM CT-DNA and 2 μM H33258 was excited at 338 nm and its emission spectrum was recorded between 390-650 nm, corresponding to the excitation and emission wavelengths of H33258.[176] 50 μL portions of 150 μM PRuT or DRuT were added and a decrease in the emission of H33258 was observed (Figure 33).

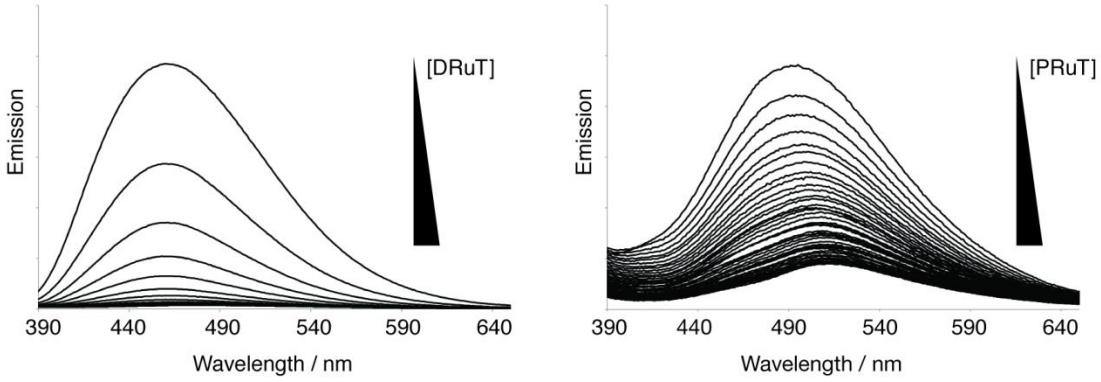

Figure 33: Graphs of emission intensity between 390-650 nm for solutions of H33258 and CT-DNA with increasing concentrations of (left) DRuT and (right) PRuT added. In both cases a decrease in emission intensity occurs, showing the complexes are displacing the H33258, however this effect is stronger for DRuT.

The decrease in H33258 emission upon the addition of PRuT shows that it does non-covalently bind to DNA, as it displaces H33258. As expected this effect is also observed for DRuT. Qualitatively the suppression in the H33258 emission is much stronger for DRuT than PRuT, showing that the same amount of DRuT displaces more H33258 than PRuT. This is consistent with DRuT having a stronger DNA binding affinity than PRuT, which is to be expected as intercalation is a very strong mode of binding. However, since the displacement of the groove binder H33258 is observed for the intercalator DRuT as well as the non-intercalator PRuT, this data cannot be used to speculate on the mode of reversible DNA binding for PRuT.

The difference between the reversible binding affinities of DRuT and PRuT could be quantitatively defined by calculating their respective DNA binding constants. One method used in the literature is to plot a Scatchard Plot using a method described by Boger et al,[177] henceforth referred to as Boger's method. The number of equivalents of the compound of interest is plotted against change in fluorescence, and from this a saturation point is observed. The change in fluorescence at this point is used to produce the Scatchard Plot which should be a straight line graph with a gradient of -K (binding constant of the compound of interest). This method relies upon three equations, Equation 1, Equation 2 and Equation 3.

$$\left(\frac{\Delta F_x}{\Delta F_{sat}}\right)\frac{1}{X} = fraction\ of\ DNA - bound\ complex$$

Equation 1

$$\left[1 - \left(\frac{\Delta F_x}{\Delta F_{sat}}\right)\frac{1}{X}\right] = fraction\ of\ free\ complex$$

Equation 2

$$[DNA]_T\left[X - \frac{\Delta F_x}{\Delta F_{sat}}\right] = [free\ complex]$$

Equation 3

Where ΔF_x is the change in fluorescence, ΔF_{sat} is the change in fluorescence at the point of saturation, X is the molar equivalent of complex compared to DNA, $[DNA]_T$ is total DNA concentration and [free complex] is concentration of unbound complex.

The first graph plotted allows ΔF_{sat} to be determined and so the concentration of free complex can be calculated using Equation 3. The Scatchard plot, which is the result of Equation 3, can then be plotted, allowing the calculation of the binding constant. These graphs were plotted for DRuT and PRuT (Figure 34).

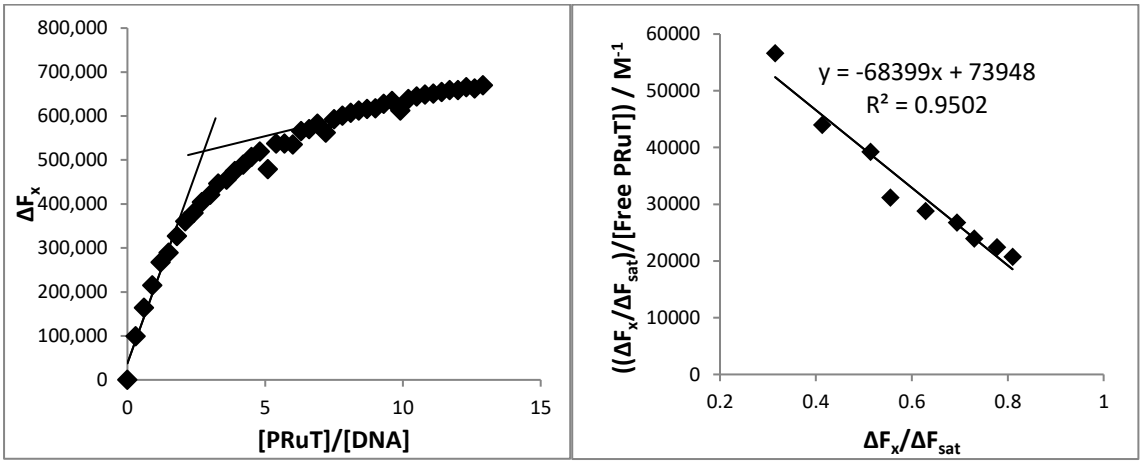

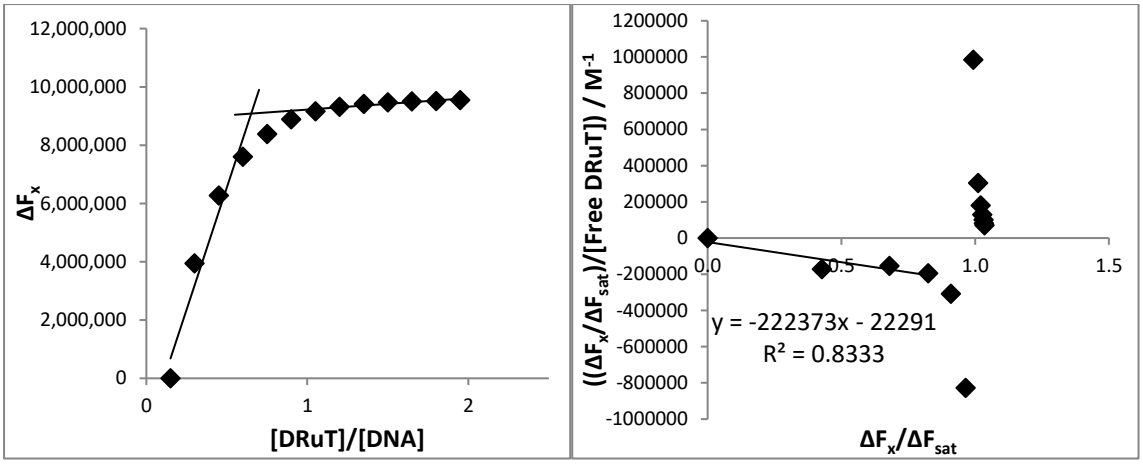

Figure 34: Saturation curves (left) and Scatchard Plots (right) for the DNA competition titration between H33258 and PRuT (top) and DRuT (bottom). In the case of PRuT a straight line Scatchard Plot and binding constant are obtained. Unusually in the case of DRuT in the linear region of the graph the y axis values are negative. For this graph the line of best fit is only applied to the first 4 points.

In both cases the graph of [complex]/[DNA] against ΔF_x gives a saturation curve. The saturation point is calculated from the point of intersection of the lines of best fit of the first and last sections of the data. According to Boger's method the value of [complex]/[DNA] at this point corresponds to the stoichiometry of binding. For PRuT this is 2.77, which suggests that one PRuT binds per 3 base pairs on the DNA. For DRuT it is 0.65, suggesting that around 1.5 DRuT molecules bind per base pair. This does not seem reasonable, as if one molecule intercalated into each available space between base pairs the ratio of DRuT to base pairs should be around 1:1. This discrepancy calls the analysis of this data using Boger's method into question. Errors may arise as the binding of the complexes to DNA is not being measured directly, rather the displacement of the H33258 is measured. It is not certain that one complex molecule displaces one H33258 molecule, the actual ratio could be different. However this effect has been observed in other studies of complexes containing DPPZ. It has been theorised that it is due to some complex molecules binding to the surface of DNA in addition to those that intercalate.[178]

The value of ΔF_x at the saturation point is ΔF_{sat}. This point is determined by calculating the point of intersection between two lines of best fit of the first and last roughly linear sections of the graph. Using this the Scatchard Plot is created and the points prior to the saturation point should form a straight line with a negative gradient which is equal to –K. For PRuT this is the case and from the gradient the binding constant is $6.8X10^4\,M^{-1}$. This is reasonable for a groove binder. However for DRuT the region of interest is negative in the y axis. The reason for this is that [free DRuT], i.e. the concentration of unbound DRuT, is calculated to be negative. This implies that more DRuT has bound to the DNA than there is DRuT in total which is clearly not possible. This may again be due to a different displacement stoichiometry than 1:1. If one DRuT molecule displaces more than one H33258 molecule then it would appear that more DRuT has bound to the DNA than is actually the case.

Nevertheless the points before the saturation point form a straight line with a negative gradient. This gives a binding constant of $2.2X10^5\,M^{-1}$. This is a reasonable binding constant for a monocationic metal

intercalator. The fact that the calculated binding constant for DRuT is higher than that for PRuT is also expected.

Another method used to calculate binding constants from displacement assays is using the binding constant of the compound being displaced, in this case H33258. A value of the binding constant of H33258 of $5X10^6$ M^{-1} was used for this analysis, as it is a rough average of values found in the literature.[179-180] The equation used is Equation 4.

$$K_{H33258}[H33258]_{50\%} = K_{app}[complex]_{50\%}.$$

Equation 4

Where K_{H33258} is the DNA-binding constant of H_{33258}, $[H33258]_{50\%}$ is the concentration of H33258 at a 50% reduction in fluorescence, K_{app} is the apparent DNA-binding constant of the complex of interest and $[complex]_{50\%}$ is the concentration of the complex of interest at a 50% reduction in fluorescence.

From Equation 4 the values of K_{app} calculated for DRuT and PRuT were $1.4X10^6$ M^{-1} and $2.1X10^5$ M^{-1}. These are both around one order of magnitude higher than those calculated from Boger's method and are more in line with those for typical intercalators and groove binding metal complexes. However, this method would also assume that one complex molecule displaces one H33258 molecule, which may not be the case. The values obtained using this method depend heavily upon the value of K used for H33258. There are a range of values for this quoted in the literature ranging from around 10^4 M^{-1} to around 10^7 M^{-1},[181] influenced by the fact that there is more than one binding mode depending on the particular system. Using values at either end of this spectrum would give different K_{app} values for DRuT and PRuT. Because of this Boger's method could be considered more accurate as it only uses the experimental data. A way to make the K_{app} method more accurate would have been to first calculate a value of K for H33258 using the same CT-DNA sample and the same experimental conditions as are used for the displacement assays.

Overall these results confirm that DRuT and PRuT both reversibly bind to DNA. DRuT intercalates whereas PRuT doesn't and DRuT binds to DNA with a higher binding constant than PRuT. PRuT may be a groove binder, although this cannot be confirmed from the data in this study.

3.5 Conclusion

The covalent and non-covalent binding modes of DRuT and PRuT to DNA have been investigated and discussed. Results suggest that PRuT covalently binds, although not with as high an affinity as an equivalent concentration of cisplatin. DRuT does not appear to covalently bind, or at least not with nearly as high an affinity as PRuT. Both complexes non-covalently bind, with experiments showing that DRuT intercalates into DNA and PRuT binds through an alternative, unknown reversible binding mode. DRuT has a higher non-covalent binding affinity than PRuT.

These differences in DNA binding properties may help to explain the different effects that DRuT and PRuT display in cells. These will be investigated further in the next chapter.

4. Mechanistic Studies in a Human Ovarian Carcinoma Model

4.1 Introduction

Previous work, outlined in chapter 2: introduction, has shown that DRuT and PRuT have interesting and distinct biological activities in the human ovarian carcinoma cell lines A2780 and A2780 CIS. Both compounds are cytotoxic towards these cells lines with DRuT being the most cytotoxic, especially towards the cisplatin-resistant cell line A2780 CIS. Although both complexes have been shown to cause cells to undergo apoptosis, the most intriguing results came from western blots aimed at investigating DNA damage and cell death pathways. Like cisplatin, PRuT treatment causes the phosphorylation of Chk1 and Chk2, as well as γ-H2AX. However, although DRuT causes the phosphorylation of Chk1, it does not cause phosphorylation of Chk2 or γ-H2AX.

This gives rise to the question of why there is a difference in mechanisms of action between these similar complexes. Chapter 3: synthesis and binding studies, presented results showing differences between the ways these two complexes bind to DNA. If their primary mode of action is through disrupting cellular processes through DNA binding, then it is probable that the differences in biological activities arise from these differences in DNA binding. This hypothesis is investigated in this chapter through a range of experiments involving A2780 CIS cells.

One important question arising from the observations described above is how does DRuT cause cell death through Chk1 activation but not Chk2 activation? Chk1 activation is normally considered to be a cell survival pathway. This issue is also investigated.

One possible reason for the difference between the toxicities of the complexes is differing rates of uptake into cells. Gaining insight into the rates of uptake could also help to clarify some conclusions from chapter 3: synthesis and binding studies, in particular those from the DNA ICP-MS experiment. Whole cell ICP-MS experiments are used to examine this.

Although DRuT and PRuT both bind to DNA, it is possible that DNA is not their primary target in cells. An alternative mechanism that could lead to cell death is damage to the mitochondria, or some combination of both. These ideas are considered in this chapter.

4.2 Cellular Uptake

Both DRuT and PRuT are presumed to enter cells as they both cause cell death and they were both associated with DNA extracted from treated cells in an ICP-MS experiment (see chapter 3: synthesis and binding studies). However it is not known whether one is taken up more quickly than the other, and what their intracellular concentrations are at various timepoints during treatment. A difference in uptake kinetics could contribute to the differing cytotoxicities of the complexes, and might also help to explain the DNA binding ICP-MS results discussed in chapter 3: synthesis and binding studies.

Size and lipophilicity of small molecules are two factors which influence how easily they are transported into cells.[182] As both complexes are identical apart from the two extra aromatic rings on the polypyridyl ligand of DRuT, DRuT is probably the more lipophilic of the two and therefore might be predicted to enter cells faster. On the other hand PRuT is slightly smaller and so it could equally exhibit the faster rate of uptake. Therefore it is difficult to predict what the actual difference, if any, in cellular uptake might be.

A common method for determining levels of cellular uptake for ruthenium polypyridyl complexes is to take advantage of their luminescent properties and use microscopy. However this is not possible as neither DRuT nor PRuT are luminescent. Therefore, ICP-MS was used to measure levels of cellular uptake. As with the experiment in chapter 3: synthesis and binding studies, ICP-MS was used to measure ruthenium content in a sample. In this case the sample was of whole cells treated with DRuT and PRuT.

A2780 CIS cells were treated with 50 μM DRuT and PRuT, the same concentration used in the DNA binding ICP-MS experiments. At various timepoints up to 24 hours the cells were harvested and counted. The samples were heated in nitric acid to break them down and ensure that any ruthenium present was fully dissolved. The ruthenium content of these samples was measured by ICP-MS. The volume of one A2780 CIS cell can be estimated as roughly 2 pL, so the intracellular ruthenium concentration could be calculated.

These experiments initially gave very variable results, making them difficult to interpret. This could be due to errors in experimental technique, for example inaccurate cell counting or loss of material when transferring between containers. However, it is also possible that the complexes quickly enter cells and then are rapidly expelled over a relatively short amount of time, leading to large variance in the results.

To improve the reliability of the results a number of changes were made to the experimental procedure. Notably the accuracy of cell counting was improved by decreasing the concentration of cells, and the samples were sonicated for 10 seconds prior to and after heating in nitric acid to ensure that any residual

cell material was broken down. Using this improved method more reliable results were obtained for 1 and 3 hour timepoints (Figure 35).

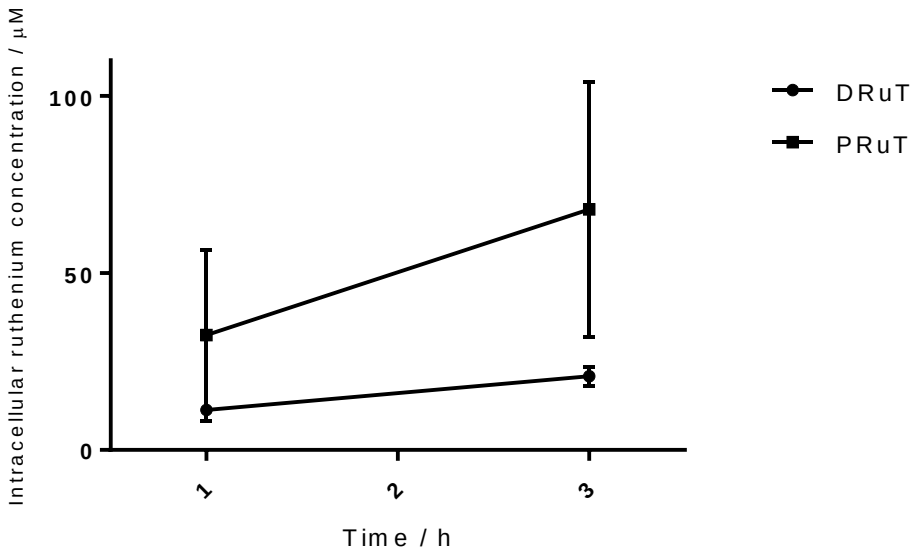

Figure 35: Intracellular ruthenium concentration after treatment of A2780 CIS cells with DRuT or PRuT (50 µM) for 1 and 3 hours, determined by ICP-MS, showing that PRuT enters cells at a higher concentration than DRuT after 3 hours. Error bars, representing standard deviation, are very large for PRuT, demonstrating the issues with obtaining reliable results in this experiment.

The data for PRuT still suffered from a large degree of variance. This mirrors the large variation seen in ruthenium contents of PRuT treated samples in the DNA binding ICP-MS experiments. In that experiment it was hypothesised that this was due to some cells dying quickly after PRuT treatment. However, in this case, the timepoints are 1 and 3 hours and it seems unlikely that enough cells could die quickly enough so as to affect the results to the extent observed, especially given that DRuT was found to be more cytotoxic. It may be that PRuT has a more complicated uptake mechanism than DRuT, perhaps PRuT is taken in to cells and expelled more easily than DRuT. So DRuT simply accumulates in cells over time whereas the levels of PRuT vary more over time.

Overall, the intracellular ruthenium concentration was higher for PRuT than DRuT at both timepoints, with the concentration at 3 hours being approximately 3 times higher. It is unclear whether this remains the case at longer timepoints, whether the concentration of PRuT relative to DRuT increases further over time, or whether at longer timepoints the uptake of DRuT overtakes that of PRuT. However this result could explain the 4-fold difference in ruthenium concentration in the DNA samples in the DNA binding ICP-MS experiments between PRuT and DRuT.

These results do not explain why DRuT is more cytotoxic than PRuT in the A2780 CIS cell line. PRuT clearly enters cells more quickly than DRuT, and this ties in with the observation that the morphology of PRuT treated cells changes more quickly after treatment. However, DRuT seems to have a more potent effect, even at a lower intracellular concentration.

4.3 Effects on DNA

4.3.1 Pulsed Field Gel Electrophoresis

The western blots for p-Chk1, p-Chk2 and γ-H2AX, shown in chapter 2: introduction, suggest that the association of PRuT with DNA results in the appearance of DNA DSBs whereas this is not the case with DRuT. This is because Chk2 phosphorylation is strongly associated with, and indicative of, DSBs[183] and γ-H2AX is a post-translationally modified histone marker which is recruited in response to DSBs and in turn recruits other repair proteins.[184] In fact, the presence of γ-H2AX is often used as a marker for the presence of DSBs in experiments.[185]

Given that the results from chapter 3: synthesis and binding studies, suggest that only PRuT binds covalently to DNA, it was hypothesised that this covalent binding leads to DSBs, and that DRuT does not covalently bind and therefore does not cause DSBs. An experiment was devised to directly determine whether PRuT causes DSBs while DRuT does not, or whether the actual situation is more nuanced. For example, PRuT could cause more DSBs than DRuT, but DRuT could still cause a limited quantity of DSBs, below the threshold required to observe Chk2 and γ-H2AX phosphorylation in western blots.

Pulsed-field gel electrophoresis (PFGE) is one of a few techniques that can be used to detect DSBs in genomic DNA, and it was used for this investigation. It is a technique that was developed in the 1980s to solve the problem that large fragments of DNA (larger than around 50 kb) could not be separated by traditional electrophoresis techniques. This inability is due to the fact that DNA molecules with higher molecular weights are too large to move through the pores in agarose gel under usual electrophoresis conditions.[186]

PFGE can be used to establish the extent of chromosomal DNA fragmentation arising from DSBs. Unbroken chromosomal DNA is too large to migrate significantly over the time course of the electrophoresis experiment and thus remains close to the origin in the gel, but DNA fragments, arising from the presence of DSBs, migrate at rates inversely proportional to their size. DSBs distributed throughout chromosomal DNA generate a wide range of different sized fragments that electrophorese at different rates, resulting in a characteristic streak.[187]

The level of DSB formation was measured in cells treated with either 50 μM DRuT or PRuT for 6 or 7 hours, as under these conditions western blots show clear phosphorylation of Chk2 and γ-H2AX for PRuT but not DRuT. Cells treated with 33 μM cisplatin for 24 hours were used as a positive control for DSB formation and untreated cells were used as a negative control.

A2780 CIS cells were treated and then harvested, counted and made into agarose plugs. They were lysed before being electrophoresed on an agarose gel containing ethidium bromide. The DNA was visualised using ethidium bromide and imaged using a ChemiDoc XRS+ System (Figure 36).

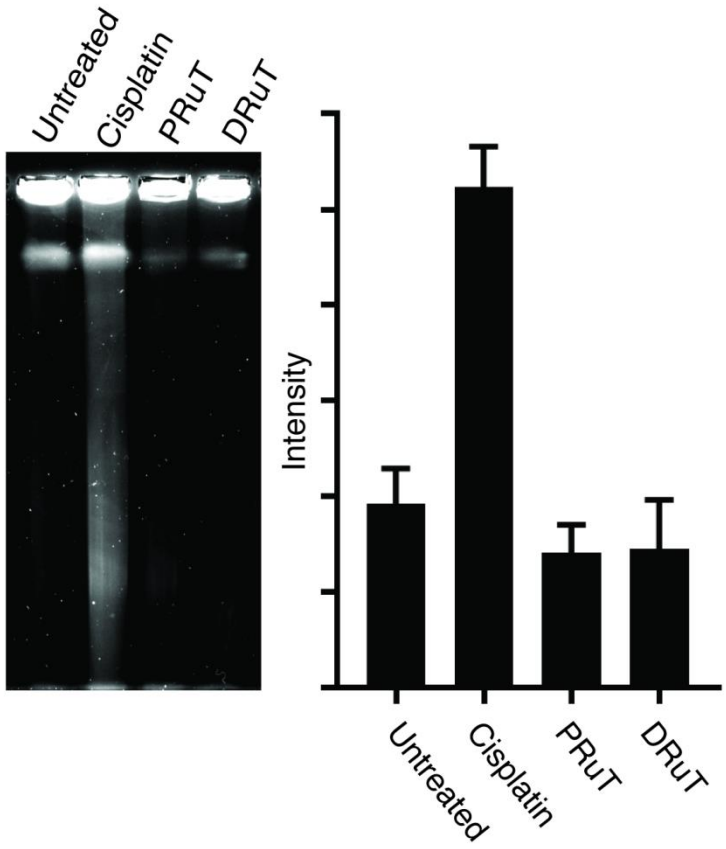

Figure 36: An image of a PFGE gel showing the impact on the DNA of A2780 CIS cells treated with cisplatin (33 μM, 24 hours), DRuT and PRuT (50 μM, 6 or 7 hours), as well as an untreated control, showing that neither DRuT nor PRuT causes a significant number of DSBs. A graph showing the average relative intensity of each lane with error bars representing the range over two experiments. The average intensity for the cisplatin lane was over two times higher than that for any other lane.

A streak is visible in the cisplatin lane, confirming that the DSBs caused by cisplatin are detected by this technique. Surprisingly there are no streaks in the DRuT or PRuT lanes, suggesting that neither DRuT nor PRuT causes DSBs. The results were quantified by measuring the total intensity of each lane. This shows that the average relative lane intensity for untreated cells was 19, for PRuT treated cells it was 14 and for DRuT treated cells it was 14. For cisplatin treated cells it was 52.

This experiment confirms that DRuT does not cause DSBs, showing that its mechanism of causing apoptosis is not due to causing an overwhelming DNA damage response due to DSBs. However, the result for PRuT is highly unexpected as it shows a lack of DSBs. The presence of γ-H2AX phosphorylation but not DSBs is unusual and warranted further investigation.

4.3.2 Fluorescence-Activated Cell Sorting

Flow cytometry is a technique in which cells in suspension are passed individually through a detector in order to analyse the properties of a large population of cells. A useful application is fluorescence-activated cell sorting (FACS). In this technique, cells can be sorted into separate populations based on their light scattering or fluorescence properties. Using multiple fluorescently-conjugated antibodies that recognise unique molecules within cells, or organelle-specific dyes, multiple parameters can be measured simultaneously.

Among other applications, flow cytometry can be used to analyse the cell cycle characteristics of populations of cells. This can be done by measuring the cells' DNA contents, as during S phase cells double their DNA content. Cells can be categorised as either being in G0/G1, S or G2/M phases, according to their DNA content. The quantification of DNA is achieved by treating cells with a fluorescent molecule that binds to DNA, such as propidium iodide (PI), an intercalating DNA stain.

The first experiment performed was an attempt to reproduce previous results obtained showing the effect that treatment with DRuT has on the cell cycle. This showed that compared with a population of untreated cells, there was an increase in the number of cells in S phase, indicating that the fraction of time treated cells spent in this phase of the cell cycle had increased (Figure 37).

Another parameter measured in this experiment was the incorporation of BrdU. This is a synthetic nucleotide which becomes incorporated into the DNA of any cells that are engaged in DNA replication. Using antibodies for BrdU and fluorescently conjugated secondary antibodies, the level of BrdU incorporation into each cell can be detected and quantified. This data can be displayed as a plot with the cell cycle histogram to show the different rates of DNA replication throughout the cell cycle. In a population of healthy cells a characteristic horseshoe shape is observed. The rate of DNA replication can be seen to increase rapidly at the beginning of S phase, reach a peak, and then decline towards the end of S phase.

For this experiment cells were treated with DRuT or PRuT at IC_{50} concentrations. After incubation, the cells were pulse-labelled with BrdU and then harvested and fixed with ethanol. They were probed with anti-BrdU antibodies, then stained with fluorescent secondary antibodies and PI. The samples then underwent FACS analysis and the results are displayed in Figure 37. For the univariate graphs, PI intensity (representing DNA content) was plotted against cell number. For bivariate graphs, PI intensity was plotted against Alexa Fluor 488 (AF488) intensity, representing BrdU incorporation. Colour contours show the number of cells in each area of the graph. Gates were used to count the number of cells in each stage of the cell cycle including stalled S (cells in S phase that were not incorporating BrdU). These results are summarised in the graphs.

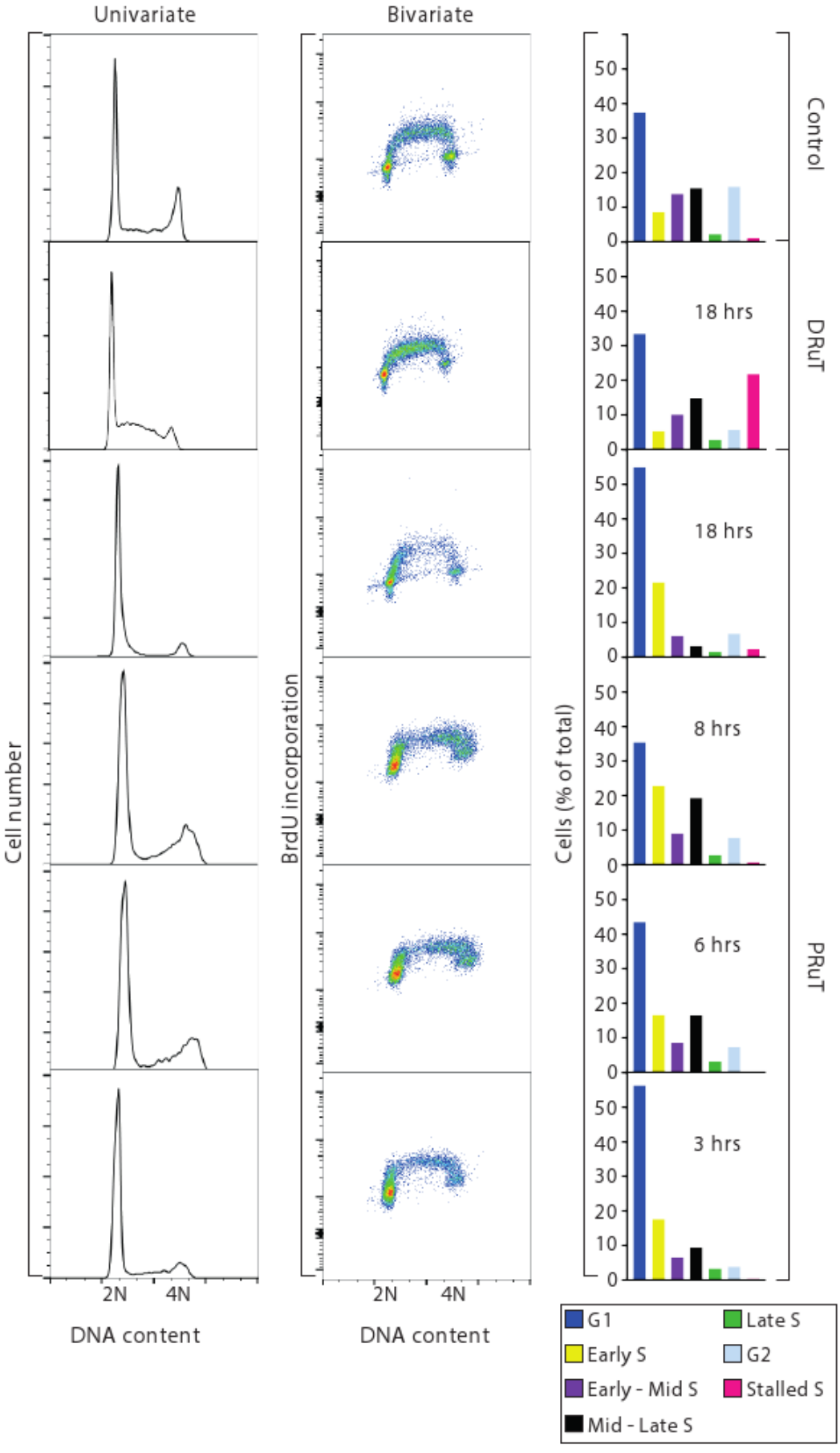
Univariate
Bivariate
Cell number
BrdU incorporation
2N
4N
DNA content
2N
4N
DNA content
Cells (% of total)
Control
18 hrs
DRuT
18 hrs
8 hrs
6 hrs
PRuT
3 hrs
G1
Late S
Early S
G2
Early - Mid S
Stalled S
Mid - Late S

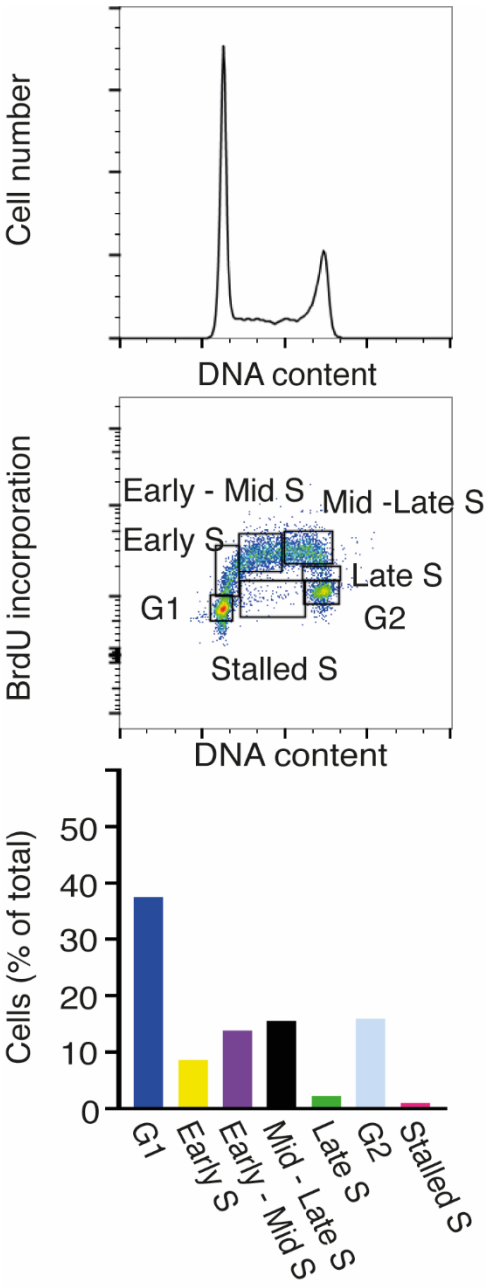

Figure 37: Graphs showing the results of FACS experiments, PI staining reveals the stage in the cell cycle, showing that DRuT causes cells to accumulate in S phase, and PRuT causes cells to accumulate in early S phase. PI staining graphs show cell number on the y axis against PI intensity on the x axis. BrdU reveals the rate of DNA replication, showing that treatment with DRuT inhibits DNA replication of the cells in S phase, whereas treatment with PRuT allows the initiation of DNA replication but it does not continue after this point. PI and AF488 staining graphs show PI intensity on the x axis, AF488 intensity on the y axis and cell number represented as colour contours. Bar charts show the number of cells in each cell cycle phase and the gates used to calculate this are shown.

The untreated cells follow the expected pattern in terms of the number of cells in each cell cycle phase and the variation in the levels of BrdU incorporation. As expected a higher proportion of cells treated with DRuT were in S phase. The horseshoe shape showing BrdU incorporation was also less pronounced, although it was not as flattened as in the previous results (see chapter 2: introduction). This shows that DRuT inhibits DNA replication which may be a reason for its toxicity. It explains the phosphorylation of Chk1 in DRuT-treated cells as Chk1 is phosphorylated in response to replication

stress and is recruited to stalled replication forks. This result also suggests that DNA is indeed a cellular target of DRuT.

After partially reproducing the results of the previous work, the impact of PRuT on the cell cycle and DNA replication was investigated. Initially the experiment was performed under the same treatment conditions as for DRuT (IC_{50} concentration for 18 hours). However shorter timepoints between 3 and 8 hours were also tested (Figure 37). Treatment with PRuT for 18 hours caused an accumulation of cells in early S phase. The univariate result alone appears to show cells arrested in G1, but the bivariate analysis reveals that these cells form the first part of the characteristic horseshoe shape, showing that cells are able to enter S phase but not proceed beyond a certain stage of DNA replication. Results for shorter treatment times support this as they show a gap appearing following the beginning of S phase, indicating the inability of cells to proceed past this specific point of the cell cycle. The cells that are already past this stage prior to PRuT treatment are presumably able to continue through mitosis and are arrested in early S phase in their next cell cycle.

These results indicate that PRuT has an impact on DNA replication but not in the same way as DRuT, where replication is inhibited. For PRuT treated cells, it appears that replication is initiated but does not continue. There are various mechanisms through which this could occur, for example, PRuT could be an inhibitor of DNA polymerase δ or ε, which control the elongation of the lagging and leading strands respectively,[188] but not DNA polymerase α, which initiates DNA replication.[189]

Alternatively PRuT could be a topoisomerase inhibitor. Topoisomerases are enzymes that allow supercoiled DNA to unwind as replication occurs. Other cancer chemotherapy drugs are known to be topoisomerase inhibitors, so this is an interesting hypothesis. To test this theory A2780 CIS cells were treated with two topoisomerase inhibitors, etoposide and camptothecin.

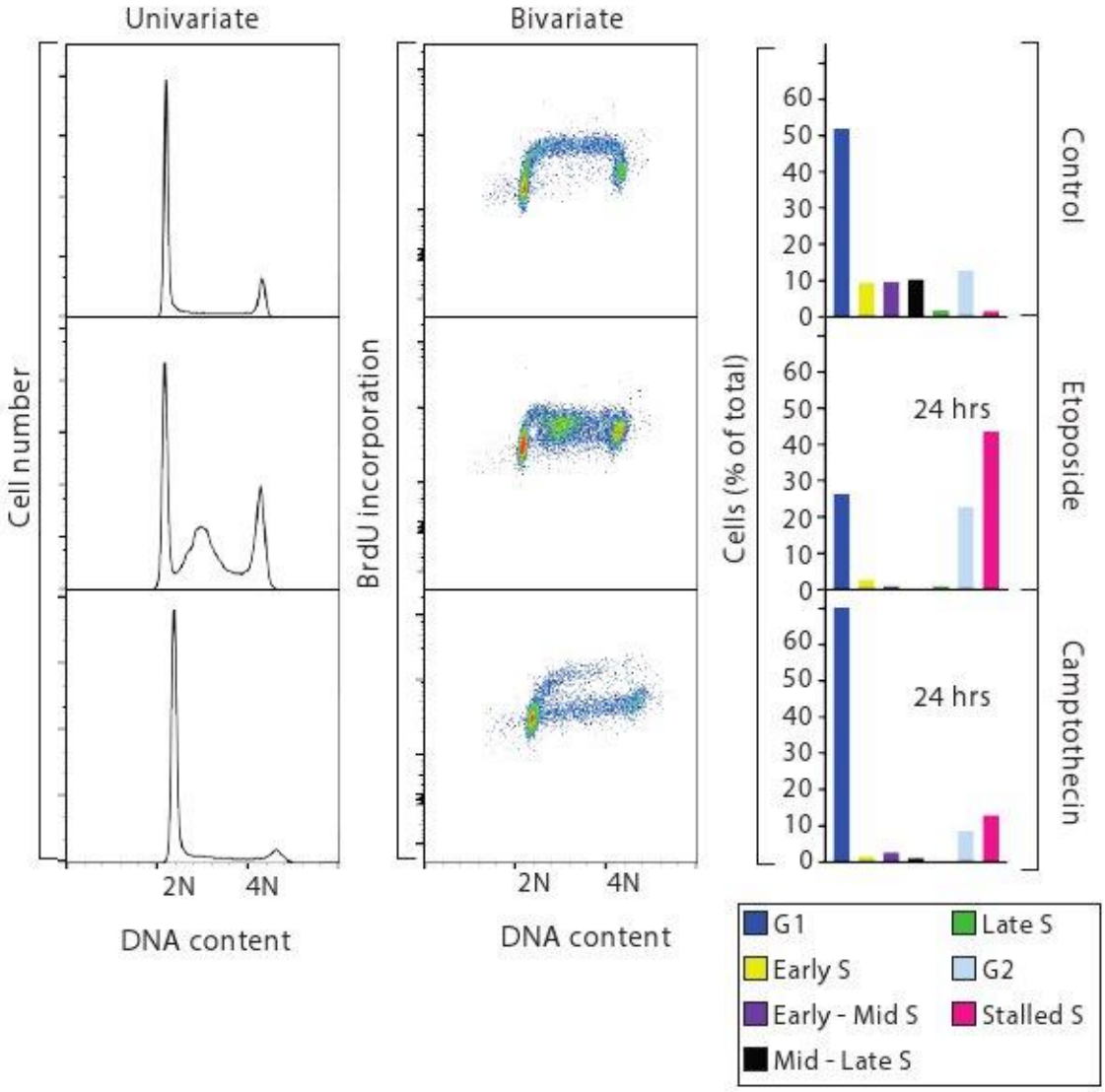

Figure 38: Graphs showing the results of FACS experiments, PI staining reveals the stage in the cell cycle. PI staining graphs show cell number on the y axis against PI intensity on the x axis. BrdU reveals the rate of DNA replication. PI and AF488 staining graphs show PI intensity on the x axis, AF488 intensity on the y axis and cell number represented as colour contours. Bar charts show the number of cells in each cell cycle phase.

Figure 38 shows that the topoisomerase II inhibitor etoposide causes a large accumulation of cells in S phase, combined with a decrease in BrdU incorporation for these cells. This shows that etoposide causes a block in DNA replication and therefore stops cells from progressing from S phase. The topoisomerase I inhibitor camptothecin causes an accumulation of cells in G1, showing that it causes a cell cycle arrest in this phase. Of the cells that are in S phase, many show a marked decrease in BrdU incorporation, confirming that camptothecin also has an impact on DNA replication.

Of the two topoisomerase inhibitors, the cell cycle profile of PRuT is most similar to that of camptothecin. However, PRuT causes a higher proportion of cells to stall in early S phase, whereas camptothecin causes most cells to stall in G1 phase. This suggests that PRuT has a mechanism of action that is distinctly different from etoposide and camptothecin and thus is not a topoisomerase inhibitor.

4.3.3 Polymerase chain reaction inhibition

PCR is a method for hugely amplifying a small amount of DNA. Since its invention it has been used in countless applications and has become an indispensable laboratory technique.

The method involves cycling through a range of temperatures and makes use of heat-stable DNA polymerases which are isolated from bacteria found in environments typically hostile to most enzymes, such as hot springs, making them able to operate at high temperatures. Two short oligonucleotide primers which are complimentary to the ends of the two strands of the DNA of interest are also used and allow the polymerase to extend them.

The first step in the reaction is at a temperature above the melting temperature of the DNA, usually 96 ^{o}C. This separates the strands of DNA to yield single-stranded DNA. Next the reaction is cooled to between 55-65 ^{o}C to allow the primers to anneal to their complementary sequences on the DNA strands. The temperature is then increased to 72 ^{o}C which allows the polymerase to extend the primers, synthesising new DNA strands. These steps are then repeated, typically 25-35 times, amplifying the quantity of DNA over several orders of magnitude.

Here PCR was used as a way to further investigate DRuT and PRuT's inhibition of DNA synthesis. The cell-free method of PCR makes conclusions about any inhibitory effects easier to draw owing to the fewer unknown variables than in cellular models. Any inhibition would either result from the complex binding to the DNA, or from the inhibition of the polymerase. This provides more information about DRuT and PRuT's inhibition of DNA replication by narrowing down the causes.

A known PCR system was used to amplify pACT-PCN1. DRuT and PRuT were added at varying concentrations to identify and quantify any PCR inhibition caused. The amount of DNA produced in a reaction was visualised by running samples on agarose gels and staining with ethidium bromide.

Figure 39 shows that both DRuT and PRuT have inhibitory effects on PCR. DRuT is the stronger inhibitor as no DNA was detected, apart from treatment with DRuT at its lowest concentration of 0.5 μM. PRuT showed a weaker effect but as its concentration increased, the amount of DNA produced in the reaction clearly decreased. At a concentration of 20 μM of PRuT, no DNA was visible on the gel.

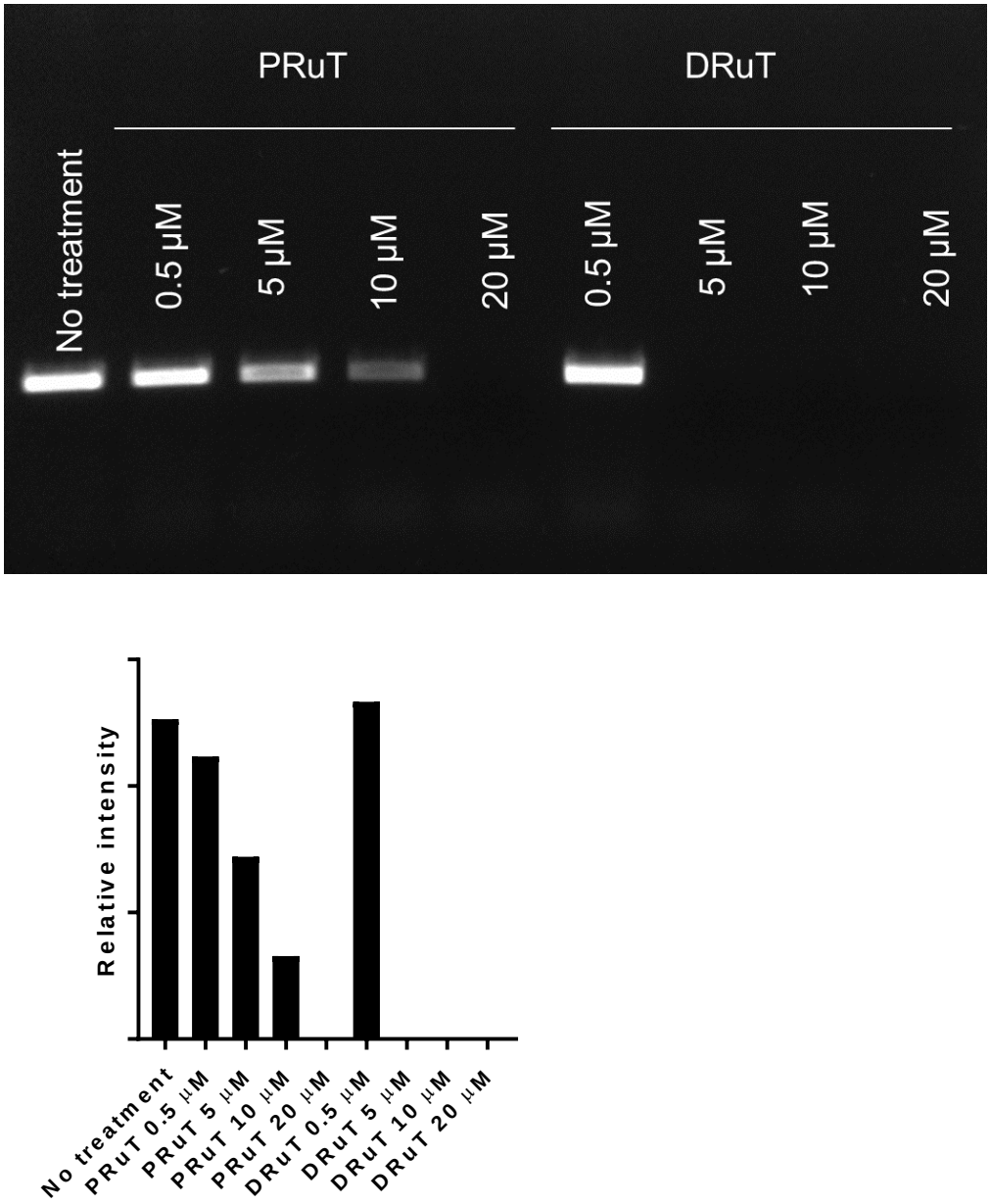

Figure 39: An agarose gel visualising the product of a PCR reaction with varying concentrations of DRuT and PRuT added to investigate their inhibitory effect. DRuT completely inhibits PCR at all concentrations but the lowest tested, 0.5 µM, whereas PRuT inhibits PCR increasingly as its concentration is increased, with full inhibition at 20 µM. A graph showing the relative intensities of the bands for each condition.

These results show that both DRuT and PRuT inhibit DNA synthesis. For DRuT this is in agreement with the flow cytometry data and it provides strong evidence that the inhibition of DNA replication for both PruT and DRuT is a result of their interactions with DNA. The only other possibility in this system is that they inhibit the polymerase.

As comparisons, the inhibitory effects of the intercalating molecules $[Ru(bpy)_2(dppz)]^{2+}$ and DRAQ5, and the groove binding molecule DAPI, were also tested. Figure 40 shows that a concentration of 20 µM all of these compounds inhibited PCR to the extent that no synthesised DNA was observed. This

shows that PRuT and DRuT both have effects consistent with other intercalating and groove binding molecules.

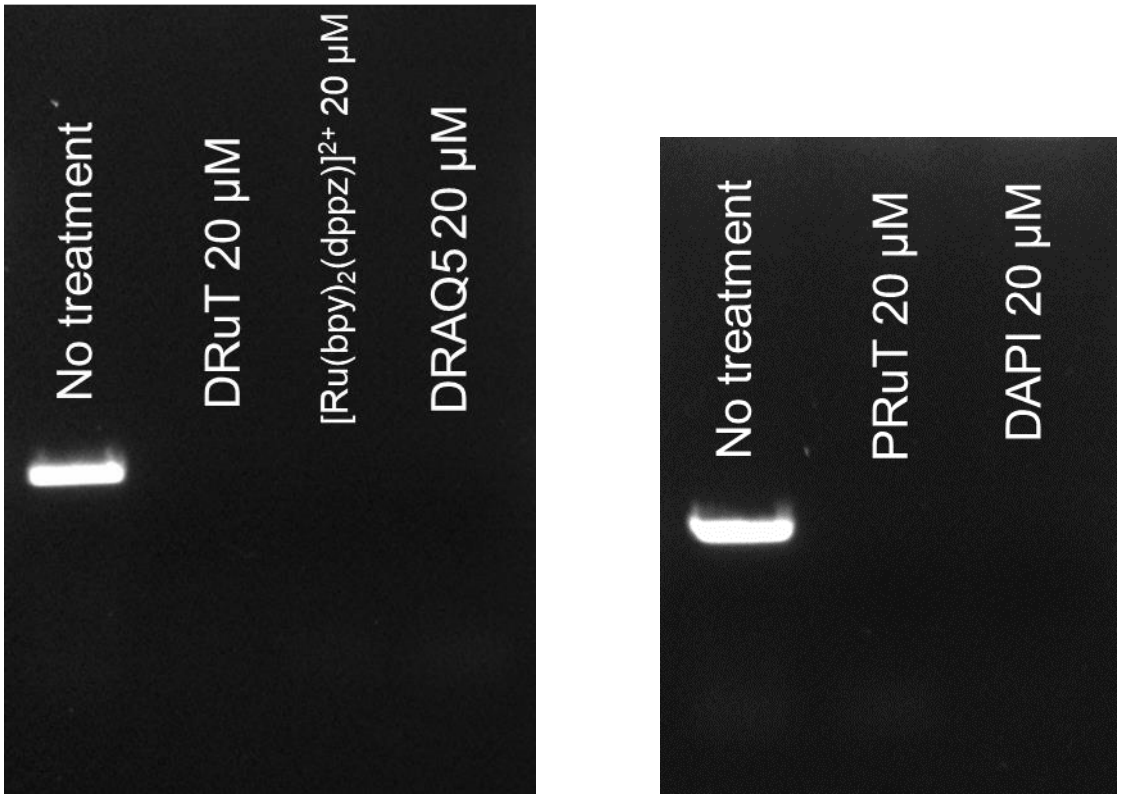

Figure 40: Agarose gels visualising the product of a PCR reaction with 20 µM DRuT, $[Ru(bpy)_2(dppz)]^{2+}$, DRAQ5, PRuT and DAPI added to investigate their inhibitory effect. All compounds tested inhibited PCR at this concentration to the extent that no synthesised DNA was observed.

Taken together with the FACS results the evidence suggests that DRuT inhibits DNA replication by binding to DNA and preventing replication forks from continuing along the double helix. The mechanism of action for PRuT is still illusive. PRuT shows signs of inhibiting DNA replication to a lesser extent than DRuT. From the FACS data, this seems to be as a result of allowing replication to initiate but not continue.

These differences may be because DRuT non-covalently binds to DNA more strongly than PRuT. The replication fork may displace or pass over PRuT lesions more easily than DRuT lesions. A higher proportion of DRuT molecules would also be bound to the DNA, meaning that there are more obstacles for the replication fork. However if this was the only difference between DRuT and PRuT, then PRuT would have the same effect as DRuT but be less potent. Although this was indicated by the PCR results, it is not the case for FACS analysis, so it appears that their differences in mechanisms of action must be due to other reasons.

4.3.4 DNA Fibre Analysis

DNA fibre analysis is a technique used to gain insight into DNA replication stress events in cells. It involves imaging individual strands of DNA from cells labelled with chlorodeoxyuridine (CldU) followed by iododeoxyuridine (IdU). From the length of the DNA fibres, the speed of travel of the replication fork can be calculated. This can provide information on replication fork speed, fork stalling and new origin formation. This powerful technique provides real insight into DNA replication at the level of individual DNA molecules from treated cells.

This technique was used to determine whether the observed DNA replication effects in the PCR inhibition experiment are also observed in cells. A2780 CIS cells were treated with DRuT and PRuT at their IC_{50} concentrations for various amounts of time, before treatment with the synthetic nucleosides CldU and IdU. Cells were first treated with CldU for precisely 20 minutes, followed by IdU for precisely 20 minutes. These precise timings allow DNA strand length to be converted to fork speed. Cells were lysed in a drop on microscope slides, and the slides were then propped up at an angle so the drops ran down the slides, spreading the DNA fibres before the slides were fixed with methanol and acetic acid. The DNA was denatured using HCl and then stained with antibodies specific to the CldU and IdU. The DNA fibres were imaged using a microscope, and the length of the DNA fibres were then measured.

DNA fibre length was measured using the software FIJI. An example of a fibre used for measurement is shown in Figure 41. The equation used to convert fibre length to speed is shown in Equation 5.

$$Speed/kbmin^{-1} = \frac{length/\mu m \times 2.59/kb\mu m^{-1}}{20\ min}$$

Equation 5

Figure 41 shows the replication fork speed for A2780 CIS cells treated with IC_{50} concentrations of DRuT and PRuT for 2, 5 and 24 hours.

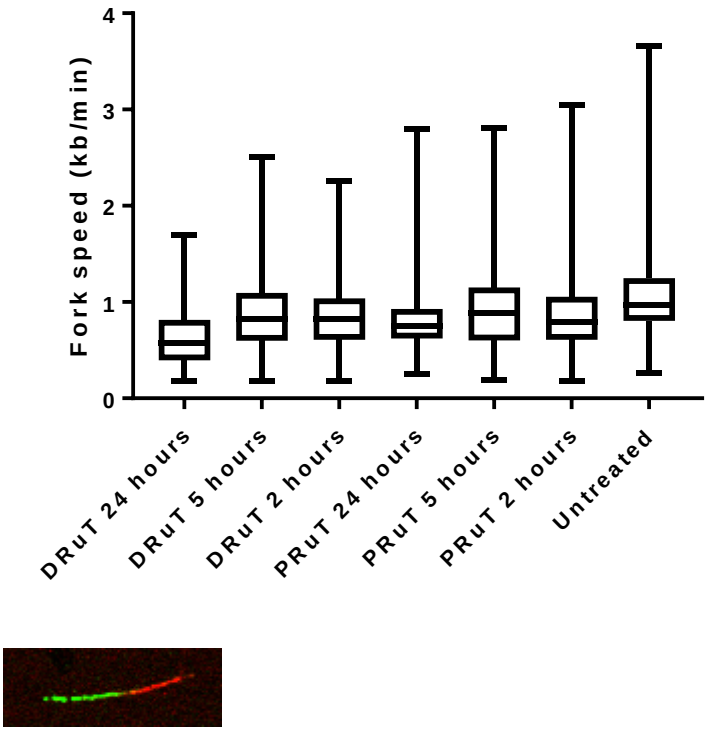

Figure 41: A box and whisker plot showing the results of DNA fibre analysis on CldU - and IdU – labelled DNA from A2780 CIS cells treated with IC_{50} concentrations of DRuT and PRuT for 2, 5 and 24 hours. Fork speed was calculated using Equation 5 after measuring the length of individual fibres. The boxes represent the interquartile range of the data, the middle line represents the median and the whiskers represent the range. 24 hour treatments of both DRuT and PRuT caused decreases in median fork speed compared to the untreated control, with DRuT having the largest effect. 2 and 5 hour treatments with both compounds caused similar modest decreases in median fork speed. An example DNA fibre stained with CldU (red) and IdU (green) is shown.

Figure 41 shows that the highest median fork speed is in untreated cells (0.96 kb/min), so all treatments had an effect on fork speed to some degree. The median fork speed after 24 hours of treatment with DRuT was 0.57 kb/min, and this treatment caused the greatest decrease in median fork speed of the conditions tested. Treatment with DRuT for 5 and 2 hours caused modest effects with median fork speeds of 0.82 and 0.83 kb/min respectively. PRuT treatment also caused a decrease in median fork speed, with 24 hours of treatment leading to a median fork speed of 0.75 kb/min. This is still a significant decrease compared to the untreated sample but the effect is smaller than that caused by DRuT. Treatment with PRuT for 5 and 2 hours caused median fork speeds of 0.88 and 0.80 kb/min respectively, similar to the results for equivalent lengths of treatment with DRuT.

These results suggest that at short timepoints (up to 5 hours) the effects of IC_{50} treatment with DRuT and PRuT on the rate of DNA replication in A2780 CIS cells are similar. However after 24 hours of treatment, DRuT causes greater retardation of replication than PRuT, though both do have an effect. This is consistent with the FACS and PCR inhibition data, which both show that DRuT causes a larger inhibition of DNA replication.

Fork asymmetry can be used to estimate the amount of replication fork stalling. This refers to a longer DNA strand on one side of an origin than the other, which suggests that one side has undergone fork stalling. An example of a new origin, used to measure fork asymmetry, is shown in Figure 42.

Two methods are commonly used to determine the frequency of replication fork stalling using DNA fibre analysis. The first involves identifying the frequency of asymmetrical forks and the second is identifying the frequency of fibres that contain only CldU, which suggests that the replication fork has stalled before the IdU treatment. In the experiments reported here, the first method was used, as not enough data was collected to draw conclusions using the second method.

To determine the amount of fork asymmetry, fibres were identified that were stained with CldU in the middle and IdU on either side. The lengths of both of the IdU stained fibres were measured and the ratio between the two lengths was calculated. If this is less than 0.75 then the replication from this origin is considered asymmetric. This suggests that one of the replication forks on either side of the origin has stalled. Figure 42 shows the percentage of asymmetrical forks under each treatment condition.

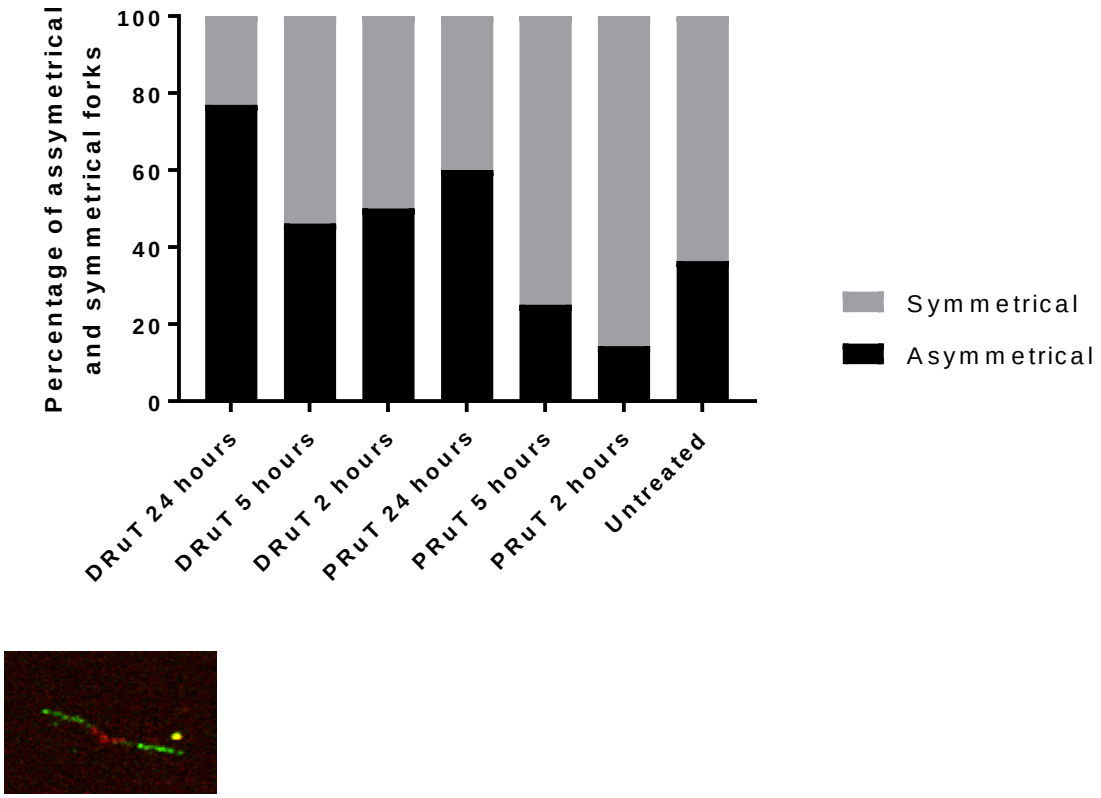

Figure 42: A bar graph showing the results of DNA fibre analysis on CldU – and IdU – labelled DNA from A2780 CIS cells treated with IC_{50} concentrations of DRuT and PRuT for 2, 5 and 24 hours. Fork asymmetry is measured from new origins, defined as a fibre stained with CldU (red) in the middle and IdU (green) on either side. The lengths of the two IdU fibres were measured and the ratio of lengths calculated. Ratios of less than 0.75 were counted as asymmetrical forks. 24 hours of treatment with both DRuT and PRuT caused an increase in the amount of fork stalling, with DRuT having the largest effect. DRuT treatment for 2 and 5 hours also caused modest increases in fork stalling, but PRuT treatment for these amounts of time did not. An example of a new origin is shown.

Figure 42 shows that the untreated sample has a relatively low number of asymmetrical forks (36%), although two other samples, PRuT 5 hours and PRuT 2 hours, have 25% and 14% asymmetrical forks respectively, which is lower than the untreated sample. This is likely due to the low number of forks counted for each condition (between 4 and 15), rather than being due to low timepoint PRuT treatments protecting against fork stalling, which seems unlikely given that overall these treatments both decreased fork speed (Figure 41). A larger number of repeats of this experiment would give a better indication of the true effects of all treatments, so results from this analysis must be treated with caution.

DRuT treatment for 24 hours causes the largest percentage of asymmetrical forks (77%), which is consistent with the results from the fork speed analysis and suggests that DRuT slows average fork speed by causing replication forks to stall. DRuT treatment for 5 and 2 hours also caused an increase in the number of asymmetric forks, with 46% and 50% asymmetrical forks respectively, suggesting that DRuT starts to have an effect on DNA replication within this timeframe. This is consistent with western blots showing some Chk1 phosphorylation after 1 hour, and a large amount of phosphorylation after 3 hours.

PRuT treatment for 24 hours causes an increase in the number of asymmetrical forks (60%). As in the case of overall fork speed this is a smaller effect than that caused by DRuT, in agreement with the PCR inhibition data. As previously mentioned 2 and 5 hours of PRuT treatment caused a lower number of asymmetrical forks than no treatment in this experiment, which does not suggest that PRuT has any effect on DNA replication at these timepoints. However this contradicts the fork speed data which is likely to be more reliable due to the much larger number of data points.

Overall these results confirm the effect that PRuT and, particularly, DRuT, have on DNA replication. However the DNA fibre technique used in this way cannot distinguish between stalled and collapsed replication forks, which could be needed to explain the differences in activity between these two complexes. This is discussed further in the Rad51 Immunofluorescence (IF) section.

4.3.5 Rad51 Immunofluorescence

One still unanswered question is: why does PRuT cause a γ-H2AX signal in treated cells but not appear to cause DSBs? This could be answered by further investigating the effect PRuT has on DNA replication. Collapsed replication forks can be turned into DSBs by cells, or cause unusual DNA structures such as so-called ‘chicken foot structures’ which can be mistaken by the cell for DSBs, due to the presence of an exposed DNA end.[190] This could be the reason for the γ-H2AX signal.

Rad51 is a DNA repair protein.[191] It is involved in the HR of DSBs, and also in the stabilisation of stalled replication forks in an effort to protect them from collapsing into DSBs. It is known to form

nuclear foci in response to replication fork collapse as it becomes involved in HR to repair these collapses. However it doesn't form foci when it is simply stabilising stalled, but not collapsed, replication forks.[21] For this reason, monitoring the formation of Rad51 foci by IF after treatment with DRuT and PRuT, was used to investigate the hypothesis that PRuT causes the widespread collapse of replication forks and DRuT does not.

HU treatment was used as a positive control for this experiment. HU causes a depletion of nucleotide pools and therefore causes replicative stress. After 1 or 2 hours, replication forks simply stall, however over longer periods stalled forks collapse, leading to the formation of Rad51 foci. After a treatment of 24 hours many replication forks will have collapsed and Rad51 foci should be noticeably formed. Therefore, in order to test the validity of the experiment it was performed first 24 hours after 2 mM HU treatment.

IF was used to visualise Rad51 foci. For this technique cells are grown on coverslips, then fixed and permeabilised. They are probed with antibodies for a protein of interest (in this case Rad51) and then stained with fluorescent secondary antibodies. Fluorescence microscopy is used to image the cells, for example widefield or confocal microscopy.

4.3.5.1 Protocol Optimisation

A2780 CIS cells were grown on coverslips and treated with 2 mM HU for 24 hours. They were fixed and permeabilised, then Rad51 was stained by use of a primary antibody and an AF488 conjugated secondary antibody. Cells were also stained with the nuclear dye DAPI and were visualised by deconvolution widefield microscopy. Nuclear foci were counted and an average number of foci per cell was calculated.

Initially cells were fixed with a mixture of acetone and methanol. This permeabilises the cells as well as fixing them. 0.2% fish skin gelatin (FSG) in PBS was used as a blocking buffer and the primary antibody was used at a concentration of 1:500. The mounting agent Prolong Gold was used to mount the coverslips. This protocol gave rise to high levels of consistent staining throughout the cells and nuclei (Figure 43). Foci were observed and appeared to be more prevalent in HU treated cells, but there were foci outside of the nuclei as well as inside which should not have been observed given that Rad51 foci should appear at sites of DNA damage.

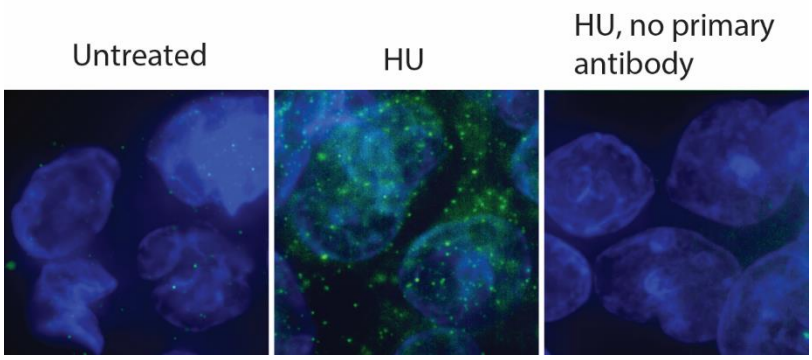

Figure 43: IF images showing results of the first protocol used to visualise Rad51 foci. DAPI is shown in blue and Rad51 in green. Images are shown for untreated, HU treated and HU treated with no primary antibody used. As expected no Rad51 is seen in the sample with no primary antibody. The HU treatment has caused a large increase in Rad51 compared with no treatment, however some of the Rad51 is not formed into foci and many foci are outside of the nucleus.

The protocol was repeated using paraformaldehyde (PFA) fixation rather than acetone/methanol. PFA fixes cells by crosslinking proteins, forming methylene bridges between primary amines. It does not permeabilise cell membranes as acetone/methanol does, so this is achieved after fixation by treating with 0.2% Triton X-100 (a detergent) in PBS. This protocol did cause distinct foci (Figure 44) but again these were observed outside of the nuclei as well as inside.

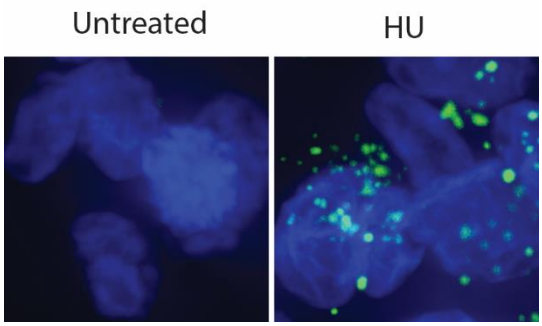

Figure 44: IF images visualising Rad51 foci after PFA fixation rather than acetone/methanol. Again, HU treatment has caused a large increase in Rad51 foci, however they are outside as well as inside the nuclei.

In an attempt to improve the signal:noise ratio higher primary antibody concentrations up to 1:100 were used and HU was used at a higher concentration of 20 mM. However, this did not improve the result (Figure 45), and from literature searches it was determined that 2 mM HU is generally sufficient to cause DNA damage.[21]

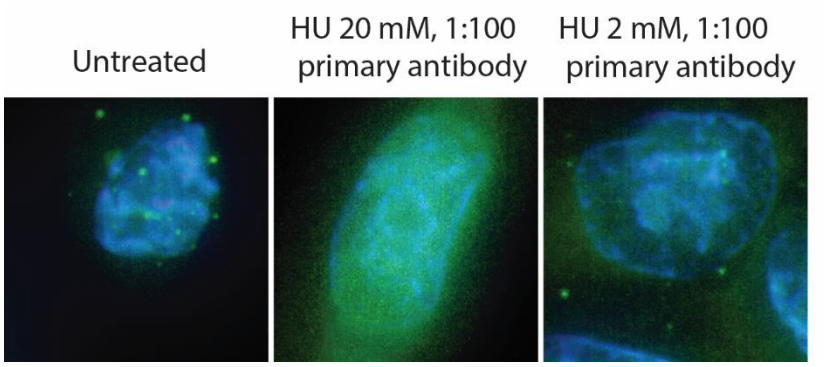

Figure 45: IF images visualising Rad51 foci, using higher primary antibody and HU concentrations. These changes did not increase the number of Rad51 foci in treated samples compared to untreated, but they did increase the levels of background staining.

A major issue with the protocol was that of background staining: Rad51 that appeared to be distributed evenly throughout the cell rather than formed into foci. Removal of this background staining would improve the signal and so a pre-extraction step was added to the protocol. Prior to fixation, cells were incubated on ice with 0.2% Triton X-100 for 10 minutes. This was combined with both PFA and acetone/methanol fixation to determine the optimal conditions. In addition the mounting agent was changed from Prolong Gold to Duolink as Prolong Gold was found to adversely affect the morphology of the cells at the point of imaging, possibly by dehydrating them. This protocol did reduce the background staining (Figure 46). Although some foci were observed, the signal was weak, many foci appeared outside of the nucleus and there did not appear to be a significant difference between the number of foci in treated and untreated cells. Attempted optimisation of the fixation and permeabilisation conditions did not improve the results (Figure 47).

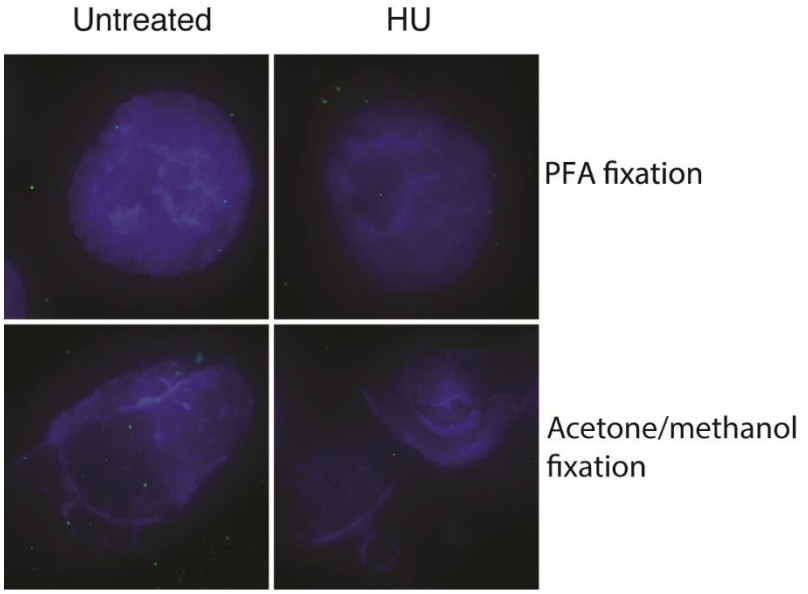

Figure 46: IF images visualising Rad51 foci after the addition of a pre-extraction step in the protocol. PFA and acetone/methanol fixation are compared. The amount of background staining is greatly reduced by the pre-extraction, but there is no noticeable difference between treated and untreated samples and many foci appear outside the nuclei.

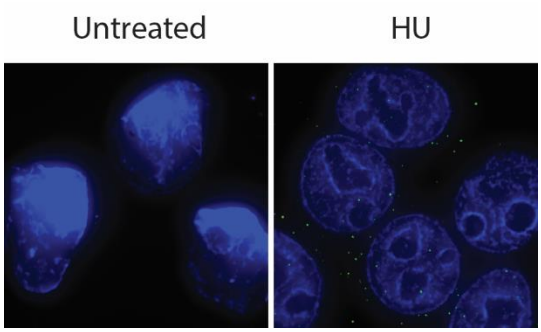

Figure 47: IF images visualising Rad51 foci following further optimisation of the protocol by altering fixation and permeabilisation conditions. The difference between treated and untreated samples is more obvious in this case, but there are still many foci appearing outside the nuclei.

The foci appearing outside of the nuclei was a particularly concerning issue, as foci formation is linked to DNA repair and should only be taking place in the nucleus. In some samples foci appeared just as concentrated outside the nuclei as inside, suggesting that the signal observed could be just background staining and was not indicative of DNA damage caused by HU treatment.

It was hypothesised that the non-nuclear foci were due to repair of mitochondrial DNA, as Rad51 has been shown to accumulate in the mitochondria in response to DNA damage.[192] In order to test this, cells were stained with Mitotracker Red (a mitochondria dye) in addition to the usual protocol, to determine whether the non-nuclear foci colocalised with the Mitotracker. Figure 48 shows that the Mitotracker did not generally colocalise with the green signal outside the nucleus. Therefore the hypothesis that these foci were related to mitochondrial DNA was discounted.

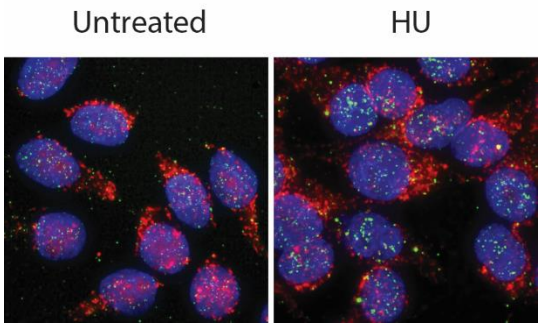

Figure 48: IF images visualising Rad51 foci. Cells were stained with Mitotracker (shown in red) to determine whether Rad51 foci outside of nuclei were caused by repair of mitochondrial DNA. The Mitotracker does not colocalise with the Rad51 foci, disproving this hypothesis.

Another possibility was that this issue was cell-line specific. There are few examples of Rad51 IF in A2780 CIS cells in the literature, this could be due to difficulty in observing Rad51 foci in this cell line. The specific mechanism of cisplatin resistance in this cell line has not been fully determined, and if this cell line has defects in DNA repair mechanisms this could mean that HR cannot occur, meaning that Rad51 foci may not be observed after DNA damaging treatment. To test this, the human osteosarcoma cell line U2OS was used for a parallel experiment. This cell line has been used extensively in the literature showing Rad51 foci after HU treatment and is used because the cells are relatively large and flat, offering an advantage for imaging. The cells were also stained with Mitotracker. In this cell line

foci did appear more concentrated in the nuclei, however there were still a significant number outside (Figure 49). These non-nuclear foci did not colocalise with the Mitotracker, again providing evidence against the hypothesis that they are caused by mitochondrial DNA repair.

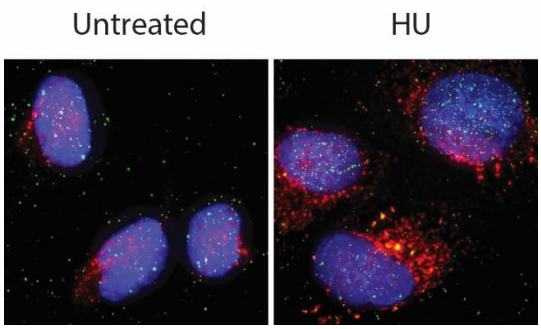

Figure 49: IF images visualising Rad51 foci in U2OS cells. Cells were stained with Mitotracker (shown in red). The results are an improvement over those in A2780 CIS cells as there is an obvious increase in the number of foci in treated compared to untreated cells, and a lot of foci are located in the nuclei. However there are still a significant number of foci outside of the nuclei and these do not colocalise with the Mitotracker.

Another plausible explanation for the issue of foci outside of the nuclei is that they are the result of background staining caused by the primary antibody not penetrating the nuclei of the cells. For some nuclear IF, specific protocols are employed designed to penetrate nuclei. To test this hyothesis, a protocol specifically designed for nuclear proteins was used with A2780 CIS cells. This involved incubating treated cells with a permeabilisation buffer which was 0.5 % Triton X-100, 0.2 µg/ml EDTA and 1% BSA in PBS. Cells were incubated in permeabilisation buffer on ice for 15 minutes, and then fixed with methanol. For this experiment, cells were blocked in 3% goat serum in PBS. Although this seemed to remove non-nuclear staining, the number of foci appeared equivalent in the treated and untreated samples (Figure 50).

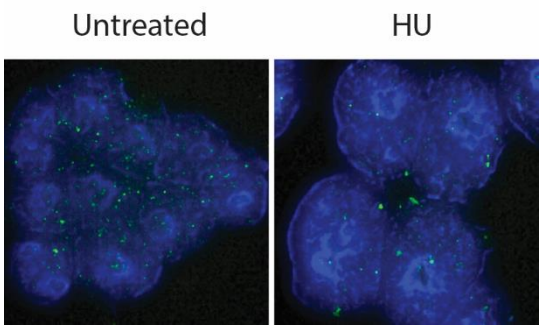

Figure 50: IF images visualising Rad51 foci after a nuclear permeabilisation protocol was used in A2780 CIS cells. This removed foci outside of the nuclei, however it decreased the difference in the number of foci between treated and untreated cells.

In addition, the original protocol was used with goat serum as the blocking agent instead of FSG. However this did not appear to alter the results (Figure 51).

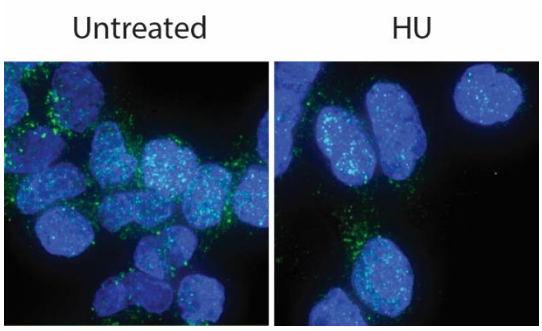

Figure 51: IF images visualising Rad51 foci using the previous optimised protocol but with blocking buffer containing goat serum rather than fish skin gelatin. This did not improve the appearance of the images.

In order to troubleshoot the experiment, the primary antibody was tested with a western blot on lysates of A2780 CIS cells treated with 2 mM HU. This showed a band at around 37 kDa, the expected molecular weight of Rad51. There was an issue with lysate spilling into adjacent lanes when loading the gel, as can be seen by bands present in lanes that were not loaded. The intensities of the bands were quantified, normalised to the intensities of the β-actin bands. No non-specific bands were visible unless the Rad51 band was highly overexposed, showing that the antibody was specific for Rad51 (Figure 52). In addition, these lysates were used in a western blot for γ-H2AX to confirm that the treatment conditions were inducing DNA damage as expected. Figure 53 shows that HU treated cells caused an increase in the amount of γ-H2AX in the cell lysate compared to untreated cells. This confirms that HR should be occurring more in the treated cells, and therefore Rad51 should be forming foci in these cells. Similar issues with loading were encountered with this western blot, and again band intensities are quantified and normalised to the intensities of the β-actin bands.

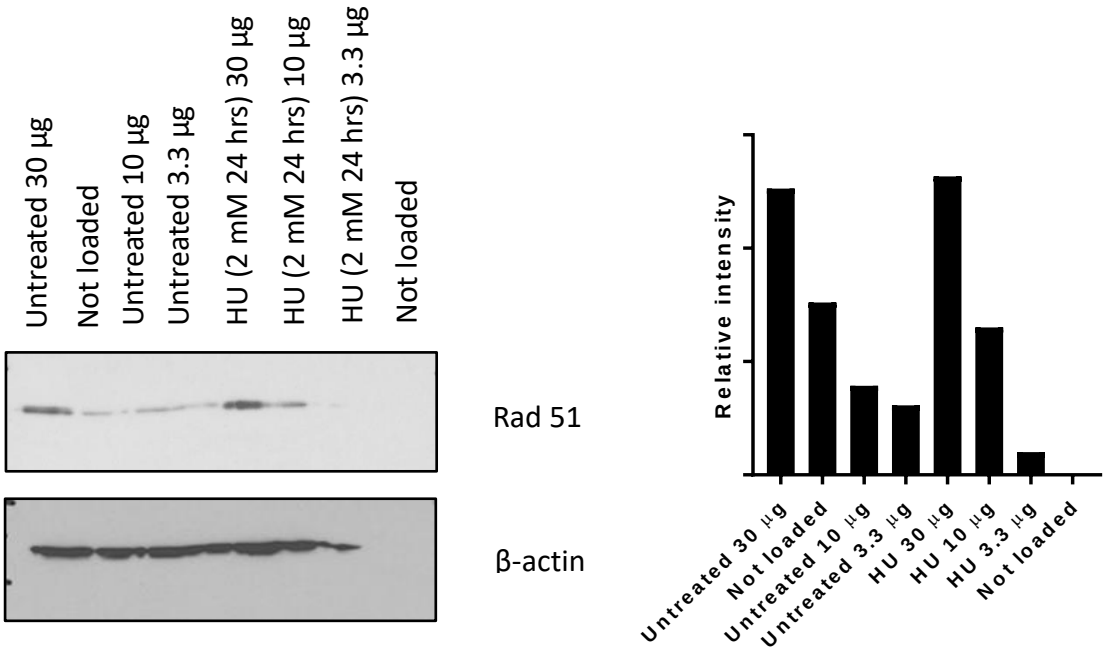

Figure 52: Rad51 western blot on HU treated cells, showing that HU treatment increases Rad51 levels in cells. Quantification of the intensity of the Rad51 bands normalised to the intensities of the β-actin bands.

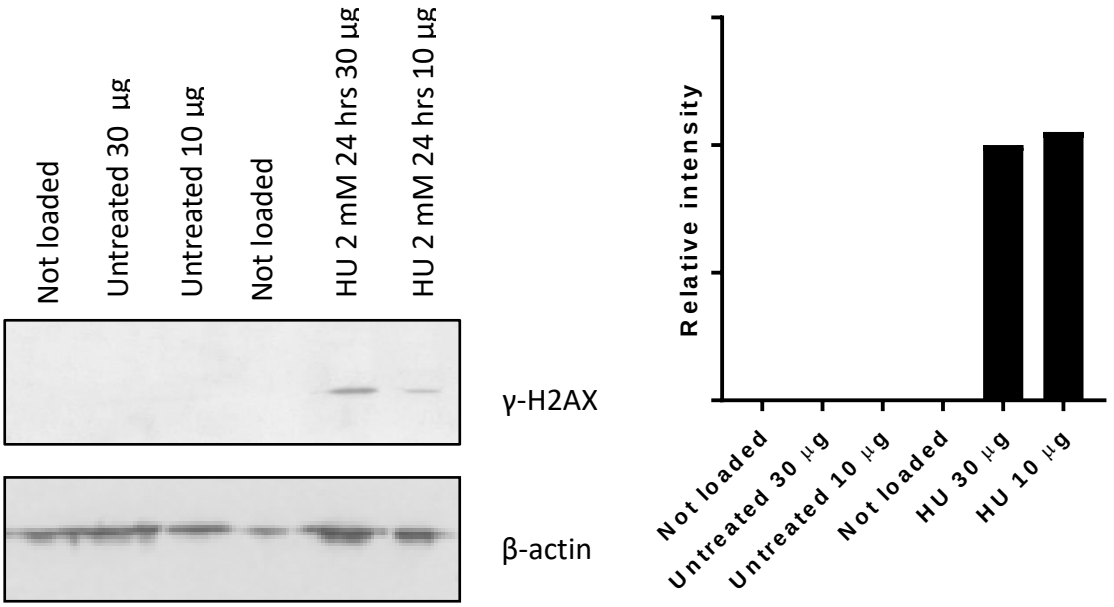

Figure 53: γ-H2AX western blot on A2780 CIS cells, showing that HU treatment causes γ-H2AX activation, confirming that the HU treatment conditions used induce DNA damage. Quantification of the intensity of the γ-H2AX bands normalised to the intensities of the β-actin bands.

Ultimately several adjustments were made to the protocol used, leading to a clear difference between HU positive and negative cells being observed, and a great reduction in non-nuclear staining. These changes are outlined below.

It was important to ensure that cells were not highly confluent before seeding onto coverslips (not more than around 60%). This is because confluent cells may enter senescence and not be actively progressing through the cell cycle. HR occurs after the collapse of replication forks which can only occur during S phase.

Fixation and permeabilisation conditions of 4% PFA and 0.1% Triton X-100 in PBS were used. Washes were performed after fixation and between antibody treatments but there was no other blocking step. The washing buffer used was 0.15% BSA and 0.1% Triton X-100 in PBS. The washes were all performed with gentle shaking which may have resulted in more effective washing.

The antibodies were diluted in 3% BSA in PBS and the primary antibody treatment was incubated overnight at 4 ^{o}C rather than for one hour at room temperature. This may have allowed for a better signal to noise ratio.

The experiment was performed in U2OS cells as well as A2780 CIS cells to compare results between the two; these are shown in Figure 54. The protocol improved the results over previous experiments in both cell lines in that background staining was reduced, foci outside of nuclei were reduced and the difference between treated and untreated cells was more pronounced. More background staining was observed in A2780 CIS cells; however it was at a level that was deemed acceptable. A2780 CIS cells were used for further experiments.

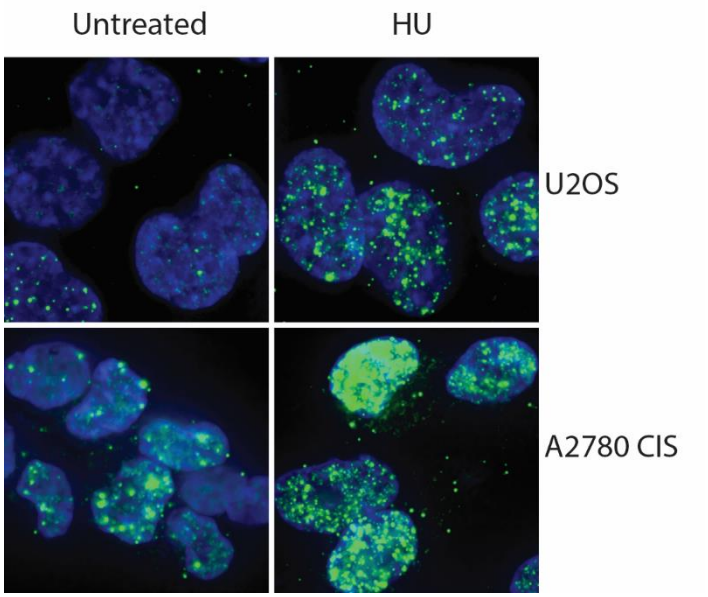

Figure 54: IF images visualising Rad51 foci using the new protocol. A2780 CIS and U2OS cells are compared. For both cell lines the difference between treated and untreated cells is more pronounced, and foci are mainly confined to the nuclei.

The results of this experiment were quantified by counting the number of foci per cell using the software FIJI. The numbers of foci per cell were grouped into the categories 0 to 5 (considered negative for Rad51 foci), 6 to 10, 10 to 15 and 15 to 20 (intermediately positive) and > 20 (very positive). Figure 55 shows the histogram produced. The histograms for HU treated and untreated cells have opposite

distributions. For untreated cells, 63% have 0 to 5 foci and 7% have over 20 foci. In contrast, of the treated cells 15% had 0 to 5 foci and 53% over 20 foci. This is a clear indication that the HU treatment caused a high level of DNA damage - and therefore Rad51 foci - compared with untreated cells, and this can be used as a positive control for the experiment comparing DRuT and PRuT. If the hypothesis on the difference between DRuT and PRuT is correct then the distribution for PRuT should be more similar to that for HU and the distribution for DRuT should be comparable to that for untreated cells.

4.3.5.2 Comparison of DRuT and PRuT

The optimised protocol was used to determine the levels of foci after treatment of A2780 CIS cells with 50 μM DRuT and PRuT for 8 hours (Figure 55). Visually both treatments appear to cause some Rad51 foci and they are difficult to distinguish. The analysis performed on this data was used to distinguish between the two data sets. Histograms showing the number of foci per cell for DRuT and PRuT treatments are in Figure 55.

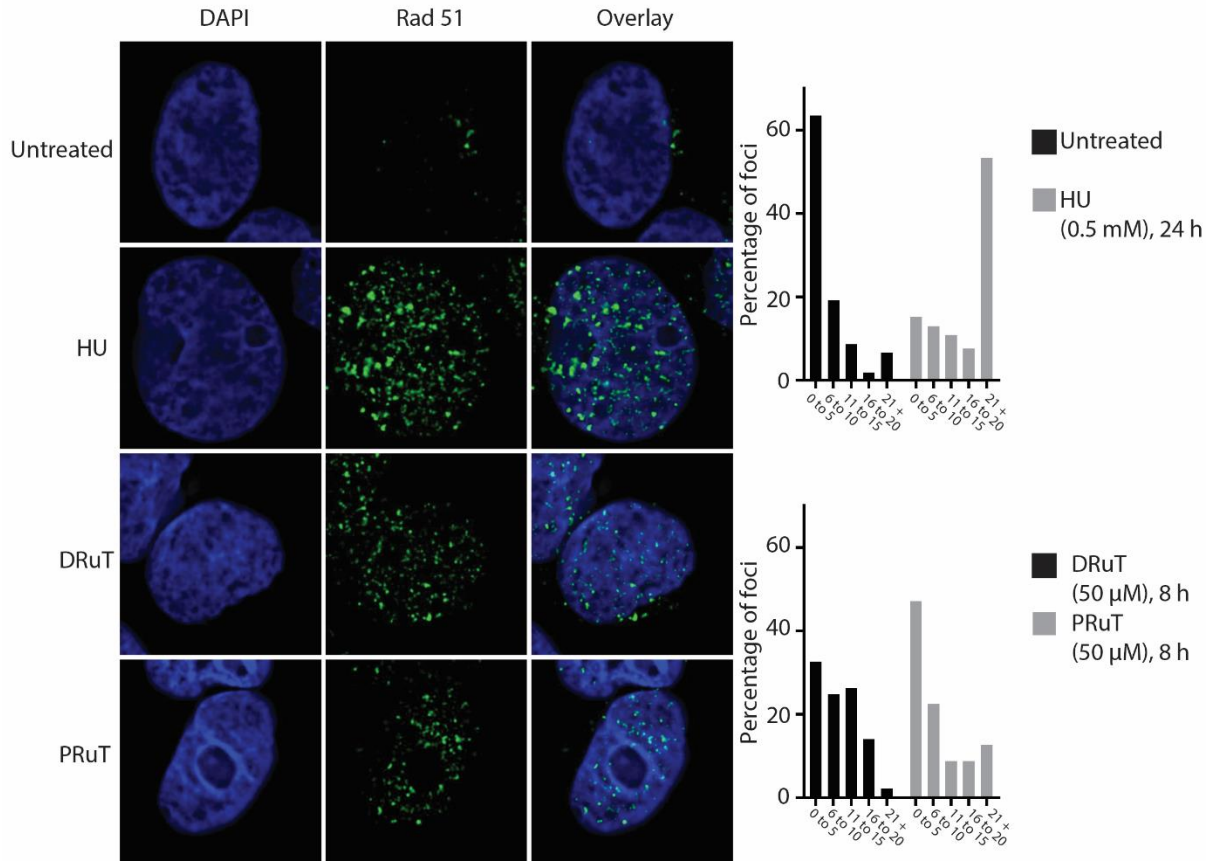

Figure 55: IF images visualising Rad51 foci in A2780 CIS cells treated with HU, DRuT and PRuT. Graphs quantifying the images, showing the number of cells with different numbers of foci. Untreated and HU treated cells have opposite distributions, showing that HU causes significant numbers of Rad51 foci.

For PRuT 47% of cells have 0 to 5 foci compared to 33 % for DRuT, which does not support the hypothesis. However, for PRuT 13% of cells have over 20 foci compared with 2% for DRuT. This does support the hypothesis, showing that PRuT causes more cells to have high levels of Rad51 foci. The median number of Rad51 foci per cell is 6 for PRuT and 9 for DRuT. This suggests that overall PRuT does not cause an increased number of Rad51 foci compared to DRuT. However both medians are higher than that for untreated, which is 4.

This evidence is inconclusive. The larger number of cells very positive for Rad51 foci after PRuT treatment could indicate that in these cells there are enough collapsed replication forks to trigger Chk2 and γ-H2AX phosphorylation. However, the median values, and the fact that PRuT treatment caused a larger number of cells negative for Rad51 foci, suggest that replication fork collapse vs stalling may not be the reason for the difference between the cellular effects of PRuT and DRuT.

4.4 Mitochondrial effects

In addition to adversely affecting DNA replication, presumably through binding to DNA, DRuT and PRuT may have direct effects on the mitochondria of cells, leading to cell death. In recent years evidence has been found that cisplatin acts in this way in addition to its DNA damaging properties (see chapter 2: introduction). This has paved the way for other metal-based drugs to be studied to determine whether they exhibit similar effects.

4.4.1 Mitochondrial membrane potential

In general, the mitochondrial health of a population of cells can be determined by measuring mitochondrial membrane potential. A decrease in mitochondrial membrane potential is one of the early stages of mitochondrial apoptosis. Simple assays can be employed to determine whether changes in mitochondrial membrane potential occur in response to drug treatments. These can then help determine whether more detailed assays are necessary.

Tetramethylrhodamine, ethyl ester (TMRE) is a positively charged dye used in live cells which accumulates in negatively charged mitochondria. If the mitochondrial membrane potential decreases then the mitochondria become less positively charged and so less TMRE accumulates in them. The amount of TMRE present can be determined by measuring its fluorescence intensity as it has an emission at 575 nm.

Cisplatin has been shown to cause disruption to the mitochondrial membrane. DRuT and PRuT may also have effects, such as this, in cells which are not related to their DNA binding properties. TMRE assays could be used as a simple method to determine whether DRuT and PRuT disrupt mitochondrial membrane potential.

To achieve this a microplate TMRE assay was performed. A2780 CIS cells were seeded in a 96-well plate, and after 24 hours wells were treated in triplicate with IC_{50} concentrations of DRuT and PRuT. Cells were treated for 24, 8, 3 and 1 hours. Untreated control wells were treated with equivalent concentrations of DMSO. 20 μM FCCP (carbonyl cyanide-p-trifluoromethoxyphenylhydrazone) treatment for 1 hour was used as a positive control for decreasing mitochondrial membrane potential. Cisplatin at IC_{50} concentration for 24 hours was also used as a positive control.

After compound incubation, TMRE was added to wells and incubated for 20 minutes. The media was then removed, cells were washed once with 0.2% BSA in PBS, which was then replaced for fluorescence measurement. Fluorescence was measured using a microplate reader with an excitation

wavelength of 544 nm and an emission wavelength of 590 nm. The fluorescence intensity was plotted for each condition and is shown in Figure 56.

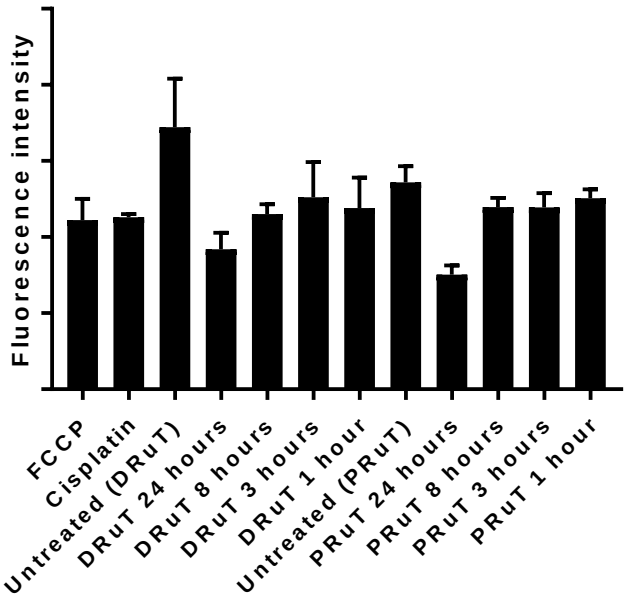

Figure 56: A graph showing the results of a TMRE assay on A2780 CIS cells treated with FCCP, DRuT and PRuT. The fluorescence intensity corresponds to the amount of TMRE retained in the mitochondria of the cells, and a higher value indicates a higher mitochondrial membrane potential. The positive control, FCCP, causes a small decrease in fluorescence intensity, and both DRuT and PRuT cause a larger decrease at the 24 hour timepoint.

Higher fluorescence intensity corresponds to a larger amount of TMRE retained in the mitochondria of the cells, and therefore a higher mitochondrial membrane potential. A lower fluorescence intensity shows that the mitochondrial membrane potential has been lowered.

FCCP was a positive control in this experiment and caused a lowering in mitochondrial membrane potential from a fluorescence intensity of 34400 for untreated (DMSO concentration equal to DRuT samples) to 22200. The fluorescence intensity for untreated (DMSO concentration equal to PRuT samples) was 27200, so the difference between this and the FCCP result was much less, likely due to the higher DMSO concentration.

The results show that after 24 hours of IC_{50} treatment, DRuT caused a substantial decrease in mitochondrial membrane potential, with fluorescence intensity decreasing from 34400 to 18400, a reduction of almost half and a larger effect than FCCP and cisplatin. This shows that DRuT does indeed have an effect on the mitochondrial membrane potential. However care should be taken in interpreting the 24 hour timepoint as by this point cells may have started to undergo apoptosis, which involves the disruption of the mitochondrial membrane. It is plausible that cellular apoptosis could be the result of DRuT's DNA binding effects, which causes the decrease in mitochondrial membrane potential observed in this assay.

At the shorter timepoints DRuT caused a smaller effect on mitochondrial membrane potential. After 8 hours of treatment the fluorescence intensity decreased from 34400 to 23000. After 3 hours it was 25200 and after 1 hour it was 23800. The result from the 8 hour timepoint was significantly different to untreated with a p value of <0.05, however the 3 and 1 hour timepoints were not significantly different to untreated with p values of >0.05. Statistics were calculated using unpaired 2-tailed t tests. This suggests that DRuT does not have a large effect on mitochondrial membrane potential quickly after treatment, however it does appear to have an effect after 8 hours. This effect could be independent of DRuT's DNA binding properties.

Similarly, PRuT causes a substantial decrease in mitochondrial membrane potential after 24 hours of IC_{50} treatment. The fluorescence intensity decreased from 27200 to 15100. This is a slightly smaller decrease than DRuT caused over 24 hours, but the effects are similar in magnitude. At the 8, 3 and 1 hour timepoints for PRuT the fluorescence intensities were 23900, 23900 and 25100 respectively, none of which are significantly different from untreated. This suggests that PRuT has a smaller effect on mitochondrial membrane potential than DRuT and has no effect at timepoints up to 8 hours.

These results suggest that one of the reasons DRuT is more cytotoxic towards A2780 CIS cells than PRuT is that it has a larger effect on mitochondrial membrane potential, possibly independent of its DNA binding properties. It is possible that these two properties work in tandem to induce apoptosis. The mitochondrial effects could help DRuT to induce apoptosis in the absence of Chk2 and γ-H2AX activation.

4.4.2 Autophagy and mitophagy

Autophagy is a process whereby cells degrade and recycle components of themselves. It is part of the normal functioning of cells but can increase in times of cellular stress. Mitophagy is a form of autophagy where mitochondria undergo autophagy. Mitochondria that are damaged will be degraded and recycled by mitophagy, so damage to mitochondria will increase the amount of mitophagy occurring in a cell.

If mitochondria are damaged by DRuT and PRuT there may be an increase in autophagy, and specifically mitophagy. Therefore, an experiment was devised to determine whether this is the case.

A fluorescently tagged protein was used for this experiment. LC3 is a marker for autophagosomes. The protein used was ptfLC3 which is tagged with both green fluorescent protein (GFP) and red fluorescent protein (RFP).[193] The protein can be transfected into cells which are then imaged using confocal microscopy. Autophagosomes can be located as they are marked by both green and red fluorescence and thus appear yellow.

In the later stage of autophagy, autophagosomes fuse with lysosomes for degradation, which have an acidic pH. GFP degrades in an acidic environment whereas RFP does not. For this reason when autolysosomes are formed, and green emission is removed, the fluorescence changes from yellow to red.

For this experiment various positive controls were used. Serum starvation induces autophagy and this was achieved by incubating cells with EBSS (Earle's Balanced Salt Solution) medium for 4 hours. EBSS combined with bafilomycin treatment for 2 hours was used as a positive control for autolysosome formation as it blocks autophagy at this stage. Carbonyl cyanide m-chlorophenyl hydrazone (CCCP) was also used as a positive control for mitophagy.

A2780 CIS cells were seeded on coverslips and after 24 hours were transfected with ptfLC3 plasmid using Lipofectamine according to the manufacturer's instructions. The transfection lasted for 48 hours, and, at the appropriate times, cells were treated with IC_{50} concentrations of DRuT, PRuT, and the positive controls. After treatment, cells were washed and fixed with PFA. They were treated with DAPI and coverslips were mounted using Prolong Gold. Cells were imaged using confocal microscopy. Figure 57 shows an example of images obtained.

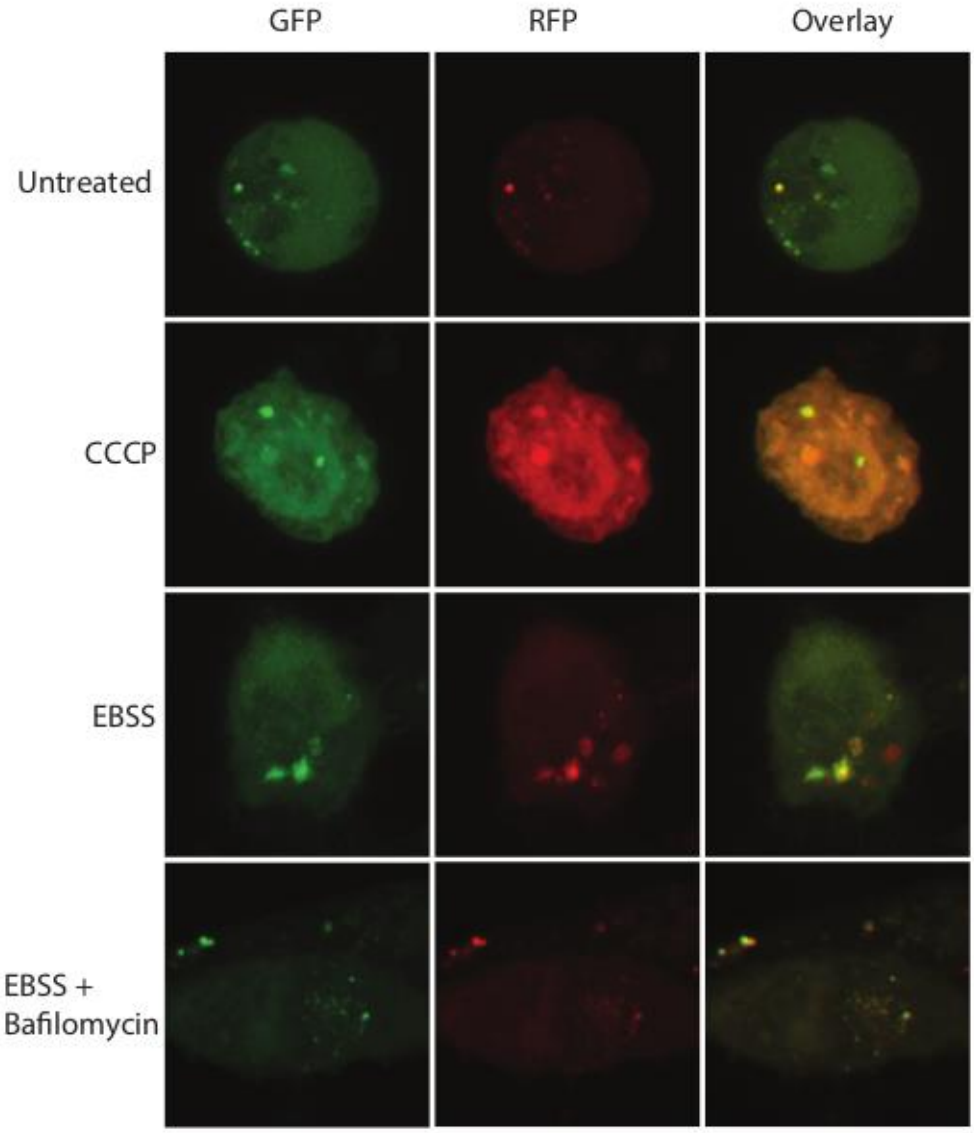
GFP
RFP
Overlay
Untreated
CCCP
EBSS
EBSS +
Bafilomycin

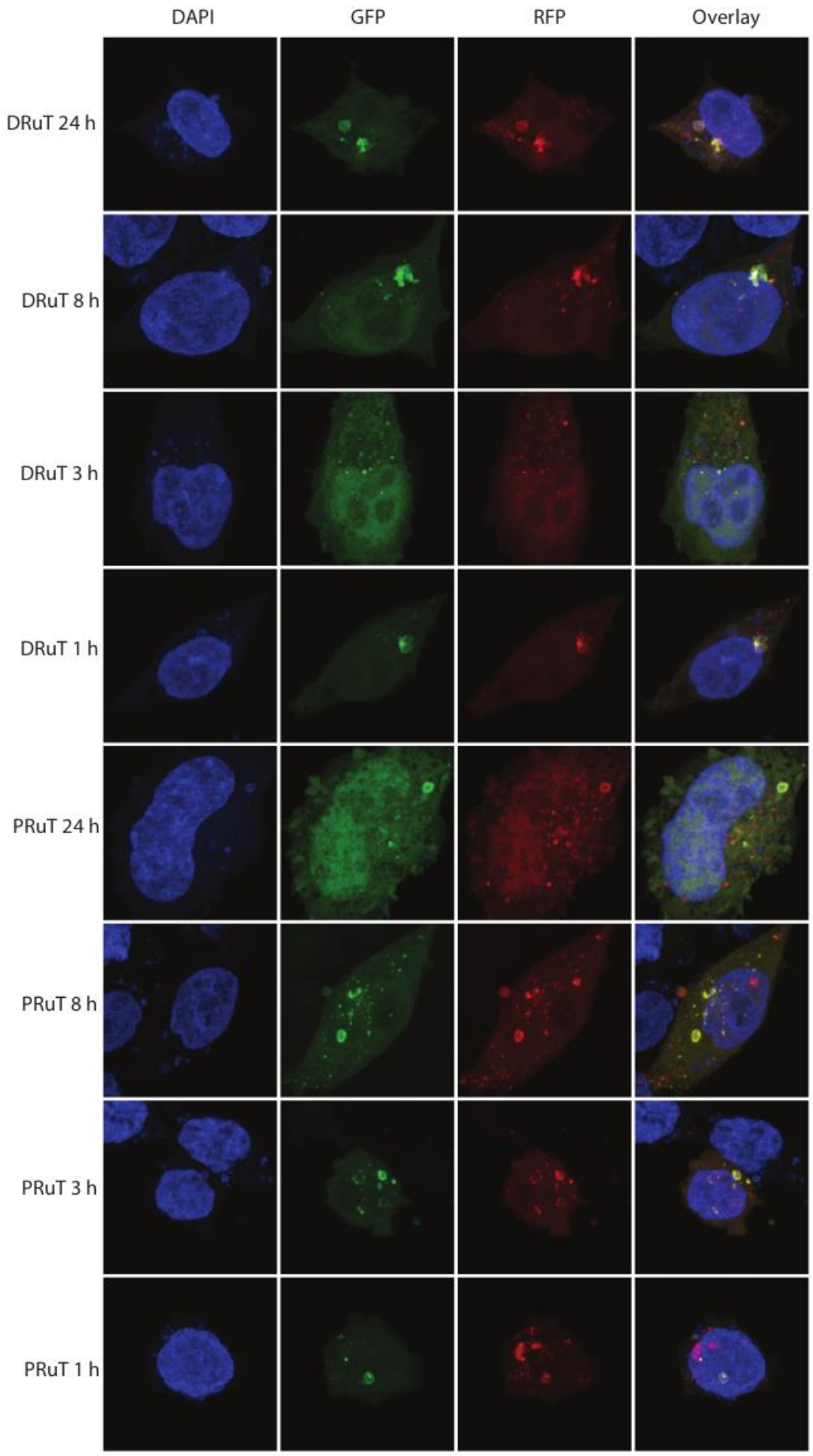
DAPI
GFP
RFP
Overlay
DRuT 24 h
DRuT 8 h
DRuT 3 h
DRuT 1 h
PRuT 24 h
PRuT 8 h
PRuT 3 h
PRuT 1 h

Figure 57: Confocal microscopy images of ptfLC3 protein in A2780 CIS cells treated with positive controls, DRuT and PRuT. The DRuT and PRuT treated cells are also stained with DAPI. Yellow foci show autophagosomes and red foci show autolysosomes.

Foci were quantified using the software FIJI. Yellow foci, representing autophagosomes, and red foci, representing autolysosomes, were counted separately. The results of the quantification are shown in Figure 58.

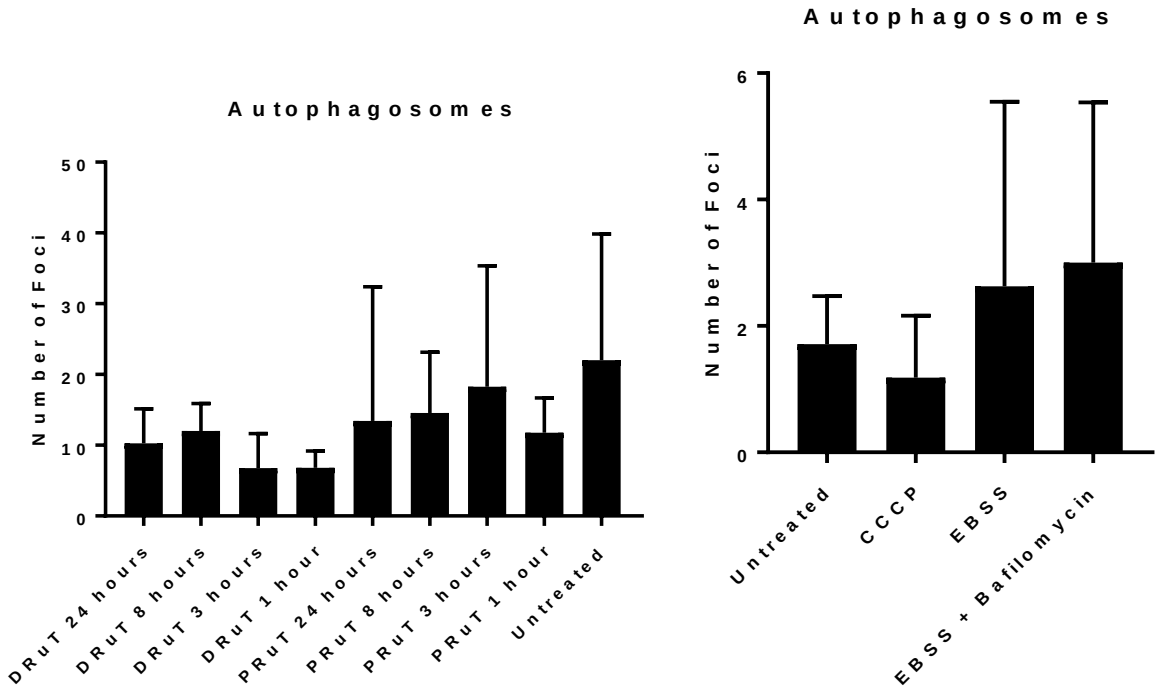

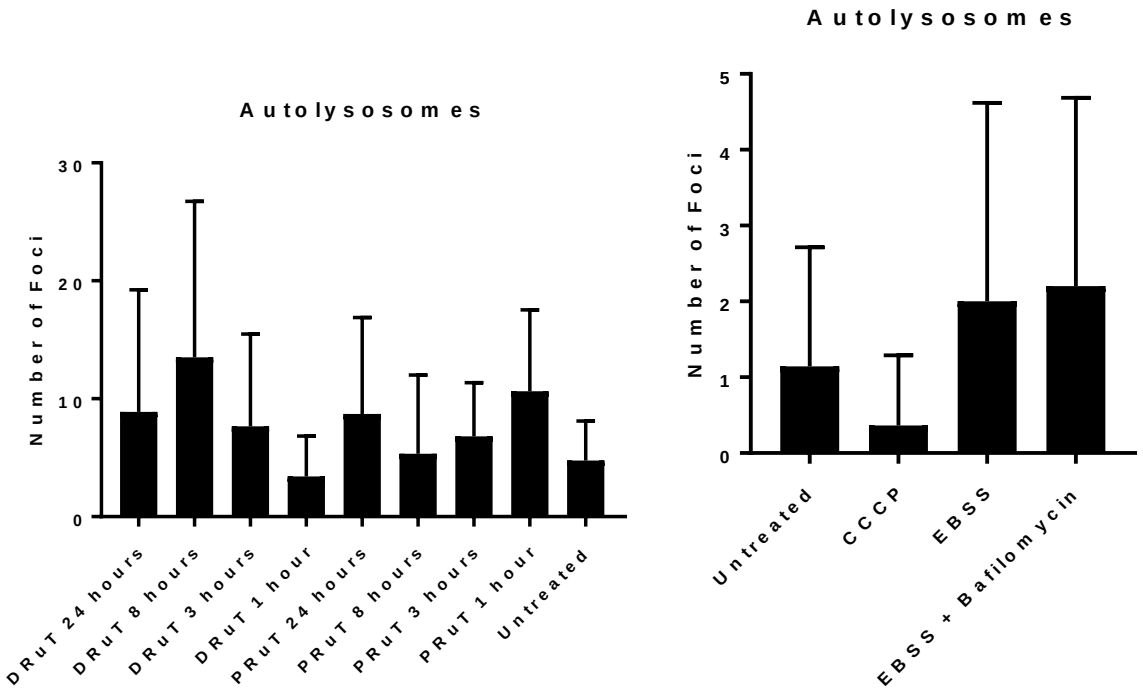

Figure 58: Quantification of ptfLC3 foci. The number of yellow foci per cell (autophagosomes) and the number of red foci per cell (autolysosomes) are shown. The conditions are: untreated, CCCP (a positive control for mitophagy), EBSS (a positive control for autophagy), EBSS + bafilomycin (a positive control for autolysosome formation), DRuT and PRuT at IC_{50} concentrations for 1, 3, 8 and 24 hours. Error bars represent standard deviation.

Considering the results overall, the error bars, representing standard deviation, are generally very large. This may be partly due to the fact that only a small number of cells were analysed in each experiment due to time constraints. Imaging and analysing more cells may improve this. However these bars are representative of the large spread in the data. In addition, the positive controls were tested in a separate experiment from DRuT and PRuT. The average number of foci is different between the two experiments, this is likely due to different imaging conditions used in each case. Therefore the number of foci cannot be directly compared between the experiments.

EBSS (serum starvation for 4 hours) would be expected to cause an increase in the number of autophagosomes. Indeed it increased the average number of yellow foci per cell from 1.7 for untreated to 2.6. However analysing the results using a 2-tailed unpaired t-test there is no statistically significant difference between the two conditions with a p value of >0.05.

EBSS and Bafilomycin would be expected to cause an increase in the number of autolysosomes. The average number of red foci per cell is 1.1 for untreated and 2.2 for EBSS + Bafilomycin, indicating that this condition did indeed cause an increase in the number of autolysosomes. However, as with the EBSS condition this result is not statistically significant.

As a positive control for mitophagy, a form of autophagy, CCCP would be expected to cause an increase in autophagosomes and autolysosomes. However, in this experiment it caused a decrease in both. The

average number of yellow foci per cell was 1.2 compared to 1.7 for untreated, and the average number of red foci per cell was 0.4 compared to 1.1. However neither of these results is statistically significant. In the TMRE assay the CCCP positive control did not produce as large an effect as expected, and the same CCCP sample was used in this experiment. It is possible that this particular sample of CCCP is not effective in reducing mitochondrial membrane potential and therefore inducing mitophagy.

More cells would need to be analysed to achieve statistically significant results and to confirm whether the EBSS and EBSS + Bafilomycin results do indeed have the effects expected, and whether the CCCP positive control doesn't.

DRuT did not cause an increase in the number of autophagosomes under any of the conditions tested. In fact, all conditions caused a decrease in the number of yellow foci per cell compared to the untreated control. 24, 8, 3 and 1 hours of DRuT treatment caused 10.3, 12.0, 6.8 and 6.8 yellow foci per cell respectively compared to 22.0 for untreated. However none of these results were statistically significant. Some DRuT treatment conditions caused an increase in the number of autolysosomes. The average number of red foci per cell was 4.8 for untreated, and 8.9, 13.5, 7.7 and 3.4 for 24, 8, 3 and 1 hours of DRuT treatment respectively. However, again these results were not statistically significant.

The large error bars in these results cast doubt upon the reliability of the results for the untreated control. From these results it cannot be stated that DRuT treatment definitively causes a decrease in autophagosomes and an increase in autolysosomes. From the TMRE assay results, it would be expected that DRuT treatment would cause an increase in both, as mitochondria damaged by a decrease in membrane potential would be degraded by mitophagy. More work is required to obtain statistically significant results to determine definitively whether this is the case or not.

Similarly, all PRuT conditions caused a decrease in autophagosomes compared to untreated control. The decreases are not as large as those caused by DRuT, but the error bars are notably larger. The number of yellow foci per cell for 24, 8, 3 and 1 hours are 13.4, 14.6, 18.3 and 11.8 respectively, compared to 22.0 for untreated. The larger error bars for PRuT treated samples compared to DRuT is consistent with observations from other experiments, for example ICP-MS. As with DRuT, PRuT treatment caused an increase in the number of autolysosomes, with the average number of red foci per cell being 8.7, 5.3, 6.8 and 10.6 for 24, 8, 3 and 1 hours of PRuT treatment respectively, compared to 4.8 for untreated. None of the results for PRuT are statistically significant.

The lack of statistically significant results from the controls also suggests that the system as a whole may not be working well. One possible explanation is researcher bias in selecting cells for imaging. The transfection efficiency of the plasmid was not high and so cells were chosen for imaging by manually selecting those that appeared to have been transfected successfully in the green microscope channel. It is likely that brighter cells were chosen preferentially, so it is possible that a number of the very brightest cells with the largest numbers of foci were chosen for each sample, rather than a representative sample

of all the cells. This issue could be addressed by imaging a broader selection of cells. In particular if the transfection was optimised cells could be chosen for imaging using DAPI, so there would be no bias as to the brightness of the green channel. For this experiment, the transfection was not optimised due to time constraints.

It is difficult to draw any conclusions from this data as to the effects of DRuT and PruT treatment on autophagy or mitophagy. However, the data collected suggest that there is no dramatic effects in either case, as this would likely have been observed even with large errors. Improvements to the experiment, such as those suggested above, are needed to obtain reliable results from which conclusions could be drawn.

4.5 Conclusion

A variety of studies have been undertaken to investigate the mechanisms of action of DRuT and PRuT in the A2780 CIS cell line.

ICP-MS experiments revealed that PRuT enters cells more rapidly than DRuT over short (1-3 hours) timepoints.

Pulsed-field gel electrophoresis unexpectedly confirmed that neither DRuT nor PRuT causes significant DNA DSBs, contrary to expectations from western blots presented in the introduction. However, FACS analysis showed a difference in the mechanisms of action between the two complexes. DRuT caused a decrease in DNA replication and cells accumulated in S phase, whereas PRuT caused the cell cycle to arrest in early S phase. A hypothesis that PRuT may be a topoisomerase inhibitor was discounted as its FACS profile did not match that of either a topoisomerase I inhibitor or a topoisomerase II inhibitor.

A PCR inhibition experiment confirmed that DRuT strongly inhibits DNA replication and showed that PRuT also inhibits DNA replication, but only at higher concentrations. DNA fibre analysis gave more insight into the DNA replication inhibition effects of DRuT and PRuT in cells. It showed that both complexes cause a decrease in the speed of DNA replication forks at timepoints as short as 2 hours, and especially at 24 hours.

Rad51 IF was used to determine whether the reason for PRuT causing Chk2 and γ-H2AX phosphorylation but not DNA DSBs, was that it causes replication forks to collapse, whereas DRuT only causes them to stall. The results showed that PRuT did cause an increase in the number of cells with very high numbers of foci compared to DRuT, which supports the hypothesis. However, PRuT also caused an increase in the number of cells with <5 foci which contradicts the hypothesis. The median number of foci per cell for DRuT was higher than for PRuT, so overall we cannot say that the Rad51 data supports the hypothesis that PRuT causes more replication forks to collapse than DRuT. The question of why PRuT causes Chk2 and γ-H2AX phosphorylation in the absence of DNA DSBs remains.

As well as the investigation into the effects of the DNA binding properties of DRuT and PRuT, the effect of these complexes on mitochondria in A2780 CIS cells was examined. A TMRE assay showed that both complexes caused a decrease in mitochondrial membrane potential after 24 hours of treatment, with DRuT causing a smaller effect at shorter timepoints. This led to an experiment investigating whether DRuT and PRuT cause an increase in autophagy due to damaged mitochondria being degraded by mitophagy. Results from this experiment did not suggest that either complex caused an increase in autophagy, however the results were inconclusive due to experimental issues.

Overall the experiments in this chapter provide insight into the mechanisms of action of DRuT and PRuT in A2780 CIS cells. The next chapter will present results to determine whether the toxicities and mechanisms of action of DRuT and PRuT are the same or different in the NSCLC cell line A549. This will be used to consider whether either compound warrants further investigation as a potential effective therapeutic for NSCLC.

5. Mechanistic Studies in a Human Non-Small Cell Lung Cancer Model

5.1 Introduction

The ruthenium complexes DRuT and PRuT have been established as effective potential anticancer therapeutic leads in a human ovarian carcinoma cell model, in particular in the cisplatin-resistant A2780 CIS cell line. However, lung cancer has a much higher incidence rate and a lower survival rate than ovarian cancer, so there is an immediate need for effective lung cancer treatments (see chapter 2: introduction).[194] Targeted and personalised therapies are prominent in cancer research at present, however these are far from ubiquitous, and at the current time traditional chemotherapy is still a mainstay of cancer treatment. Issues with platinum-based chemotherapy, such as side effects and resistance, offer a challenge to be overcome and in previous chapters, DRuT in particular has been identified as a compound that could potentially help to overcome these problems.

For this reason DRuT and PRuT will be tested for their potential to treat NSCLC using the A549 cell line. Their cytotoxicities towards this cell line will be determined using the MTT assay and the results will be compared to those from the A2780 and A2780 CIS cell lines. The mechanisms of action of these drugs in A549 cells will be determined and compared to those in A2780 CIS cells. From this DRuT and/or PRuT's suitability to go forward as candidates for NSCLC treatment will be assessed.

In A2780 CIS cells, DRuT and PRuT's cytotoxicities have been linked to their DNA binding properties. Experiments will be performed to determine whether these factors are similar or different in A549 cells to determine whether DRuT and PRuT have the same mechanisms of action in both cell lines. In particular, FACS analysis will be used to determine their effects on the cell cycle and DNA replication.

In addition, the effects of DRuT and PRuT on mitochondria in A549 cells will be investigated. This will be achieved using the same techniques as were used for A2780 CIS cells, namely a TMRE assay and transfection with ptfLC3. The TMRE assay will determine whether the compounds cause a decrease in mitochondrial membrane potential and the ptfLC3 experiment will determine whether they cause an increase in autophagy.

Together these experiments will be used to determine whether DRuT and PRuT are toxic towards A549 cells, and therefore whether they could be suitable as therapeutics for NSCLC. These studies will be used to assess whether the complexes display the same mechanisms of action in the two cell lines, specifically with regards to their effects on DNA replication and mitochondria.

5.2 MTT Toxicity Assay

The MTT assay is used to determine the toxicity of compounds, in this case potential drugs, to a given cell line. It involves the reduction of the yellow tetrazolium salt MTT to formazan, an insoluble purple product by NAD(P)H-dependent oxidoreductase enzymes in viable cells. The amount of formazan produced can be used to measure the number of viable cells in a sample.[195] By comparing the number of viable cells in samples treated with various concentrations of a compound of interest to the number in untreated control samples, the toxicity of the compound can be calculated. The compound concentration corresponding to a 50% reduction in cell viability can be calculated by interpolation of the data. This is known as the IC_{50} concentration. IC_{50} concentrations should not be directly compared between experiments as the results are specific to the conditions used in a particular experiment. However, comparisons can be made within experiments, controls are routinely used, and values can be used as an indication of the toxicity of a compound.

As IC_{50} concentrations for DRuT and PRuT in A2780 and A2780 CIS cells have already been determined, the first step to assess whether either compound could be an effective treatment for NSCLC is to determine their IC_{50} concentrations against the A549 cell line of this cancer. As for the assays using A2780 and A2780 CIS cells, cisplatin was used as a control compound.

A549 cells were seeded in a 48-well plate. Wells were treated with concentrations of DRuT, PRuT and cisplatin between 0.1 and 200 μM in triplicate. As DMSO was used to dissolve the compounds, the DMSO concentration was kept constant in all wells, including untreated control wells. After 48 hours of treatment the culture media was removed and replaced with MTT diluted in serum-free media. Cells were then incubated for 30-45 minutes, until purple formazan crystals were visible in the wells. The media was removed leaving the crystals, which were then dissolved in isopropanol. The absorbance at 595 nm was measured for each well using a plate reader. The results were then plotted and the IC_{50} values were determined. The experiment was repeated three times for each compound and the average IC_{50} value was calculated. An example of a graph showing cell viability against compound concentration is shown in Figure 59. This shows that for both cisplatin and DRuT the number of viable cells decreases as compound concentration increases, meaning the two complexes are toxic towards A549 cells. Figure 59 also shows the IC_{50} concentrations of DRuT, PRuT and cisplatin. For PRuT the IC_{50} was higher than the highest concentration tested (200 μM), so the value shown is a minimum estimate of its IC_{50}.

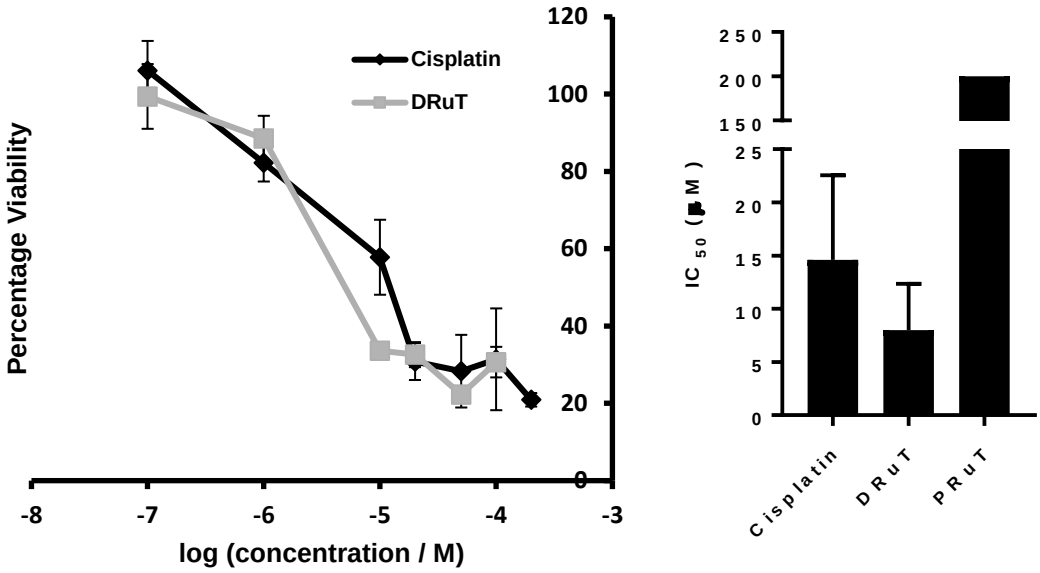

Figure 59: Graphs showing results from MTT assays. An example of a cell viability against compound concentration graph, and the IC_{50} concentrations of cisplatin, DRuT and PRuT. The IC_{50} of PRuT was higher than the highest concentration tested (200 μM), so 200 μM is a minimum estimate of its IC_{50}. Error bars represent standard deviation.

Both cisplatin and DRuT are toxic towards A549 cells. The IC_{50} for cisplatin is 15 μM and for DRuT it is 8 μM. DRuT's lower IC_{50} value means that under these conditions it is more toxic than cisplatin, a currently used clinical treatment for NSCLC. This shows that DRuT has great potential to be an effective treatment against this type of cancer. DRuT's IC_{50} value is lower than that in A2780 CIS cells (19 μM) but around the same as that in A2780 cells (7 μM). This is not unexpected as A549 is not a cisplatin-resistant cell line, and the difference between IC_{50} values for A2780 and A2780 CIS cells shows that DRuT does display some cross-resistance with cisplatin. Interestingly, PRuT does not show significant toxicity towards A549 cells and the IC_{50} is > 200 μM. It is surprising that there is such a large difference in IC_{50} between DRuT and PRuT given that their toxicity profiles are quite similar in the ovarian cancer cell lines. This suggests that the difference in mechanism of action already explored between DRuT and PRuT is of greater significance in A549 cells. The reason is unlikely to be a result of PRuT's higher cross-resistance with cisplatin as A549 cells are not particularly resistant to cisplatin. One possibility is that slower uptake of PRuT into A549 cells results in the lower activity of the complex.

Due to DRuT's high toxicity in this cell line and PRuT's lack of toxicity, DRuT was taken forward as the compound of interest for NSCLC. Further experiments were undertaken to probe its mechanism of action in this cell line. PRuT was used as a comparison in only some experiments.

5.3 Effects on DNA

5.3.1 Western Blots

An interesting property of DRuT in A2780 CIS cells is its ability to cause apoptosis through activation of Chk1 but not Chk2 or γ-H2AX. Western blots were employed to determine whether this effect is also observed in A549 cells as this would indicate that DRuT is a very interesting therapeutic lead for NSCLC due to the previously discussed benefits of avoiding DSBs and Chk2 activation in terms of drug side effects and cisplatin cross resistance (see chapter 2: introduction).

Western blots were performed for Chk1, p-Chk1, Chk2 and p-Chk2. Lysates of cells treated with 8 µM DRuT (IC_{50} concentration) for 1, 3, 8 and 24 hours were used. Cisplatin and HU were used as positive controls for p-Chk1 and p-Chk2. Cisplatin was used at 15 µM, its IC_{50} concentration, for 24 hours and HU was used at 2 mM for 24 hours, the same conditions used to induce Rad51 foci in A2780 CIS cells (see chapter 4: mechanistic studies in a human ovarian carcinoma model). The western blot for Chk1 is shown in Figure 60.

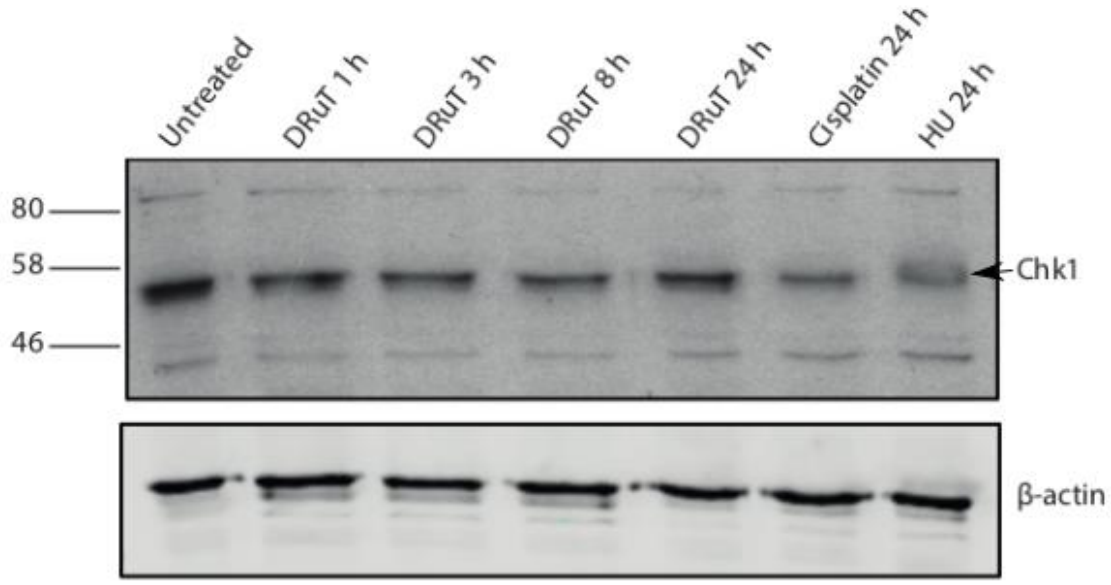

Figure 60: An image of a western blot for Chk1. A549 cells were treated with DRuT at IC_{50} concentration for 1, 3, 8 and 24 hours, and cisplatin and HU were used as positive controls. A band is visible at the expected molecular weight for Chk1 in all lanes and vertical smudging of the band, particularly visible in the HU lane, indicates phosphorylation.

The predicted molecular weight of Chk1 is 56 kDa and in all lanes a band is observed below the 58 kDa molecular weight marker, with the expected electrophoretic mobility. Some low-intensity non-specific bands are also visible above and below the Chk1 band. The β-actin loading control bands

confirm that the loading is equal in all lanes. The Chk1 band appears slightly diffuse in some lanes, most notably in the lane containing lysates derived from cells exposed to HU. Previous work[196] has shown that this is due to the presence of multiple phosphorylated forms of Chk1 each with slightly different electrophoretic mobility compared to non-phosphorylated Chk1, and indicates that some of the Chk1 protein is indeed phosphorylated under these treatment conditions.[21]

The western blot for p-Chk1 is shown in Figure 61.

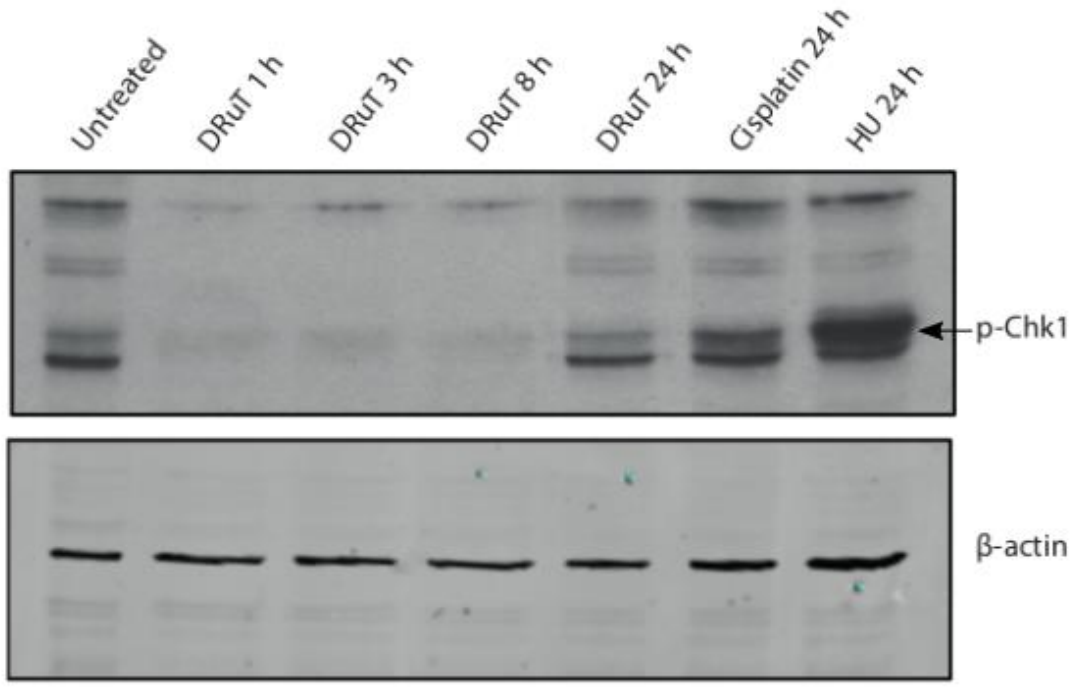

Figure 61: An image of a western blot for p-Chk1. A549 cells were treated with DRuT at IC_{50} concentration for 1, 3, 8 and 24 hours. Cisplatin and HU were used as positive controls. A band is visible for p-Chk1 in lanes 1, 5, 6 and 7. This shows that in this cell line DRuT causes Chk1 phosphorylation after 24 hours.

A band corresponding to p-Chk1 was observed in some lanes as well as some non-specific bands at higher molecular weights. The β-actin loading control confirms that the loading is equal between the lanes. There is a band for p-Chk1 in the untreated lane, which is unexpected, but could be due to replication stress or DNA damage being inadvertently caused during cell culture. As expected cisplatin and HU treatment both cause Chk1 phosphorylation, with HU treatment causing the greatest extent of phosphorylation. There is also a band visible in the DRuT 24 hour lane, showing that extended exposure of cells to DRuT results in Chk1 phosphorylation. However there are no bands corresponding to phosphorylated Chk1 at shorter exposure times. In A2780 CIS cells DRuT-H_2O causes some Chk1 phosphorylation after 1 hour, and significant Chk1 phosphorylation after 3 and 8 hours (see chapter 2: introduction). This suggests that DRuT takes longer to induce replication stress in A549 cells than A2780 CIS cells. However, this result suggests that DRuT does cause replication stress in A549 cells. In all lanes where it is visible the p-Chk1 band appears as 2 bands at very close

molecular weights. This is likely due to the presence of multiple phosphorylation sites in Chk1, resulting in small changes in electrophoretic mobility; Chk1 has been shown to have multiple phosphorylation sites.[197] The antibody used for this experiment detects Chk1 phosphorylated at serine 345, which is responsible for its activation. Chk1 subsequently undergoes autophosphorylation leading to additional band shifting.[196]

The western blot for Chk2 is shown in Figure 62.

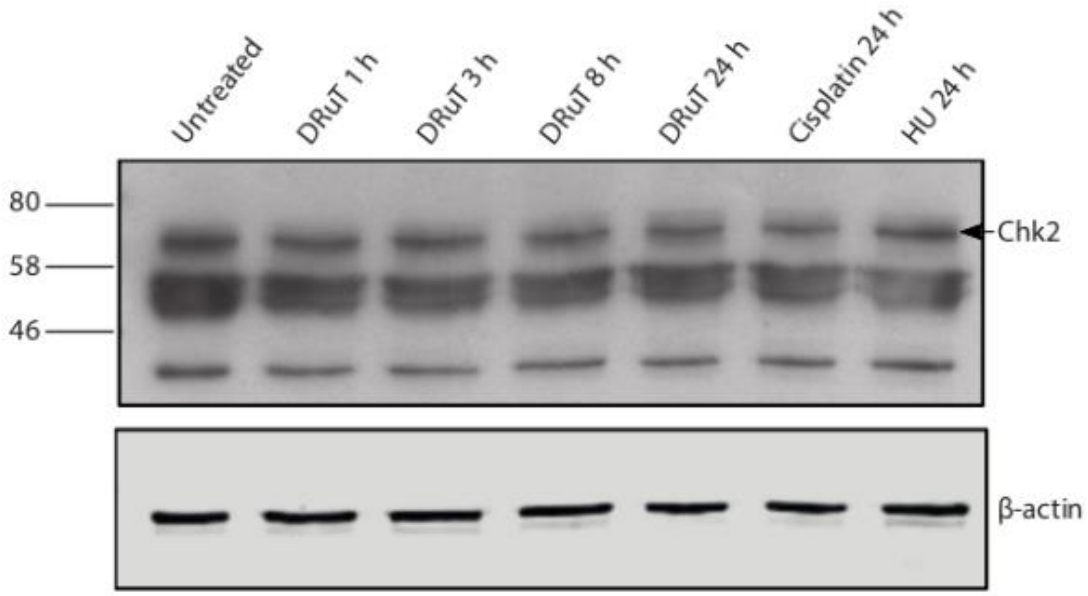

Figure 62: An image of a western blot for Chk2. A549 cells were treated with DRuT at IC_{50} concentration for 1, 3, 8 and 24 hours. Cisplatin and HU were used as positive controls. A band appears at the expected molecular weight for Chk2 in all lanes, however there are other bands close in molecular weight so it is difficult to identify which band represents Chk2.

The molecular weight of Chk2 is 64 kDa and a band appears above the 58 kDa molecular marker in all lanes, apparently representing Chk2. The β-actin loading control confirms that all lanes were loaded equally. However, there are two bands close in molecular weight below the 58 kDa molecular weight marker and it is also possible that these bands represent Chk2, especially as they are more intense than the band at the higher molecular weight so they don't appear to be non-specific bands. It is also possible that these bands are caused by keratin contamination in the western blot which could have been accidentally introduced from a number of sources. Keratin bands normally appear between 50-68 kDa.[198] All bands appear fairly equal in intensity across the lanes, confirming that Chk2 is present in all samples.

The western blot for p-Chk2 is shown in Figure 63.

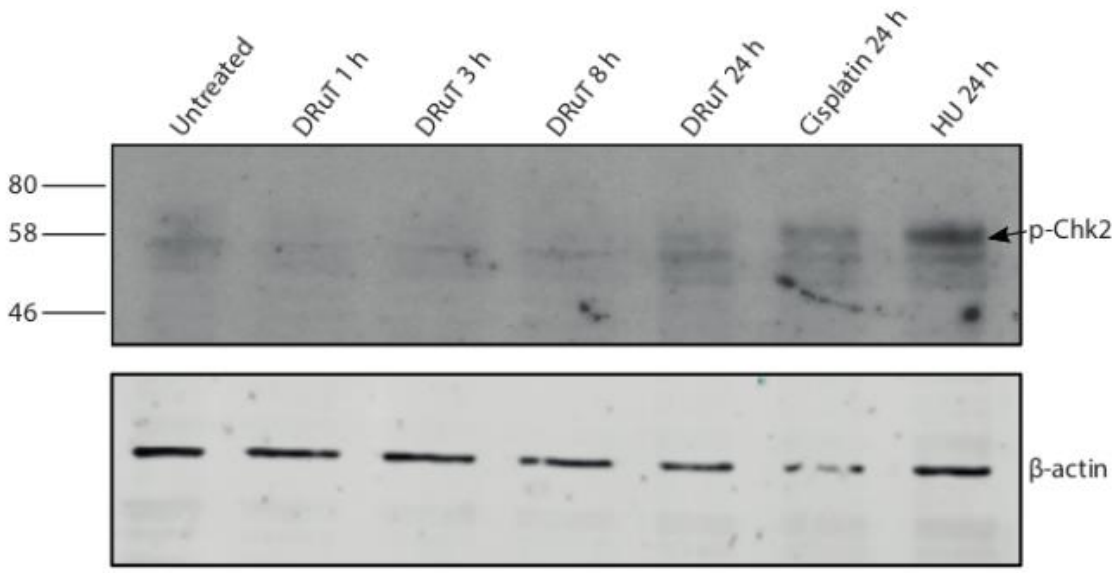

Figure 63: An image of a western blot for p-Chk2. A549 cells were treated with DRuT at IC_{50} concentration for 1, 3, 8 and 24 hours. Cisplatin and HU were used as positive controls. A band at the expected molecular weight is visible in the cisplatin and HU lanes.

A band is visible above the 58 kDa molecular weight marker in the cisplatin and HU lanes, and it is particularly intense in the HU lane. It is not visible in any of the DRuT lanes or the untreated lane, confirming that DRuT does not cause Chk2 phosphorylation in A549 cells. The β-actin loading control confirms that the loading is equal in all lanes. The β-actin band appears broken in the cisplatin lane, this could be due to an issue with the transfer from gel to membrane. A band at a slightly lower molecular weight than the p-Chk2 band is visible in some lanes, particularly in the DRuT 24 hour, cisplatin and HU lanes. This could be due to non-phosphorylated Chk2.

Overall these western blots suggest that DRuT may have a similar mechanism of action in A549 cells as in A2780 CIS cells. As in A2780 CIS cells, exposure to DRuT causes Chk1 phosphorylation, suggesting replication stress, but not Chk2 phosphorylation. The major difference is that it takes up to 24 hours for Chk1 phosphorylation to be observed, as opposed to 1 hour in A2780 CIS cells. This could be due, for example, to slower uptake of DRuT in A549 cells. However it is interesting given that DRuT is still very toxic towards A549 cells. This suggests that if DRuT's cytotoxicity is caused by its DNA binding properties in A549 cells then it must have a large effect soon after 24 hours.

5.3.2 FACS Analysis

FACS analysis of A549 cells, measuring the PI and BrdU content of treated cells, was used in the same way as in A2780 CIS cells, to determine whether DRuT has a similar effect on cell cycle and DNA replication in both lines. If the effect is the same as in A2780 CIS cells, an increase in S phase cells and

a decrease in BrdU incorporation (increase in stalled S phase) would be expected following DRuT treatment of A549 cells at IC_{50} concentration.

The experiment was performed in the same way as in A2780 CIS cells (see chapter 4: mechanistic studies in a human ovarian carcinoma model). Briefly, A549 cells were treated with DRuT, and then pulse-treated with BrdU. Cells were fixed and then stained with an anti-BrdU antibody and an AF488-conjugated secondary antibody, and with PI. Flow cytometry was then performed.

As Chk1 phosphorylation, indicating replication stress, was not observed until 24 hours, the long timepoints of 20 hours and 26 hours of DRuT treatment were used. The results of the FACS analysis are shown in Figure 64.

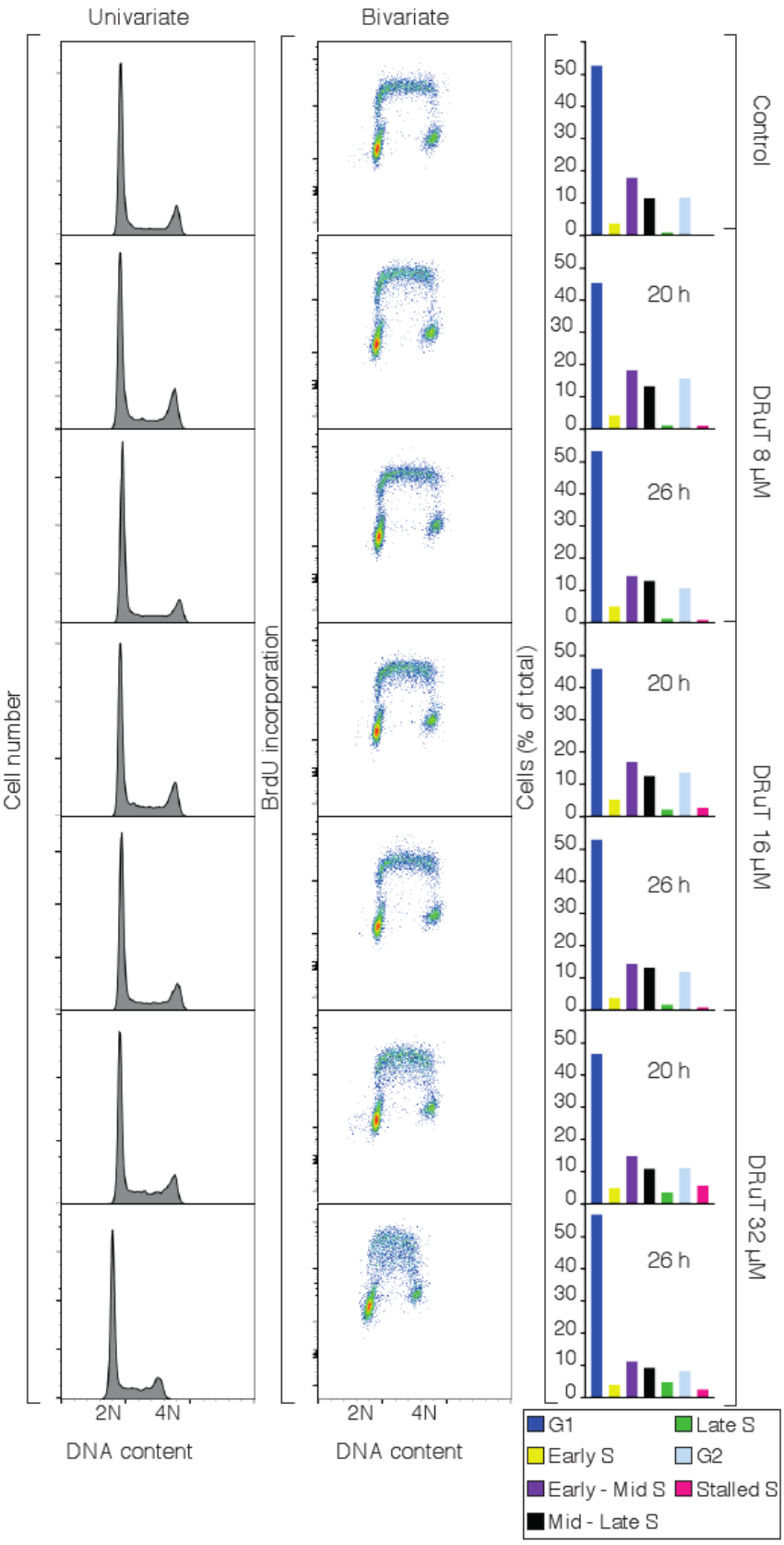

Figure 64: Graphs showing the results of FACS experiments, PI staining reveals the stage in the cell cycle, showing cell number on the y axis against PI intensity on the x axis. BrdU reveals the rate of DNA replication. PI and AF488 staining graphs show PI intensity on the x axis, AF488 intensity on the y axis and cell number represented as colour contours. Bar

charts show the number of cells in each cell cycle phase and the gates used to calculate this are the same as those used for A2780 CIS cells (see chapter 4: mechanistic studies in a human ovarian carcinoma cell line).

As shown in Figure 64, DRuT concentrations of 8 µM, 16 µM and 32 µM were used. This is because the IC_{50} concentration of 8 µM did not cause a significant effect on the cell cycle or BrdU incorporation.

DRuT treatment caused a small increase in the overall number of S phase cells, particularly at higher treatment concentrations. However, overall under most treatment conditions the univariate cell cycle profile is similar. The bivariate profiles are more revealing. The proportion of cells stalled in S phase - i.e. in S phase but not replicating DNA - revealed by decreased BrdU incorporation, is higher for all treatment conditions compared to untreated. This effect is most pronounced in the 32 µM 20 hour sample. The bivariate graph indicates that the 32 µM 26 hour sample appears to have more cells in stalled S phase, however the quantification reveals that the proportion of cells in this phase is lower as more cells are in G1. The proportions of cells in other phases are similar between samples, although the proportion of cells in G1 is variable. This could be due to factors such as confluence of the cells in dishes causing cells to enter G0. These cells would appear to be in G1 in the FACS analysis due to their DNA content.

Overall, these results show that DRuT does cause inhibition of DNA replication in A549 cells. However this effect is not as pronounced as in A2780 CIS cells and is only significant at concentrations double and quadruple the IC_{50}. This, combined with the slower phosphorylation of Chk1 in A549 cells following DRuT treatment, suggests that the effects on DNA may not be as important to the cytotoxicity of DRuT in A549 cells as in A2780 CIS cells.

5.4 Mitochondrial Effects

As DRuT does not appear to have as large an effect on DNA replication in A549 cells as in A2780 CIS cells, it is likely that there is another target of DRuT in this cell line. In A2780 CIS cells DRuT has been shown to have an effect on mitochondria, therefore this is also a possible target in A549 cells. Experiments were therefore performed to determine whether DRuT has a damaging effect on mitochondria in A549 cells. PRuT was also used in these experiments for comparison.

5.4.1 TMRE Assay

The first experiment used to determine whether DRuT or PRuT damage mitochondria in A549 cells was the TMRE assay. As described in chapter 4: mechanistic studies in a human ovarian carcinoma model, both DRuT and PRuT cause a decrease in mitochondrial membrane potential in the A2780 CIS cell line after 24 hours of treatment. For both compounds the effect was larger than that caused by the positive control compound FCCP. Cisplatin treatment for 24 hours at IC_{50} concentration also caused a decrease in mitochondrial membrane potential similar in magnitude to the effect caused by FCCP.

In A549 cells it was hypothesised that DRuT would cause a large decrease in mitochondrial membrane potential but PRuT would not. This could explain the difference in cytotoxicity between the compounds.

The experiment was performed in the same way as in A2780 CIS cells. Briefly, A549 cells in a 96-well plate were treated with DRuT at IC_{50} concentration, 50 µM PRuT, cisplatin at IC_{50} concentration and 20 µM FCCP, as well as untreated control wells containing DMSO. After compound incubation, cells were treated with TMRE for 20 minutes which was then removed. The fluorescence intensity of the wells was measured using a plate reader with excitation wavelength 544 nm and emission wavelength 590 nm. The results of this experiment are shown in Figure 65.

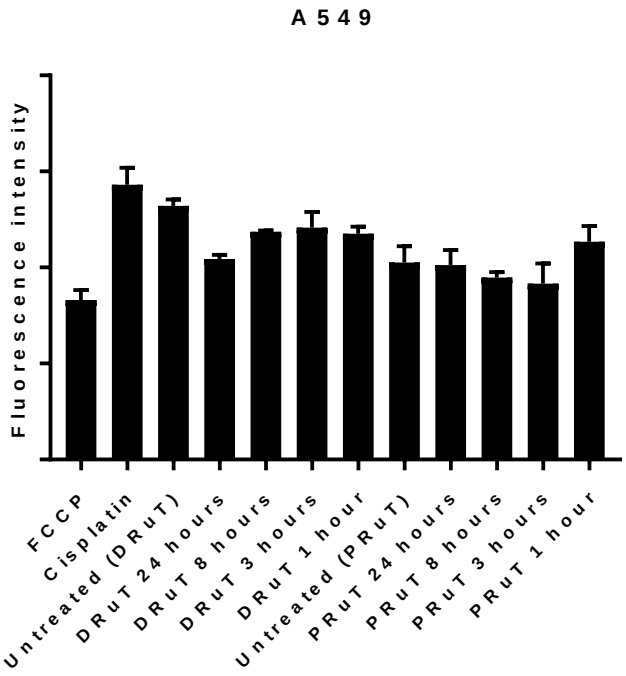

Figure 65: A graph showing the results of a TMRE assay on A549 cells treated with FCCP, DRuT and PRuT. The fluorescence intensity corresponds to the amount of TMRE retained in the mitochondria of the cells, and a higher value indicates a higher mitochondrial membrane potential. The positive control, FCCP, causes a decrease in fluorescence intensity, and DRuT causes a small decrease at the 24 hour timepoint.

A lower fluorescence intensity corresponds to a lower concentration of TMRE in the mitochondria and therefore a lowered mitochondrial membrane potential. The positive control, FCCP, caused a substantial decrease in fluorescence intensity, from 52900 to 33200, corresponding to a 37% decrease. Interestingly, cisplatin did not cause a decrease in mitochondrial membrane potential, in fact the fluorescence intensity increased slightly from 52900 to 57200. However, this difference is not statistically significant. This suggests that, in this cell line, cisplatin has minimal effect on mitochondrial function. Cisplatin has been shown to cause damage to mitochondria in some cell lines,[199] however this experiment suggests that in this cell line mitochondrial damage is not a major contributing factor to cisplatin's toxicity. This also suggests that large numbers of cells have not entered apoptosis after 24 hours, as an early stage of apoptosis is a decrease in mitochondrial membrane potential.[200]

DRuT treatment for 24 hours did cause a small decrease in mitochondrial membrane potential in this cell line, with fluorescence intensity decreasing from 52900 to 41800. This is a statistically significant result, however it is just a 21% decrease, compared with a 47% decrease for 24 hours of DRuT treatment in A2780 CIS cells. This suggests that DRuT has a smaller effect on mitochondria in A549 cells than in A2780 CIS cells. DRuT treatment for 8, 3 and 1 hours caused fluorescence intensities of 47400, 48300 and 47000 respectively. These are very small decreases and suggest that DRuT treatment causes minimal mitochondrial damage at these timepoints.

PRuT treatment for 24 hours caused only a 1% decrease in fluorescence intensity, from 41100 to 40500; this is not a statistically significant change. The fluorescence intensities at 8, 3 and 1 hours are 37900, 36600 and 45300 respectively. The 8 and 3 hour timepoints caused a larger decrease in fluorescence intensity than the 24 hour timepoint, however none of these changes are statistically significant.

Overall this suggests that PRuT treatment has no significant effect on mitochondrial membrane potential in A549 cells. This may be one reason why PRuT is not cytotoxic towards this cell line. As DRuT does have some effect on mitochondrial membrane potential in this cell line this could be a reason why it is much more cytotoxic than PRuT in the A549 cell line. However, as DRuT only has a small effect it is unlikely that this difference is the sole cause of the difference in toxicities.

5.4.2 Autophagy and Mitophagy

In A2780 CIS cells the ptfLC3 construct was used to determine whether autophagy increased with DRuT or PRuT treatment. This is because damaged mitochondria would be expected to be degraded by mitophagy, a form of autophagy. The same experiment was used in A2780 CIS cells (see chapter 4: mechanistic studies in a human ovarian carcinoma model), but the results were inconclusive. Here, the same experiment is performed in A549 cells to determine whether an effect could be observed in this cell line.

LC3 is a marker for autophagosomes. ptfLC3 is conjugated to both GFP and RFP. In autophagosomes, both fluorophores can be observed by microscopy. However, in the later stage of autophagy, in autolysosomes, the acidic environment causes the GFP to degrade, and only the RFP is visible. Through measuring the amount of yellow and red fluorescence, the amount and stage of autophagy can be quantified following the treatment of interest, in this case DRuT and PRuT treatment.

The same positive controls used in the A2780 CIS experiment were employed. Serum starvation (EBSS media for 4 hours) was used to induce autophagy as a positive control. EBSS and bafilomycin treatment for 2 hours was used as a positive control for autolysosome formation, and CCCP treatment was used as a positive control for mitophagy. This treatment should increase the amount of autophagy, as mitophagy is a form of autophagy.

The method used was the same as in A2780 CIS cells. To briefly recap, A549 cells were seeded on coverslips and transfected with ptfLC3 plasmid. Wells were treated with DRuT at IC_{50} concentration for 24, 8, 3 and 1 hours, and PRuT at 50 μM at the same timepoints. Wells were also treated with the positive controls. Cells were then fixed with PFA, and in some cases stained with DAPI, coverslips were mounted onto microscope slides and imaged using confocal microscopy. Figure 66 shows an example of images obtained.

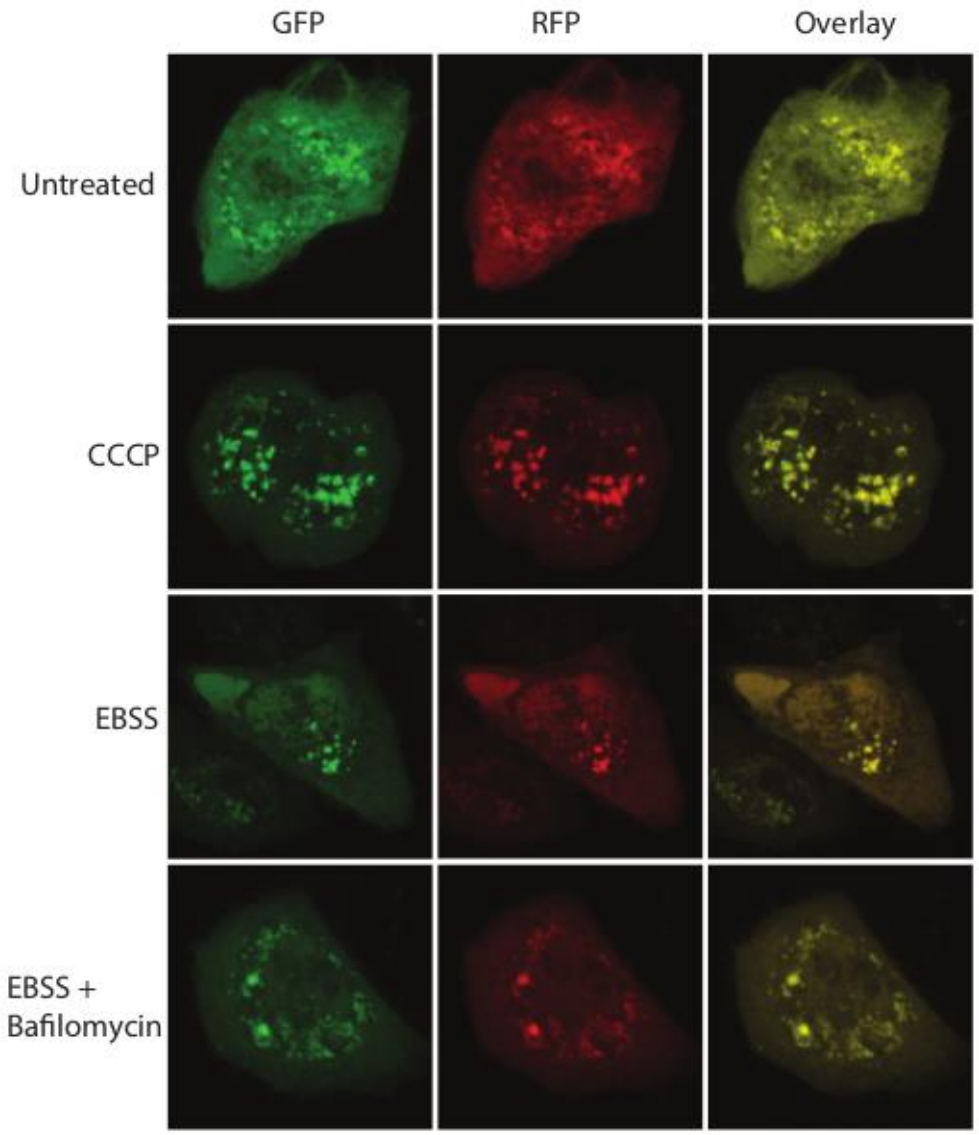
GFP
RFP
Overlay
Untreated
CCCP
EBSS
EBSS +
Bafilomycin

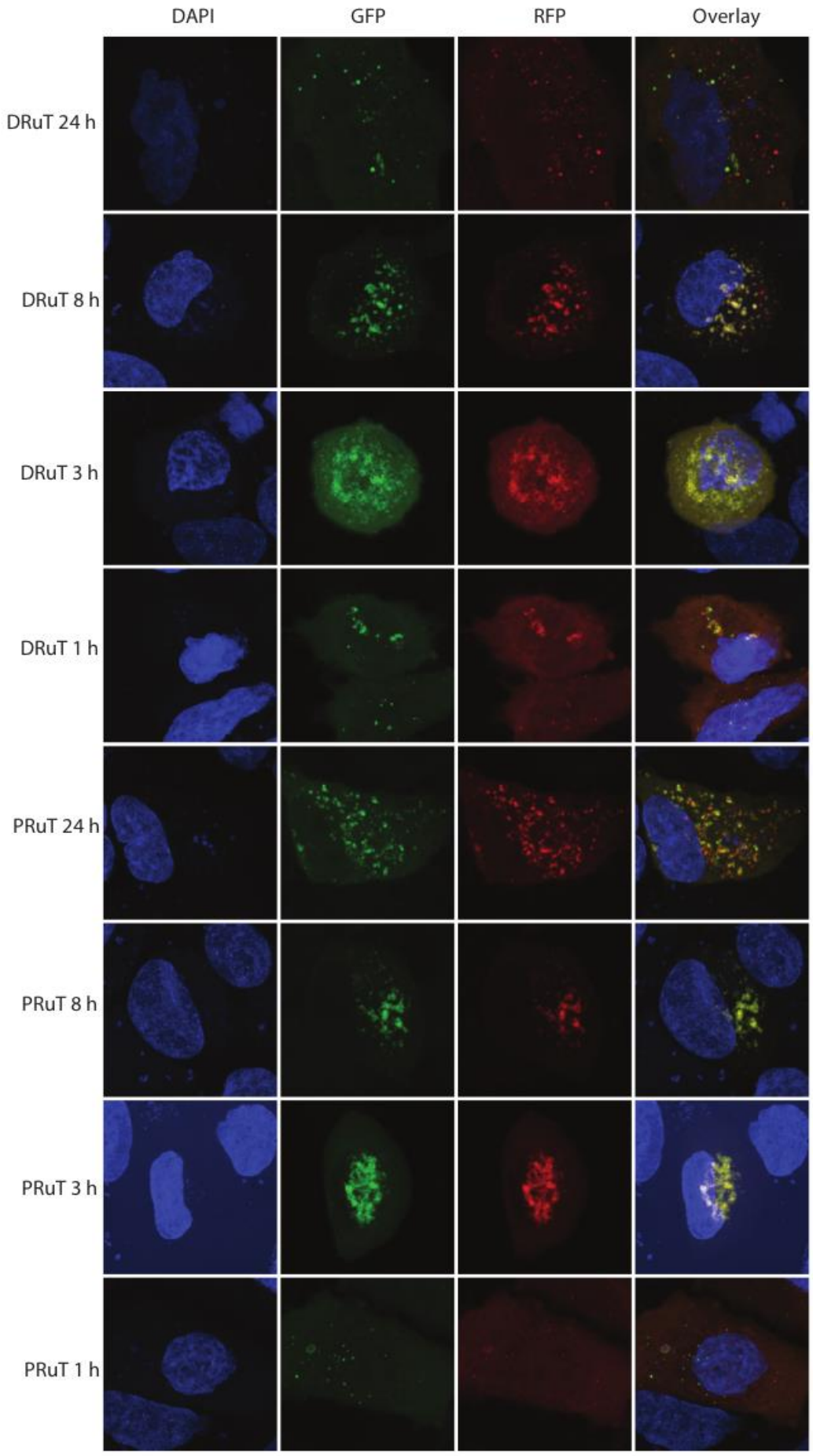
DAPI
GFP
RFP
Overlay
DRuT 24 h
DRuT 8 h
DRuT 3 h
DRuT 1 h
PRuT 24 h
PRuT 8 h
PRuT 3 h
PRuT 1 h

Figure 66: Confocal microscopy images of ptfLC3 protein in A549 cells treated with positive controls, DRuT and PRuT. The DRuT and PRuT treated cells were also stained with DAPI. Yellow foci show autophagosomes and red foci show autolysosomes.

Foci were counted using the software FIJI. Yellow foci, representing autophagosomes, and red foci, representing autolysosomes, were quantified separately. The results of the quantification are shown in Figure 67.

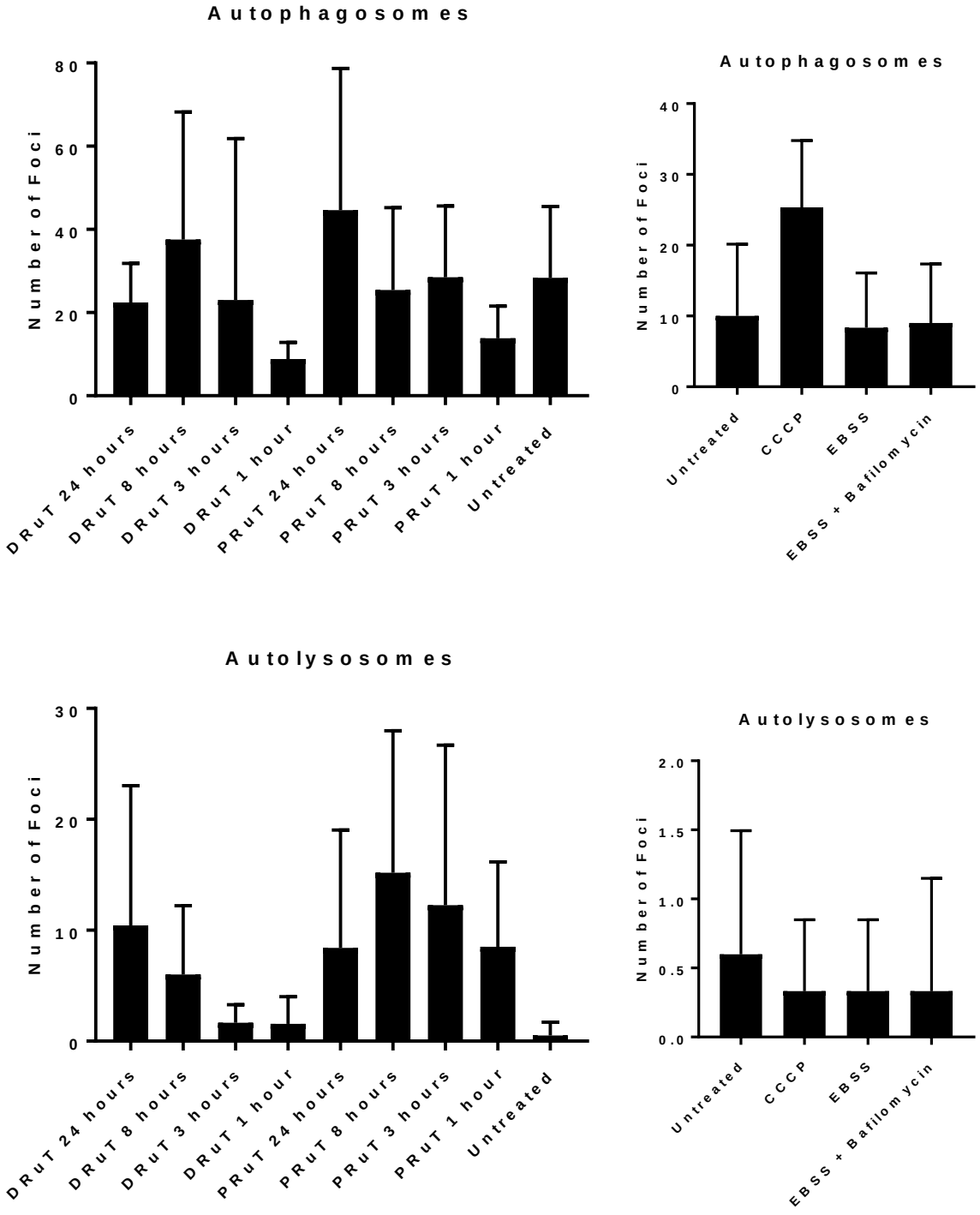

Figure 67: Quantification of ptfLC3 foci. The number of yellow foci per cell (autophagosomes) and the number of red foci per cell (autolysosomes) are shown. The conditions are: untreated, CCCP (a positive control for mitophagy), EBSS (a positive

control for autophagy), EBSS + bafilomycin (a positive control for autolysosome formation), DRuT at IC_{50} concentration and PRuT at 50μM for 1, 3, 8 and 24 hours. Error bars represent standard deviation.

As with the experiment in A2780 CIS cells, the error bars from this experiment are large. Again, this is likely due to the small number of cells counted for each condition (between 5 and 11). A larger sample size would likely decrease errors. In addition, in the same way as the experiment in A2780 CIS cells, the positive controls were tested in a separate experiment from the DRuT and PRuT treatments with different imaging conditions. Therefore, numbers of foci cannot be directly compared between experiments.

EBSS treatment (serum starvation) is a positive control for inducing autophagy and would be expected to cause an increase in autophagosomes. However, the number of yellow foci per cell was 8 after EBSS treatment, compared to 10 for untreated cells. CCCP is a positive control for mitophagy and this did indeed cause an increase in the number of autophagosomes, with an average of 25 per cell. This result was statistically significant, suggesting that CCCP was an effective positive control in this cell line, despite it not being so in the A2780 CIS experiment.

The number of red foci per cell in all samples in the control experiment was very low. It was 0.6 for the untreated sample and 0.3 for all other conditions. The EBSS + Bafilomycin treatment would be expected to cause an increase in the number of autolysosomes, as bafiomycin inhibits late stages in the autophagic process,[201] however this was not the case.

For DRuT treatment at IC_{50} concentration the number of yellow foci per cell was 22, 38, 23 and 9 for 24, 8, 3 and 1 hours respectively. For the untreated sample in this experiment there were on average 28 foci per cell. Therefore, all DRuT treatment conditions apart from 8 hours, did not cause an increase in the number of autophagosomes. However, the only statistically significant change was for the 1 hour sample which decreased the number of autophagosomes.

For the untreated sample the number of red foci per cell was 0.5. This is very low and so all treatment conditions caused an increase. For DRuT treatment the number of red foci per cell was 10, 6, 2 and 2 for 24, 8, 3 and 1 hours respectively. The fact that the number of autolysosomes is higher for the higher timepoints adds credibility to these results. However, it seems implausible that the number of autolysosomes would increase but not the number of autophagosomes, as autophagosomes are a precursor to autolysosomes. These results are not statistically significant so these changes are likely due to the large variance in the data.

For PRuT treatment at 50 μM the number of yellow foci per cell was 45, 25, 29 and 14 for 24, 8, 3 and 1 hours of treatment respectively, compared to 28 for the untreated sample. None of these results are statistically significant so PRuT does not appear to have an effect on autophagosome formation. The number of red foci per cell after PRuT treatment was 8, 15, 12 and 9 for 24, 8, 3 and 1 hours respectively, compared to 0.5 for the untreated sample. As with DRuT, all treatment conditions for PRuT caused an

increase in red foci, as the average number of foci for the untreated sample is very low. Again, it is unlikely that PRuT would cause an increase in autolysosomes without also increasing the number of autophagosomes.

Overall, these results do not provide any evidence that either DRuT or PRuT cause an increase in mitophagy. For PRuT this is in agreement with the data from the TMRE assay which showed that PRuT treatment did not cause a decrease in mitochondrial membrane potential. However, the TMRE assay showed that DRuT did cause a decrease in mitochondrial membrane potential and this is not reflected by an increase in autophagy shown in this experiment. However, as with this experiment in A2780 CIS cells, the errors are large and most of the results are not statistically significant. The lack of robust positive controls shows that the experiment does not give reliable results. The number of cells counted for each treatment condition was not high enough. In addition, similar issues with a lack of a high transfection efficiency were experienced here as with A2780 CIS cells. This meant that the cells imaged were not chosen at random and selection bias may have influenced the results. Improvements to this experiment, outlined in chapter 4: mechanistic studies in a human ovarian carcinoma model, could lead to more informative results being obtained.

5.5 Conclusion

In conclusion, studies have been carried out in the cell line A549 to determine whether DRuT could be an effective potential chemotherapy agent for NSCLC.

In A549 cells it was found that DRuT is more cytotoxic, and PRuT is less cytotoxic, than cisplatin. The difference in cytotoxicities is much larger in this cell line than in A2780 or A2780 CIS. It was also determined that, in A549 cells like in A2780 CIS cells, DRuT causes Chk1 phosphorylation but not Chk2 phosphorylation. However, Chk1 phosphorylation is not observed until 24 hours of treatment, compared with 1 hour in A2780 CIS cells.

FACS analysis revealed that at IC_{50} concentration DRuT treatment caused little noticeable effect on the cell cycle or DNA replication of A549 cells. Only at concentrations double and quadruple the IC_{50} was a partial inhibition of DNA replication observed. This explains the fact that Chk1 is activated late, as it is phosphorylated due to replication stress, and the FACS data shows that little replication stress is caused at IC_{50} concentration.

The TMRE assay showed that DRuT causes a decrease in mitochondrial membrane potential in A549 cells whereas PRuT does not. This may help to explain why DRuT is more cytotoxic. However, the lowering of mitochondrial membrane potential that DRuT causes in A549 cells is not as large as in A2780 CIS cells and is unlikely to be the sole reason for the difference.

The ptfLC3 experiment was performed to determine whether the decrease in mitochondrial membrane potential caused by DRuT translates into an increase in autophagy, as would be expected. However, the results of this experiment were not conclusive due to the large variance in the data. It did not show a large increase in autophagy following either DRuT or PRuT treatment.

One other possible reason for the difference in toxicities between DRuT and PRuT is a difference in rates of uptake in A549 cells. In A2780 CIS cells PRuT was shown to have a faster uptake rate at short timepoints, however DRuT could have a faster uptake rate in A549 cells. This warrants further investigation.

Overall the toxicity of DRuT in A549 cells, together with the fact that it does not cause Chk2 phosphorylation, suggests that it does warrant further investigation as a chemotherapy drug for NSCLC. As PRuT is not toxic in this cell line it is not an appropriate compound for this aim. However, the reasons for DRuT's toxicity and PRuT's lack of toxicity have yet to be revealed. DRuT does not appear to have as large an effect on DNA replication in A549 cells as in A2780 CIS, and although it does have an effect on mitochondria, this effect is modest. Additional work is required to investigate this further.

6. Conclusion and Future Work

6.1 Conclusion

Two ruthenium complexes, DRuT and PRuT, were synthesised and their DNA binding properties were investigated. The understanding of their mechanisms of cytotoxicity was extended in A2780 CIS cells, and finally, to determine their suitability as candidates for the treatment of NSCLC, their cytotoxicities and mechanisms of action were assessed in A549 cells.

DRuT and PRuT were initially synthesised prior to this project as part of a series of ruthenium complexes with the general formula $[Ru(tpm)(N\text{-}N)X]^{n+}$ where N-N is a polypyridyl ligand (DPPZ or phen), X is a monodentate ligand and n is either 1 or 2. The series of complexes was designed to investigate the effect in cells of differing DNA binding properties. The polypyridyl ligand was either DPPZ, an intercalating ligand, or phen, a non-intercalating ligand. A selection of monodentate ligands were used which were either labile or inert. It was found that the complexes that were the most cytotoxic towards A2780 and A2780 CIS cells were those with labile monodentate ligands.

The three complexes that were significantly cytotoxic were DRuT, PRuT, and DRuT-H_2O. It was assumed that DRuT and DRuT-H_2O were equivalent in terms of biological activity because the chloride ligand would presumably substitute for a water ligand in aqueous solution.

A viscosity experiment showed that DRuT-H_2O intercalates into DNA but PRuT does not. Mechanistic studies showed that DRuT causes cells to die via apoptosis. Western blots showed that PRuT, like cisplatin, causes the activation of p-Chk1, p-Chk2 and γ-H2AX. DRuT and DRuT-H_2O cause the activation of p-Chk1 but not p-Chk2 or γ-H2AX. Finally, FACS analysis showed that DRuT treatment causes cells to accumulate in S phase, and inhibits DNA replication.

This project aimed to build on the aforementioned work to fill gaps in knowledge. First, the DNA binding properties of DRuT and PRuT were thoroughly investigated. It was assumed that they would both be capable of covalently binding to DNA through substitution of their monodentate ligands, but it was not known whether this actually occurred in cells. DNA ICP-MS and NMR experiments were used to attempt to answer this question, however the results were not conclusive. A restriction enzyme inhibition experiment was used which suggested that PRuT covalently binds to DNA but DRuT does not.

It was known that DRuT reversibly binds to DNA via intercalation, but it was not known whether PRuT covalently binds, and if so, how. However it was known that PRuT does not intercalate. A competition DNA binding titration was used to determine PRuT's reversible DNA binding characteristics. It was

found that PRuT does reversibly bind to DNA, but with a lower affinity than DRuT. DNA binding constants were difficult to calculate due to issues with the data, however they were estimated using two different methods and in both cases the binding constant for DRuT was found to be an order of magnitude larger than that for PRuT. This is consistent with PRuT being a groove binder, however this is not categorically proven.

All experiments used to determine DNA binding had various issues, and so the DNA binding properties of DRuT and PRuT were not determined beyond doubt.

The knowledge obtained through the binding studies provided a context to mechanistic studies aimed at determining DRuT and PRuT's mechanisms of action in A2780 CIS cells. It was hypothesised that DRuT is particularly cytotoxic due to its intercalating properties, which cause the inhibition of DNA replication. It was also hypothesised that PRuT causes DNA DSBs due to it covalently binding to DNA, through a similar mechanism to cisplatin.

One reason the results of the DNA ICP-MS experiment were not conclusive was because they could have been influenced by differing cellular uptake rates of the compounds tested. For this reason ICP-MS was used to determine the rates of cellular uptake of DRuT and PRuT. Unfortunately it was difficult to obtain reliable results from this experiment, however it was determined that over the first 3 hours after treatment PRuT enters cells faster than DRuT.

To test the hypothesis that PRuT causes DNA DSBs, PFGE was used. It was found that neither DRuT nor PRuT causes DSBs, which was unexpected. FACS analysis confirmed that DRuT causes replication inhibition, although the effect was smaller than that observed previously. As expected, PRuT caused a different effect on the cell cycle and DNA replication. The cell cycle was arrested in early S phase and it appeared that replication was initiated but did not continue.

A PCR inhibition experiment was used to determine whether DRuT's inhibition of DNA replication was due to its DNA binding properties, and to confirm whether PRuT would also be observed to inhibit replication. As expected, DRuT was found to strongly inhibit DNA replication, and PRuT was found to inhibit DNA replication at higher concentrations. This suggested that both compounds have effects on the cell cycle and DNA replication due to their DNA binding properties.

DNA fibre analysis was used to gain extra insight into the DNA replication inhibition properties of DRuT and PRuT in A2780 CIS cells. In agreement with the PCR inhibition experiment it was found that both DRuT and PRuT slowed replication fork speed, with DRuT having a larger effect.

It was hypothesised that the reason that PRuT causes phosphorylation of Chk2 and γ-H2AX but does not cause DNA DSBs is that PRuT causes replication forks to stall and then collapse, causing 'chicken foot' DNA structures. This would cause the formation of Rad51 foci which would accumulate at collapsed fork sites to repair the DNA damage. Rad51 IF was used to measure this and if the hypothesis

was true then PRuT would cause more Rad51 foci that DRuT. The results were inconclusive; PRuT treatment caused a higher number of cells with less than 5 foci, but also a higher number of cells with over 20 foci. Collapsed replication forks could account for some of the Chk2 and γ-H2AX phosphorylation, however it seems unlikely to be responsible for all of it. There may be other factors involved that have yet to be clarified.

The effects of DRuT and PRuT on mitochondria in A2780 CIS cells were also investigated as a potential alternative cytotoxicity mechanism to DNA binding. A TMRE assay showed that both DRuT and PRuT cause a decrease in mitochondrial membrane potential of similar magnitude, meaning that they both damage mitochondria. The plasmid ptfLC3 was used to attempt to determine whether DRuT or PRuT causes an increase in autophagy, which should be caused following damage to mitochondria. However, the experiment did not give conclusive results. Overall these experiments show that DRuT and PRuT do damage mitochondria, however the mechanism of this is not known and further work is needed to determine this, as well as how this effect interacts with the effects on DNA, and which effect causes the cytotoxicity of the complexes in A2780 CIS cells.

The overall aim of the project was to determine whether a ruthenium complex could be an effective treatment for NSCLC. Once details of DRuT and PRuT's mechanisms of action had been explored in A2780 CIS cells, a NSCLC cell line was needed to determine whether their toxicities and mechanisms of action are similar in this cell line. The A549 cell line was used for this purpose.

The cytotoxicities of DRuT and PRuT were determined in A549 cells using MTT assays. It was found that DRuT is cytotoxic, but PRuT is not. The large difference in IC_{50} values was unexpected due to the similarities in their structures. Western blots were used to determine whether DRuT causes Chk1 phosphorylation but not Chk2 or γ-H2AX phosphorylation as it does in A2780 CIS cells. It was found that it indeed does not cause Chk2 or γ-H2AX phosphorylation and does cause Chk1 phosphorylation, however not as quickly as in A2780 CIS cells.

Due to Chk1 not being phosphorylated as quickly in A549 cells after DRuT treatment, FACS analysis was used to determine whether DRuT treatment causes DNA replication inhibition in A549 cells in the same way as in A2780 CIS cells. It was found that concentrations of DRuT 2-3 times higher than the IC_{50} caused a slight inhibition of DNA replication, but not to the extent observed in A2780 CIS cells, and not at the IC_{50} concentration. This suggested that DRuT's effects on DNA replication are not as important to the cytotoxicity of DRuT in A549 cells as in A2780 CIS cells.

The effects of DRuT and PRuT on mitochondria were investigated as it was hypothesised that the mitochondrial effects were the main reason for DRuT's cytotoxicity in this cell line. A TMRE assay showed that DRuT caused a small decrease in mitochondrial membrane potential and PRuT did not cause a decrease. This suggests that DRuT has some damaging effects to mitochondria in A549 cells but as these are small they are, like the effects on DNA replication, probably not fully responsible for

DRuT's cytotoxicity in this cell line. An experiment using the plasmid ptfLC3 was performed but, like in A2780 CIS cells, the results were not conclusive.

Overall this work showed that DRuT could potentially be an effective treatment for NSCLC, although its mechanism of action in this cell line is not fully understood.

6.2 Future Work

Future work should focus on taking DRuT forwards as a candidate for NSCLC treatment. Mice with xenograft tumours are commonly used initially to test new compounds. For this immunocompromised mice are injected with human or mouse cancer cells either under the skin or into the organ of interest. These cells develop into a tumour uninhibited by the mice's immune systems. Since these mice are immunocompromised, results found using them are not fully representative of naturally occurring cancer in humans. However, they give an idea of the efficacy and toxicity of compounds which are used to decide whether to study a particular compound further.[202]

3D tumour models represent a stage of study between cell culture and animal testing. These models are similar to monolayer cell cultures, but as they are 3D they more accurately represent the tumour microenvironment.[203] A 3D model of NSCLC could be used to study DRuT's toxicity, followed by studies in xenograft tumours in mice.

If DRuT is found to be an effective treatment in mice, then more work will need to be done to determine its mechanism of action against NSCLC. In addition to further cell studies, results from the studies in mice could be used to explore this. For example, in recent years patient-derived xenograft models have been used in which patient tumour tissue forms the xenograft rather than a cell line. In this case tumour subpopulations following treatment can be studied to discover mechanisms of drug resistance.[204]

Another interesting aspect of this thesis is the DNA binding studies of DRuT and PRuT. Although some progress was made, the true modes of binding of both complexes are still not fully understood. One way to gain significant insight into this would be to create NMR structures of both complexes bound to oligonucleotides.

The question of why PRuT causes γ-H2AX activation and Chk2 phosphorylation but does not cause DNA DSBs was not fully answered. This could be explored further as it is not a widely reported phenomenon.

7. Experimental

7.1 Synthesis

7.1.1 Synthesis of 1,10-phenanthroline-5,6-dione (DPQ)

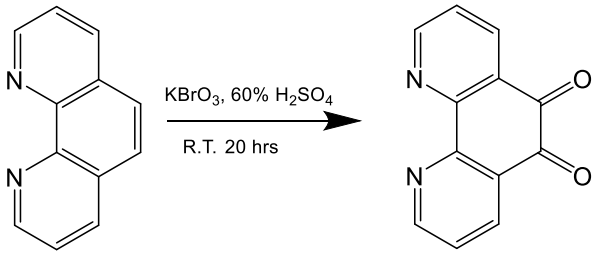

31%

1,10-phenanthroline (2.70 g, 15 mmol, 1 eq) was dissolved in 60% sulphuric acid (35 ml). Potassium bromate (2.76 g, 16.5 mmol, 1.1 eq) was added over a period of 30 minutes. The mixture was stirred at room temperature for 20 hours and then poured over ice. Saturated sodium hydroxide solution was added until the mixture was orange and cloudy at around pH 5. It was filtered, extracted with CH_2Cl_2 and the solvent was removed under reduced pressure. The solid was recrystallized from methanol to give 1,10-phenanthroline-5,6-dione (0.75 g, 23 %) as a yellow solid, δ_H (400 MHz; $CDCl_3$) 7.62 ppm (2H, dd, *J* 7.9 and 4.7 Hz), 8.54 ppm (2H, dd, *J* 7.9 and 1.9 Hz), 9.15 ppm (2H, dd, *J* 4.7 and 1.9 Hz).

7.1.2 Synthesis of DPPZ

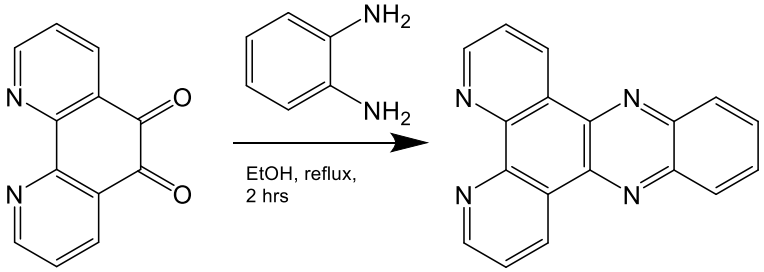

80%

DPQ (1.08 g, 5.16 mmol) and o-phenylenediamine (0.56 g, 5.16 mmol) were dissolved in ethanol (60 ml). The solution was heated to reflux for two hours. The solvent was removed under reduced pressure and the resulting solid was recrystallized from 50:50 ethanol:water and washed with cold ethanol and

water to give dppz (1.16 g, 80%) as a pale orange solid, δ_H (400 MHz; DMSO-d6) 7.96 ppm (2H, dd, *J* 8.1 and 4.4 Hz), 8.07 ppm (2H, dd, *J* 6.5 and 3.4 Hz), 8.40 ppm (2H, dd, *J* 6.5 and 3.4 Hz), 9.22 ppm (2H, dd, *J* 4.4 and 1.8 Hz), 9.55 ppm (2H, dd, *J* 8.1 and 1.7 Hz).

7.1.3 Synthesis of [Ru(tpm)Cl$_3$]

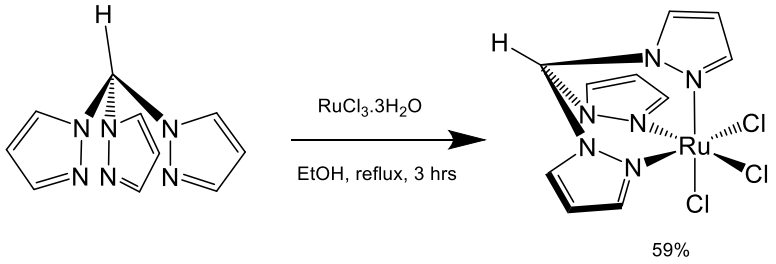

[$RuCl_3$].3H_2O (1.22 g, 4.67 mmol) was dissolved in ethanol (50 ml). Under N_2 TPM (1.00 g, 4.67 mmol) was added and the mixture was heated to reflux for three hours. The mixture was filtered and the solid was washed with cold ethanol and diethyl ether to give [Ru(tpm)Cl_3].3H_2O (1.30 g, 59%) as a dark brown solid, *m/z* (ESI) 388 (M^+-Cl).

7.1.4 Synthesis of [Ru(tpm)(phen)Cl]$^+$

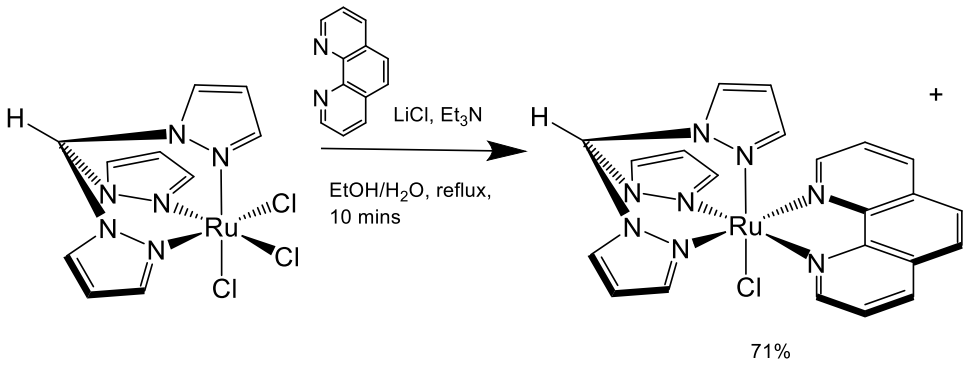

[Ru(tpm)Cl_3].3H_2O (0.50 g, 1.05 mmol) and 1,10-phenanthroline (0.23 g, 1.28 mmol, 1.2 eq) were dissolved in a mixture of 3:1 ethanol:water (100 ml) containing lithium chloride (0.5 g). Under N_2 the mixture was heated to reflux for five minutes after which triethylamine (12 drops) was added. The mixture was refluxed for a further 10 minutes and then filtered hot through celite. Aqueous ammonium hexafluorophosphate solution was added to precipitate the product which was collected by centrifuge and washed with water and diethyl ether. This was dissolved in the minimum volume of acetonitrile, diethyl ether was added and the precipitate was collected by centrifuge and washed with water and

diethyl ether to give [Ru(tpm)(phen)Cl](PF_6) (0.28 g, 71%) as a dark brown solid, δ_H (400 MHz; CDCN) 9.11 ppm (2H, dd, *J* 5.2 and 1.1 Hz), 9.02 ppm (1H, s), 8.60 ppm (2H, dd, *J* 8.2 and 1.1 Hz), 8.48 ppm (2H, d, *J* 2.7 Hz), 8.41 ppm (2H, d, *J* 1.9 Hz), 8.31 ppm (1H, d, *J* 2.8 Hz), 8.26 ppm (2 H, s), 7.87 ppm (2H, dd, *J* 8.2 and 5.3 Hz), 6.75 ppm (2H, t, *J* 2.6 Hz), 6.32 ppm (1H, d, *J* 2.1 Hz), 6.17 ppm (1 H, t, *J* 2.5 Hz), *m/z* (ESI) 531 (M^+-PF_6).

7.1.5 Synthesis of [Ru(tpm)(dppz)Cl]$^+$

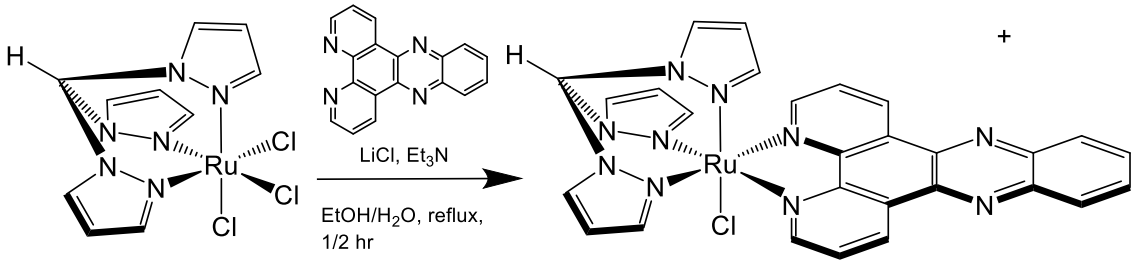

11
%

[Ru(tpm)Cl_3].3H_2O (1.09 g, 2.58 mmol), dppz (0.80 g, 2.84 mmol, 1.1 eq) and lithium chloride (0.4 g) were dissolved in a mixture of 3:1 ethanol:water (57 ml). The mixture was heated to reflux under N_2 for 10 minutes. Triethylamine (12 drops) was added and the mixture continued to reflux for three hours. The solvent was removed under reduced pressure and the residue dissolved in methanol (20 ml) and filtered through celite. Aqueous ammonium hexafluorophosphate solution was added to precipitate the product which was collected by centrifuge and washed with water and diethyl ether to give a dark brown solid. This was dissolved in the minimum volume of acetonitrile, diethyl ether was added and the precipitate was collected by centrifuge and washed with water and diethyl ether. This was purified by column chromatography on neutral alumina using acetonitrile:toluene 50:50 to 60:40 to give [Ru(tpm)(dppz)Cl]PF_6 (0.22 g, 11%) as a dark brown solid, δ_H (400 MHz; CDCN) 9.66 ppm (2H, dd, *J* 8.2 and 1.3 Hz), 9.20 ppm (2H, dd, *J* 5.4 and 1.3 Hz), 9.00 ppm (1H, s), 8.53 ppm (2H, dd, *J* 6.6 and 3.4 Hz), 8.49 ppm (2H, dd, *J* 2.9 and 0.6 Hz), 8.45 ppm (2H, d, *J* 2.1 Hz), 8.33 ppm (1H, dd, *J* 2.9 and 0.5 Hz), 8.16 ppm (2H, dd, *J* 6.6 and 3.4 Hz), 8.02 ppm (2H, dd, *J* 8.1 and 5.4 Hz), 6.78 ppm (2H dd, *J* 2.9 and 2.2 Hz), 6.57 ppm (1H, d, *J* 2.3 Hz), 6.23 Hz (1H, dd, *J* 2.9 and 2.3 Hz), *m/z* (ESI) 633 (M^+-PF_6).

7.1.6 Synthesis of $[Ru(tpm)(dppn)Cl]^+$

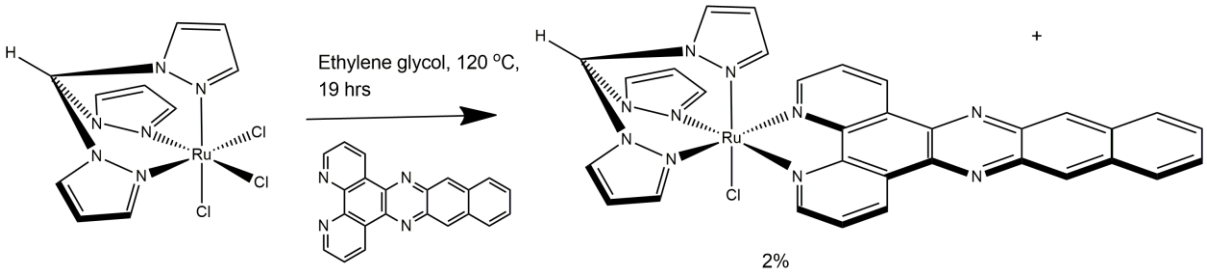

$[Ru(tpm)Cl_3].3H_2O$ (0.5 g, 1.05 mmol) and dppn (0.39 g, 1.16 mmol, 1.1 eq) were dissolved in ethylene glycol (120 ml). The mixture was heated under N_2 in the absence of light to 120 °C overnight. The mixture was cooled, methanol (300 ml) was added and the mixture was filtered through celite. The solvent was removed as far as possible under reduced pressure. Aqueous ammonium hexafluorophosphate solution was added to precipitate the product which was collected by centrifuge and washed with water and diethyl ether to give a dark brown solid. This was dissolved in the minimum volume of acetonitrile, diethyl ether was added and the precipitate was collected by centrifuge and washed with water and diethyl ether. This was purified by column chromatography on neutral alumina using acetonitrile:toluene 50:50 to 60:40 to give $[Ru(tpm)(dppn)Cl]PF_6$ (0.02 g, 2%) as a dark brown solid, δ_H (400 MHz; CDCN), 9.63 ppm (2H, dd, *J* 8.1 and 1.2 Hz), 9.18-9.15 ppm (4H, m), 8.99 ppm (2H, s), 8.49 ppm (2H, dd, *J* 13.9 and 2.9 Hz), 8.41 ppm (2H, dd, *J* 6.5 and 3.3 Hz), 8.34 ppm (2H, d, *J* 2.9 Hz), 8.00 ppm (2H, dd, *J* 8.1 and 5.4 Hz), 7.79 ppm (2H, dd, *J* 6.7 and 3.2 Hz), 6.79 ppm (2H, t, *J* 2.7 Hz), 6.63 ppm (1H, d, *J* 2.2), 6.25 ppm (1H, t, *J* 2.4 Hz), *m/z* (ESI) 683 (M^+-PF_6).

7.1.7 Synthesis of $[Ru(bpy)_2Cl_2]$

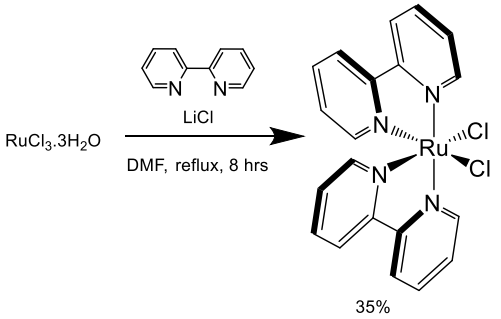

$RuCl_3.3H_2O$ (0.78 g, 2.98 mmol) and 2,2-bipyridine (0.94 g, 6.00 mmol, 2 eq) were dissolved in dimethyl formamide (DMF) (5 ml) containing lithium chloride (0.84 g, 0.2 mmol). The mixture was heated to reflux under N_2 for 8 hours, after which acetone (25 ml) was added and the mixture cooled to 4 °C overnight. The precipitate was filtered and washed with water and diethyl ether to give $[Ru(bpy)_2Cl_2]$ (0.54 g, 35%) as a black solid, δ_H (400 MHz; CDCN), 10.08 ppm (2H, s), 8.39 (2H, d, *J*

7.5 Hz), 8.25 ppm (2H, d, *J* 7.4 Hz), 8.02 ppm (2H, t, *J* 7.8 Hz), 7.69 ppm (2H, t, *J* 6.4 Hz), 7.60 ppm (4H, t, *J* 7.6 Hz), 7.03 ppm (2H, t, *J* 6.1 Hz).

7.1.8 Synthesis of $[Ru(bpy)_2(dppz)]^{2+}$

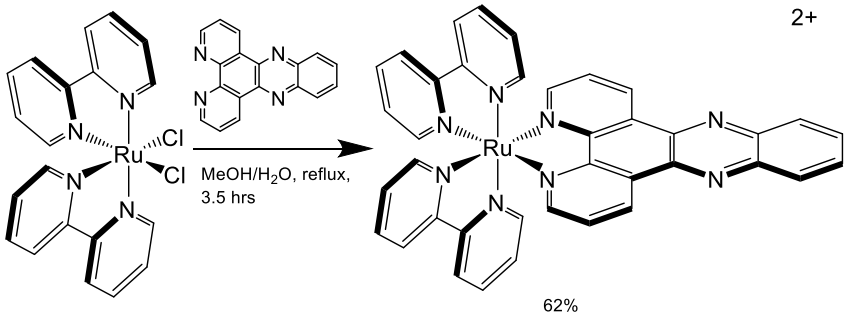

$[Ru(bpy)_2Cl_2]$ (0.13 g, 0.26 mmol) and DPPZ (0.08 g, 0.29 mmol, 1.1 eq) were dissolved in a mixture of 1:1 methanol:water (34 ml). The mixture was refluxed under N_2 for 3.5 hours. The volume was reduced before aqueous ammonium hexafluorophosphate was added. The resulting precipitate was collected and washed with cold water and diethyl ether. This was dissolved in the minimum volume of acetonitrile, diethyl ether was added and the precipitate was collected and washed with water and diethyl ether to yield $[Ru(bpy)_2(dppz)](PF_6)_2$ (0.16 g, 62%) as an orange solid, δ_H (400 MHz; CDCN), 9.70 ppm (2H, dd *J* 8.2 and 1.3 Hz), 8.56 ppm (4H, dd, *J* 13.3 and 8.1 Hz), 8.51 ppm (2H, dd, *J* 6.6 and 3.4 Hz), 8.26 – 8.10 ppm (6H, m), 8.05 ppm (2H, td, *J* 7.9 and 1.5 Hz), 7.92 ppm (2H, dd, *J* 8.3 and 5.4 Hz), 7.88 ppm (2H, d, *J* 4.9 Hz), 7.75 ppm (2H, d, *J* 5.0 Hz), 7.49 ppm (2H, ddd, *J* 7.6, 5.6 and 1.3 Hz), 7.29 ppm (2H, t, *J* 6.1 Hz).

7.1.9 Synthesis of $[Ru(bpy)_3]^{2+}$

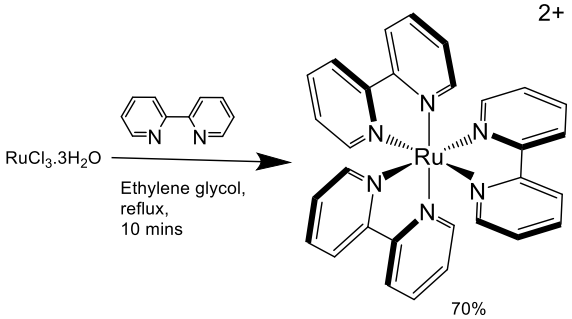

$RuCl_3.3H_2O$ (0.1 g, 0.38 mmol) and 2,2-bipyridine (0.18 g, 1.14 mmol, 3 eq) were dissolved in ethylene glycol (10 ml) and heated to reflux under N_2 for 10 minutes. Once cool aqueous ammonium

hexafluorophosphate was added and the resulting precipitate was collected and washed with water to give $[Ru(bpy)_3](PF_6)_2$ (0.23 g, 70%) as an orange solid, δ_H (400 MHz; CDCN) 8.52 ppm (4H, d, *J* 8.2 Hz), 8.08 ppm (4H, t, *J* 7.9 Hz), 7.75 ppm (4H, d, *J* 5.5 Hz), 7.42 ppm (4H, t, *J* 6.2 Hz), *m/z* (ESI) 285 (M^{2+}-2(PF_6)).

7.1.10 Formation of chloride salts

Complexes were converted from hexafluorophosphate salts to water soluble chloride salts by dissolving in the minimum volume of acetone and adding tetrabutylammonium chloride dissolved in acetone. The precipitate was filtered and washed with acetone to give the products as chloride salts.

7.1.11 Preparation of stock solutions

In the case of all complexes other than DRuT: complexes were dissolved in PBS (generally 500 μM) and filtered through a 0.20 μm filter. Stock solutions were made to the relevant concentrations for experiments with growth medium. In the case of DRuT and sometimes PRuT, they were dissolved in DMSO to a concentration of 10 mM, made to the relevant concentration for experiments in growth medium, and filtered through a 0.20 μm filter.

7.2 Biological Studies

7.2.1 Cell culture

A2780 and A2780 CIS cells were grown in a monolayer in RPMI-1640 (Roswell Park Memorial Institute 1640) medium supplemented with 100 IU ml^{-1} penicillin, 100 $\mu g ml^{-1}$ streptomycin and 10% fetal bovine serum (FBS). A549 and U2OS cells were grown in a monolayer in DMEM (Dulbecco's Modified Eagle Medium) supplemented with 2 mM L-glutamine, 100 IU ml^{-1} penicillin, 100 $\mu g ml^{-1}$ streptomycin and 10% fetal bovine serum (FBS).

Cell cultures were grown in a humidified incubator at 37 ^{o}C and 5% CO_2 and passaged regularly. For A2780 CIS cells growth medium was supplemented with 2 μM cisplatin every fourth passage to maintain cisplatin resistance.

7.2.2 DNA ICP-MS

A2780 CIS cells were grown in 10 cm dishes for at least 24 hours, then treated with cisplatin or Ru complexes (50 μM) for 24 hours. Cells were washed with PBS and harvested by trypsinisation, and the DNA was extracted using a Mammalian Genomic DNA Miniprep Kit from Sigma Aldrich. This involved cell lysis and treatment with proteinase K and RNAse A, followed by purification of the DNA through a spin column. The purity of the DNA was assessed by measuring the A_{260}/A_{280} ratio using a NanoDrop spectrophotometer and any samples with A_{260}/A_{280} outside the range of 1.6-1.9 were discarded. To precipitate the DNA, to each 400 μL sample sodium acetate (3M, pH 5.2, 40 μL) and 96% ethanol (800 μL) were added, the samples were mixed and cooled at – 20 ^{o}C overnight. The DNA was collected by centrifugation, washed with ice cold 70% ethanol (1 ml) and dissolved in TMAH/EDTA buffer. Samples were analysed by an Agilent 7500CE ICP-MS instrument to determine ruthenium content. Ruthenium mass 101 was measured against a calibration graph produced from standards of known Ru concentrations. Any matrix changes were corrected by the online addition of Rh which was monitored at mass 103.

7.2.3 NMR

Ruthenium complexes were dissolved in DMF-d7 to a concentration of 10 mM and then made up to 0.8 ml with D_2O to a final concentration of 200 μM. In the experiments in which it was used guanosine was also dissolved in the D_2O to a concentration of 200 μM. During incubation times the NMR tubes were kept protected from light and spectra were taken as soon as possible after mixing and then after the specified amounts of time. Spectra were taken using a Bruker Avance III HD 500 MHz spectrometer.

7.2.4 Restriction Enzyme Inhibition

The plasmid FCHo1-pmCherryCl was a gift from Christien Merrifield (Addgene plasmid # 27690).[1] Plasmid (1 μg) was incubated with cisplatin, DRuT or PRuT at concentrations specified in the experiment at room temperature for 5 hours.

For samples incubated with cisplatin a Qiagen Qiaquick PCR purification kit was used according to the manufacturer's instructions to purify the plasmid. Buffer PB (500 μL) was added to the sample, which was then added to a silica column. This was centrifuged at room temperature at 13000 RPM for 1 minute (all subsequent centrifuge steps were performed under these conditions). The flow through was removed and buffer PE (750 μL) was added to the column. This was centrifuged, and flow through was discarded and the centrifugation was repeated. MilliQ water (50 μL) was added to the column to elute the plasmid and after 1 minute incubation at room temperature the column was centrifuged into a fresh Eppendorf tube. The concentration of the resulting plasmid solution was then measured using the absorbance at 260 nm, and the A_{260}/A_{280} ratio was measured, using a Nanodrop.

For samples incubated with DRuT or PRuT the plasmid was purified by ethanol precipitation. NaOAc (3M, pH 5.2, 5 μL) was added to the sample, followed by ethanol (96%, 100 μL). The sample was inverted 10 times and then incubated at -20 ^{o}C overnight. It was then centrifuged at 14000 RPM at 4 ^{o}C for 20 minutes. The supernatant was removed and ice-cold 70% ethanol (200 μL) was added. The sample was briefly vortexed and then centrifuged at 14000 RPM at 4 ^{o}C for 15 minutes. This ethanol wash step was repeated a further 4 times. After the final supernatant was removed the Eppendorf was heated to 37 ^{o}C with the lid open until all residual ethanol had evaporated. MilliQ water (50 μL) was added and pipetted up and down to mix, before being incubated at 65 ^{o}C for 15 minutes to dissolve the DNA. The DNA concentration was measured using the absorbance at 260 nm, and the A_{260}/A_{280} ratio was measured using a Nanodrop.

The purified plasmid DNA was used in a restriction enzyme reaction with the restriction enzyme EcoRI. This was done according to the manufacturer's instructions (Promega) and the plasmid was mixed with water, Buffer H, BSA and EcoRI. The mixture was pipetted to mix and briefly centrifuged. It was then incubated at 37 ^{o}C for 2 hours. The resulting samples were visualised using a 0.8% agarose gel and ethidium bromide.

7.2.5 DNA titrations

Luminescence spectra were recorded using a Jobin-Yvon FluoroMax-3 spectrophotometer. A solution of 20 μM CT-DNA and 2 μM H33258 in 5 mM tris, 25 mM NaCl, pH 7.4 at 26.9 ^{o}C was excited at 338 nm and its emission spectrum was recorded between 390-650 nm. 50 μL portions of 150 μM DRuT or PRuT were titrated in and upon each addition the solution was allowed to equilibrate for five minutes before a spectrum was recorded.

7.2.6 Cellular Uptake ICP-MS

A2780 CIS cells were grown in 10 cm dishes. After 24 hours they were treated with DRuT or PRuT (50 μM) for the amount of time specified in the experiment. Following this the media was removed and the cells washed with 3 X 10 ml PBS. They were trypsinised and collected in centrifuge tubes. They were then washed with 3 ml serum-free media, before the pellet was resuspended in serum-free media (100 μL). The cells were counted using a haemocytometer. Samples were then stored at -20 ^{o}C overnight. Nitric acid (60%, 2 ml) was added to each sample and they were heated to 60 ^{o}C overnight. The samples were made up to 10 ml with distilled water. Samples were analysed by an Agilent 7500CE ICP-MS instrument to determine ruthenium content. Ruthenium mass 101 was measured against a calibration graph produced from standards of known Ru concentrations. Any matrix changes were corrected by the online addition of Rh which was monitored at mass 103.

7.2.7 Pulsed-Field Gel Electrophoresis

A2780 CIS cells were grown in 6 cm dishes for at least 24 hours and then treated with cisplatin or ruthenium complexes at the appropriate times and concentrations. They were then washed with PBS, trypsinised, washed twice with PBS (5 ml) and suspended in PBS (100 μL). This was mixed in a 1:1 ratio with 1.6 % low melting point agarose and made into plugs. These were incubated in lysis buffer

(EDTA (0.3 M, pH 8), lauryl sarcosinate (10 mg/ml), proteinase K (1 mg/ml)) at 50 °C for 40 hours, then incubated in rinsing buffer (tris (10 mM), EDTA (10 mM), HCl (10 mM), pH 7.5) at 4 °C for 48 hours, during which time the buffer was changed twice. The plugs were run in a 1.3 % agarose gel in 0.5 % TBE buffer on a Bio Rad CHEF-DR-II machine for 36 hours at 6.0 V cm^{-2}. The initial switch time was 80 s and the final switch time was 20 s. Gels were visualised with ethidium bromide.

7.2.8 Fluorescence-Activated Cell Sorting

A2780 CIS or A549 cells were grown in culture dishes and after 24 hours were given the treatment of interest, for example 50 μM DRuT. 30 minutes before the end of the desired treatment time BrdU was added to a final concentration of 25 μM. After 30 minutes cells were washed with PBS and trypsinised, before being collected by centrifugation and washed again with PBS. Cells were then centrifuged, the supernatant was removed and the pellet was resuspended in PBS (0.5 ml). This mixture was added dropwise to 4.5 ml ice-cold 70% ethanol. Samples were then chilled at -20 °C overnight

Cells were centrifuged at 1000 RPM for 5 minutes. The supernatant was removed and the pellet was resuspended in ice-cold PBS (10 ml). The centrifugation was repeated, after which the supernatant was removed and the pellet was resuspended in ice-cold wash buffer (0.5% BSA in PBS) (1 ml). This was centrifuged at 4 °C at 2200 RPM for 5 minutes (all further centrifugation steps were performed under these conditions). The supernatant was removed and the pellet was resuspended in HCl (2 M, 1 ml) and incubated at room temperature for 20 minutes. After this ice-cold wash buffer (0.5 ml) was added and the mixture was centrifuged. The supernatant was removed and the pellet was resuspended in ice-cold wash buffer (1 ml). The mixture was centrifuged, the supernatant removed and the pellet was resuspended in sodium borate (0.1 M, pH 8.5, 0.5 ml). The mixture was then incubated at room temperature for 3 minutes. After this the sample was centrifuged and then washed with ice-cold wash buffer (1 ml). The pellet was then resuspended in ice-cold dilution buffer (0.5% BSA and 0.2% Tween-20 in PBS) (0.1 ml). Anti-BrdU antibody (BD Biosciences 347580) was added at a concentration of 1:38 and the mixture was incubated at 4 °C for 2 hours with occasional mixing.

After incubation ice-cold wash buffer (1 ml) was added, the mixture was centrifuged and the supernatant removed. The pellet was then washed with ice-cold wash buffer (1 ml). The pellet was resuspended in ice-cold dilution buffer (0.1 ml) and AF488 goat anti mouse antibody was added at a concentration of 1:50. The mixture was incubated at 4 °C for 1 hour.

Following incubation ice-cold wash buffer (0.5) ml was added, the mixture was centrifuged and the supernatant removed. The pellet was then washed twice with ice-cold wash buffer (1 ml). The pellet

was then resuspended in ice-cold PBS (1 ml) containing PI (20 µg/ml) and RNAse A (200 µg/ml). Samples were then stored at 4 ^{o}C before analysis.

Samples were analysed with a BD LSR II flow cytometer, exciting cells with a blue laser. 10000 cells were counted for each sample.

Data was analysed using the software FlowJo. A forward scatter vs. side scatter plot was used and a gate was applied to remove debris. Next, an area vs. width plot in the blue 660_20 channel was used and a gate was applied to remove doublets. Finally, the blue 660_20 A channel was plotted as a histogram (univariate plots) and the blue 660_20 A channel was plotted against the blue 530_30 A channel (bivariate plots). Gates were applied to the bivariate plots by eye to count the number of cells in each cell cycle phase.

7.2.9 Polymerase Chain Reaction Inhibition

A pACT-PCN1 plasmid was used with appropriate primers. The pACT-PCN1 (260 ng/µL, 0.5 µL) was incubated with DRuT, PRuT, DRAQ5, $[Ru(bpy)_2(dppz)]^{2+}$ at the concentrations specified in each experiment, or water, for 30 minutes at room temperature. Following this, forward and reverse primers were added, as well as High Fidelity PCR Master Mix. This mixture was put in 25 PCR cycles. Afterwards the samples were visualised on a 1% agarose gel using ethidium bromide.

7.2.10 DNA Fibre Analysis

A2780 CIS cells were seeded in 6-well plates (200000 cells per well). After 24 hours cells were treated with DRuT (19 µM) and PRuT (38 µM) for the amounts of time specified in the experiment. 40 minutes before the end of the incubation time CldU (2.5 mM, 20 µL) was added to each well. After 20 minutes IdU (2.5 mM, 200 µL) was added to each well and incubated for a further 20 minutes. Wells were then washed with ice-cold PBS. PBS (300 µL) was added to each well and the cells were scraped and transferred to eppendorfs on ice. Cells were counted using a haemocytometer and the mixtures were made up to a concentration of approximately 400000 cells/ml.

Each mixture was briefly vortexed and then 2 µL was pipetted onto a microscope slide (Menzel-Glaser, Fisher Scientific MNJ-200-010H) near the top. After incubating for 3 minutes at room temperature spreading buffer (200 mM Tris-HCl pH 7.4, 50 mM EDTA, 0.5% SDS, 7 µL) was added and mixed with a pipette tip. This was incubated at room temperature for 2 minutes. Slides were then propped at an angle on the edge of a 96-well plate lid so the drop slowly moved down the slide with gravity. The

angle was adjusted to ensure that the drop reached the bottom of the slide in approximately 3 minutes. The slide was incubated horizontally at room temperature until the liquid had evaporated. Methanol/acetic acid (3:1, 0.5 ml) was pipetted over the slide to cover it. Once dried, the slides were stored overnight at 4 °C.

Slides were dipped in water twice, before being dipped in HCl (2.5 M) and then submerged in HCl (2.5 M) for 1 hour. Slides were then dipped into PBS several times, dipped in blocking solution (PBS, 1% BSA, 0.1% Tween-20) and then submerged in blocking solution for 1 hour. Primary antibody solution (monoclonal rat anti-BrdU, clone BU1/75 (ICRI) (AbD Serotec) 1:1000, monoclonal mouse anti-BrdU (clone B44) (BD Biosciences 347580) 1:750 in blocking solution) was pipetted over each slide in a horizontal position and slides were incubated in a humidified chamber at room temperature for 1 hour.

Slides were dipped in PBS several times to wash, then PFA (4% in PBS, 1 ml) was pipetted over in a horizontal position. Slides were incubated at room temperature in a humidified chamber for 10 minutes. Slides were dipped in PBS several times, then dipped in blocking solution 3 times. Secondary antibody solution (Alexa Fluor 555 (AF555) goat-anti-rat 1:500, AF488 goat-anti-mouse 1:500 in blocking solution) was pipetted over slides in a horizontal position and they were incubated at room temperature in a humidified chamber for 1 hour.

Slides were dipped twice in PBS, dipped 3 times in blocking solution and twice more in PBS. Coverslips were mounted on slides using Immumount mounting agent. After 1 hour slides were stored at 4 °C overnight.

Slides were imaged using an Olympus FV1200 confocal microscope. The lengths of green and red fibres were measured using the software FIJI. The length of fibres in µm was converted to replication speed in kb/min using Equation 6.[205]

$$Replication\ speed = \frac{length\ X\ 2.59}{20}$$

Equation 6

At least 50 fibres were counted for each treatment condition. To measure fork asymmetry forks labelled with CldU in the centre and IdU on the outside were identified. The lengths of the two IdU-labelled portions were measured and the ratio of their lengths counted. Forks with ratios of less than 0.7 were considered to be asymmetric.

7.2.11 Rad51 Immunofluorescence

A2780 CIS cells were seeded on coverslips in 6-well plates at a concentration of 200000 cells per well. After 24 hours cells were treated with HU (0.5 mM) for 24 hours, DRuT or PRuT (50 µM) for 8 hours.

After the incubation cells were washed twice with PBS (2ml), and then fixed with PFA (4% in PBS with 0.1% Triton X-100) at room temperature for 20 minutes. Cells were washed 4 times with PBS-tx (0.15% BSA and 0.1% Triton X-100 in PBS) for 5 minutes with gentle shaking. Coverslips were covered in 100 µL of a solution of anti-Rad51 antibody (Santa Cruz Biotechnology sc-8349) (1:500 in 3% BSA in PBS). Coverslips were placed in a humidified chamber and incubated at 4 ^{o}C overnight.

Cells were washed 4 times with PBS-tx for 5 minutes with gentle shaking. Coverslips were covered in 100 µL of a solution of Alexa Fluor 568 (AF568) conjugated goat-anti-rabbit antibody (1:500 in 3% BSA in PBS). Coverslips were placed in a humidified chamber in the absence of light and incubated at room temperature for 1 hour. Cells were washed twice with PBS-tx and once with PBS for 5 minutes with gentle shaking in the absence of light. Coverslips were then dipped in MilliQ water and allowed to dry completely in the absence of light. They were then mounted onto microscope slides using Duolink with DAPI mounting agent.

Slides were imaged using a Nikon Dual Cam widefield microscope. DAPI was excited with a 395 nm laser and AF568 was excited with a 555 nm laser. Rad51 foci were counted using the software FIJI.

7.2.12 TMRE Assay

An Abcam TMRE assay kit was used according to the manufacturer's instructions. A2780 CIS or A549 cells were seeded in a 96-well plate at a density of 10000 cells per well for A2780 CIS or 6000 cells per well for A549. After 24 hours cells were treated with DRuT (IC_{50} concentration) or PRuT (IC_{50} concentration for A2780 CIS or 50 µM for A549) for the amounts of time specified in the experiment. Alternatively, cells were treated with FCCP (20 µM) for 1 hour or cisplatin (IC_{50} concentration) for 24 hours. Wells were treated in triplicate. 20 minutes prior to the end of the incubation time cells were treated with TMRE (1 µM).

At the end of the incubation period cells were washed with PBS containing 0.2% BSA (100 µL) twice. Finallly, PBS containing 0.2% BSA (100 µL) was added to each well and the fluorescence intensity was measured using a microplate reader. The excitation wavelength was 544 nm and the emission wavelength was 590 nm.

7.2.13 ptfLC3 Transfection and Imaging

ptfLC3 was a gift from Tamotsu Yoshimori (Addgene plasmid # 21074).[206] A2780 CIS or A549 cells were seeded on sterilised coverslips in 6-well plates at a concentration of 500000 cells per well. After

24 hours cells were transfected with ptfLC3 using Lipofectamine 2000 according to the manufacturer's instructions. Lipofectamine (9 µL per well), diluted in serum-free media, was added to ptfLC3 plasmid (2.4 µg/mL, 5.9 µL per well) also diluted in serum-free media. This was incubated at room temperature for 5 minutes. The mixture was then added to each well and cells were incubated for 48 hours total prior to fixation. At the amount of time prior to fixation specified in the experiment, cells were treated with DRuT (IC_{50} concentration) or PRuT (IC_{50} concentration for A2780 CIS or 50 µM for A549). Alternatively for controls, 4 hours before fixation cells were washed with PBS and then treated with EBSS media, 4 hours before fixation cells were treated with CCCP (10 µM), and 2 hours before fixation some of the cells treated with EBSS were treated with bafilomycin (500 nM).

Following incubation cells were washed with PBS (2 ml). They were then fixed with PFA (4% in PBS) at room temperature for 20 minutes. Cells were washed with PBS (2 X 2 mL), then each coverslip was dipped in MilliQ water and mounted onto a microscope slide with Prolong Gold mounting agent. These were incubated at room temperature in the absence of light for 24 hours to dry.

Slides were imaged using a Zeiss Airyscan confocal microscope. GFP was excited using a 488 nm laser and RFP was excited using a 561 nm laser. Airyscan processing was used to sharpen images.

Images were analysed using the software FIJI. Z stacks were merged into a maximum intensity projection, then yellow and red foci were counted manually in each cell.

7.2.14 MTT Assay

A2780 CIS or A549 cells were seeded in a 48-well plate at a concentration of 10000 cells per well. After 24 hours wells were treated in triplicate with the compound of interest at concentrations of 200, 100, 50, 20, 10, 1 and 0.1 µM. Cells were treated with cisplatin at the same concentrations. Control wells were untreated. Where DMSO was used to dissolve the compound of interest, DMSO concentration was kept constant in all wells. Cells were incubated for 48 hours.

Media was removed and replaced with MTT (0.5 mg/mL) diluted in serum-free media. Cells were incubated for approximately 45 minutes, until purple formazan crystals were observed in the bottom of wells. The media was aspirated and isopropanol (130 µL) was added to each well to dissolve the formazan. Once the formazan had dissolved with the aid of gentle shaking, 100 µL from each well was transferred to a 96-well plate. The absorbance at 595 nm was measured using a microplate reader.

Cell viability for each treatment condition was calculated as the ratio of the absorbance of wells given that treatment compared to the absorbance of untreated control wells. Cell viability was plotted against compound concentration for each compound, and IC_{50} concentration was calculated by interpolating the data to find the compound concentration corresponding to 50% cell viability.

7.2.15 Western Blotting

7.2.15.1 Lysate Preparation

A2780 CIS or A549 cells were seeded in 10 cm dishes. After 24 hours dishes were treated with the compound of interest at the concentration, and for the amount of time, specified in the experiment. After the incubation dishes were transferred to ice. Cells were washed 3 times with ice-cold PBS (10 ml) then lysis buffer (300 µL) was added. Dishes were incubated at room temperature for 5 minutes. Following this cells were scraped to remove them from the surface and pipetted into Eppendorf tubes on dry ice. Lysate samples were frozen and thawed 3 times and then centrifuged at 4 ºC at 13000 RPM for 5 minutes. The supernatant was collected and the solid pellet discarded. Protein concentration in lysates was calculated by a Bradford Assay.

7.2.15.2 Western Blotting

Lysates were mixed with water and sample buffer in the appropriate quantities so that the amount of protein in each sample was equal. Samples were boiled, briefly centrifuged and loaded into an acrylamide gel of the appropriate concentration for the protein of interest, in a tank containing running buffer (25 mM Tris, 190 mM glycine, 0.1% SDS). Commercial molecular weight ladders were also loaded. Gels were run at 130 V until proteins had moved sufficiently, judged by the positions of the molecular weight markers. The proteins were then transferred from the gel to nitrocellulose membrane in transfer buffer (25 mM Tris, 190 mM glycine, 20% methanol) at 100 V for 75 minutes.

The membrane was then submerged in blocking buffer (dependent upon the protein, either 5% milk or BSA in tris-buffered saline (TBS), with or without 0.1% Tween-20) for 1 hour at room temperature with gentle shaking. The membrane was submerged in a solution of the appropriate primary antibody for the protein of interest at the appropriate concentration in blocking buffer, either for 1 hour at room temperature or overnight at 4 ºC, with gentle shaking.

The membrane was then washed 4 times for 5 minutes with TBS or TBS-T (0.1% Tween-20 in TBS). It was then submerged in a solution of the appropriate secondary antibody (either fluorescently conjugated or anti- horseradish peroxidase (HRP)) in blocking buffer for 1 hour at room temperature with gentle shaking. The 4 washes were then repeated. Proteins were imaged either using LICOR or with film.

For membranes imaged with film an ECL kit was used according to the manufacturer's instructions. Membranes were then put in contact with film in the absence of light and the film was then developed.

8. References

1. Walker, M. G. Modular ruthenium complexes containing both DNA groove binding and intercalative units. University of Sheffield, 2013.
2. D., W. J.; Crick, F. H. C., A Structure for Deoxyribose Nucleic Acid. *Nature* **1953,** *171*, 737-738.
3. Belmont, P.; Constant, J.-F.; Demeunynck, M., Nucleic acid conformation diversity: from structure to function and regulation. *Chemical Society Reviews* **2001,** *30* (1), 70-81.
4. Hang, B., Formation and Repair of Tobacco Carcinogen-Derived Bulky DNA Adducts. *Journal of Nucleic Acids* **2010,** *2010*, 29.
5. Jowsey, P. A.; Williams, F. M.; Blain, P. G., DNA damage responses in cells exposed to sulphur mustard. *Toxicology letters* **2012,** *209* (1), 1-10.
6. Thomas*, T.; Thomas, T. J., Polyamines in cell growth and cell death: molecular mechanisms and therapeutic applications. *CMLS, Cell. Mol. Life Sci.* **2001,** *58* (2), 244-258.
7. Bloomfield, V. A., DNA condensation by multivalent cations. *Biopolymers* **1997,** *44* (3), 269-282.
8. Lerman, L. S., Structural considerations in the interaction of DNA and acridines. *Journal of Molecular Biology* **1961,** *3* (1), 18-IN14.

9.Chaires, J. B., Energetics of drug–DNA interactions. *Biopolymers* **1997,** *44* (3), 201-215.

10. Suh, D.; Chaires, J. B., Criteria for the mode of binding of DNA binding agents. *Bioorganic & Medicinal Chemistry* **1995,** *3* (6), 723-728.
11. Kopka, M. L.; Yoon, C.; Goodsell, D.; Pjura, P.; Dickerson, R. E., Binding of an antitumor drug to DNA: Netropsin and C-G-C-G-A-A-T-T-BrC-G-C-G. *Journal of Molecular Biology* **1985,** *183* (4), 553-563.
12. Kopka, M. L.; Yoon, C.; Goodsell, D.; Pjura, P.; Dickerson, R. E., The molecular origin of DNA-drug specificity in netropsin and distamycin. *Proceedings of the National Academy of Sciences* **1985,** *82* (5), 1376-1380.
13. Alberts, B., The Cell as a Collection of Protein Machines: Preparing the Next Generation of Molecular Biologists. *Cell* **1998,** *92* (3), 291-294.
14. Crick, F., Central Dogma of Molecular Biology. *Nature* **1970,** *227*, 561 - 563.
15. Hartwell, L. H.; Weinert, T. A., Checkpoints: controls that ensure the order of cell cycle events. *Science* **1989,** *246* (4930), 629-34.
16. M., O. C. C.; Adams, J. U., *Essentials of Cell Biology*. NPG Education: Cambridge, MA, 2010.

17. Murakami, Y.; Hurwitz, J., DNA polymerase alpha stimulates the ATP-dependent binding of simian virus tumor T antigen to the SV40 origin of replication. *Journal of Biological Chemistry* **1993,** *268* (15), 11018-27.
18. Waga, S.; Stillman, B., THE DNA REPLICATION FORK IN EUKARYOTIC CELLS. *Annual Review of Biochemistry* **1998,** *67* (1), 721-751.
19. Baker, T. A.; Bell, S. P., Polymerases and the Replisome: Machines within Machines. *Cell* **1998,** *92* (3), 295-305.
20. Berg, J. M.; J.L., T.; L., S., *Biochemistry*. 5th edition ed.; W H Freeman: New York, 2002.
21. Petermann, E.; Orta, M. L.; Issaeva, N.; Schultz, N.; Helleday, T., Hydroxyurea-Stalled Replication Forks Become Progressively Inactivated and Require Two Different RAD51-Mediated Pathways for Restart and Repair. *Molecular Cell* **2010,** *37* (4), 492-502.
22. Jossen, R.; Bermejo, R., The DNA damage checkpoint response to replication stress: A Game of Forks. *Frontiers in Genetics* **2013,** *4*.
23. Méchali, M., Eukaryotic DNA replication origins: many choices for appropriate answers. *Nat Rev Mol Cell Biol* **2010,** *11* (10), 728-738.
24. Brenner, S.; Jacob, F.; Meselson, M., An Unstable Intermediate Carrying Information from Genes to Ribosomes for Protein Synthesis. *Nature* **1961,** *190* (4776), 576-581.
25. Grünberg, S.; Hahn, S., Structural insights into transcription initiation by RNA polymerase II. *Trends in Biochemical Sciences* **2013,** *38* (12), 603-611.
26. Liu, X.; Bushnell, D. A.; Kornberg, R. D., RNA polymerase II transcription: Structure and mechanism. *Biochimica et Biophysica Acta (BBA) - Gene Regulatory Mechanisms* **2013,** *1829* (1), 2-8.
27. Steitz, T. A., A structural understanding of the dynamic ribosome machine. *Nat Rev Mol Cell Biol* **2008,** *9* (3), 242-253.
28. Erdmann, V. A.; Barciszewski, J., 2011: 50th Anniversary of the Discovery of the Genetic Code. *Angewandte Chemie International Edition* **2011,** *50* (41), 9546-9552.
29. Saibil, H., Chaperone machines for protein folding, unfolding and disaggregation. *Nat Rev Mol Cell Biol* **2013,** *14* (10), 630-642.
30. Voorhees, R. M.; Ramakrishnan, V., Structural Basis of the Translational Elongation Cycle. *Annual Review of Biochemistry* **2013,** *82* (1), 203-236.
31. Jaenicke, R., Protein Folding and Protein Association. *Angewandte Chemie International Edition in English* **1984,** *23* (6), 395-413.
32. Hartl, F. U.; Bracher, A.; Hayer-Hartl, M., Molecular chaperones in protein folding and proteostasis. *Nature* **2011,** *475* (7356), 324-332.
33. Rass, U.; Ahel, I.; West, S. C., Defective DNA Repair and Neurodegenerative Disease. *Cell* **2007,** *130* (6), 991-1004.

34. Hjertvik, M.; Erixon, K.; Ahnström, G., Repair of DNA damage in mammalian cells after treatment with UV and dimethyl sulphate: discrimination between nucleotide and base excision repair by their temperature dependence. *Mutation Research/DNA Repair* **1998,** *407* (2), 87-96.
35. Li, T.; Wang, Z.; Zhao, Y.; He, W.; An, L.; Liu, S.; Liu, Y.; Wang, H.; Hang, H., Checkpoint protein Rad9 plays an important role in nucleotide excision repair. *DNA Repair* **2013,** *12* (4), 284-292.
36. Chan, C. Y.; Galli, A.; Schiestl, R. H., Pol3 is involved in nonhomologous end-joining in Saccharomyces cerevisiae. *DNA Repair* **2008,** *7* (9), 1531-1541.
37. Li, X.; Heyer, W.-D., Homologous recombination in DNA repair and DNA damage tolerance. *Cell Res* **2008,** *18* (1), 99-113.
38. Hickman, J., Apoptosis induced by anticancer drugs. *Cancer Metast Rev* **1992,** *11* (2), 121-139.
39. Paus, R.; Rosenbach, T.; Haas, N.; Czarnetzki, B. M., Patterns of cell death: the significance of apoptosis for dermatology. *Experimental Dermatology* **1993,** *2* (1), 3-10.
40. Earnshaw, W. C.; Martins, L. M.; Kaufmann, S. H., Mammalian Caspases: Structure, Activation, Substrates, and Functions During Apoptosis. *Annual Review of Biochemistry* **1999,** *68* (1), 383-424.
41. Ashkenazi, A., Targeting the extrinsic apoptosis pathway in cancer. *Cytokine & Growth Factor Reviews* **2008,** *19* (3), 325-331.
42. Elmore, S., Apoptosis: A Review of Programmed Cell Death. *Toxicologic pathology* **2007,** *35* (4), 495-516.
43. Jiang, X.; Wang, X., Cytochrome C-Mediated Apoptosis. *Annual Review of Biochemistry* **2004,** *73* (1), 87-106.
44. Hanahan, D.; Weinberg, R. A., The Hallmarks of Cancer. *Cell* **2000,** *100* (1), 57-70.
45. Hanahan, D.; Weinberg, Robert A., Hallmarks of Cancer: The Next Generation. *Cell* **2011,** *144* (5), 646-674.
46. Malkin, D.; Li, F. P.; Strong, L. C.; Fraumeni, J. F.; Nelson, C. E.; Kim, D. H.; Kassel, J.; Gryka, M. A.; Bischoff, F. Z.; Tainsky, M. A.; et, a., Germ line p53 mutations in a familial syndrome of breast cancer, sarcomas, and other neoplasms. *Science* **1990,** *250* (4985), 1233-1238.
47. Wrzeszczynski, K. O.; Varadan, V.; Byrnes, J.; Lum, E.; Kamalakaran, S.; Levine, D. A.; Dimitrova, N.; Zhang, M. Q.; Lucito, R., Identification of Tumor Suppressors and Oncogenes from Genomic and Epigenetic Features in Ovarian Cancer. *PLoS ONE* **2011,** *6* (12), e28503.
48. *http://www.cancerresearchuk.org/cancer-info/cancerstats/survival/england-and-wales-cancer-survival-statistics*.
49. *http://www.cancerresearchuk.org/funding-for-researchers/how-we-deliver-research/our-research-strategy*.

50. https://www.cancer.org/cancer/non-small-cell-lung-cancer/about/what-is-non-small-cell-lung-cancer.html.
51. *https://www.lungcancer.org/find_information/publications/163-lung_cancer_101/268-types_and_staging*.
52. *https://www.lungcancer.org/find_information/publications/163-lung_cancer_101/269-non-small_cell_lung_cancer_treatment*.
53. *https://www.cancerresearchuk.org/about-cancer/causes-of-cancer*.
54. Doll, R.; Peto, R., The causes of cancer: quantitative estimates of avoidable risks of cancer in the United States today. *J Natl Cancer Inst* **1981,** *66* (6), 1191-308.
55. *http://www.who.int/cancer/prevention/en/*.
56. Krtolica, A.; Parrinello, S.; Lockett, S.; Desprez, P.-Y.; Campisi, J., Senescent fibroblasts promote epithelial cell growth and tumorigenesis: A link between cancer and aging. *Proceedings of the National Academy of Sciences* **2001,** *98* (21), 12072.
57. Parkin, D. M.; Boyd, L.; Walker, L. C., 16. The fraction of cancer attributable to lifestyle and environmental factors in the UK in 2010. *British Journal Of Cancer* **2011,** *105*, S77.
58. Wolin, K. Y.; Carson, K.; Colditz, G. A., Obesity and Cancer. *The Oncologist* **2010,** *15* (6), 556-565.
59. Rigel, D. S., Cutaneous ultraviolet exposure and its relationship to the development of skin cancer. *Journal of the American Academy of Dermatology* **2008,** *58* (5), S129-S132.
60. Chan, D. S. M.; Lau, R.; Aune, D.; Vieira, R.; Greenwood, D. C.; Kampman, E.; Norat, T., Red and Processed Meat and Colorectal Cancer Incidence: Meta-Analysis of Prospective Studies. *PLOS ONE* **2011,** *6* (6), e20456.
61. Block, G.; Patterson, B.; Subar, A., Fruit, vegetables, and cancer prevention: A review of the epidemiological evidence. *Nutrition and Cancer* **1992,** *18* (1), 1-29.
62. Friedenreich, C. M.; Neilson, H. K.; Lynch, B. M., State of the epidemiological evidence on physical activity and cancer prevention. *European Journal of Cancer* **2010,** *46* (14), 2593-2604.
63. Boffetta, P.; Hashibe, M., Alcohol and cancer. *The Lancet Oncology* **2006,** *7* (2), 149-156.
64. Burd, E. M., Human Papillomavirus and Cervical Cancer. *Clinical Microbiology Reviews* **2003,** *16* (1), 1-17.
65. Raaschou-Nielsen, O.; Andersen, Z. J.; Beelen, R.; Samoli, E.; Stafoggia, M.; Weinmayr, G.; Hoffmann, B.; Fischer, P.; Nieuwenhuijsen, M. J.; Brunekreef, B.; Xun, W. W.; Katsouyanni, K.; Dimakopoulou, K.; Sommar, J.; Forsberg, B.; Modig, L.; Oudin, A.; Oftedal, B.; Schwarze, P. E.; Nafstad, P.; De Faire, U.; Pedersen, N. L.; Östenson, C.-G.; Fratiglioni, L.; Penell, J.; Korek, M.; Pershagen, G.; Eriksen, K. T.; Sørensen, M.; Tjønneland, A.; Ellermann, T.; Eeftens, M.; Peeters, P. H.; Meliefste, K.; Wang, M.; Bueno-de-Mesquita, B.; Key, T. J.; de Hoogh, K.; Concin, H.; Nagel, G.; Vilier, A.; Grioni, S.; Krogh, V.; Tsai, M.-Y.; Ricceri, F.; Sacerdote, C.; Galassi, C.; Migliore, E.; Ranzi, A.; Cesaroni, G.; Badaloni, C.; Forastiere, F.;

Tamayo, I.; Amiano, P.; Dorronsoro, M.; Trichopoulou, A.; Bamia, C.; Vineis, P.; Hoek, G., Air pollution and lung cancer incidence in 17 European cohorts: prospective analyses from the European Study of Cohorts for Air Pollution Effects (ESCAPE). *The Lancet Oncology* **2013,** *14* (9), 813-822.

66. Darby, S.; Hill, D.; Auvinen, A.; Barros-Dios, J. M.; Baysson, H.; Bochicchio, F.; Deo, H.; Falk, R.; Forastiere, F.; Hakama, M.; Heid, I.; Kreienbrock, L.; Kreuzer, M.; Lagarde, F.; Mäkeläinen, I.; Muirhead, C.; Oberaigner, W.; Pershagen, G.; Ruano-Ravina, A.; Ruosteenoja, E.; Rosario, A. S.; Tirmarche, M.; Tomáscaron; ek, L.; Whitley, E.; Wichmann, H. E.; Doll, R., Radon in homes and risk of lung cancer: collaborative analysis of individual data from 13 European case-control studies. *BMJ* **2005,** *330* (7485), 223.
67. Brown, K. F.; Rumgay, H.; Dunlop, C.; Ryan, M.; Quartly, F.; Cox, A.; Deas, A.; Elliss-Brookes, L.; Gavin, A.; Hounsome, L.; Huws, D.; Ormiston-Smith, N.; Shelton, J.; White, C.; Parkin, D. M., The fraction of cancer attributable to modifiable risk factors in England, Wales, Scotland, Northern Ireland, and the United Kingdom in 2015. *British Journal of Cancer* **2018,** *118* (8), 1130-1141.
68. Pronk, G. J.; Bos, J. L., The role of p21ras in receptor tyrosine kinase signalling. *Biochimica et Biophysica Acta (BBA) - Reviews on Cancer* **1994,** *1198* (2), 131-147.
69. Sporn, M. B., The war on cancer. *The Lancet* **1996,** *347* (9012), 1377-1381.
70. Hubenak, J. R.; Zhang, Q.; Branch, C. D.; Kronowitz, S. J., Mechanisms of injury to normal tissue after radiotherapy: a review. *Plastic and reconstructive surgery* **2014,** *133* (1), 49e-56e.
71. Bentzen, S. M., Preventing or reducing late side effects of radiation therapy: radiobiology meets molecular pathology. *Nature Reviews Cancer* **2006,** *6*, 702.
72. Coates, A.; Abraham, S.; Kaye, S. B.; Sowerbutts, T.; Frewin, C.; Fox, R. M.; Tattersall, M. H., On the receiving end--patient perception of the side-effects of cancer chemotherapy. *European journal of cancer & clinical oncology* **1983,** *19* (2), 203-8.
73. Partridge, A. H.; Burstein, H. J.; Winer, E. P., Side effects of chemotherapy and combined chemohormonal therapy in women with early-stage breast cancer. *Journal of the National Cancer Institute. Monographs* **2001,** (30), 135-42.
74. Jacobsen, P. B.; Stein, K., Is Fatigue a Long-term Side Effect of Breast Cancer Treatment? *Cancer control : journal of the Moffitt Cancer Center* **1999,** *6* (3), 256-263.
75. Ahles, T. A.; Saykin, A. J.; Furstenberg, C. T.; Cole, B.; Mott, L. A.; Skalla, K.; Whedon, M. B.; Bivens, S.; Mitchell, T.; Greenberg, E. R.; Silberfarb, P. M., Neuropsychologic impact of standard-dose systemic chemotherapy in long-term survivors of breast cancer and lymphoma. *Journal of clinical oncology : official journal of the American Society of Clinical Oncology* **2002,** *20* (2), 485-93.
76. Weiner, L. M.; Surana, R.; Wang, S., Antibodies and cancer therapy: versatile platforms for cancer immunotherapy. *Nature reviews. Immunology* **2010,** *10* (5), 317-327.

77. Dranoff, G., Cytokines in cancer pathogenesis and cancer therapy. *Nat Rev Cancer* **2004,** *4* (1), 11-22.

78. Finn, O. J., Cancer Immunology. *New England Journal of Medicine* **2008,** *358* (25), 2704-2715.

79. Perica, K.; Varela, J. C.; Oelke, M.; Schneck, J., Adoptive T Cell Immunotherapy for Cancer. *Rambam Maimonides Medical Journal* **2015,** *6* (1), e0004.

80. Loges, S.; Mazzone, M.; Hohensinner, P.; Carmeliet, P., Silencing or fueling metastasis with VEGF inhibitors: antiangiogenesis revisited. *Cancer Cell* **2009,** *15* (3), 167-70.

81. Ledermann, J.; Harter, P.; Gourley, C.; Friedlander, M.; Vergote, I.; Rustin, G.; Scott, C. L.; Meier, W.; Shapira-Frommer, R.; Safra, T.; Matei, D.; Fielding, A.; Spencer, S.; Dougherty, B.; Orr, M.; Hodgson, D.; Barrett, J. C.; Matulonis, U., Olaparib maintenance therapy in patients with platinum-sensitive relapsed serous ovarian cancer: a preplanned retrospective analysis of outcomes by BRCA status in a randomised phase 2 trial. *The Lancet. Oncology* **2014,** *15* (8), 852-61.

82. Samol, J.; Ranson, M.; Scott, E.; Macpherson, E.; Carmichael, J.; Thomas, A.; Cassidy, J., Safety and tolerability of the poly(ADP-ribose) polymerase (PARP) inhibitor, olaparib (AZD2281) in combination with topotecan for the treatment of patients with advanced solid tumors: a phase I study. *Invest New Drugs* **2012,** *30* (4), 1493-500.

83. Fricker, S. P., Metal based drugs: from serendipity to design. *Dalton Transactions* **2007,** (43), 4903-4917.

84. Kelland, L., The resurgence of platinum-based cancer chemotherapy. *Nat Rev Cancer* **2007,** *7* (8), 573-584.

85. Galluzzi, L.; Vitale, I.; Michels, J.; Brenner, C.; Szabadkai, G.; Harel-Bellan, A.; Castedo, M.; Kroemer, G., Systems biology of cisplatin resistance: past, present and future. *Cell Death &Amp; Disease* **2014,** *5*, e1257.

86. Bergamo, A.; Dyson, P. J.; Sava, G., The mechanism of tumour cell death by metal-based anticancer drugs is not only a matter of DNA interactions. *Coordination Chemistry Reviews* **2018,** *360*, 17-33.

87. Fraval, H. N. A.; Roberts, J. J., Excision Repair of Diamminedichloroplatinum(II)-induced Damage to DNA of Chinese Hamster Cells. *Cancer Research* **1979,** *39* (5), 1793.

88. Siddik, Z. H., Cisplatin: mode of cytotoxic action and molecular basis of resistance. *Oncogene* **2002,** *22*, 7265.

89. Gonzalez, V. M.; Fuertes, M. A.; Alonso, C.; Perez, J. M., Is Cisplatin-Induced Cell Death Always Produced by Apoptosis? *Molecular Pharmacology* **2001,** *59* (4), 657.

90. Yu, F.; Megyesi, J.; Price, P. M., Cytoplasmic initiation of cisplatin cytotoxicity. *American Journal of Physiology-Renal Physiology* **2008,** *295* (1), F44-F52.

91. Brenner, C.; Grimm, S., The permeability transition pore complex in cancer cell death. *Oncogene* **2006,** *25*, 4744.

92. Tajeddine, N.; Galluzzi, L.; Kepp, O.; Hangen, E.; Morselli, E.; Senovilla, L.; Araujo, N.; Pinna, G.; Larochette, N.; Zamzami, N.; Modjtahedi, N.; Harel-Bellan, A.; Kroemer, G., Hierarchical involvement of Bak, VDAC1 and Bax in cisplatin-induced cell death. *Oncogene* **2008,** *27*, 4221.

93. Chipuk, J. E.; Kuwana, T.; Bouchier-Hayes, L.; Droin, N. M.; Newmeyer, D. D.; Schuler, M.; Green, D. R., Direct Activation of Bax by p53 Mediates Mitochondrial Membrane Permeabilization and Apoptosis. *Science* **2004,** *303* (5660), 1010.

94. Bragado, P.; Armesilla, A.; Silva, A.; Porras, A., Apoptosis by cisplatin requires p53 mediated p38α MAPK activation through ROS generation. *Apoptosis* **2007,** *12* (9), 1733-1742.

95. Hodeify, R.; Megyesi, J.; Tarcsafalvi, A.; Safirstein, R. L.; Price, P. M., Protection of cisplatin cytotoxicity by an inactive cyclin-dependent kinase. *American Journal of Physiology-Renal Physiology* **2010,** *299* (1), F112-F120.

96. Zhu, S.; Pabla, N.; Tang, C.; He, L.; Dong, Z., DNA Damage Response in Cisplatin-Induced Nephrotoxicity. *Archives of Toxicology* **2015,** *89* (12), 2197-2205.

97. Wheate, N. J.; Walker, S.; Craig, G. E.; Oun, R., The status of platinum anticancer drugs in the clinic and in clinical trials. *Dalton Transactions* **2010,** *39* (35), 8113-8127.

98. Neidle, S.; Ismail, I. M.; Sadler, P. J., The structure of the antitumor complex cis-(diammino) (1,1-cyclobutanedicarboxylato)-Pt(II): X ray and nmr studies. *Journal of Inorganic Biochemistry* **1980,** *13* (3), 205-212.

99. Frey, U.; Ranford, J. D.; Sadler, P. J., Ring-opening reactions of the anticancer drug carboplatin: NMR characterization of cis-[Pt(NH3)2(CBDCA-O)(5'-GMP-N7)] in solution. *Inorganic Chemistry* **1993,** *32* (8), 1333-1340.

100. Holzer, A. K.; Manorek, G. H.; Howell, S. B., Contribution of the Major Copper Influx Transporter CTR1 to the Cellular Accumulation of Cisplatin, Carboplatin, and Oxaliplatin. *Molecular Pharmacology* **2006,** *70* (4), 1390-1394.

101. Mistry, P.; Kelland, L. R.; Abel, G.; Sidhar, S.; Harrap, K. R., The relationships between glutathione, glutathione-S-transferase and cytotoxicity of platinum drugs and melphalan in eight human ovarian carcinoma cell lines. *British Journal of Cancer* **1991,** *64* (2), 215-220.

102. Johnson, S. W.; Swiggard, P. A.; Handel, L. M.; Brennan, J. M.; Godwin, A. K.; Ozols, R. F.; Hamilton, T. C., Relationship between Platinum-DNA Adduct Formation and Removal and Cisplatin Cytotoxicity in Cisplatin-sensitive and -resistant Human Ovarian Cancer Cells. *Cancer Research* **1994,** *54* (22), 5911.

103. Ferry, K. V.; Hamilton, T. C.; Johnson, S. W., Increased nucleotide excision repair in cisplatin-resistant ovarian cancer cells: Role of ercc1–xpf. *Biochemical Pharmacology* **2000,** *60* (9), 1305-1313.

104. Chang, I.-Y.; Kim, M.-H.; Kim, H. B.; Lee, D. Y.; Kim, S.-H.; Kim, H.-Y.; You, H. J., Small interfering RNA-induced suppression of ERCC1 enhances sensitivity of human cancer cells to cisplatin. *Biochemical and Biophysical Research Communications* **2005,** *327* (1), 225-233.

105. Aebi, S.; Kurdi-Haidar, B.; Gordon, R.; Cenni, B.; Zheng, H.; Fink, D.; Christen, R. D.; Boland, C. R.; Koi, M.; Fishel, R.; Howell, S. B., Loss of DNA Mismatch Repair in Acquired Resistance to Cisplatin. *Cancer Research* **1996,** *56* (13), 3087.

106. Bassett, E.; Vaisman, A.; Tropea, K. A.; McCall, C. M.; Masutani, C.; Hanaoka, F.; Chaney, S. G., Frameshifts and deletions during in vitro translesion synthesis past Pt–DNA adducts by DNA polymerases β and η. *DNA Repair* **2002,** *1* (12), 1003-1016.

107. Ndagi, U.; Mhlongo, N.; Soliman, M. E., Metal complexes in cancer therapy - an update from drug design perspective. *Drug design, development and therapy* **2017,** *11*, 599-616.

108. Mojžišová, G.; Mojžiš, J.; Vašková, J., Organometallic iron complexes as potential cancer therapeutics. *Acta Biochimica Polonica* **2014,** *61* (4), 651-654.

109. Butler, J. S.; Sadler, P. J., Targeted delivery of platinum-based anticancer complexes. *Current Opinion in Chemical Biology* **2013,** *17* (2), 175-188.

110. Maeda, H.; Wu, J.; Sawa, T.; Matsumura, Y.; Hori, K., Tumor vascular permeability and the EPR effect in macromolecular therapeutics: a review. *Journal of Controlled Release* **2000,** *65* (1–2), 271-284.

111. Kobayashi, H.; Watanabe, R.; Choyke, P. L., Improving Conventional Enhanced Permeability and Retention (EPR) Effects; What Is the Appropriate Target? *Theranostics* **2014,** *4* (1), 81-89.

112. Tripisciano, C.; Kraemer, K.; Taylor, A.; Borowiak-Palen, E., Single-wall carbon nanotubes based anticancer drug delivery system. *Chemical Physics Letters* **2009,** *478* (4–6), 200-205.

113. Dhar, S.; Daniel, W. L.; Giljohann, D. A.; Mirkin, C. A.; Lippard, S. J., Polyvalent Oligonucleotide Gold Nanoparticle Conjugates as Delivery Vehicles for Platinum(IV) Warheads. *Journal of the American Chemical Society* **2009,** *131* (41), 14652-14653.

114. Min, Y.; Mao, C.; Xu, D.; Wang, J.; Liu, Y., Gold nanorods for platinum based prodrug delivery. *Chemical Communications* **2010,** *46* (44), 8424-8426.

115. Jennette, K. W.; Lippard, S. J.; Vassiliades, G. A.; Bauer, W. R., Metallointercalation Reagents. 2-Hydroxyethanethiolato(2,2′,2″-terpyridine)-platinum(II) Monocation Binds Strongly to DNA By Intercalation. *Proceedings of the National Academy of Sciences* **1974,** *71* (10), 3839-3843.

116. Barton, J. K.; Danishefsky, A.; Goldberg, J., Tris(phenanthroline)ruthenium(II): stereoselectivity in binding to DNA. *Journal of the American Chemical Society* **1984,** *106* (7), 2172-2176.

117. Wong, Y.-S.; Lippard, S. J., X-Ray crystal structure of a 2:2 chloroterpyridineplatinum(II)-adenosine-5[prime or minute]-monophosphate intercalation complex. *Journal of the Chemical Society, Chemical Communications* **1977,** (22), 824-825.

118. Dwyer, F. P.; Mayhew, E.; Roe, E. M.; Shulman, A., Inhibition of Landschütz Ascites Tumour Growth by Metal Chelates Derived from 3,4,7,8-Tetramethyl-1,10-phenanthroline. *Br J Cancer* **1965,** *19* (1), 195-199.

119. Levina, A.; Mitra, A.; Lay, P. A., Recent developments in ruthenium anticancer drugs. *Metallomics* **2009,** *1* (6), 458-470.

120. Han Ang, W.; Dyson, P. J., Classical and Non-Classical Ruthenium-Based Anticancer Drugs: Towards Targeted Chemotherapy. *European Journal of Inorganic Chemistry* **2006,** *2006* (20), 4003-4018.

121. Novakova, O.; Kasparkova, J.; Vrana, O.; van Vliet, P. M.; Reedijk, J.; Brabec, V., Correlation between Cytotoxicity and DNA Binding of Polypyridyl Ruthenium Complexes. *Biochemistry* **1995,** *34* (38), 12369-12378.

122. Novohradsky, V.; Bergamo, A.; Cocchietto, M.; Zajac, J.; Brabec, V.; Mestroni, G.; Sava, G., Influence of the binding of reduced NAMI-A to human serum albumin on the pharmacokinetics and biological activity. *Dalton Transactions* **2015,** *44* (4), 1905-1913.

123. Sava, G.; Zorzet, S.; Turrin, C.; Vita, F.; Soranzo, M.; Zabucchi, G.; Cocchietto, M.; Bergamo, A.; DiGiovine, S.; Pezzoni, G.; Sartor, L.; Garbisa, S., Dual Action of NAMI-A in Inhibition of Solid Tumor Metastasis: Selective Targeting of Metastatic Cells and Binding to Collagen. *Clinical Cancer Research* **2003,** *9* (5), 1898-1905.

124. Sava, G.; Pacor, S.; Mestroni, G.; Alessio, E., Na[trans-RuCl4(DMSO)Im], a metal complex of ruthenium with antimetastatic properties. *Clinical & Experimental Metastasis* **1992,** *10* (4), 273-280.

125. Rademaker-Lakhai, J. M.; van den Bongard, D.; Pluim, D.; Beijnen, J. H.; Schellens, J. H. M., A Phase I and Pharmacological Study with Imidazolium-trans-DMSO-imidazole-tetrachlororuthenate, a Novel Ruthenium Anticancer Agent. *Clinical Cancer Research* **2004,** *10* (11), 3717-3727.

126. Leijen, S.; Burgers, S. A.; Baas, P.; Pluim, D.; Tibben, M.; van Werkhoven, E.; Alessio, E.; Sava, G.; Beijnen, J. H.; Schellens, J. H. M., Phase I/II study with ruthenium compound NAMI-A and gemcitabine in patients with non-small cell lung cancer after first line therapy. *Investigational New Drugs* **2015,** *33* (1), 201-214.

127. Hartinger, C. G.; Jakupec, M. A.; Zorbas-Seifried, S.; Groessl, M.; Egger, A.; Berger, W.; Zorbas, H.; Dyson, P. J.; Keppler, B. K., KP1019, A New Redox-Active Anticancer Agent – Preclinical Development and Results of a Clinical Phase I Study in Tumor Patients. *Chemistry & Biodiversity* **2008,** *5* (10), 2140-2155.

128. Trondl, R.; Heffeter, P.; Kowol, C. R.; Jakupec, M. A.; Berger, W.; Keppler, B. K., NKP-1339, the first ruthenium-based anticancer drug on the edge to clinical application. *Chemical Science* **2014,** *5* (8), 2925-2932.

129. Burris, H. A.; Bakewell, S.; Bendell, J. C.; Infante, J.; Jones, S. F.; Spigel, D. R.; Weiss, G. J.; Ramanathan, R. K.; Ogden, A.; Von Hoff, D., Safety and activity of IT-139, a ruthenium-based compound, in patients with advanced solid tumours: a first-in-human, open-label, dose-escalation phase I study with expansion cohort. *ESMO Open* **2016,** *1* (6).

130. Heffeter, P.; Böck, K.; Atil, B.; Reza Hoda, M. A.; Körner, W.; Bartel, C.; Jungwirth, U.; Keppler, B. K.; Micksche, M.; Berger, W.; Koellensperger, G., Intracellular protein binding patterns of the anticancer ruthenium drugs KP1019 and KP1339. *JBIC Journal of Biological Inorganic Chemistry* **2010,** *15* (5), 737-748.

131. Long, E. C.; Barton, J. K., On demonstrating DNA intercalation. *Accounts of Chemical Research* **1990,** *23* (9), 271-273.

132. Rehmann, J. P.; Barton, J. K., Proton NMR studies of tris(phenanthroline) metal complexes bound to oligonucleotides: characterization of binding modes. *Biochemistry* **1990,** *29* (7), 1701-1709.

133. Rehmann, J. P.; Barton, J. K., Proton NMR studies of tris(phenanthroline) metal complexes bound to oligonucleotides: structural characterizations via selective paramagnetic relaxation. *Biochemistry* **1990,** *29* (7), 1710-1717.

134. Satyanarayana, S.; Dabrowiak, J. C.; Chaires, J. B., Neither .DELTA.- nor .LAMBDA.-tris(phenanthroline)ruthenium(II) binds to DNA by classical intercalation. *Biochemistry* **1992,** *31* (39), 9319-9324.

135. Satyanarayana, S.; Dabrowiak, J. C.; Chaires, J. B., Tris(phenanthroline)ruthenium(II) enantiomer interactions with DNA: Mode and specificity of binding. *Biochemistry* **1993,** *32* (10), 2573-2584.

136. Friedman, A. E.; Chambron, J. C.; Sauvage, J. P.; Turro, N. J.; Barton, J. K., A molecular light switch for DNA: Ru(bpy)2(dppz)2+. *Journal of the American Chemical Society* **1990,** *112* (12), 4960-4962.

137. Gill, M. R.; Thomas, J. A., Ruthenium(ii) polypyridyl complexes and DNA-from structural probes to cellular imaging and therapeutics. *Chemical Society Reviews* **2012,** *41* (8), 3179-3192.

138. Jenkins, Y.; Friedman, A. E.; Turro, N. J.; Barton, J. K., Characterization of dipyridophenazine complexes of ruthenium(II): The light switch effect as a function of nucleic acid sequence and conformation. *Biochemistry* **1992,** *31* (44), 10809-10816.

139. Lu, X.-H.; Shi, S.; Yao, J.-L.; Gao, X.; Huang, H.-L.; Yao, T.-M., Two structurally analogous ruthenium complexes as naked-eye and reversible molecular “light switch” for G-quadruplex DNA. *Journal of Inorganic Biochemistry* **2014,** *140* (0), 64-71.

140. Blackburn, G. M.; Gait, M. J.; Loakes, D.; Williams, D. M., *Nucleic Acids in Chemistry and Biology*. 3rd ed.; The Royal Society of Chemistry: Cambridge, 2006.

141. Jiang, Y.; Fang, X.; Bai, C., Signaling Aptamer/Protein Binding by a Molecular Light Switch Complex. *Analytical Chemistry* **2004,** *76* (17), 5230-5235.

142. Gill, M. R.; Garcia-Lara, J.; Foster, S. J.; Smythe, C.; Battaglia, G.; Thomas, J. A., A ruthenium(II) polypyridyl complex for direct imaging of DNA structure in living cells. *Nature Chemistry* **2009,** *1*, 662-667.

143. Tian, X.; Gill , M. R.; Cantón, I.; Thomas, J. A.; Battaglia, G., Live Cell Luminescence Imaging As a Function of Delivery Mechanism. *ChemBioChem* **2011,** *12* (4), 548-551.

144. Sreedharan, S.; Sinopoli, A.; Jarman, P. J.; Robinson, D.; Clemmet, C.; Scattergood, P. A.; Rice, C. R.; Smythe, C. G. W.; Thomas, J. A.; Elliott, P. I. P., Mitochondria-localising DNA-binding biscyclometalated phenyltriazole iridium(iii) dipyridophenazene complexes: syntheses and cellular imaging properties. *Dalton Transactions* **2018,** *47* (14), 4931-4940.

145. Gill, M. R.; Jarman, P. J.; Halder, S.; Walker, M. G.; Saeed, H. K.; Thomas, J. A.; Smythe, C.; Ramadan, K.; Vallis, K. A., A three-in-one-bullet for oesophageal cancer: replication fork collapse, spindle attachment failure and enhanced radiosensitivity generated by a ruthenium(ii) metallo-intercalator. *Chemical Science* **2018,** *9* (4), 841-849.

146. Sreedharan, S.; Gill, M. R.; Garcia, E.; Saeed, H. K.; Robinson, D.; Byrne, A.; Cadby, A.; Keyes, T. E.; Smythe, C.; Pellett, P.; Bernardino de la Serna, J.; Thomas, J. A., Multimodal Super-resolution Optical Microscopy Using a Transition-Metal-Based Probe Provides Unprecedented Capabilities for Imaging Both Nuclear Chromatin and Mitochondria. *Journal of the American Chemical Society* **2017,** *139* (44), 15907-15913.

147. Saeed, H. K.; Jarman, P. J.; Archer, S.; Sreedharan, S.; Saeed, I. Q.; McKenzie, L. K.; Weinstein, J. A.; Buurma, N. J.; Smythe, C. G. W.; Thomas, J. A., Homo- and Heteroleptic Phototoxic Dinuclear Metallo-Intercalators Based on Ru(II) (dppn) Intercalating Moieties: Synthesis, Optical, and Biological Studies. *Angewandte Chemie (International ed. in English)* **2017,** *56* (41), 12628-12633.

148. Trofimenko, S., Recent advances in poly(pyrazolyl)borate (scorpionate) chemistry. *Chemical Reviews* **1993,** *93* (3), 943-980.

149. Holford, J.; Sharp, S. Y.; Murrer, B. A.; Abrams, M.; Kelland, L. R., In vitro circumvention of cisplatin resistance by the novel sterically hindered platinum complex AMD473. *British Journal of Cancer* **1998,** *77* (3), 366-373.

150. Waywell, P.; Gonzalez, V.; Gill, M. R.; Adams, H.; Meijer, A. J. H. M.; Williamson, M. P.; Thomas, J. A., Structure of the Complex of [Ru(tpm)(dppz)py]2+ with a B-DNA Oligonucleotide—A Single-Substituent Binding Switch for a Metallo-Intercalator. *Chemistry – A European Journal* **2010,** *16* (8), 2407-2417.

151. Harrington, H. A.; Ho, K. L.; Ghosh, S.; Tung, K. C., Construction and analysis of a modular model of caspase activation in apoptosis. *Theoretical Biology & Medical Modelling* **2008,** *5*, 26-26.

152. Xiao, Z.; Chen, Z.; Gunasekera, A. H.; Sowin, T. J.; Rosenberg, S. H.; Fesik, S.; Zhang, H., Chk1 Mediates S and G2 Arrests through Cdc25A Degradation in Response to DNA-damaging Agents. *Journal of Biological Chemistry* **2003,** *278* (24), 21767-21773.

153. Zhao, H.; Piwnica-Worms, H., ATR-Mediated Checkpoint Pathways Regulate Phosphorylation and Activation of Human Chk1. *Molecular and Cellular Biology* **2001,** *21* (13), 4129-4139.

154. Pabla, N.; Huang, S.; Mi, Q.-S.; Daniel, R.; Dong, Z., ATR-Chk2 Signaling in p53 Activation and DNA Damage Response during Cisplatin-induced Apoptosis. *Journal of Biological Chemistry* **2008,** *283* (10), 6572-6583.

155. Rogakou, E. P.; Pilch, D. R.; Orr, A. H.; Ivanova, V. S.; Bonner, W. M., DNA Double-stranded Breaks Induce Histone H2AX Phosphorylation on Serine 139. *Journal of Biological Chemistry* **1998,** *273* (10), 5858-5868.

156. Kisova, A.; Zerzankova, L.; Habtemariam, A.; Sadler, P. J.; Brabec, V.; Kasparkova, J., Differences in the Cellular Response and Signaling Pathways between Cisplatin and Monodentate Organometallic Ru(II) Antitumor Complexes Containing a Terphenyl Ligand. *Molecular Pharmaceutics* **2011,** *8* (3), 949-957.

157. Albani, B. A.; Peña, B.; Leed, N. A.; de Paula, N. A. B. G.; Pavani, C.; Baptista, M. S.; Dunbar, K. R.; Turro, C., Marked Improvement in Photoinduced Cell Death by a New Tris-heteroleptic Complex with Dual Action: Singlet Oxygen Sensitization and Ligand Dissociation. *Journal of the American Chemical Society* **2014,** *136* (49), 17095-17101.

158. Gill , M. R. DNA-binding ruthenium complexes: cellular imaging and cytotoxicity. University of Sheffield, 2010.

159. Zheng, R. H.; Guo, H. C.; Jiang, H. J.; Xu, K. H.; Liu, B. B.; Sun, W. L.; Shen, Z. Q., A new and convenient synthesis of phendiones oxidated by KBrO3/H2SO4 at room temperature. *Chinese Chemical Letters* **2010,** *21* (11), 1270-1272.

160. Llobet, A.; Doppelt, P.; Meyer, T. J., Redox properties of aqua complexes of ruthenium(II) containing the tridentate ligands 2,2':6',2''-terpyridine and tris(1-pyrazolyl)methane. *Inorganic Chemistry* **1988,** *27* (3), 514-520.

161. Sullivan, B. P.; Salmon, D. J.; Meyer, T. J., Mixed phosphine 2,2'-bipyridine complexes of ruthenium. *Inorganic Chemistry* **1978,** *17* (12), 3334-3341.

162. Amouyal, E.; Homsi, A.; Chambron, J.-C.; Sauvage, J.-P., Synthesis and study of a mixed-ligand ruthenium(II) complex in its ground and excited states: bis(2,2[prime or minute]-bipyridine)(dipyrido[3,2-a : 2[prime or minute],3[prime or minute]-c]phenazine-N4N5)ruthenium(II). *Journal of the Chemical Society, Dalton Transactions* **1990,** (6), 1841-1845.

163. Yamada, K.; Kato, N.; Takagi, A.; Koi, M.; Hemmi, H., One-milliliter wet-digestion for inductively coupled plasma mass spectrometry (ICP-MS): determination of platinum-DNA

adducts in cells treated with platinum(II) complexes. *Anal Bioanal Chem* **2005,** *382* (7), 1702-1707.

164. Wu, B.; Ong, M. S.; Groessl, M.; Adhireksan, Z.; Hartinger, C. G.; Dyson, P. J.; Davey, C. A., A Ruthenium Antimetastasis Agent Forms Specific Histone Protein Adducts in the Nucleosome Core. *Chemistry – A European Journal* **2011,** *17* (13), 3562-3566.
165. Barbas, C. F.; Burton, D. R.; Scott, J. K.; Silverman, G. J., Quantitation of DNA and RNA. *Cold Spring Harbor Protocols* **2007,** *2007* (11), pdb.ip47.
166. Wilfinger, W. W.; Mackey, K.; Chomczynski, P., Effect of pH and ionic strength on the spectrophotometric assessment of nucleic acid purity. *BioTechniques* **1997,** *22* (3), 474-6, 478-81.
167. Liu, J.-G.; Ye, B.-H.; Li, H.; Zhen, Q.-X.; Ji, L.-N.; Fu, Y.-H., Polypyridyl ruthenium(II) complexes containing intramolecular hydrogen-bond ligand: syntheses, characterization, and DNA-binding properties. *Journal of Inorganic Biochemistry* **1999,** *76* (3–4), 265-271.
168. Marcelis, A. T. M.; van Kralingen, C. G.; Reedijk, J., The interactions of cis- and trans-diammineplatinum compounds with 5′-guanosine monophosphate and 5′-deoxyguanosine monophosphate. A proton nmr investigation. *Journal of Inorganic Biochemistry* **1980,** *13* (3), 213-222.
169. Rilak, A.; Bratsos, I.; Zangrando, E.; Kljun, J.; Turel, I.; Bugarčić, Ž. D.; Alessio, E., New Water-Soluble Ruthenium(II) Terpyridine Complexes for Anticancer Activity: Synthesis, Characterization, Activation Kinetics, and Interaction with Guanine Derivatives. *Inorganic Chemistry* **2014,** *53* (12), 6113-6126.
170. Guéron, M.; Plateau, P.; Decorps, M., Solvent signal suppression in NMR. *Progress in Nuclear Magnetic Resonance Spectroscopy* **1991,** *23* (2), 135-209.
171. Brabec, V.; Balcarova, Z., Restriction-enzyme cleavage of DNA modified by platinum(II) complexes. *European Journal of Biochemistry* **1993,** *216* (1), 183-187.
172. Choudhury, J. R.; Rao, L.; Bierbach, U., Rates of intercalator-driven platination of DNA determined by a restriction enzyme cleavage inhibition assay. *J Biol Inorg Chem* **2011,** *16* (3), 373-80.
173. Sitlani, A.; Dupureur, C. M.; Barton, J. K., Enantiospecific palindromic recognition of 5'-d(CTCTAGAG)-3' by a novel rhodium intercalator: analogies to a DNA-binding protein. *Journal of the American Chemical Society* **1993,** *115* (26), 12589-12590.
174. Hintermann, G.; Fischer, H. M.; Crameri, R.; Hütter, R., Simple procedure for distinguishing CCC, OC, and L forms of plasmid DNA by agarose gel electrophoresis. *Plasmid* **1981,** *5* (3), 371-373.
175. Chen, Y.-M.; Liu, Y.-J.; Li, Q.; Wang, K.-Z., pH- and DNA-induced dual molecular light switches based on a novel ruthenium(II) complex. *Journal of Inorganic Biochemistry* **2009,** *103* (10), 1395-1404.

176. Huang, H.; Zhang, P.; Chen, H.; Ji, L.; Chao, H., Comparison Between Polypyridyl and Cyclometalated Ruthenium(II) Complexes: Anticancer Activities Against 2D and 3D Cancer Models. *Chemistry – A European Journal* **2014,** *21* (2), 715-725.

177. Boger, D. L.; Fink, B. E.; Brunette, S. R.; Tse, W. C.; Hedrick, M. P., A Simple, High-Resolution Method for Establishing DNA Binding Affinity and Sequence Selectivity. *Journal of the American Chemical Society* **2001,** *123* (25), 5878-5891.

178. Nair, R. B.; Teng, E. S.; Kirkland, S. L.; Murphy, C. J., Synthesis and DNA-Binding Properties of [Ru(NH3)4dppz]2+. *Inorganic Chemistry* **1998,** *37* (1), 139-141.

179. Sahoo, B. K.; Ghosh, K. S.; Bera, R.; Dasgupta, S., Studies on the interaction of diacetylcurcumin with calf thymus-DNA. *Chemical Physics* **2008,** *351* (1), 163-169.

180. Loontiens, F. G.; Regenfuss, P.; Zechel, A.; Dumortier, L.; Clegg, R. M., Binding characteristics of Hoechst 33258 with calf thymus DNA, poly[d(A-T)] and d(CCGGAATTCCGG): multiple stoichiometries and determination of tight binding with a wide spectrum of site affinities. *Biochemistry* **1990,** *29* (38), 9029-9039.

181. Pjura, P. E.; Grzeskowiak, K.; Dickerson, R. E., Binding of Hoechst 33258 to the minor groove of B-DNA. *Journal of Molecular Biology* **1987,** *197* (2), 257-271.

182. Yang, N. J.; Hinner, M. J., Getting Across the Cell Membrane: An Overview for Small Molecules, Peptides, and Proteins. *Methods in molecular biology (Clifton, N.J.)* **2015,** *1266*, 29-53.

183. Buscemi, G.; Perego, P.; Carenini, N.; Nakanishi, M.; Chessa, L.; Chen, J.; Khanna, K.; Delia, D., Activation of ATM and Chk2 kinases in relation to the amount of DNA strand breaks. *Oncogene* **2004,** *23*, 7691.

184. Paull, T. T.; Rogakou, E. P.; Yamazaki, V.; Kirchgessner, C. U.; Gellert, M.; Bonner, W. M., A critical role for histone H2AX in recruitment of repair factors to nuclear foci after DNA damage. *Current Biology* **2000,** *10* (15), 886-895.

185. Kuo, L. J.; Yang, L. X., Gamma-H2AX - a novel biomarker for DNA double-strand breaks. *In Vivo* **2008,** *22* (3), 305-9.

186. Maule, J., Pulsed-Field Gel Electrophoresis. In *The Nucleic Acid Protocols Handbook*, Rapley, R., Ed. Humana Press: Totowa, NJ, 2000; pp 81-104.

187. Ager, D. D.; Dewey, W. C.; Gardiner, K.; Harvey, W.; Johnson, R. T.; Waldren, C. A., Measurement of Radiation-Induced DNA Double-Strand Breaks by Pulsed-Field Gel Electrophoresis. *Radiation Research* **1990,** *122* (2), 181-187.

188. Miyabe, I.; Kunkel, T. A.; Carr, A. M., The Major Roles of DNA Polymerases Epsilon and Delta at the Eukaryotic Replication Fork Are Evolutionarily Conserved. *PLOS Genetics* **2011,** *7* (12), e1002407.

189. Muzi-Falconi, M.; Giannattasio, M.; Foiani, M.; Plevani, P., The DNA Polymerase _-Primase Complex: Multiple Functions and Interactions. *TheScientificWorldJOURNAL* **2003,** *3*.

190. Maric, C.; Bénard, M., Replication forks reverse at high frequency upon replication stress in Physarum polycephalum. *Chromosoma* **2014,** *123* (6), 577-585.

191. Tarsounas, M.; Davies, A. A.; West, S. C., RAD51 localization and activation following DNA damage. *Philosophical Transactions of the Royal Society B: Biological Sciences* **2004,** *359* (1441), 87-93.

192. Sage, J. M.; Gildemeister, O. S.; Knight, K. L., Discovery of a Novel Function for Human Rad51: MAINTENANCE OF THE MITOCHONDRIAL GENOME. *Journal of Biological Chemistry* **2010,** *285* (25), 18984-18990.

193. Kimura, S.; Noda, T.; Yoshimori, T., Dissection of the Autophagosome Maturation Process by a Novel Reporter Protein, Tandem Fluorescent-Tagged LC3. *Autophagy* **2007,** *3*, 452-60.

194. *https://www.cancerresearchuk.org/health-professional/cancer-statistics/survival#heading-One*.

195. Mosmann, T., Rapid colorimetric assay for cellular growth and survival: Application to proliferation and cytotoxicity assays. *Journal of Immunological Methods* **1983,** *65* (1), 55-63.

196. Feijoo, C.; Hall-Jackson, C.; Wu, R.; Jenkins, D.; Leitch, J.; Gilbert, D. M.; Smythe, C., Activation of mammalian Chk1 during DNA replication arrest: a role for Chk1 in the intra-S phase checkpoint monitoring replication origin firing. *The Journal of Cell Biology* **2001,** *154* (5), 913-924.

197. Okita, N.; Minato, S.; Ohmi, E.; Tanuma, S.-i.; Higami, Y., DNA damage-induced CHK1 autophosphorylation at Ser296 is regulated by an intramolecular mechanism. *FEBS Letters* **2012,** *586* (22), 3974-3979.

198. Lee, T. F.; McNellis, T. W., Elimination of keratin artifact bands from western blots by using low concentrations of reducing agents. *Analytical Biochemistry* **2008,** *382* (2), 141-143.

199. Kumar, S.; Tchounwou, P. B., Molecular mechanisms of cisplatin cytotoxicity in acute promyelocytic leukemia cells. *Oncotarget* **2015,** *6* (38), 40734-40746.

200. Ly, J. D.; Grubb, D. R.; Lawen, A., The mitochondrial membrane potential ($\Delta\psi m$) in apoptosis; an update. *Apoptosis* **2003,** *8* (2), 115-128.

201. Mauvezin, C.; Neufeld, T. P., Bafilomycin A1 disrupts autophagic flux by inhibiting both V-ATPase-dependent acidification and Ca-P60A/SERCA-dependent autophagosome-lysosome fusion. *Autophagy* **2015,** *11* (8), 1437-1438.

202. Jung, J., Human Tumor Xenograft Models for Preclinical Assessment of Anticancer Drug Development. *Toxicological Research* **2014,** *30* (1), 1-5.

203. Zanoni, M.; Piccinini, F.; Arienti, C.; Zamagni, A.; Santi, S.; Polico, R.; Bevilacqua, A.; Tesei, A., 3D tumor spheroid models for in vitro therapeutic screening: a systematic approach to enhance the biological relevance of data obtained. *Scientific Reports* **2016,** *6*, 19103.

204. Moro, M.; Bertolini, G.; Tortoreto, M.; Pastorino, U.; Sozzi, G.; Roz, L., Patient-derived xenografts of non small cell lung cancer: resurgence of an old model for investigation of modern

concepts of tailored therapy and cancer stem cells. *Journal of biomedicine & biotechnology* **2012,** *2012*, 568567.

205. Quinet, A.; Carvajal-Maldonado, D.; Lemacon, D.; Vindigni, A., Chapter Three - DNA Fiber Analysis: Mind the Gap! In *Methods in Enzymology*, Eichman, B. F., Ed. Academic Press: 2017; Vol. 591, pp 55-82.

206. Kimura, S.; Noda, T.; Yoshimori, T., Dissection of the autophagosome maturation process by a novel reporter protein, tandem fluorescent-tagged LC3. *Autophagy* **2007,** *3* (5), 452-60.